MAX-PLANCK-INSTITUT
FÜR BIOANORGANISCHE CHEMIE

DESIGNED SYNTHESIS OF EXCHANGE-COUPLED OXIMATE-BASED POLYNUCLEAR COMPLEXES

Dissertation for the degree of **Doktor der Naturwissenschaften** in the Fakultät für Naturwissenschaften (Department Chemie) at the Universität Paderborn

Presented by
Sumit Khanra

MÜLHEIM AN DER RUHR, 2005

This work was independently carried out between June 2002 and April 2005 at the **Max-Planck-Institut für Bioanorganische Chemie**, Muelheim an der Ruhr, Germany.

Submitted on: 08.08.2005 Examination: 16.09.2005

Publications:

1. A Magnetostructural Study of Linear $Ni^{II}Mn^{III}Ni^{II}$, $Ni^{II}Cr^{III}Ni^{II}$ and Triangular Ni^{II}_3 Species Isolated from (Pyridine-2-aldoximato)nickel(II) Unit as a Building Block.

   Thomas Weyhermüller, Rita Wagner, **Sumit Khanra** and Phalguni Chaudhuri

   Dalton. Trans. **2005**, 2539

2. Self-assembly of a Nonanuclear Nickel(II) Complex and its Magnetic Properties

   Sumit Khanra, Thomas Weyhermüller, Eva Rentschler and Phalguni Chaudhuri

   Inorg. Chem. **2005**, 8176

3. Photoinduced Intramolecular Proton Transfer of Phenol-containing Ligands and their Zn-Complexes.

   Helmut Görner, **Sumit Khanra**, Thomas Weyhermüller and Phalguni Chaudhuri

   J. Phys. Chem., **2005,** in press

4. Deliberate Synthesis for Magnetostructural Study of Linear Tetranuclear $B^{III}Mn^{II}Mn^{II}B^{III}$, $Mn^{III}Mn^{II}Mn^{II}Mn^{III}$, $Mn^{IV}Mn^{II}Mn^{II}Mn^{IV}$, $Fe^{III}Mn^{II}Mn^{II}Fe^{III}$ and $Cr^{III}Mn^{II}Mn^{II}Cr^{III}$ Complexes Using the Idea of “Metal Complexes” as Ligands.

   Sumit Khanra, Thomas Weyhermüller and Phalguni Chaudhuri

   Inorg. Chem. **2005**, Will be submitted soon.

5. A Magnetostructural Study of Butterfly Heterotetranuclear $Fe^{III}_2Cu^{II}_2$ and $Cr^{III}_2Cu^{II}_2$ Core Congeners with Strong (O…H…O) Bonding, Generated from $[Cu(dapdoH_2)]^{2+}$ Building Block: Competing Exchange Interaction and Irregular Spin State Structure.

   Sumit Khanra, Thomas Weyhermüller and Phalguni Chaudhuri

   Inorg. Chem. **2005**, Manuscript in preparation

6. Synthesis, Crystal Structure and Magnetic Properties of an Endogenous-alkoxo and Exogenous-hydroxo bridged Nonanuclear Copper(II) Metallamacrocyclic Core.

Sumit Khanra, Thomas Weyhermüller, Eva Rentschler and Phalguni Chaudhuri

Dalton Trans. **2005**, Manuscript in preparation

7. Tridentate Facial Ligation of Tris (Pyridine-2-aldoximato)nickel(II) to Generate $Mn^{III}Ni^{II}$, $Ni^{II}Ni^{II}$, $Zn^{II}Ni^{II}$ and Electrochemically Generated $Mn^{IV}Ni^{II}$, $Mn^{II}Ni^{II}$, $Zn^{II}Ni^{III}$, $Ni^{II}Ni^{III}$ Species : Magnetostructural, Electrochemical, Spectroscopic EPR and MCD Studies.

Phalguni Chaudhuri, Thomas Weyhermüller, Rita Wagner, **Sumit Khanra**, Stergios Piligkos, Eckhard Bill and Eberhard Bothe.

Inorg. Chem. **2005**, Manuscript in preparation

Examination Committee:

Prof. Dr. Phalguni Chaudhuri (Referent)

Prof. Dr. G. Henkel(Koreferent)

Prof. Dr. K. Hubber (Prüfer)

Prof. Dr. W. Bremser (Vorsitzender)

Examination: 16.09.2005

Acknowledgements

I would like to mention that submission of this thesis of mine would not have been possible at all had I not been bestowed with the benign association of the scientific elite of the Max Planck Institute, Muelheim an der Ruhr, Germany.

First of all, I humbly offer my deepest obeisance to **Prof. Dr. P. Chaudhuri**, who offered me the scope to be one of the Research- scholars under him. His constant guidance, hour-long invaluable discussions, perpetual inspiration with occasional reformatory thrashings always acted as motivating factors to my research works. Prof. Dr. P. Chaudhuri, in the truest sense, played the ideal role of the philosopher, the friend and the guide to me.

I am very much thankful to **Prof. Dr. K. Wieghardt** for the opportunity of working in his research group, providing with all needed laboratory facilities and also for intricate scientific discussion, invaluable guidance.

I am very much indebted to **Dr. E. Bill** for extending his warm hand for me in the field of Molecular Magnetism. Hour- long discussions with him on some intricate scientific issues infused a sense of confidence in me to complete this thesis.

I am indebted to **Dr. T. Weyhermüller** and **Mrs. H. Schucht** for their elegant work with the X-ray crystallography.

I cannot do justice to myself unless I acknowledge the contribution of Prof. **Dr. E. Rentschler**, Universität Mainz, Germany, who in spite of her busy schedule, spent her valuable time to teach and help me to simulate magnetic data for polynuclear complexes by **ITO** formalism

Thanks to **Dr. E. Bothe** and Mrs. P. Höfer for their help during electrochemical measurements, discussions and fruitful suggestions.

Dr. J. F. Barry and Dr. P. Larsen for suggestion and correction to complete this thesis.

I am thankful to Mr. A. Göbels, Mr. F. Reikowski, and Mr. B. Mienert for discussions and measurements of EPR, SQUID, and Mössbauer.

I am thankful to Frau. R. Wagner and Herr. U. Pieper, for technical assistance in the laboratory and due to their suggestions.

Mrs U. Westhoff and Mrs**.** M. Trinoga for skillfull GC and LC analysis.

Frau **J. Theurich**, Frau**. B. Deckers** and Herr W. Schlamann for their helpfulness in general.

Dr. K. Chlopek, Dr. L. Slep, Dr. K. Merz, Dr N. Aliaga-Alcalde, Dr. L. Benisvy, Dr Y. Song, Dr. S. Piligkos, and S. Kokattam, for a cordial working atmosphere and invaluable friendship.

Dr. Apurba Patra, Amin Khan, Shivani, Chandan Mukherjee, Dr. Kallol Ray**,** Dr. Tapan Paine, Dr. Soumen Mukherjee, Dr. Sourav Chaterjeee, Mamtha, for a nice homely atmosphere outside the laboratory and a wonderful friendship that I will cherish forever.

I will ever be thankful to **Dr. Ruta Kapre** and **Dr. Sachin Kinge** for a friendship and help that will remain in my heart for ever. Ruta and Sachin, thanks for being such nice friends.

Family Basak and Shila to make the life easier in Mülheim an der Ruhr.

Nivedita and Iowanna for wonderful friendship and encouragement.

I am thankful to my Parents, Parents in law**,** Amit and Ananda for their constant inspiration and encouragement.

I am highly indebted to my wife **Suchismita** for her understanding, inspiration, invaluable support and having faith in me.

DFG and **MPG** are greatfully acknowledged for financial assistance

Last but not the least in the list of my well wishers and aides, is the convoy of my research- mates in this Institute, my friends and fraternities outside, who stood by me in my weal and woe during my academic career in the Max Planck Institute for Bioinorganic Chemistry, Muelheim, Germany.

CONTENTS

DESIGNED SYNTHESIS OF EXCHANGE-COUPLED OXIMATE-BASED POLYNUCLEAR COMPLEXES

Abbreviations:

Technical terms:

AF: antiferromagnetic

Ag / $AgNO_3$: reference electrode

av.: average

B: magnetic field

CT: charge transfer

D: zero-field splitting

deg.: degree (°)

e^- : electron

E: total energy

exp.: experimental

F: ferromagnetic

fac.: facial

Fc^+/Fc: internal electrochemical standard

g: Landé factor

H: Hamiltonian

h.s: high spin

I: nuclear spin

IS: intermediate spin

J: coupling constant (cm^{-1})

KD: Kramer doublet

LF: ligand field

m/z: mass per charge

$[M]^+$: molecular ion peak

M: molar magnetization

mer.: meridional

MP: melting point

PI: paramagnetic impurity

rt: room temperature (293K)

S: electron spin

sim: simulated

TIP: temperature independent paramagnetism

ZFS: zero-field splitting

Techniques:

CV: cyclic voltammetry

EA: elemental analysis

EI: electron ionization

EPR: electron paramagnetic resonance

ESI: electrospray ionization

IR: infrared spectroscopy

LC: liquid chromatography

MS: mass spectroscopy

NMR: nuclear magnetic resonance

SQUID: superconducting quantum interface device

SW: square wave voltammetry

UV-Vis: ultraviolet-visible spectroscopy

VTVH: Variable-temperature variable field

Units:

Å: angstrom (10^{-10} m)

cm: centimeter

emu: electromagnetic unit

G: gauss

K: Kelvin

M : molar

mm : millimeter

nm : nanometer (10^{-9} m)

ppm: parts per million

s: second

T : tesla

V : volts

μ_B : bohr magnetron

Latin expressions:

ca.: around

et al: and coworkers

e.g.: for example

i.e.: namely

vs.: versus, against

Symbols:

λ: wavelength (nm)

ε: extinction coefficient ($M^{-1}cm^{-1}$)

IS: isomer shift (mms^{-1})

μ_{eff}: magnetic moment (μ_B)

ΔE_Q: quadrupole splitting (mm/s)

δ: isomer shift (mm/s)

Solvents and reagents:

Bu_4NOMe : tetrabutylammoniummethoxide

Et_3N: triethylamine

$TBAPF_6$: tetrabutylammonium hexafluorophosphate

TMS: tetramethylsilane

[9]-aneN_3: triazacyclononane = 1,4,7-triazacyclononane

Me_3Tacn: tmtacn = 1,4,7-trimethyl-1,4,7-triazacyclononane

Ligands used in this work:

PyAH: syn-2-pyridine-aldoxime

$SaloxH_2$: salicylaldoxime

$DapdoH_2$: 2,6-diacetylpyridyl dioxime

$DfmpH_3$: 2,6-diformyl-4-methyl phenol dioxime

Hppi: 2-pyridylmethyl-2-hydroxyphenylimine

H_2L: dioxime from m-xylenediamine

H_3L^1: N,N'-(2-hydroxypropane-1,3-diyl)bis(benzoylacetoneimine)

List of complexes synthesized with their numbers:

$[Ni^{II}(PyA)_3Mn^{III}(PyA)_3Ni^{II}](ClO_4)$ (1)

$[Ni^{II}(PyA)_3Cr^{III}(PyA)_3Ni^{II}](ClO_4)$ (2)

$[Ni^{II}{}_3(PyA)_5(PyAH)](ClO_4).CH_3CN$ (3)

$[MeB\{dfmp)_3Mn^{II}Mn^{II}\}BMe](Et_3NH)$ (4)

$[(Me_3Tacn)Mn^{III}\{dfmp)_3Mn^{II}Mn^{II}\}Mn^{III}(Me_3Tacn)](ClO_4)$ (5)

$[(Me_3Tacn)Mn^{IV}\{dfmp)_3Mn^{II}Mn^{II}\}Mn^{IV}(Me_3Tacn)](ClO_4)_3$ (6)

$[(Me_3Tacn)Fe^{III}\{dfmp)_3Mn^{II}Mn^{II}\}Fe^{III}(Me_3Tacn)](ClO_4)$ (7)

$[(Me_3Tacn)Cr^{III}\{dfmp)_3Mn^{II}Mn^{II}\}Cr^{III}(Me_3Tacn)](ClO_4)$ (8)

$[(Me_3Tacn)_2Fe^{III}{}_2(dapdo)_2Cu^{II}{}_2(O..H..O)Cl]\ (ClO_4)_2$ (9)

$[(Me_3Tacn)_2Cr^{III}{}_2(dapdo)_2Cu^{II}{}_2(OH)_2Br_2]\ (ClO_4)_2$ (10)

$[Mn^{II}{}_4(ppi)_6](BF_4)_2\ .2CH_3CN.\ H_2O$ (11)

$[Mn^{III}{}_4(salox)_4(salox\ H)_4]\ .2.5\ CH_3OH$ (12)

$[(dapdo)_2(dapdoH)_4|(\mu\text{-}O)_2(\mu\text{-}OMe)_2Mn^{III}{}_4Mn^{II}{}_2](ClO_4)_2$ (13)

$[(dapdo)_2(dapdoH)_4|(\mu\text{-}O)_2(\mu\text{-}OH)_2Mn^{III}{}_4Mn^{II}{}_2](ClO_4)_2$ (14)

$[L_3(\mu\text{-}O..H..O\text{-}\mu)Cu^{II}{}_6(H_2O)_6](BF_4)_3$ (15)

$[Ni^{II}{}_9(PyA)_{10}(\mu_3\text{-}OH)_2(\mu_2\text{-}OH)_2(\mu_2\text{-}OH_2)_2(H_2O)_6](ClO_4)_4\ .12\ H_2O$ (16)

$[Cu^{II}{}_9L_4(\mu_3\text{-}OH)_4(MeOH)_2](ClO_4)_2\ .6\ MeOH$ (17)

OUTLINE OF THE THESIS

The principles of coordination chemistry e.g. ligand field theory constitute a common ground for molecular magnetism, biomimetics and bioinspired chemistry. The subject of *molecular magnetism* is the center of this thesis. Summarily, this thesis mainly describes *exchange-coupled* homo and heteropolynuclear complexes, containing different paramagnetic metal ions, with particular emphasis on the interactions of spin carriers based on different *topological* approach with irregular *spin state structures* towards building *high-spin* molecules. These polynuclear complexes described here are characterized structurally and spectroscopically so that magnetostructural *correlations* can be made.

This work is divided into eight chapters. The first chapter gives an introduction relevant to this work, considering the background of "*Molecular Magnetism*" and the importance of the *exchange coupled* polynuclear complexes in "*molecular magnetism"* and *magnetic molecular materials*. The importance of oxime ligands as backbones for polynuclear complexes due to their versatility at bonding modes is discussed. A few examples of well characterized *high spin* molecules, relevant to this thesis, are reviewed.

The second chapter is concerned with the synthesis, characterization and magnetostructural study of *exchange coupled* trinuclear oximate complexes. It is to be mentioned here that new exchange pathways can be expected for heteropolynuclear complexes where unusual sets of magnetic orbitals can be made to overlap with each other and hence investigations of a series of heteropolynuclear complexes might be more informative in comparison to those of homometal complexes. Three trinuclear complexes, $\mathbf{Ni^{II}Mn^{III}Ni^{II}}$ **1**, $\mathbf{Ni^{II}Cr^{III}Ni^{II}}$ **2** and $\mathbf{Ni^{II}_3}$ **3** based on (pyridine-2-aldoximato)nickel(II) units are described. Two of them, **1** and **2**, contain metal-centers in linear arrangement, as is revealed by X-ray diffraction. Complex **3** is a homonuclear complex in which the three nickel(II) centers are disposed in a triangular fashion. The compounds were characterized by various physical methods including cyclic voltammetric and variable-temperature (2–290 K) susceptibility measurements. Complexes **1** and **3** display antiferromagnetic exchange coupling of the neighboring metal centers, while weak ferromagnetic spin exchange between the adjacent Ni^{II} and Cr^{III} ions in **2** is observed. The experimental magnetic data were simulated by using appropriate models.

The third chapter presents linear tetranuclear "*homo and heteropolymetallates*" constructed using a dinucleating oxime ligand. One dinuclear and four tetranuclear

complexes, **$Mn^{II}Mn^{II}$ 4, $Mn^{III}Mn^{II}Mn^{II}Mn^{III}$ 5, $Mn^{IV}Mn^{II}Mn^{II}Mn^{IV}$ 6, $Fe^{III}Mn^{II}Mn^{II}Fe^{III}$ 7** and **$Cr^{III}Mn^{II}Mn^{II}Cr^{III}$ 8** based on (2,6-diformyl-4 methyl phenoldioximato)manganese(II) units are described. All of them contain metal-centers in linear arrangement, as is revealed by X-ray diffraction. The compounds were characterized by various physical methods including cyclic voltammetric and variable-temperature (2–290 K) susceptibility measurements. Complexes display overall antiferromagnetic exchange coupling with extremely low-lying states.

The fourth and fifth chapters discuss the building up of high spin polynuclear complexes based on different *molecular topology* such as, butterfly, star-shaped etc, and a "parallel spin coupled" system using "accidental ferromagnetism" and "planned ferromagnetism" both governed by the common principle of orthogonal orbital overlap. It also discusses *irregular spin state structures* due to *spin frustration* or *competing exchange interaction.* Two tetranuclear complexes, **$Fe^{III}_2Cu^{II}_2$ 9**, **$Cu^{II}_2Cr^{III}_2$ 10** based on (2,6-diacetyl pyridinealdoximato)copper(II) units and $Me_3TacnMX_3$ (where M = Fe(III), Cr(III) and X = Cl or Br) are described. Both of them, **9** and **10**, contain metal-centers disposed in "butterfly" fashion with M(III) as the "wing" and Cu(II) as the "body", as is revealed by X-ray diffraction. The compounds were characterized by various physical methods including variable-temperature (2–290 K) susceptibility and variable-temperature variable-field (VTVH) magnetic measurements. The experimental magnetic data were simulated by using appropriate models Complexes **9** and **10** display antiferromagnetic exchange coupling of the neighboring metal centers, due to the "spin-frustration" or more precisely competing exchange interactions between the spin carriers complex **10** exhibits irregular spin state structure with $S_T = 2$ ground state. While strong wing-body interactions over body-body interaction, stabilizes $S_T = 4$ ground state in complex **9**.

Two tetranuclear complexes, **Mn^{II}_4 11**, **Mn^{III}_4 12** based on salicylaldoxime ligand are described. One of them, **11** contains metal-centers in "star-shaped" arrangement while the complex **12** in which the four manganese(III) centers are disposed in a tetrahedral fashion, as is revealed by X-ray diffraction. The compounds were characterized by various physical methods including variable-temperature (2–290 K) susceptibility and variable-temperature variable-field (VTVH) magnetic measurements. The experimental magnetic data were simulated by using appropriate models Complexes **11** and **12** display weak ferromagnetic exchange coupling of the neighboring metal centers, and yield high-spin $S_T = 10$ and $S_T = 8$ ground states for the complexes **11** and **12** respectively.

Also hexa-and nonanuclear complexes have been synthesized and are described in chapters six and seven. The hexanuclear complexes, composed of two edge-sharing triangular units, are also subjected to magnetostructural studies as described in chapter five, while sixth chapter describes two rare examples of nonanuclear Ni(II) and Cu(II) complexes**.** Two nonanuclear complexes, $\mathbf{Ni^{II}_9}$ **16**, $\mathbf{Cu^{II}_9}$ **17** based on (pyridine-2-aldoximato)nickel(II) unit and N,N'-(2-Hydroxypropane-1,3-diyl)bis(benzoylacetoneimine) respectively are described. Both of them, **16** and **17**, contain two irregular tetrahedra connected to a centrally placed M(II) ions, as is revealed by X-ray diffraction. The compounds were characterized by various physical methods including variable-temperature (2–290 K) susceptibility measurements and variable-temperature variable-field (VTVH) magnetic measurements. Complexes **16** and **17** display antiferromagnetic exchange coupling of the neighbouring metal centers. The experimental magnetic data were simulated by using appropriate models.

CHAPTER -1

INTRODUCTION AND OBJECTIVES

1.1 Background:

Molecular magnetism[1,7,15] is a field of research where the investigation of the magnetic properties of isolated molecules as well as of assemblies of molecules is undertaken. These molecules may contain one or more magnetic centers. Assemblies of molecules occurring in the solid state may be characterized by weak interactions between the molecular entities, thus displaying magnetic behavior very similar to that of the isolated molecules or may consist of extended systems built from molecular precursors in a way that maximizes the interactions between these molecular precursors, yield bulk magnetic properties. Solid state systems (metal oxides or metallic compounds) that also display highly interesting magnetic properties but do not consist of molecular entities or do not derive from molecular precursors are not included within the framework of the definition on molecular magnetism. In molecular magnetism the magnetic properties of paramagnetic molecules and how these properties affect the bulk magnetic properties of molecular materials are described.

This field concerns the chemistry and the physics of open shell molecules and molecular assemblies containing open-shell units. The main facets of molecular magnetism may be summarized as follows:

(i) Designing of open-shell molecules, the main emphasis being on molecules containing at least two magnetic centers where spin communication is possible between the spin carriers. These spin carriers may be transition metal ions as well as organic radicals. Efforts will be given to the design of polynuclear complexes containing tri, tetra and even if higher nuclearity spin clusters of transition metal ions.

(ii) Determination of the spectra of the low-lying states for such open-shell molecules, using various techniques such as magnetic susceptibility and magnetization measurements, EPR and optical spectroscopies or inelastic neutron scattering.

(iii) Chemistry and physics of transition metal compounds exhibiting a spin conversation or spin-transition between two different spin states.

(iv) The relations among magnetic properties, structure and reactivity of metalloenzymes and model compounds. This facet may be defined as biomagnetism.

(v) Three-dimensional effects in molecular assemblies, containing open-shell units. The main issues deal with molecular-based compounds exhibiting a spontaneous magnetization below a critical temperature T_c.

A prominent site of *molecular magnetism* is its interdisciplinary nature. It has already been pointed out that molecular magnetism has common frontiers with quite a few other areas such as supramolecular chemistry, theoretical chemistry and physics, material and life sciences and also molecular electronics.

Certainly the subject of "Molecular magnetism" has become increasingly accessible in recent years through many authoritative reviews and books.[1-11] As basic ideas and concepts related to magnetic interactions are described in these excellent reviews and books, we refrain here from repeating the same. Instead a description of the concepts of "***spin-frustration***", "***irregular spin-state structure***",[16,19] "***molecular topology***" etc. which are directly related to this research, is presented.

1.2 Objectives:

The objectives underlying the thesis are:

(i) Designed Synthesis:

One of the challenges in the field of exchange coupling in polymetallic systems is the design of complexes with predicted magnetic properties. To achieve this goal, the influence of parameters such as the symmetry of magnetic orbitals, the nature of bridging and terminal ligands, and changes in coordination geometry have been studied.[12] Surprisingly, very few studies of the influence of the molecular topology[26] on the magnetic properties of coordination complexes have been performed. For example, the chromium analogue of the Werner's hexol, $[Cr^{III}\{(OH)_2Cr^{III}en_2\}_3](ClO_4)_6$ by Anderson and Berg exhibits a high-spin $S_T = 3$ ground state owing to its topology,[25,26] shown below.

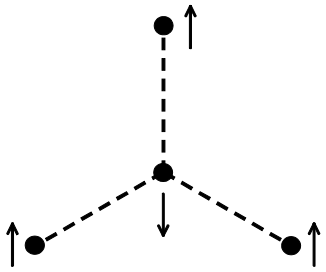

A ferromagnetic-like behavior is obtained with a ground state characterized by a large spin, although the interaction between nearest neighbor Cr^{III} ions ($S_{Cr} = {}^3/_2$) is

antiferromagnetic. This effective ferromagnetic coupling between the outer ions is highly interesting in the context of synthesizing "high spin" molecules. The best result would be obtained in a topology, in which a maximum number of spins point in the same direction as show in the previous page. Similarly other tetranuclear complexes of the formula $[\{Cu(oxpn)\}_3Mn](ClO_4)_2.2H_2O$ by Lloret et.al[24a] and $[Cr(ox)\{Ni(Me_6\text{-}(14)ane\text{-}N_4)\}_3](ClO_4)_3$ abbreviated as Cu_3Mn and $CrNi_3$ respectively, by Kahn et. al exhibit $S_T = 1$ and $S_T = 9/2$ ground state, respectively and it is to be noted that in case of Cu_3Mn, however, the pairwise interaction is antiferromagnetic but stabilizes a nondiamagnetic ground state due to the topology described above.

Recently more exciting result appeared, dealing with homometal tetranuclear nickel(II) planar trigonal-shaped species[30] $[Ni_4(HL)_3](ClO_4)_2$ where H_3L is 1,4,7-tris(acetophenoxime)-1,4,7-triazacyclononane. This tetranuclear nickel (II) complex with local spins $S_{Ni} = 1$ exhibits antiferromagnetic exchange interaction and yields a high-spin ground state $S_T = 2$ owing to the topology of the spin carriers as shown in the Figure above.

The other two topological possibilities for tetranuclear complexes, namely the square and the linear arrangements of the spin carriers, lead in the case of identical metal ions, to a diamagnetic ground state due to the equal number of spins in each direction, as illustrated schematically below

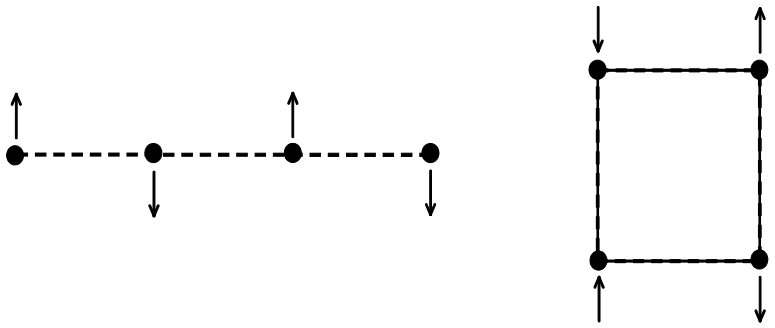

Thus the challenge for the chemists is to design real molecules having the following topologies for polymetallic complexes containing n paramagnetic ions, where n = 3, 4 or 5.

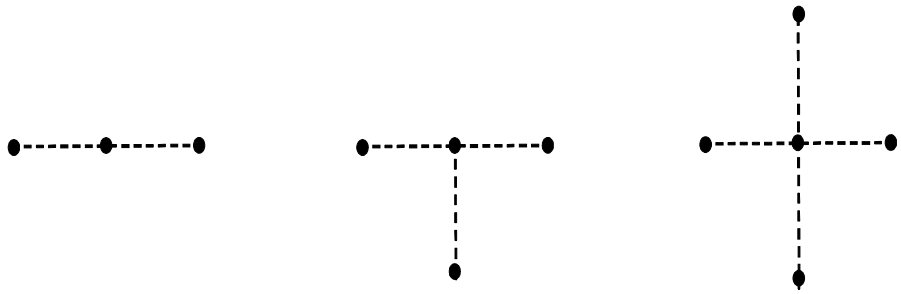

If the two border cases are considered for a heterometallic system, two possible situations arise for the spin coupling: i) the smaller spins may be located outside with the large spin at the center, yielding an overall "low spin"ground state, in which the outer spins partially cancel the central spin and ii) the reverse arrangement, i.e. the larger spins outside; the smaller spin located at the center polarizes the outer spins, thus resulting in a "high spin" ground state. Chaudhuri et.al used this strategy in the synthesis of a linear trinuclear $Fe^{III}Cu^{II}Fe^{III}$ complex[27] with an $S_T = {}^9/_2$ ground state, demonstrating the point of molecular topology is a very important factor determining the magnetic properties of polynuclear complexes with more than two metal ions. It is noteworthy that the actual geometry does not govern the spin structure for $n \geq 3$ metal ions. Thus it is possible to tune the magnetic properties of polynuclear complexes by controlling the topology and the nature of the ions in interaction. This approach is particularly promising for the synthesis of "high spin" molecules and needs systematic exploration.

In the field of magnetic molecular materials, one of the main challenges is the design of molecular ferromagnets. One approach to this consists of first synthesizing molecular entities with a large spin in the ground state and then of assembling this molecules within the crystal lattice in a ferromagnetic fashion. One strategy to obtain ferromagnetic interactions within a molecular entity is to make use of the orthogonality of the magnetic orbitals of the interacting magnetic centers. These symmetry requirements are difficult to achieve. Another strategy based on the concept of *irregular spin state structures*[19] leads to new molecular systems with a large spin in the ground state. It must be emphasized that the former strategy of orthogonality is not more efficient than the latter.

The basic idea of an irregular spin state structure can be described in the following way: The two ${}^5/_2$ local spins on the terminal iron(III) ions, for example, are aligned along a common direction through the antiferromagnetic interaction with the central local spin ${}^1/_2$ of the copper(II) ion, which is depicted below:

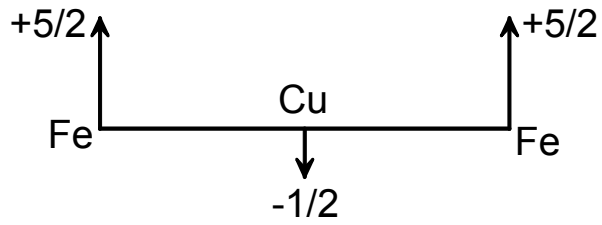

In some way, the small central spin polarizes the two large terminal spins in a ferromagnetic-like fashion. It is to be noted that J_{13}, the exchange interaction between the two terminal paramagnetic centers, has a profound effect on the spin-state energy-splitting pattern and depending on its magnitude a variability of the ground state might result. The spin-level ordering is a result of the mutual influence of two different interactions, $J_{12} = J_{23}$ and J_{13}, which may lead to "ground-state variability".[31a]

The key point is to focus on the bridging ligands which have already allowed the design of molecular based magnets. To date, these bridges are oxamato, oxamido, oxalato, oximato, carboxylato and cyano. Certain complexes involve such as in Fig. (a) organic bridging ligand between two similar or dissimilar modules. In (b) and (c) two mononuclear dissimilar modules generate heterobinuclear entities, in (d) a single metal ion acts as bridge between two mononuclear subunits giving rise to linear symmetric heterotrinuclear species. The same approach is used in (e) and (f), but in these cases the central metal ions are coordinated in bridging ligands producing heterotri and-tetranuclear complexes. Case (g) demonstrates the schematical presentation of two modules connected in a butterfly fashion.

These large, mostly linear polynuclear species received the name *baukasten* or *modular* complexes. The ligands facially bonded to the terminal ions are called end-caps, whereas the intermediate ones are referred to as bridging ligands. The most frequently encountered building blocks for modular synthesis have been described previously in the review article by chaudhuri, [30] and some of the pertinent concepts are described below.

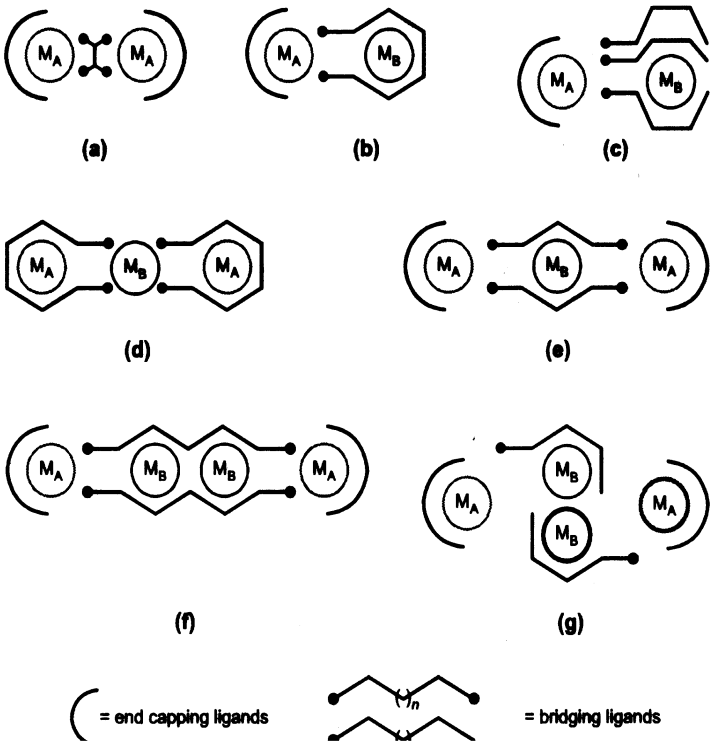

Figure 1.1: Schematical drawings of dinuclear (a-c), trinuclear (d, e) and tetranuclear (f, g) homo-and heterometal complex.

The synthetic organization of paramagnetic metal centers into close spaced arrays with useful magnetic properties is a challenge, and is generally achieved by having small bridging groups, which produce extended 2D and 3D structural arrangements. Cyanide has proven to be useful in this regard and with orthogonally connected metal orbitals, long range ferromagnetic ordering can be achieved. The optimal organization of paramagnetic transition metal centers into extended bridge structures with very short metal ion spacing can only be achieved with single atom bridges; this can be approached with e.g., oxygen based bridges. The last few years have experienced the ongoing development in the area of small 2D arrays with many examples of [3 X 3] magnetic grids with Co(II), Cu(II) and Mn(II), where M...M separations are of the order of 4Å . [2 X 2] self assembled Fe^{II}_4 grid reported by Lehn, based on a pyramidine bridging framework shows novel spin crossover behavior induced by pressure, temperature or light perturbations. These important unit molecule attributes can only be exploited if individual molecules can be successfully synthesized.

The oxamide dianion can adopt bidentate and bis bidentate coordination modes in its metal complexes, like the parent oxalate, to yield polynuclear complexes[39]. The strong electron donating capability of its deprotonated nitrogen amide atoms accounts for the

greater stability of its metal complexes when comparing with those of the oxalate. Moreover the lower electro negativity of the nitrogen atoms with respect to the oxygen atoms allows for stronger magnetic interactions between metal centers through oxamidato bridging ligands and several polynuclear complexes of this kind of ligand have been reported with magnetostructural studies. On the other hand, bimetallic oxamidato-bridged complexes are well known in magnetochemistry because they are suitable candidates in designing molecular based magnets.

Metal oximates have proven to be versatile for this approach as will be evident from the structurally and magnetochemically characterized compounds described later. The dimensions of structurally characterized oxime groups involve a C=N distance of ~ 1.26-1.28 Å and a N-O distance of 1.36-1.42 Å. The vicinal groups in solids are stabilized by the presence of C=N-O....H-O-N=C hydrogen bonds and the C-N-O angles vary from 110 to 114°. There are different modes of bonding in oxime complexes, these modes emerge from the potential ambidentate character through nitrogen and/or oxygen coordination. Some of the bonding modes are depicted in the Figure 1.2 below:

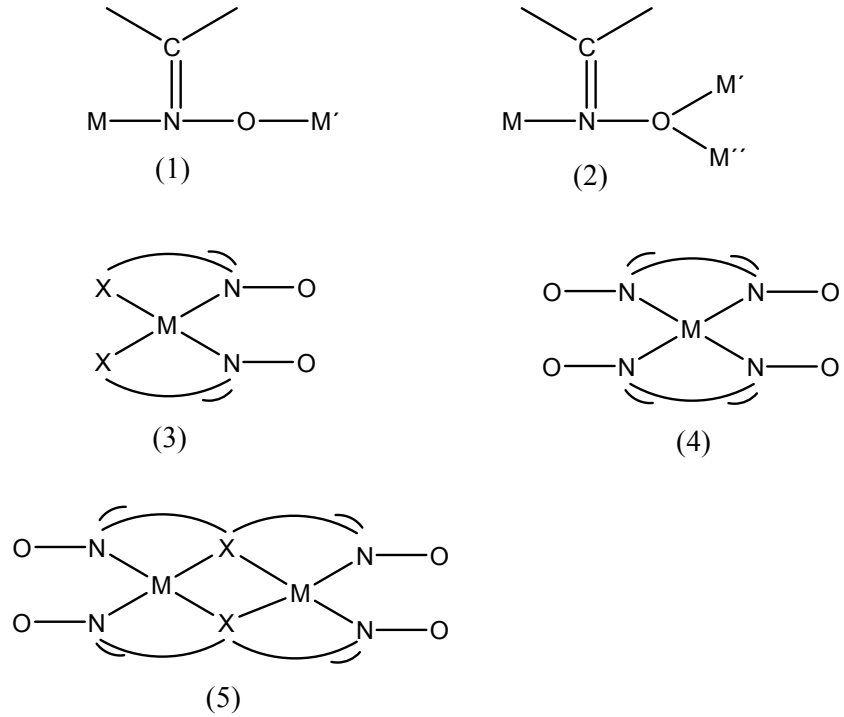

Figure 1.2: Bonding modes in oximes.

Due to this versatility of bonding modes, oximes are excellent bridging units in modular synthesis. In the last few years, the idea of synthesizing polynuclear complexes involving "metal oximates" as building blocks has become quite popular. The modular preparation with oximato ligands enables the synthesis of linear symmetrical and

asymmetrical cores M_AM_A,[30,32] M_AM_B,[30,32] $M_AM_BM_A$,[27,31a-b] $M_AM_BM_BM_A$[36] (M_A, M_B being two different metal ions). The synthesis of asymmetric heterotrinuclear complexes $M_AM_BM_C$ and of $M_A(\mu_3\text{-}O)_2$ M_B butterfly cores have also been achieved. The uniqueness of oximates providing diatomic N-O-bridging is demonstrated by several series of isostructural complexes with different metal ions like Cr(III), Mn(III), Mn(IV), Fe(III), Co(III). Such isostructural series[30] are not available for any other bridging ligands.

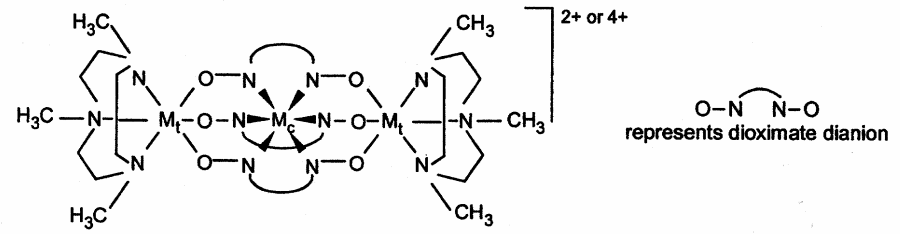

General formula **A**: M_t = Fe(III), Mn(III), Mn(IV), Cr(III) or Co(III)
M_c = Zn(II), Cu(II), Ni(II), Fe(II), Mn(II).

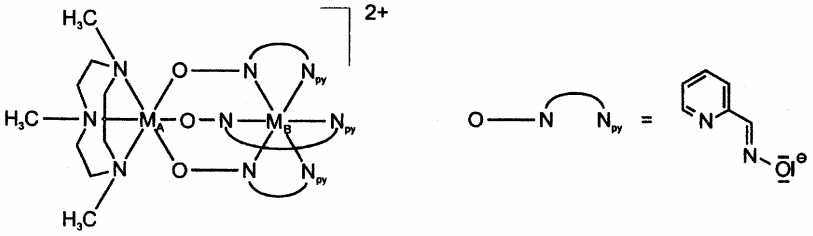

General formula **B**: M_A = Fe(III), Mn(III), Mn(IV), Cr(III) or Co(III) and
M_B = Zn(II), Cu(II), Ni(II), Fe(II), Mn(II).

Several different end-cap ligands have been reported. The function of such ligands is to prevent undesired oligomerization processes. Many acyclic polyamines including di-, tri-, and tetra-amines and bipyridine have been used as end cap ligands due to their ready commercial availability. Although not so readily available and obtainable only by a lengthy multistep synthesis, a very versatile end-cap ligand is the cyclic amine 1,4,7- trimethyl-1,4,7-triazacyclononan (Me_3Tacn). This amine is a facially coordinating tridentate nitrogen ligand and a significant number of both thermodynamically and kinetically, stable complexes of this ligands are known.[27, 30,31a-b]

The synthesis and characterization of homo and heteropolynuclear complexes with Me_3Tacn and oxime ligands using a modular approach has been one of the main goal of Chaudhuri and coworkers in recent years. Emphasis is given to the structural and

magnetochemical characterization. Recently it has been reported[32] that tris(pyridine-2-aldoximato) metallates, $[M^{II}(L)_3]^-$, are capable of acting as ligands to give rise to various asymmetric dinuclear complexes $[(Me_3Tacn)M^{III}(L)_3M^{II}]^{2+}$ where M^{III} = Cr(III), Mn(III) or Fe(III) and M^{II} = Mn(II), Fe(II), Ni(II), Cu(II) and Zn(II) containing three oximato groups (=N-O) as bridging ligands, which can mediate the exchange interactions of varying range.

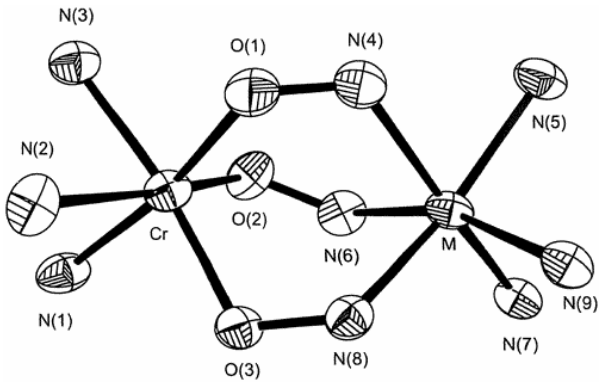

The oxime bridged tetranuclear complexes reported until now are of two types:

(i) Linear tetranuclear complexes are relatively rare. Using a modular synthesis some examples of $\mathbf{M_AM_BM_BM_A}$ and $\mathbf{M_AM_AM_AM_A}$ type containing the dinucleating oxime were synthesized.[36]

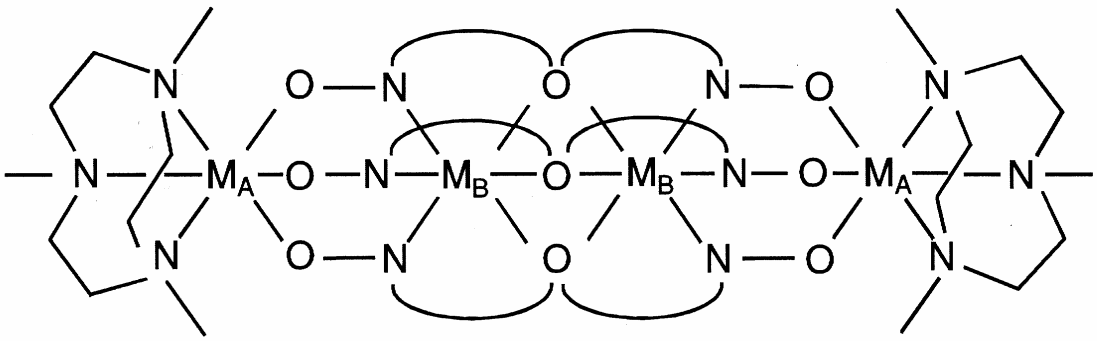

Polynucleating ligands, on the other hand, have structural attributes that combine separate coordination pockets, and in cases where they are contiguously arranged, metal ions are bound in close proximity and can be linked directly by endogenous or exogenous ligand fragments, leading to spin communication between metals. The interest in polynuclear complexes started with a class of dinucleating phenol containing ligands, where the dinucleating phenol provides an ideal focus for the simultaneous coordination

of two metal ions in close proximity and in further extension by the deprotonation of the dioximate oxygen to bind more metal ions for the modular synthesis of linear tetranuclear complexes in designed way.

Compounds with $Fe^{III}Ni^{II}Ni^{II}Fe^{III}$ and $Mn^{III}Ni^{II}Ni^{II}Mn^{III}$ cores, reported[36] earlier are similar to $Mn^{III}Mn^{II}Mn^{II}Mn^{III}$, $Mn^{IV}Mn^{II}Mn^{II}Mn^{IV}$, $Fe^{III}Mn^{II}Mn^{II}Fe^{III}$ and $Cr^{III}Mn^{II}Mn^{II}Cr^{III}$ congeners (Chapter-3)

(ii) Butterfly structures with the cores $\mathbf{[(M_A)_2(\mu_3\text{-}O)_2(M_B)_2]^{8+}}$ and $\mathbf{[(M_A)_4(\mu_3\text{-}O)_2]^{8+}}$

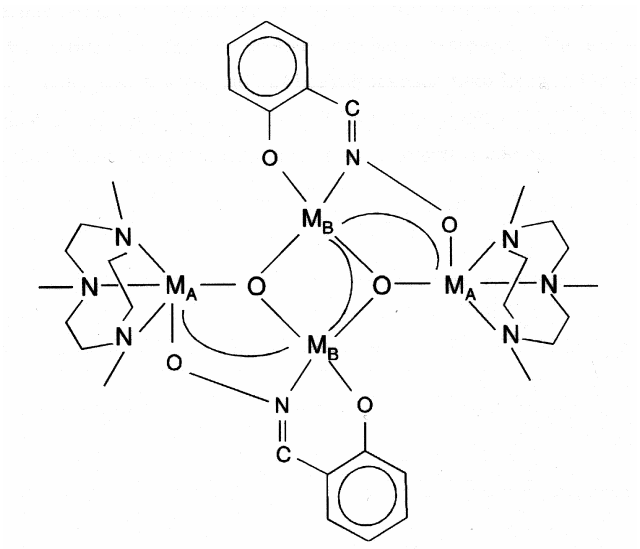

So far the reported tetranuclear butterfly clusters are based on homonuclear tetramanganese and tetrairon cores. Recently heterotetranuclear butterfly cluster was reported by Chaudhuri and coworkers in connection with magnetostructural correlation studies. And a series of exchange coupled homo and hetero tetranuclear butterfly clusters with $[Fe_4O_2]^{8+}$, $[Mn_4O_2]^{8+}$, $[Fe_2Mn_2O_2]^{8+}$ cores congeners were structurally and magnetochemically characterized.[37] Although the intrinsic interaction between the body manganese ions of the butterfly is antiparallel in nature, there is frustration in the spin alignment or competing interaction in the cluster associated with two manganese ions, causing the alignment to be parallel and gives rise to ground state variability.

So due to the lack of studies on heteronuclear butterfly clusters it allows us to investigate such ground state variation of the cluster based on small local spins at the body and higher local spins at the wing to have some "high spin" molecules due to the spin frustration or competing spin interaction. In this context some success was achieved in synthesizing and characterizing such heteronuclear "high spin" complexes and the competing spin interaction and irregular spin state structures will be described.

High nuclearity clusters with more than four metal centers were analyzed previously in our group with oxime ligand. An example is the hexanuclear cluster comprised of two μ_3-oxo centred trinuclear $[Cr^{III}_3(\mu_3\text{-}O)]$ units.[38] The antiferromagnetic coupling between the Cr^{III} centers reported in the literature is around - 14.0 cm^{-1}($H = -2JS_iS_j$), where exchange interaction was mediated through μ-oxo, oximate (=N-O) and also through the carboxylate bridging.

Further success was achieved in the synthesis and characterization of some hexanuclear complexes with different oxime ligands where exchange interaction mediated through oximates (=N-O) and in some complex with a combination of oxime and oxo bridge.

(ii) Evaluation of Coupling Constant:

The spin-Hamiltonian accounting for this isotropic exchange interactions may be written as $\mathbf{H = - 2 \Sigma J_{ij} S_i S_j}$, where the sum is taken over all pairwise interactions of intensity J_{ij} between spins S_i and S_j in the molecule. This model of the isotropic interaction between the spin carriers is based on the concept of magnetic orbitals and overlaps densities between pairs of such orbitals, and allows an analysis of the spin coupling. In molecular magnetism we are concerned not only with local spins associated with metal ions, but also with molecular spins associated with open-shell molecular units as a whole. It turns that the interaction between two such molecular units may not be of the same nature as the interactions between the two metal ions, belonging to a molecular unit, the other one belonging to the other molecular unit.

There are three mathematical methods for calculating the magnetic susceptibilities in polynuclear complexes:

(a) ***Vector Coupling*** (**VC**)

(b) ***Full matrix diagonalization*** (**FMD**)

(c) ***Irreducible tensor operator*** (**ITO**)

The VC method, formulated by Kambe,[40] is the easiest of three to set up and of use. It can results in the evaluation of closed form expressions for the susceptibility, which chemists feel comfortable working with. This method limited by the symmetry of the cluster system; since one has to be able to obtain appropriate and unique solutions to multivariable problems, it can therefore be used only for certain symmetries. Departure from these symmetries causes the Hamiltonian, to involve more J values, some of which may or may not be equal.

ITO or FMD methods must be then used. FMD has a major drawback in that it can result in very large matrices requiring long diagonalization times, and thus long computing times. The ITO method[41] on the other hand reduces the size of the matrices and computation times dramatically. Its drawback is that it is a bit more difficult to set up in the first case and requires a considerable degree or sophisticated mathematics. It is difficult to include single-ion effects in the ITO calculations such as zero-field splitting (ZFS). In contrast it is relatively easy to set up a matrix in FMD and to include effects such as ZFS.

(iii) Magnetizations at different fields:

A sample containing 1 mol of a molecular compound within an homogeneous magnetic field H, acquires a molar magnetization M related to H through, $\partial M / \partial H = \chi$ where χ is the molar magnetic susceptibility. When the magnetic field is weak enough, χ is independent of H, such that one can write $M = \chi H$. The molar magnetization M, is expressed in cm^3 G mol^{-1}, alternatively, M may be expressed in Nß units, N being the Avogadro's number and ß the electronic bohr magneton. The molar paramagnetic susceptibility characterizes the way in which an applied magnetic field H interacts with the angular momentum associated with the thermally populated states of a molecule. When a sample is perturbed by an external magnetic field, its magnetization is related to its energy variation through $M = - \partial E / \partial H$. This equation may be easily translated into the language of quantum mechanics. The macroscopic molar magnetization M is then obtained by a sum of the microscopic magnetizations weighted according to the Boltzmann distribution law, which leads to,

$M = [N\Sigma_n (\partial E_n / \partial H) \exp(-E_n / kT)] / \Sigma_n \exp(-E_n / kT)$, where T is the temperature and k is the Boltzmann constant. The above equation may be considered as a fundamental expression in molecular magnetism. The molar magnetic susceptibility varies as C/T, the constant C depending on the spin multiplicity of the ground state; this is the Curie law, which was proposed in 1910 from experimental data before the introduction of quantum mechanics and it is important to keep in mind that the Curie law is valid only when H / kT is small enough. The molar magnetization is then linear in H. When H / kT become large, then M must be calculated from the fundamental equation above. On the contrary, when H / kT becomes very large, M approaches the saturation value M_s, $M_s = Ng\beta S$. The saturation magnetization will be expressed in the following chapters in Nß units; its value is simply given by gS.

(iv) Different methods used for characterization of compounds:

To identify or assign the organic and inorganic compounds from the synergistic information afforded by the combination of mass (MS), infrared (IR), nuclear magnetic resonance (NMR) and UV-VIS absorption spectrum techniques will be employed. Essentially, the molecule is perturbed by these energy probes and the molecule's responses are recorded as spectra.

Infrared (IR) radiation refers broadly to that part of the electromagnetic spectrum between the visible and microwave regions. Of greatest practical use to the synthetic chemist is interested in the region between 4000 and 400 cm^{-1}. Although the IR spectrum is characteristic of the entire molecule, it is true that certain groups of atoms give rise to bands at or near the same frequency regardless of the structure of the rest of the molecule. It is the persistence of these characteristic bands that permits the chemist to obtain useful structural information by simple inspection and reference to general charts of characteristic group frequencies. Since it is not possible to use IR spectra solely for identification, a detailed analysis of the spectrum will not be required but only the assignments of the characteristic groups present in the ligand and complexes.

Various methods of producing molecular ions (including EI and ESI method) will be taken into consideration for the structure elucidation.

Electrochemical methods offer a unique access to information on chemical, biochemical and physical systems. The "Electrochemical methods", contains the most frequently utilized techniques, i.e., cyclic voltammetry, pulse and square-wave voltammetry and coulometry etc. Among the electrochemical techniques, cyclic voltammetry is frequently used because it offers wealth experimental information and insights into both the thermodynamic and kinetic details of many chemical systems. So voltametric experiments with microcrystalline particulate deposits present on the electrode surface provide information on the redox processes at the solid/solvent electrolyte interface, so for the insight into the redox processes these techniques will also be employed.

Mössbauer and EPR spectroscopy techniques will also be taken into consideration occasionally for the assignment of the oxidation state of iron atoms in the complex through Mössbauer spectroscopy and also to extract chemical information EPR spectroscopy will also be employed.

At the same time X-ray single crystal structure also important for the information of structural parameters that is necessary for better understanding of magnetostructural studies.

(v) Advantages of heteronuclear complexes over homometal complexes:

Both homo- and heteropolymetallic systems[16] provide opportunities to understand fundamental factors that govern exchange interactions. New exchange pathways can be expected for heteropolynuclear complexes where unusual sets of magnetic orbitals can be made to overlap with each other; hence investigations of a series of heteropolynuclear complexes might be more informative in comparison to those of homopolynuclear complexes. It is worth mentioning in this connection that the presence of different competing interactions in polynuclear complexes may lead to ground and other low-lying states that cannot be expected by simple combination of the local spins according to the nature of the interactions present between the spin carriers.

Another good reason for studying polynuclear complexes is that they may be building blocks for molecular-based magnetic materials. Although the pairwise exchange interactions in majority of the complexes are found to be antiferromagnetic, "spin-frustration"[17-21] in a general sense of the term, or more accurately competing spin interactions, in a polynuclear complex can result in ground states having a relatively large number of unpaired electrons. Although spin frustration is a well known magnetic phenomenon for extended lattices,[22] its application to the magnetochemistry of discrete polynuclear complexes is not widely recognized.[23] Competing spin interactions may give rise to unpredictable ground state spins and peculiar spin state structures. Thus the situation of ground state degeneracy induced by competing spin interactions is worth investigating.

"***Spin frustration***" will be used as a general case in certain topological arrangements of paramagnetic centers with competing exchange interactions of comparable magnitude preventing or frustrating the spin alignments that would otherwise be preferred in the ground state. The ground state is particularly sensitive to the relative magnitudes of the competing interactions and the spin of the ground state adopts an intermediate value rather than the lowest value that might be anticipated for an antiferromagnetically coupled system. "Spin-frustration degeneracy" of the ground state[19] leading to unusual electronic properties might be observed for some of the heteropolynuclear compounds to be synthesized here.

Linear heterotrinuclear complexes with general formula $[(Me_3Tacn)M_A(\text{oxime bridge})_{2\text{-}3}M_BM_A(Me_3Tacn)]^{2+/3+}$ were exclusively investigated. In these compounds the central oxime bridge is usually formed from dimethylglyoxime units N-cordinated to central ion M_B and bridged through the oxygen atoms to the terminal ions M_A. Depending

on the metallic ions involved, these complexes exhibit both antiferromagnetic and ferromagnetic properties. In the Cr(III) series complexes with Cu(II) and Mn(II) ions in the central position lead to ferromagnetic couplings while Ni(II) and Fe(III) result in antiferromagnetic exchange interactions. The Mn(III) series also exhibits alternate ferro- and antiferromagnetic exchange interaction. The complex Mn^{IV}_2Cu is isoelectronic with Cr^{III}_2Cu and also exhibits ferromagnetic exchange interaction. The much stronger interaction in the $Mn^{IV}_2Cu^{II}$ core can be attributed to the higher charge and consequently higher covalent character of the bonds to the Mn^{IV} ion. In contrast to the Mn(IV) series all the Fe(III) series exhibit antiferromagnetic exchange interaction.

Recently a rational assembly of a series of exchange coupled linear heterotrinuclear complexes of the type $M_AM_BM_C$ based on a strategy using metal oximates as building blocks has been reported.[35] Thus complexes $[(Me_3Tacn)M_A(L_{OX})M_BM_C]^{3+}$ where M_A = Fe(III) and Co(III) is facially coordinated to three nitrogen donors of the macrocyclic amine and M_B = Cu(II) or Ni(II) and M_C = Ni(II) or Cu(II) are embedded in a asymmetric dicompartmental imine-oxime ligand H_4L_{OX}. The compounds synthesized in this series $M_AM_BM_C$ are $Fe^{III}Cu^{II}Ni^{II}$ and $Fe^{III}Ni^{II}Cu^{II}$. The variable temperature magnetic moments reveal ground states of S_T = 3 and 2 respectively, also confirmed by the magnetization measurements

The magnetic interactions operating in this type of linear trinuclear complexes result in a ground state of high spin multiplicity, although the nearest neighbor spin alignments are antiparallel. Isoelectronic $Fe^{III}Cu^{II}Ni^{II}$ and $Fe^{III}Ni^{II}Cu^{II}$ demonstrate the strong influence of topological features on the magnetostructural properties. Following the Goodenough and Kanamori rules a qualitative rationalization for the exchange paths prevailing between neighboring and terminal spin carriers in these heterotrinuclear complexes has been presented and implies the predominance of σ-interactions over π-interactions.

The continuous development of exchange coupled heterometallic systems started with the aim of understanding interactions between two magnetic ions. The number of papers cited testifies to the uninterrupted interest in this area of coordination chemistry involving exchange coupled metal oximates. Of particular interest is the small but significant effect of bridging ligands like carboxylate anions for cooperation with the ancillary ligand, *viz* the oxime ligands to build up high nuclearity metal clusters.

To summarize, this work involves studies of magnetic properties of complexes containing paramagnetic metal centers in different molecular topology and

this thesis is devoted to the homo- and heterometallic exchange coupled polynuclear complexes.

1.3 References:

(1) O. Kahn, "*Molecular Magnetism*", VCH Weinheim, 1993

(2) J. B. Goodenough, "*Magnetism and the Chemical Bond* (Interscience, New York, 1963).

(3) E. Sinn, *Coord. Chem. Rev*., 1970, **5**, 313.

(4) A. P. Ginsberg, *Inorg. Chim. Acta Rev*., 1971, **5**, 45.

(5) W. E. Hatfield in "*Theory and Applications of Molecular Paramagnetism*", Eds. E. A. Boudreaux, L. N. Mulay, John Wiley & Sons, N. Y., 1976, p. 349.

(6) "*Magneto-Structural Correlations in Exchange Coupled Systems*", Eds. R. D. Willet, D. Gatteschi, O. Kahn, NATO ASI Series C, Vol. 140, Reidel, Dordrecht 1985.

(7) "*Magnetic Molecular Materials*", Eds. D. Gatteschi, O. Kahn, J. S. Miller, F. Palacio, NATO ASI Series E, Vol. 198, Kluwer Academic, Dordrecht, The Netherlands, 1990.

(8) R. L. Carlin, "*Magnetochemistry*", Springer Verlag, Berlin, 1986.

(9) C. J. O'Connor, *Progr. Inorg. Chem*., 1982, **29**, 203.

(10) O. Kahn, *Angew. Chem*., 1985, **97**, 837.

(11) A. Bencini, D. Gatteschi, "EPR of Exchange Coupled Systems", Springer Verlag, Berlin, 1990.

(12) G. Aromi, S. M. J. Aubin, M. A. Bolkar, G. Christou, H. J. Eppley, K. Folting, D. N. Hendrickson, J. C. Huffmann, R. C. Squire, H-L. Tsai, S.Wang and M. W. Wemple, *Polyhedron,* 1998, **17**, 3005

(13) E. C. Sanudo, W. Wernsdorfer, K. A. Abboud, and G. Christou, *Inorg. Chem* 2004, **43**, 4137; (b) M. Murugesu, M. Habrych, W. Wernsdorfer, K. A. Abboud, and G. Christou, *J.Am. Chem.Soc*., 2004,**126**,4766 .

(14) See for example: (a) R. H. Holm, E. I. Solomon, Guest Eds. *Chem. Rev*., 1996, **96**, No. 7; (b) A. L. Feig, S. J. Lippard, *Chem. Rev*., 1994, **94**, 759; (c) D. M. Kurtz, *Chem. Rev.,* 1990, **90**, 585; (d) L. Que, A. E. True, *Progr. Inorg. Chem*., 1990, **38**, 98; (e) V. L. Pecoraro, Ed. "*Manganese Redox Enzymes*", VCH Verlagsgesellschaft, Weinheim, 1992; (f) H. H. Thorp, V. L. Pecoraro, Eds. "*Mechanistic Bioinorganic Chemistry*", Advances in Chemistry Series 246, ACS, Washington DC, 1995.

(15) Selected examples: (a) "Mol. Cryst., Liq. Cryst." Eds. J. S. Miller, D. A. Dougherty, 1989, 176; (b) J. S. Miller and A. J. Epstein, *Angew. Chem. Int. Ed. Engl.*, 1994, **33**, 385;

(c) J. S. Miller, A. J. Epstein, *C & EN*, October 2 (1995), 30; (d) M. Kinoshita, *Jap. J. Appl. Phys*., 1994, **33**, 5718; (e) D. Gatteschi, *Adv. Mat*., 1994, **6**, 635; (f) H. Iwamura, J. S. Miller, Eds. "*Proceedings of the Conference on Chemistry & Physics of Molecular-Based Magnetic Materials*". *Mol. Cryst. Liq. Cryst.* 1993, 232-233; (g) N. Nakamura, K. Inone and H. Iwamura, *Angew. Chem*., 1993, **105**, 900. (h) H. O. Stumpf, L. Ouahab, Y. Pei, D. Grandjean and O. Kahn, *Science*, 1993, **261**, 447; (i) C. Kollmar and O. Kahn, *Acc. Chem. Res*., 1993, **26**, 259; (j) G. Christou, D. Gatteschi, D. N. Hendrickson and R. Sessoli, *MRS Bulletin* November 2000, p. 56; (k) E. Coronado, J. R. Galan-Mascaras, C. J. Gomez-Garcia and V. Laukhin, *Nature*, 2000, **408**, 447; (l) D. Gatteschi, R. Sessoli and A. Cornia, *J. Chem. Soc., Chem. Commun*., 2000, 725; (m) O. Sato, T. Iyoda, A. Fujishima and K. Hashimoto, *Science*, 1996, **272**, 704; (n) S. Ferlay, T. Mallah, R. Ouatrés, P. Veillet and M. Verdaguer, *Nature*, 1995, **378**, 701; (o) W. R. Entley and G. S. Girolami, *Science*, 1995, **268**, 397; (p) T. Mallah, S. Thiébaut, M. Verdaguer and P. Veillet, *Science*, 1993, **262**, 1554; (q) H. Miyasaka, N. Matsumoto, H. Okawa, N. Re, E. Gallo and C. Floriani, *J. Am. Chem. Soc*., 1996, **118**, 981. (r) S. Rajca and A, Rajca*, J. Am. Chem. Soc*., 1995, **117**, 9172; (s) H.-L. Tsai, S. Wang, K. Folting, W. E. Streib, D. N. Hendrickson and G. Christou, *J. Am. Chem. Soc*., 1995, **117**, 2503; (t) J. Solid State Chem. Special issue: "*New Horizons for Magnetic Solids Based on Molecules*", (a tribute to Oliver Kahn), Ed. K. R. Dunbar, 2001, **159**, No. 2; (u) J. S. Miller and J. L. Manson, *Acc. Chem. Res*., 2001, **34**, 563.

(16) (a) O. Kahn, *Adv. Inorg. Chem*., 1995, **43**, 179; (b) K. S. Murray, *Adv. Inorg. Chem*., 1995, **43**, 261.

(17) D. N. Hendrickson in "Research Frontiers in Magnetochemistry, Ed. C. J. O'connor, World Scientific, Singapore, 1993, p. 87.

(18) C. A. Christmas, H.-L. Tsai, L. Pardi, J. M. Kesselman, P. K. Gantzel, R. K. Chadha, D. Gatteschi, D. F. Harvey and D. N. Hendrickson*, J. Am. Chem. Soc*., 1993, **115**, 12483.

(19) O. Kahn, Chem. *Phys. Lett*., 1996, **265**, 109.

(20) R. D. Cannon, U. A. Jayasooriya, R. Wu, S. K. Arapkoske, J. A. Stride, O. F. Nielsen, R. P. White, G. J. Kearley and D. Summerfield, *Inorg. Chem*., 1994, **116**, 11869.

(21) J. E. Greedan, *J. Mater. Chem*., 2001, **11**, 37.

(22) S. Ghose, A. W. Hewat and M. Pinkney, *Solid State Commun*. 1990, **74**, 413.

(23) J. K. McCusker, E. A. Schmitt and D. N. Hendrickson in ref. 8, p. 297.

(24) (a) F. Lloret, Y. Journaux and M. Julve, *Inorg. Chem*., 1990, **29**, 3967; (b) D. J. Hodgson, K. Michelsen, E. Pedersen and D. K. Towle, *Inorg. Chem.,* 1991, **30**, 815.

(25) P. Andersen and T. Berg, *Acta Chem. Scand. Ser. A.,* 1978, **32**, 989.

(26) H. Güdel and U. Hauser, *Inorg. Chem*., 1980, **19**, 1325.

(27) P. Chaudhuri, M. Winter, P. Fleischhauer, W. Haase, U. Flörke and H.-J. Haupt, *J. Chem. Soc., Chem. Commun*., 1990, 1728.

(28) (a) E. I. Ochiai, *J. Chem. Ed.* 1993, **70**, 128; (b) J. Z. Pedersen and A. Finazzi-Agro, *FEBS Lett*. 1993, **325**, 53; (c) "*Metal Ions in Biologiical Systems*", Eds. H. Sigel and A. Sigel, Marcel Dekker, New York, Vol. 30, 1994; (d) M. M. Fontecave and J.-L. Pierre, *Bull. Soc. Chim. Fr*. 1996, **133**, 653; (e) G. T. Babcock, M. Espe, C. Hoganson, N. Lyldakis-Simantiris, J. McCracken, W. Shi, S. Styring, C. Tommos and K. Warncke, *Acta Chem. Scand*, 1997, **51**, 533; (f) J. Stubbe and W. A. Van der donk, *Chem. Rev*., 1998, **98**, 705.

(29) V. Pavlischuk, F. Birkelbach, T. Weyhermüller, K. Wieghardt and P. Chaudhuri, *Inorg. Chem*., 2002, **41**, 4405

(30) P. Chaudhuri, *Coord. Chem. Rev.,* 2003, **243**, 143

(31) (a) F. Birkelbach, U. Flörke, H-J. Haupt, C. Butzlaff, A.X. Trautwein, K. Wieghardt and P. Chaudhuri, *Inorg. Chem*.,1998, **37**, 2000; (b) D. Burdinsky, F. Birkelbach, T. Weyhermüller, U. Flörke, H-J. Haupt, M. Lengen, A.X. Trautwein, E. Bill, K. Wieghardt and P.Chaudhuri, *Inorg. Chem*., 1998, **37**,1009; (c) P. Chaudhuri, M. Winter, B. P. C. D. Vedova, P. Fleischhauer, W. Hasse, U. Flörke and H-J. Haupt, *Inorg. Chem*., 1991, **30**, 4777; (d) P. Chaudhuri, M. Winter, B. P. C. D. Vedova, E. Bill, A. Trautwein, S. Gehring, P. Fleischhauer, B. Nuber and J. Weiss *Inorg. Chem*., 1991, **30**, 2148

(32) S. Ross, T. Weyhermüller, E. Bill, K. Wieghardt and P. Chaudhuri, *Inorg. Chem*., 2001, **40**, 6656

(33) P. Basu, S. Pal, and A. Chakravorty. *Inorg. Chem*., 1988, **27**, 1848

(34) S. G. Sreerama and S.Pal. *Inorg. Chem*., 2002, **41**, 4843

(35) (a) C. N. Verani, T. Weyhermüller, E. Rentschler, E. Bill and P. Chaudhuri., *J. Chem. Soc., Chem. Commun.,* 1998, 2475; (b) C. N. Verani, E. Rentschler, T. Weyhermüller, E. Bill and P. Chaudhuri, *J. Chem. Soc. Dalton Trans.,* 2000, 4263; (c) C. N. Verani, Dissertation, Bochum, Germany, 2000

(36) (a) C. Krebs, Dissertation, Bochum, Germany, 1997; (b) C. Krebs, M. Winter, T. Weyhermüller, E. Bill, K. Wieghardt and P. Chaudhuri, *J. Chem. Soc., Chem Commun.,* 1995, 1913

(37) P. Chaudhuri, E. Rentschler, F. Birkelbach, C. Krebs, E. Bill , T. Weyhermüller and U. Flörke, *Eur. J. Inorg. Chem*., 2003, 541

(38) P. Chaudhuri, M. Hess, E. Rentschler, T. Weyhermüller and U. Flörke, *New J.Chem*., 1998, **30**, 553

(39) (a) Shi-bin Wang , Guang-ming Yang , Rong-fang Li , Yuan-fang Wang and Dai-zheng Liao, *Eur. J. Inorg. Chem*., 2004, 4907; (b) Y. Pei, Y. Jornaux and O. Kahn, *Inorg. Chem*., 1988, **27**, 399

(40) K. Kambe, *J. Phys.Soc., Jpn*. 1950, **5**, 48

(41) D. Gatteschi and L. Pardi, *Gazz. Chim. Ita*., 1993, **123**, 231

CHAPTER -2

TRINUCLEAR METAL OXIMATES: DESIGNED SYNTHESIS AND MAGNETIC PROPERTIES OF LINEAR $Ni^{II}Mn^{III}Ni^{II}$, $Ni^{II}Cr^{III}Ni^{II}$ AND TRIANGULAR Ni^{II}_3 COMPLEXES

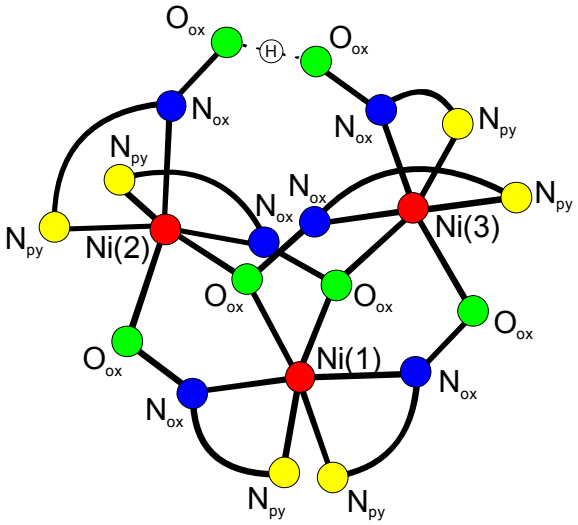

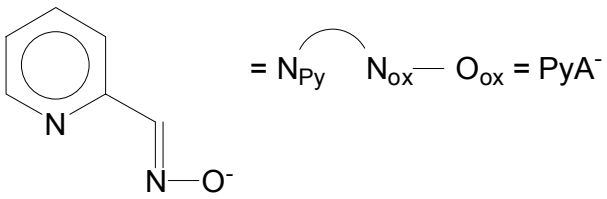

2.1 Introduction:

The homo and heteropolynuclear complexes are of interest to the inorganic chemists for their relevance to molecular magnetism (Chapter-1). This chapter describes some 3d-transition metal homo-and heterotrinuclear complexes which are relevant to the importance in magnetostructural studies. In an isosceles triangle how competing exchange interaction with two different coupling constants J and J' influences in determining the ground state will be discussed. If both the exchange coupling constants are negative, the exact nature of the ground state depends on the ratio ρ = J' / J and how this affects is also evidenced in the triangular Ni^{II}_3 (**3**) complex.

A remarkable feature of the oxime ligands[1] is their propensity to form polynuclear complexes,[2] both homo-and heteronuclear in which oxime function (>C=N-O) acts as a

bridging unit to yield magnetically interesting compounds.[3] This chapter describes the spin-spin interactions between the paramagnetic metal centers through multi-atom bridges and deals specifically with the ligation property of tris(pyridine-2-aldoximato)nickel(II), $[Ni(PyA)_3]^-$. It was prompted to study the coordination chemistry of this metal complex as a ligand because of the opportunity for its facile in-situ formation dictated by the thermodynamic stability of the resulting monoanion containing facially disposed three pendent oxime oxygen atoms for ligation.[4] So the ability of $[Ni(PyA)_3]^-$ monoanion will be explored in generating such homo-and heteropolynuclear complexes which will allow us to study exchange-coupled interactions.

2.2 Synthesis:

The reaction of Syn-2-pyridinealdoxime with $NiCl_2.6H_2O$ and $Mn(ClO_4)_2.6H_2O$; with $NiCl_2.6H_2O$ and $Cr(ClO_4)_3.6H_2O$ in 6:2:1 ratio in presence of NBu_4OMe as base yielded heterotrinuclear complexes $[Ni(PyA)_3Mn(PyA)_3Ni]$ (ClO_4) (**1**) and $[Ni(PyA)_3Cr(PyA)_3Ni]$ (ClO_4) (**2**) respectively; whereas the reaction of Syn-2-pyridinealdoxime with $Ni(ClO_4)_2.6H_2O$ in 6:3 ratio in presence of NBu_4OMe as base yielded homotrinuclear complex $[Ni_3(PyA)_5(PyAH)]$ (ClO_4) (**3**). In all the three complexes tris(pyridine-2-aldoximato)nickel(II) unit acting as a building block for the trinuclear complexes. These complexes will be abbreviated as $Ni^{II}Mn^{III}Ni^{II}$ (**1**), $Ni^{II}Cr^{III}Ni^{II}$ (**2**) and contain metal centers in linear arrangement while homotrinuclear complex as Ni^{II}_3 (**3**) where the three nickel(II) centers are disposed in triangular fashion.

2.3 Infrared and Mass Spectroscopy:

The relevant bands in IR spectra of comparable pyridine-2-aldoximato containing heteronuclear $Cr^{III}M^{II}$ and $Fe^{III}M^{II}$ complexes have been reported earlier by Ross et.al,[4] and the spectra of **1-3** are also very similar. A notable feature of the NO stretching for **3** is the sharp bands at 1130, 1125, 1031 cm^{-1}. The presence of two different coordination modes of the oxime group in **3** is consistent with the splitting.

Electrospray-ionaziation mass spectrometry (ESI-MS) in the positive ion mode has been proved to be very successful in characterizing $Ni^{II}Cr^{III}Ni^{II}$ which shows the monopositively charged species $[M\text{-}ClO_4]^+$ as the base peak. On the contrary the signal for $[M\text{-}ClO_4]^+$ of **3** is very weak, together with the base peak for the fragment $[M\text{-}ClO_4\text{-}PyA]^+$. The manganese

containing complex $Ni^{II}Mn^{III}Ni^{II}$ does not provide signals for unambiguous characterization.[19]

2.4 Solid state Structure:

2.4.1 X-ray structure of $[Ni(PyA)_3Mn(PyA)_3Ni]\ ClO_4$; H2O (1).

The lattice is built of discrete trinuclear monocations, perchlorate anions, and water molecules of crystallizations. The trinuclear complex contains two $[Ni^{II}(PyA_3)]^-$ moieties-each having a NiN_6 coordination sphere-acting as a tridentate ligand through the pendent oximato oxygen atoms to the centrally placed manganese (III) ion. A view of the cation $[Mn(PyA)_6Ni_2]^+$ ion in complex **1** is shown in Figure 2.1. Selected bond distances and angles are listed in Table2.1. The cation $[Mn(PyA)_6Ni_2]^+$ having a crystallographic threefold inversion symmetry has therefore a strictly linear arrangement of the $Ni^{II}Mn^{III}Ni^{II}$ array and the two $[Ni(PyA)_3]^-$ units necessarily have opposite chirality (Δ, Λ) making $[Mn(PyA_6)Ni_2]^+$ achiral.

The terminal nickel centers are six-fold coordinated yielding an NiN_6 core; coordination occurs facially through three pyridine nitrogen atoms $N_{py}(1)$ and three azomethine nitrogen atoms $N_{ox}(8)$, from the pyridine 2-aldoximate ligands. The Ni(1)-$N_{ox}(8)$ bond length 2.039(2) Å, is shorter than the Ni(1)-$N_{Py}(1)$, 2.107(2) Å, bond distance, as has been observed earlier for comparable complexes.[4] The Ni-N bond lengths fall within the ranges that are considered as normal covalent bonds for high spin d^8 Ni(II) ions. The facial disposition of the three $N_{py}N_{ox}$-chelate rings at each nickel atom is necessary for the ligation of the pendant oxime oxygen atom, O(9) and its equivalents, to the central manganese. The chelate rings are planar. The average chelate bite angle on the two nickel centers is 86.5°. This small but negative deviation of the bite angle from 90° necessarily implies the presence of substantial trigonal distortion. Indeed the two nickel centers can be considered to have distorted trigonal antiprismatic coordination, as is evident from the average twist angle Ψ of 38.0°, which deviates appreciably from the ideal 60° for an octahedron. The trigonal twist angle Ψ is defined as the angle between the triangular faces comprising three pyridine nitrogens, N(1) an its equivalents and three azomethine nitrogens N(8) and its equivalents. That the array Ni(N-O)Mn is not planar is shown by the dihedral angle θ of 36.5° between the planes comprising Mn(O-N) and Ni(N-O) atoms. These distortion of the 6 coordinate d^8 Ni(II) ion in complex **1** can be ascribed to both electronic LFSE and its size effects, as has been discussed earlier.[4-6]

The central manganese atom Mn(1) is surrounded by an almost perfect octahedron (deviation being less than 4°) of six oximato oxygen atoms O(9), pendent from the two [Ni $(PyA)_3]^-$ fragments. All angles at the metal between cis oxygen atoms deviate from ideal 90°, being 86.20(5)° and 93.80(5)°, the cis Mn(1)-O bond angle of 93.8(5)° represents the oxygen atoms originated from the same $[Ni(PyA)_3]^-$ fragment, where as the angle 86.20(5)° is exhibited between the oxygens of two different $[Ni(PyA)_3]^-$ fragments. The Mn(1)-O(9) distance of 2.027(1) Å is significantly shorter than the divalent manganese–oxygen distances lying in the range 2.101(4)-2.218(2) Å,[7] indicating that Mn(1) is in higher oxidation state than +II. That the central manganese ion must be ascribed to a +III (d^4 high spin) oxidation level is borne out by the facts that:(i) a perchlorate anion is present for maintaining the electroneutrality of the monocationic $[Mn(PyA_6)Ni_2]^+$ complex, (ii) the magnetic data can only be simulated by considering an S_{Mn} = 2.0 for the central Mn(1) center, and, (iii) the complex is X-band EPR silent at 4-20K.

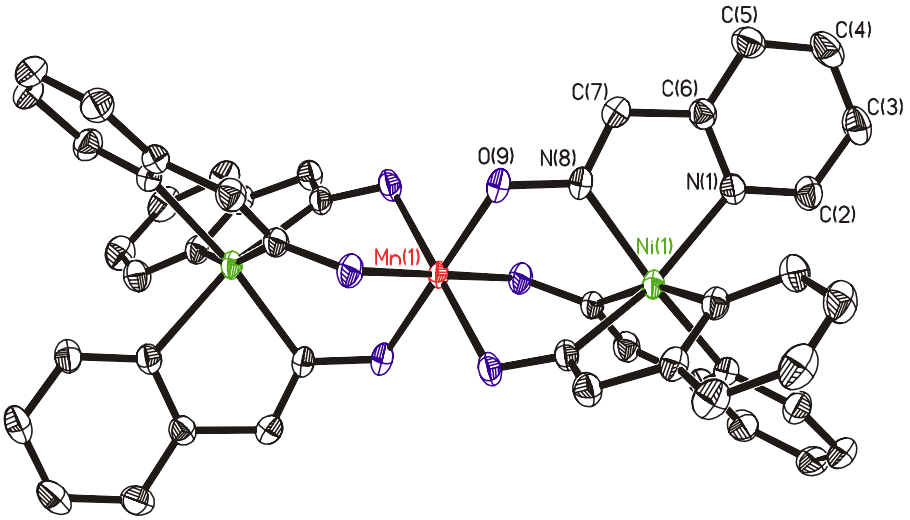

Figure 2.1: ORTEP and labeling scheme for $Ni^{II}Mn^{III}Ni^{II}$ (1)

There are rare structural data on high spin Mn(III) complexes with six identical monodentate ligands,[8] although a large number of tris(bidentate) and polydentate chelate complexes are known.[7] The Mn(1)-O(9) distance of 2.027(1) Å, found in complex **1** is completely in conformity with the Mn(III)-O distances observed in the comparable unambiguously established Mn(III)-complexes including the complexes with the Mn(III)-O_{oxime} bonds.[9-10] The cation in **1** has crystallographic site symmetry 3, (three fold inversion

symmetry)-which requires the six Mn-O bonds to be equivalent and hence the Jahn-Tellar distortion expected for a high spin d^4 Mn(III) is not observed for the octahedral $Mn(1)O_6$ polyhedron. The most reasonable explanation for the equivalence of the Mn-O bond lengths lies presumably in the dynamic Jahn-Tellar effect. It is concluded, complex **1** contains a $Ni^{II}_2Mn^{III}$ (high spin) core. Very similar oximato-bridged trinuclear MFe_2(low spin) have also been reported, although from the magnetochemical point of view they are mononuclear with central paramagnetic metal ions.[11]

Table 2.1: *Selected Bond Lengths (Å) and Angles (deg)* **[Ni(PyA)$_3$Mn(PyA)$_3$Ni] ClO$_4$; H2O (1).**

Ni(1)•••Mn(1)	3.57	Ni(1)•••Ni(1A)	7.14
Ni(1)-N(8)#1	2.039(15)	Mn(1)-O(9)	2.027(14)#3
Ni(1)-N(8)	2.039(15)	Mn(1)-O(9)	2.027(14)#4
Ni(1)-N(8)#2	2.039(15)	Mn(1)-O(9)	2.027(14)#5
Ni(1)-N(1)	2.017(15)	Mn(1)-O(9)	2.027(14)
Ni(1)-N(1)#1	2.017(15)	Mn(1)-O(9)	2.027(14)#1
Ni(1)-N(1)#2	2.017(15)	Mn(1)-O(9)	2.027(14)#2

2.4.2 X-ray structure of [Ni(PyA)$_3$Cr(PyA)$_3$Ni](ClO$_4$) (2).

The heterotrinuclear complex, **2**, $Ni^{II}Cr^{III}Ni^{II}$ also crystallizes like complex **1** in the space group R-3, with threefold inversion symmetry and is isostructural as expected with complex **1**. The trinuclear complex consists of two $[Ni^{II}(PyA)_3]^-$ moieties-each having a NiN_6 coordination sphere acting as tridentate ligand through the pendent oximato oxygen atoms to the centrally placed Cr(III) ion. A view of the cation $[Cr(PyA)_6Ni_2]^+$ in complex **2** is shown in Figure 2.2. The terminal $[Ni(PyA)_3]^-$ is very similar to that described for complex **1**.

The central chromium atom Cr(1) is surrounded by an almost perfect octahedron of six oximato oxygen atoms, O(9) and its equivalents, pendants from the terminal two $[Ni(PyA)_3]^-$ -fragments. The site symmetry $\bar{3}$ in the cation of **2** yields the six Cr(1)-O bonds to be equivalent for the octahedral $Cr(1)-O_6$ polyhedron. The Cr(1)-O(9) distance of 1.994(1) Å, found in complex **2** is completely in conformity with the Cr(III)-O observed in the comparable Cr(III)-complexes. That complex **2** is monocationic containing the $Ni^{II}Cr^{III}Ni^{II}$ ions is also evidenced by the presence of an anion perchlorate and the magnetic data described later. Selected bond distances and angles are listed in Table 2.2.

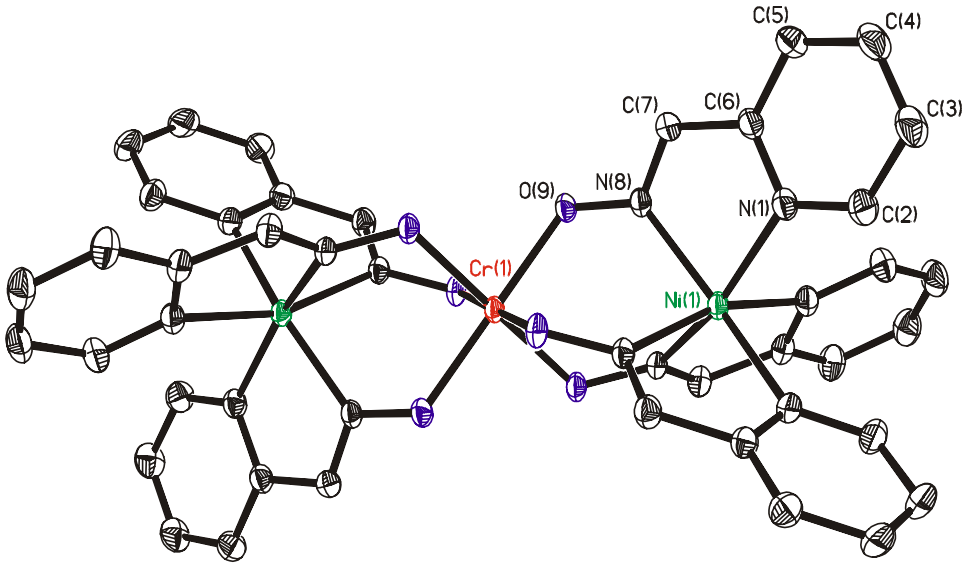

Figure 2.2: ORTEP and labeling scheme for $Ni^{II}Cr^{III}Ni^{II}$ (2)

Table 2.2: *Selected Bond Lengths (Å) and Angles (deg)* **$[Ni(PyA)_3Cr(PyA)_3Ni]\ ClO_4$; H2O (2).**

Ni(1)•••Cr(1)	3.552	Ni(1)•••Ni(1A)	7.104
Ni(1)-N(8)#1	2.036(13)	Cr(1)-O(9)	1.9936(11)#1
Ni(1)-N(8)#3	2.036(13)	Cr(1)-O(9)	1.9936(11)#2
Ni(1)-N(8)	2.036(13)	Cr(1)-O(9)	1.9936(11)#3
Ni(1)-N(1)#1	2.108(13)	Cr(1)-O(9)	1.9936(11)#4
Ni(1)-N(1)	2.108(13)	Cr(1)-O(9)	1.9937(11)#5
Ni(1)-N(1)#3	2.108(13)	Cr(1)-O(9)	1.9937(11)

2.4.3 X-ray structure of $[Ni_3(PyA)_5(PyAH)]\ ClO_4 \bullet CH_3CN$ (3).

The molecular geometry and atom-labeling scheme of the molecule has been shown in Figure 2.3. The structure of the complex consists of discrete trinuclear monocations $[Ni_3(PyA)_5(PyAH)]^+$, perchlorate anions, and acetonitrile molecules. There are three types of oximic groups: (i) two non-bridging >C= N-OH groups, O(39) and O(59) of which a proton is disordered over both sites, which is virtually the universal bonding mode for oximes, (ii) a two atom (N-O) bridging group, N(8)O(9) and N(18)O(19), as found in preponderance over

(iii), (iii) a monoatomic oximato μ_2-O bridging, O(29) and O(49). That an oxime group acts as a bridging μ_3-ligand, -N-O, is not unprecedented.[14] Accordingly, the N-O bond lengths in the oximate fragments are in the ranges 1.332(2), 1.341(2)-1.359(2) and 1.370(2)-1.373(2) Å and correspond well with those observed in the comparable structures. The bond distance $C=N_{ox}$ at average 1.291 ± 0.011 Å and the bridging bond angle $C=N_{ox}$-O of average 118.7±1° and non-bridging $C=N_{ox}$-O of 114.5 ± 0.2° fall in the range reported for complexes containing pyridine-2-aldoximato as ligands.[4,10,18] All other intraligand bond parameters are unexceptional. Figure 2.4 highlights not only the coordination spheres of the three nickel atoms, but also illustrates the three different coordination modes of pyridine-2-aldoximato(-) ion, $N_{py}N_{ox}$-O, in complex **3**. The three nickel atoms form a triangular arrangements with the separations of Ni(1)..Ni(2) 3.240, Ni(1)…Ni(3) 3.276 and Ni(2)…Ni(3) 3.951 Å.

The nickel ions all display pseudo-octahedral geometry with NiN_4O_2 coordination spheres. Ni(1) is coordinated to cis-$(N_{py})_2$, tarns-$(N_{ox})_2$ and cis-$(\mu_2\text{-}O_{ox})_2$ donor atoms, where N_{py}, N_{ox}, O_{ox} represent respectively pyridine nitrogen, oxime nitrogen and monoatomic bridging oxime oxygen. The two bridging ligands between Ni(1) and Ni(2) are the monoatomic μ_2-O(49)(which is bonded to N(48) of an oxime group), N(8)O(9). The bridging connectivities between Ni(1) and Ni(3) are also very similar with μ_2-O(29) and N(18)O(19). On the contrary Ni(2) and Ni(3) are bridged through only the two μ_2-O-oxygens, O(49) and O(49). The coordination octahedron of Ni(1) is slightly irregular, with several angles departing from right angles by 11° or so, as exemplified in Figure 2.3 by N(8)-Ni(1)-N(11) at 101.54(6)°. The distortion from octahedral geometry for Ni(2) and Ni(3) is more pronounced; the trans donor angles deviate from 180° by nearly 20°, *viz*. N(41)-Ni(3)-O(29) at 161.59(5)° and N(21)-Ni(2)-O(49) at 162.79(5)°. Selected bond lengths and angles are given in Table 2.3. The Ni(1)-N_{ox} bond lengths are shorter than the Ni(1)-N_{py} bond lengths, while for Ni(2) and Ni(3), the reverse is true. As expected the Ni-μ_2-O_{ox} bond lengths are significantly longer than the Ni-O_{ox} bond lengths involving the two atomic oximato bridges, e.g. Ni(3)-O(29) 2.116(1) Å vs. Ni(3)-O(19) 2.051(1) Å. The Ni-N and Ni-O bond distances are consistent with normal covalent bonds for high spin d^8 Ni(II) ions with oximato ligands.

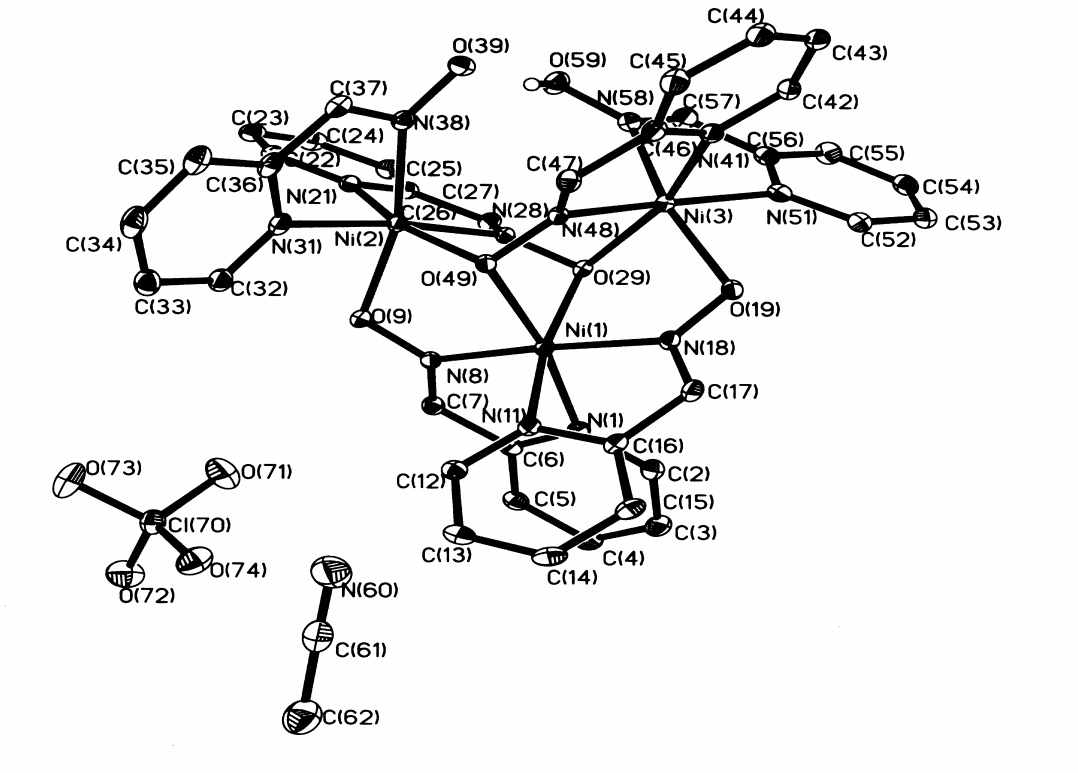

Figure 2.3: ORTEP and labeling scheme for Ni^{II}_3 (3)

The short O(39)....O(59) separation of 2.414(2) Å clearly indicates the occurrence of strong hydrogen bond interactions between these oxygen atoms, suggesting protonated uncoordinated O(59) and O(39). Indeed, a difference Fourier in the later refinement stages did reveal a peak assignable to a proton, appearing between O(39) and O(59) and it was included in this position in the final refinement cycle (occupation factor 0.5 each). The presence of a single proton per trinuclear unit with six pyridine–2-aldoximato anions is in complete accord with the charge balance considerations of the monocations in complex **3**. The oxime hydrogen was refined isotropically, and approximate bond distances within the symmetrical hydrogen bridge are about 0.9Å; O(39)-H = 0.898 and H....O(59)=0.905 Å. That the hydrogen bonding is symmetrical is also manifested in similar N-O lengths: O (39)-N (38) = 1.359(2) and O(59)-N(58)=1.341(2) Å.

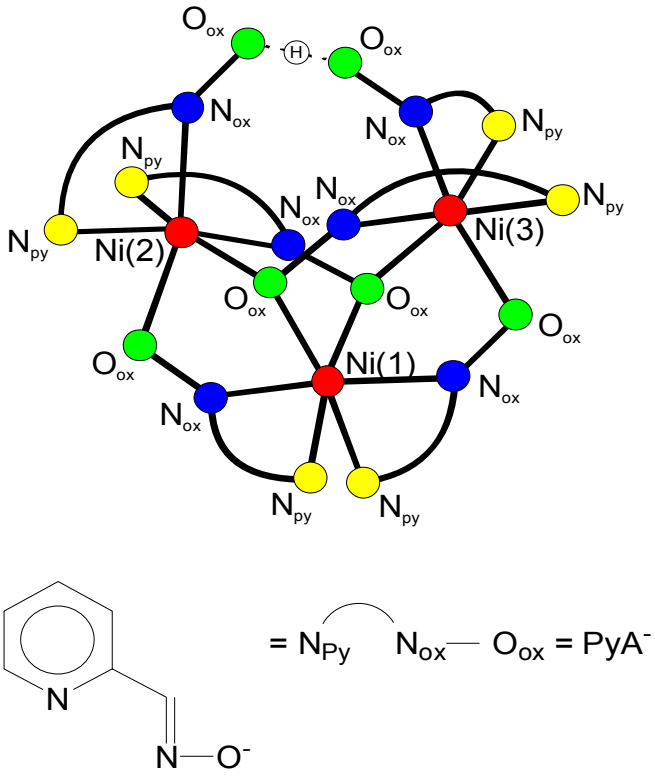

Figure 2.4: A schematic representation of the atom connectivities in the triangular trinickel(II) present in the cation of complex 3 to highlight three different coordination modes of pyridine-2-aldoximato monoanion, $N_{py}N_{ox}$-

Table 2.3: *Selected Bond Lengths (Å) and Angles (deg)* **[Ni_3 $(PyA)_5(PyAH)$] ClO_4 •CH_3CN (3).**

Ni(1)•••Ni(2)	3.240	Ni(1)•••Ni(3)	3.276
Ni(2)•••Ni(3)	3.951		
Ni(1)-N(18)	2.017(14)	Ni(3)-N(51)	2.071(15)
Ni(1)-N(8)	2.024(14)	Ni(3)-N(41)	2.072(15)
Ni(1)-N(11)	2.104(14)	Ni(3)-N(48)	2.081(14)
Ni(1)-N(1)	2.117(14)	Ni(3)-N(58)	2.164(2)
Ni(1)-O(49)	2.104(12)	Ni(3)-O(19)	2.051(12)
Ni(1)-O(29)	2.138(12)	Ni(3)-O(29)	2.116(12)
Ni(2)-N(28)	2.069(14)	Ni(3)-O(29)-Ni(1)	100.7(5)
Ni(2)-N(31)	2.070(15)	Ni(31)-O(49)-Ni(2)	100.6(5)
Ni(2)-N(21)	2.080(134		

Ni(2)-N(38)	2.123(2)
Ni(2)-O(49)	2.107(12)
Ni(2)-O(9)	2.042(13)

2.5 Magnetic Properties:

Magnetic susceptibility data for polycrystalline samples of the complexes were collected in the temperature range 2-290 K in an applied magnetic field of 1T. We use the Heisenberg spin Hamiltanonian in the form: $H= - 2J(S_1S_2+S_2S_3)-2J_{13}(S_1S_3)$, for an isotropic exchange coupling with $S_1 = S_3 = S_{Ni} = 1$ and $S_2 = S_{Mn} = 2$ for **1**, $S_1 = S_3 = S_{Ni} = 1$ and $S_2 = S_{Cr} = 3/2$ for **2**. The experimental data as the effective magnetic moments μ_{eff} versus temperature T. are displayed in Figures 2.5 and 2.6. The experimental magnetic data were simulated using a least squares fitting computer program with a full matrix diagonalization approach and the solid lines in Figures 2.5 and 2.6 represent the simulations. Table 2.4 summarizes intratrimer magnetic parameters.

The magnetic moment μ_{eff}/molecule for **1**, $Ni^{II}Mn^{III}Ni^{II}$, of 6.13 μ_B ($\chi_M \bullet T$ = 4.692 $cm^3.K.mol^{-1}$) decreases monotonically with decreasing temperature until it reaches a value of 5.199 μ_B ($\chi_M \bullet T$ = 3.38 $cm^3.K.mol^{-1}$) at 50 K and then starts to decrease further but rapidly and reaches a value of 1.639 μ_B ($\chi_M \bullet T$ = 0.336 $cm^3.K.mol^{-1}$) at 2 K. This temperature dependence is in agreement with the weak antiferromagnetic coupling between the neighboring Ni(II) and Mn(III) ions resulting in a diamagnetic $S_T = 0$ ground state for **1**. A simulation kept $J_{13} = 0$ and shown as a solid line in Figure 2.4 results in J = - 3.18cm^{-1}, g_{Ni} = 2.05, g_{Mn} = 1.97 and 2% paramagnetic impurity with S = 2.0. The observed antiferromagnetic coupling agrees well with the comparable exchange coupling constants reported earlier.[9-10]

The variable-temperature magnetic movements μ_{eff} vs. T-plot for complex **2**, $Ni^{II}Cr^{III}Ni^{II}$ also shown in Figure 2.6 exhibits in the region 293-100 K nearly temperature-independent μ_{eff} value of 5.52μ_B ($\chi_M \bullet T$ = 3.816 $cm^3.K.mol^{-1}$), which is very close to the value expected for three uncoupled spins for $S_1 = S_3 = 1.0$ and $S_2 = 3/2$ (μ_{eff} = 5.56 μ_B with g = 2.0). Below 100 K the μ_{eff} values increase very slowly to reach a peak value of 5.733μ_B ($\chi_M \bullet T$ = 4.11 $cm^3.K.mol^{-1}$) at 10 K. The increase in μ_{eff} values indicates an overall ferromagnetic coupling. A simulation shown as a solid line in Figure 2.6 results in $J = J_{12} = J_{23} = + 0.60$ cm^{-1}, $J_{13} = - 0.90cm^{-1}$, $g_{Ni} = g_1 = g_3 = 2.0$(fixed) and $g_{Cr} = g_2 = 1.95$ (fixed).

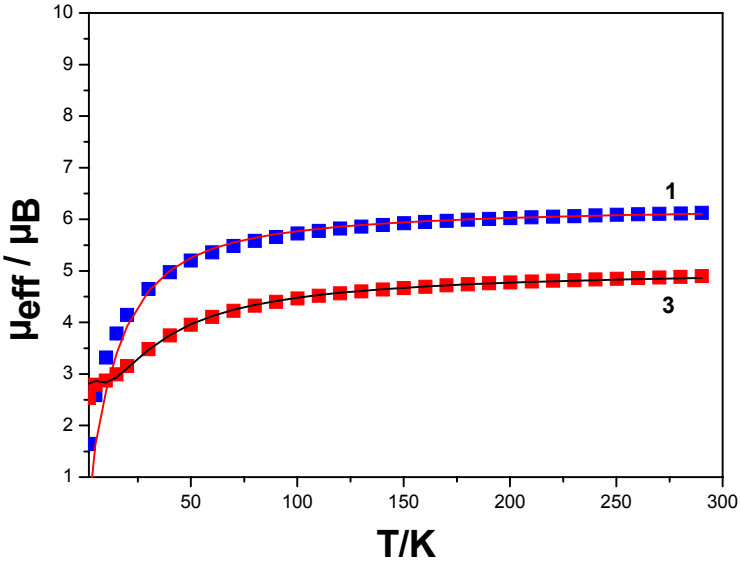

Figure 2.5: Magnetic data for $Ni^{II}Mn^{III}Ni^{II}$ (1) and $Ni^{II}{}_3$ (3) plot of μ_{eff} vs. T. The bold points represent the experimental data while the solid line represents the simulation.

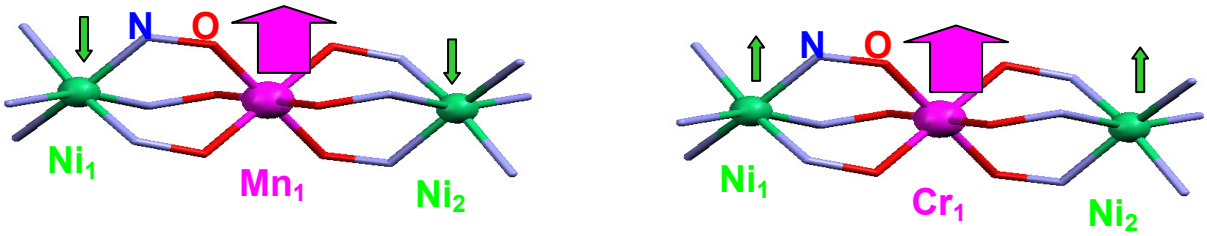

Scheme 1: Representation of the magnetic exchange coupling model.

The energy ladder of the spin-states shows that two states with S_T = 7/2 and 3/2 form the ground state, which is only 1.8 cm^{-1} below the first excited state with an another S_T = 7/2. The observed ferromagnetic coupling between Cr(III) and Ni(II) centers agrees well with the comparable exchange couplings reported in the literature and is in accord with the Goodenough-Kanamori orthogonality rule[3a] as expressed by the Ginsberg's symbols: e_g(Ni) $||\ \sigma_{NO} \perp t_{2g}$(Cr)[6,16]

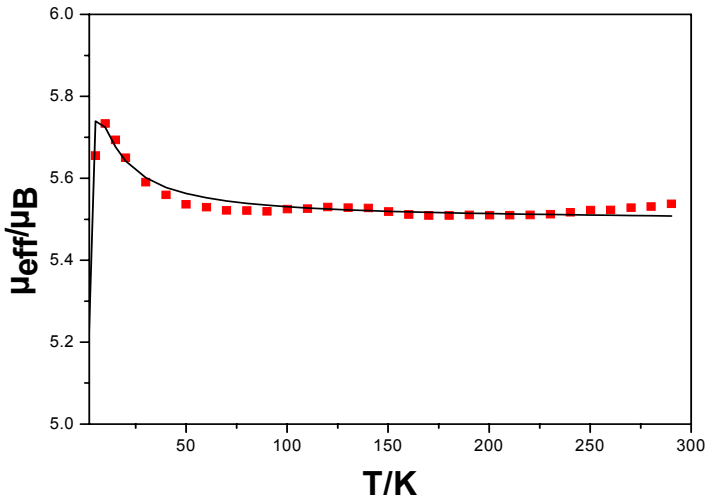

Figure 2.6: Magnetic data for $Ni^{II}Cr^{III}Ni^{II}$ (2) plot of μ_{eff} vs. T. The bold points represent the experimental data while the solid line represents the simulation.

The magnetic movement μ_{eff} vs. T plot with an applied field of 1 T for **3** in the range 2-290 K is shown in Figure 2.4. The magnetic movement μ_{eff} /molecule for **3**, Ni^{II}_3, of 4.896 μ_B (χ_M•T = 2.998 cm^3.K.mol^{-1}), at 290 K decreases monotonically with the decreasing temperature until it reaches a value of 2.790 μ_B (χ_M•T = 0.9735 cm^3.K.mol^{-1}) at 5 K, which then drops to 2.535 μ_B (χ_M•T = 0.8036 cm^3.K.mol^{-1}) at 2 K. This temperature dependence is in agreement with an antiferromagnetic coupling between the Ni(II) ions resulting in triplet S_T = 1 ground state for **3**.

On the basis of crystal structure of **3**, Ni^{II}_3 triangular unit with the $[Ni_3(PyA)_5(PyAH)]^+$ can be considered as scalene as a Ni(1)...Ni(2) (3.240 Å), Ni(1)...Ni(3) (3.276 Å) and Ni(2)...Ni(3) (3.951 Å) distances are different. Hence three pair wise exchange interactions with J_{12}, J_{13} and J_{23} at the beginning were used to simulate the experimental magnetic data. A good fit (not shown) was obtained with the fitting parameter: J_{12} = - 32.7 cm^{-1}, J_{13} = + 12.5 cm^{-1}, J_{23} = + 25.0 cm^{-1}, $g_1 = g_2 = g_3$= 2.0. As a coupling constant appear to

us to be physically unreasonable, we generated plots of the relative error for the fitting of the data as a function of "J" and g, which show clearly the strong correlation and local minimum nature of the fitting. Hence, the data for complex **3** were analyzed as an isosceles system with the "two–J" model; a similar magnetochemical analysis of another triangular oxime bridged Ni^{II}_3 complex is known in the literature.[14e] Additionally, the bridging ligands between Ni(1) and Ni(2) or Ni(3) are same, while Ni(2) and Ni(3) are bridged through only two monoatomic μ_2-O_{ox} groups, which are consistent with a "two-J" model with the $J = J_{12} = J_{13}$ and $J = J_{23}$ expected for an isosceles triangle. Thus, the spin Hamiltonian in used to describe the isotropic exchange interaction is given by; $H = - 2J(S_1S_2 + S_1S_3) - 2J'(S_2S_3)$, where the subscripts refer to the Nickel centers labeling scheme in Figure 2.4 with S = 1.0. An excellent fit of the experimental μ_{eff} vs. T data, shown as a solid line in Figure 2.5, with fitting parameters $J = - 8.20 \pm 0.20$ cm^{-1}, $J = - 2.0 \pm 0.1$ cm^{-1} and $g_1 = g_2 = g_3 = 2.07$, are obtained. No other terms were used for the simulation shown in Figure 2.5. thus, the ground state is a triplet with $|S_T, S^*\rangle = |1,2\rangle$ above which the excited states, in order of increasing energy are, $|0,1\rangle$, $|1,1\rangle$, $|2,2\rangle$, $|1,0\rangle$, $|2,1\rangle$ and $|3,2\rangle$ with the first excited state $|0,1\rangle$ only 8.4 cm^{-1} and the second excited state $|1,1\rangle$ 24.8 cm^{-1} above the $|1,2\rangle$ ground state. Such antiferromagnetic interactions in triangular Ni^{II}_3 complexes are not unprecedented.[10]

For an isosceles triangle of three spins of S = 1.0 the two antiferromagnetic exchange interactions J and J' compete with each other to determine the spin state energies as it is not possible for three spins to be aligned anti parallel to each other and thus the spin state energies become a function of the relative magnitudes of J and J', i.e., the J' / J. Ginsberg et.al.[13] have in a seminal paper pointed out for three S = 1.0 spin centers that if x = J' / J be less than 0.5 or greater than 2.0, the ground state is a triplet, $S_T = 1.0$. On the other hand, for $0.5 < x < 2$ the ground state is $|0,1\rangle$. The evaluated x (= J' / J) of 0.24 for **3** is in accord with the observed triplet ground state. We are aware of one very similar oxime bridged trinuclear Ni^{II}_3 complex[17e] in which the ratio of the evaluated exchange coupling constants was found to be x = J' / J = 0.53 for which hence a ground state of $|0,1\rangle$ is expected.

Table 2.4: Intratrimer magnetic parameters for homo-and heterotrinuclear complexes 1-3

Compounds	Magnetic core		J_{12} [cm^{-1}]	J_{13}[cm^{-1}]	J_{23}[cm^{-1}]	g_{Ni}	g_{Mn}	g_{Cr}
1	$Ni^{II}Mn^{III}Ni^{II}$	$J_{12} = J_{23}$	**- 3.18**			**2.05**	**1.97**	
2	$Ni^{II}Cr^{III}Ni^{II}$	$J_{12} = J_{23}$	**+ 0.6**	**- 0.9**		**2.00**		**1.95**
3	Ni^{II}_3	$J_{12} = J_{13}$	**- 8.2 ± 0.2**		**-2.0 ± 0.1**	**2.07**		

The evaluated exchange coupling constant J of - 8.2 cm^{-1} for **3** along the short edges Ni(1)/Ni(2) and Ni(1)/Ni(3), of the isosceles Ni(II) triangle does fall in the lower end of the range which has been observed for oximate bridge-Ni(II) complexes[1a]. This moderate coupling is consistent with its mediation by two types of oximate bridge, a single atom μ_3-O bridge and a two-atom N-O linkage, of which the later is expected to provide the main super-exchange σ-pathway along the short-edges of the triangle. A single-atom oximate μ_3-O bridges directly Ni(1) to each of Ni(2) and Ni(3) (O(49) and O(29), respectively) and thus increases the Ni(2)-μ_3-O (49) and Ni(3)-μ_3-O (29) bond lengths in comparison to those for oximate μ_2-O(O(9) and O(19)) and hence a diminution of the strength of antiferromagnetic exchange coupling is observed in a manner similar to protonation and metalaton of the μ_2-oxo bridge.[14] Additionally, a two-atom N-O-bridge along the short edges of the triangle links Ni(1) to Ni(2) and Ni(3) contributing mostly to the net coupling. Thus, the very weak coupling J' of – 2 cm^{-1} transmitted along the long edge of the Ni(II)-triangle is attributed to the μ_3-O nature of the oximate -O, O(49) and O(29).

It is pertinent at this point to mention that in a dinickel(II) complex containing only three two-atom N-O linkages, $[LNi(PyA)_3Ni]^+$ were L represents a tridentate amine 1,4,7-trimethyl-1,4,7-triazacyclononane, the J-value has been found to be – 32 cm^{-1}.[15]

By considering that in complex **3** there is only one, two-atom N-O bridge between Ni(1) and Ni(2) or Ni(3), the evaluated J-value of – 8.20cm^{-1} is in well accord with the expected value. The J and the J'-values for **3**, - 8.2 and - 2.0 cm^{-1} respectively, are similar than those in only other triangular Ni(II)-oximate complex,[17e] for which the corresponding coupling constants are - 14.4 and - 7.6 cm^{-1}. The significantly longer Ni-O bonds in complex **3** might account mostly for the weaker coupling in **3**. It must be pointed out that in the limit of weak interactions the exchange coupling constant is also sensitive to small angular changes or distortions, but to a lesser degree.

Exchange coupling parameters reported for $Ni^{II}Ni^{II}$, $Ni^{II}Mn^{III}$ and $Ni^{II}Cr^{III}$ complexes mediated through oximate (NO) ligands are summarized in the following Table 2.5.

Table 2.5: Magnetic parameters for exchange coupled oximate complexes

Compounds	Magnetic core	$J_{Ni(II)...Cr(III)}$ [cm^{-1}]	$J_{Ni(II)...Ni(II)}$ [cm^{-1}]	$J_{Ni(II)...Mn(III)}$ [cm^{-1}]	$g_{Mn(III)}$	$g_{Ni(II)}$	$g_{Cr(III)}$	Ref:
$[\{Ni(Dien)\}_2(\mu_3\text{-}OH)_2\{Ni_2(Moda)_4\}](ClO_4)_2$	$Ni^{II}Ni^{II}$		- 20.6			2.32		20b
$[Ni_3(Dtox)(Dtox\ H)_2](ClO_4)_2$	$Ni^{II}Ni^{II}$		- 14.4 ± 0.6 - 7.6 ± 1.1			2.17		17e
$[Ni_4(MeOH)_2(pko)_6](OH)(ClO_4)$	$Ni^{II}Ni^{II}$		- 24.1 - 7.25			2.2		20a
$[Ni_4(LH)_3](ClO_4)_2$	$Ni^{II}Ni^{II}$		- 13.4			2.00		17i
$K_4[Ni(H_2O)_6][Ni_8(HL)_{10}(H_2L)_2]$	$Ni^{II}Ni^{II}$		- 30.0			2.27		20e
$[(Me_3Tacn)Ni_2(PyA)_3](ClO_4)$	$Ni^{II}Ni^{II}$		- 33.6			2.16		15
$[(Me_3Tacn)Mn\{(dmg)_3Ni\}Mn(Me_3Tacn)](ClO_4)_2$	$Ni^{II}Mn^{III}$			- 5.3	1.98	1.98		9
$[Mn(5\text{-}R\text{-}saltmen)Ni(PyA)(bpy)_2]_2(ClO_4)_4$	$Ni^{II}Mn^{III}$			- 16.35	2.04	2.04		20c
$[(Me_3Tacn)MnNi(PyA)_3](ClO_4)$	$Ni^{II}Mn^{III}$			- 9.9 -14.7	1.99	2.17		15 20d
$[Mn_2(saltmen)Ni(PyA)_2(py)_2](ClO_4)_2$	$Ni^{II}Mn^{III}$							
$[(Me_3Tacn)CrNi(PyA)_3](ClO_4)_2$	$Ni^{II}Cr^{III}$	- 9.2				2.19	2.00	4b
$[(Me_3Tacn)CrNi\{P(PyA)\}_3](ClO_4)_2$	$Ni^{II}Cr^{III}$	0				2.16	1.98	4b
$[(Me_3Tacn)Cr\{(dmg)_3Ni\}Cr(Me_3Tacn)](ClO_4)_2$	$Ni^{II}Cr^{III}$	- 0.7				2.19	2.00	6

2.6 References:

(1) (a) P. Chaudhuri, *Coord. Chem. Rev.,* 2003, **243**, 143; (b)A. Chakravorty, *Coord. Chem. Rev.,* 1974, **13**, 1; (c) M. E. Keeney, K. Osseo-Ascrae and K. A. Woode. *Coord. Chem. Rev.,* 1984, **59**, 14 ; (d) V. Y. Kukushkin and A. J. L. Pombeiro, *Coord. Chem. Rev.,* 1999, **181**, 147; (e) A. G. Smith, P. A. Tasker and D. J. White, *Coord. Chem. Rev.,* 2003, **241**, 61

(2) (a) R. Beckett, R. Colton, B. F. Hoskins, R. L. Martin and D. J. Vince, *Aus. J. Chem.*, 1969, **22**, 2257; (b)D. Dutta and A. Chakravorty, *Inorg. Chem.*, 1983, **22**, 1611; (c) P. Basu, S. Pal and A. Chakravorty, *Inorg. Chem.*, 1988, **27**, 1850; (d) S. Ganguly, S. Karmakar, C. K. Pal and A. Chakravorty, *Inorg. Chem.*, 1999, **38**, 5984;

(e) H. Okawa, M. Koikawa, S. Kida, D. Luneau and H. Oshio, *J. Chem. Soc. Dalton Trans*., 1990, 469; (f) D. Luneau, H. Oshio, H. Okawa and S. Kida, *J. Chem. Soc. Dalton Trans*., 1990, 2282; (g) N. Kukita, M. Ohba, T. Shig, H. Okawa and Y. Ajiro, *J. Chem. Soc. Dalton Trans*., 2001, 64; (h) Y. Agnus, R. Louis, B. Metz, C. Boudin, J. P. Gisselbrecht and M. Gross, *Inorg. Chem.*, 1991, **30**, 3155; (i) R. Ruiz, M. Julve, J. Faus, F. Lloret, C. M. Munoz, Y. Journaoux and C. Bois, *Inorg. Chem.*, 1997, **36**, 3434; (j) D. Blaack, A. J. Blake, K. P. Dancey, A. Harrison, M. Mcpartlin, S. Parsons, P. A. Tasker, G. Whittaker and M. Schröder, *J. Chem. Soc. Dalton Trans*., 1998, 395; (k) P. Chaudhuri, M. Winter, P. Fleischhauer, W. Haase, U. Flörke, H.-J. Haupt, *J. Chem. Soc., Chem. Commun*. 1990, 1728; (l) P. Chaudhuri, M. Winter, B. P. C. D. Vedova, P. Fleischhauer, W. Hasse, U. Flörke, H-J. Haupt, *Inorg. Chem*., 1991, **30**, 4777; (m) D. Burdinsky, E. Bill, F. Birkelbach, K. Wieghardt and P.Chaudhuri, *Inorg. Chem*., 2001, **40**, 1160; (n) F. Birkelbach, M. Winter, U. Flörke, H-J. Haupt, C. Butzlaff, M. Lengen, E. Bill, A. X. Trautwein, K. Wieghardt and P.Chaudhuri, *Inorg. Chem*., 1994, **33**, 3990; (o) C. Krebs, M. Winter, T. Weyhermüller, E. Bill, K. Wieghardt and P. Chaudhuri. *J. Chem.Soc., Chem Commun.* 1995, 1913; (p) C. N. Verani, E. Rentschler, T. Weyhermüller, E. Bill and P. Chaudhuri, *J. Chem. Soc. Dalton Trans* 2000, 4263; (q) C. N. Verani, T. Weyhermüller, E. Rentschler, E. Bill and P. Chaudhuri, *J. Chem. Soc., Chem. Commun* 1998, 2475

(3) (a) O. Kahn, "*Molecular Magnetism*", VCH Weinheim, 1993; (b) *Molecular Magnetism : New Magnetic Materials*, ed. K. Itoh, M. Kinoshita, Gordon & Breach, Amstardam, The Netherlands, 2000; (c) G. Christou, D. Gatteschi, D. N. Hendrickson and R. Sessoli, *MRS Bull*. 2000, **25**, 66; (d) D. Gatteschi and R. Sessoli, *Angew. Chem. Int. Ed*., 2003, **42**, 268

(4) (a) S. Ross, T. Weyhermüller, E. Bill, E. Bothe, U. Flörke, K. Wieghardt and P. Chaudhuri, *Eur.J.Inorg.Chem*, 2004, 984; (b) S. Ross, T. Weyhermüller, E. Bill, K. Wieghardt and P. Chaudhuri, *Inorg. Chem.*, 2001, **40**, 6656

(5) (a) R. A. D. Wentworth, *Coord. Chem. Rev*., 1972/73, **9**, 171; (b) R. M. Kirchner, C. Meali, M. Bailey, N. Howe, L. P. Torre, L. J. Wilson, L.C. Andrews, N. J. Rose and E. C. Lingafelter, *Coord. Chem. Rev*., 1987, **77**, 89; (c) S. A. Kunow; K. J. Takeuchi, J. J. Grzybowski, A. J. Tireitano and V. L. Goedken, *Inorg.Chim. Acta*, 1996, **241**, 12

(6) D. Burdinsky, F. Birkelbach, T. Weyhermüller, U. Flörke, H-J. Haupt, M. Lengen, A. X. Trautwein, E. Bill, K. Wieghardt and P.Chaudhuri, *Inorg. Chem*., 1998, **37**, 1009

(7) "*Comprehensive Coordination Chemistry*", Ed. G. Wilkinson, Pergamon, England 1987, Vol. 4

(8) H. Aghalbozorg, G. J. Palenik, R. C. Stoufer and J. Summers, *Inorg. Chem*., 1982, **21**, 3903

(9) F. Birkelbach, U. Flörke, H-J. Haupt, C. Butzlaff, A. X. Trautwein, K. Wieghardt and P. Chaudhuri, *Inorg. Chem*., 1998, **37**, 2000

(10) (a) S. G. Sreerama and S.Pal, *Inorg. Chem*., 2002, **41**, 4843 ; (b) R. Clerac, H. Miyasaka, M. Yamashita and C. Coulon, *J. Am. Chem. Soc*., 2002, **124**, 12837; (c) H. Miyasaka, R. Clerac, K. Mijushima, K. Sugiura, M. Yamashita, W. Wernsdorfer and C. Coulon, *Inorg. Chem*., 2003, **42**, 8203; (d) C. J. Milios, E. Kefalloniti, C. P. Raptopoulou, A. Terzis, A. Escuer, R. Vincente and S. P. Perleples, *Polyhedron*, 2004, **23**, 83

(11) (a) S. Pal, T. Melton, R. Mukherjee, A. R. Chakravorty, M. Tomas, L. R. Falvello and A. Chakravorty, *Inorg. Chem*.,1985, **24**, 1250; (b) S. Pal, R. Mukherjee, M. Tomas, L. R. Falvello and A. Chakravorty, *Inorg. Chem*., 1986, **25**, 200; (c) V. Manivannan, S. Dutta, P. Basu and A. Chakravorty, *Inorg. Chem*., 1993, **32**, 4807

(12) (a) A. Escuer, R. Vincente, S. B. Kumar, X. Solans, M. Font-Bardia and A. Caneschi, *Inorg. Chem*., 1996, **35**, 3094; (b) A. Escuer, I. Castro, F. Mautner, M. S. El Fallah and R. Vincente, *Inorg. Chem*., 1997, **36**, 4633

(13) A. P. Ginsberg, R. L. Martin and R. C. Sherwood, *Inorg. Chem*., 1968, **7**, 392

(14) S. M. Gorun and S. J. Lippard, *Inorg. Chem*., 1991, **30**, 1625

(15) P. Chaudhuri and T. Weyhermüller, unpublished results.

(16) A. P. Ginsberg, *Inorg. Chim. Acta Rev.,*1971, **5**, 45

(17) Selected Examples: (a) M. S. Ma, R. J. Anjelici, D. Powell and R. A. Jacobson, *Inorg. Chem*., 1980, **19**, 3121; (b) P. Gouzeth, P. Jeanin, C. Rocchiaccioli-Deltcheff and F. Valentini, *J. Coord. Chem.,* 1979, **9**, 221; (c) R. Ruiz, J. Sanz, F. Lloret, M. Julve, J. Faus, C. Bois and M. Carmen-Munoz, *J. Chem. Soc. Dalton. Trans*., 1993, 3035; (d) E. Colacio, J. M. Dominguez-Vera, A. Escuer, R. Kivekas and A. Romerosa, *Inorg. Chem*., 1994, **33**, 3914; (e) V. V. Pavlischulk, S. V. Kolotilov, A. W. Addison, M. J. Prushan, R. J. Butcher and L. K. Thompson, *Inorg. Chem*., 1999, **38**, 1759; (f) P. Chaudhuri, M. Hess, E. Rentschler, T. Weyhermüller and U. Flörke, *New. J. Chem.*, 1998, **22**, 553; (g) H. Miyasaka, T. Nezu, F. Iwahori, S. Furukawa, K. Sugimoto, R. Clerac, K. Sugiura and M. Yamashita, *Inorg. Chem*., 2003, **42**, 4501; (h) Y. B. Jiang, H. Z. Kou, R-J. Wang, A. L. Cui and J. Ribas, *Inorg. Chem*. 2005, **44**, 709; (i) V.

Pavlischuk, F. Birkelbach, T. Weyhermüller, K.Wieghardt and P. Chaudhuri. *Inorg. Chem*., 2002, **41**, 4405

(18) (a) M. Orama, H. Saarinen and J. Korvenranta, *Acta Chem. Scand.Ser.A*, 1989, **43**, 717; (b) H. Saarinen and M. Orama, *Acta Chem. Scand*., 1998, **52**, 1209

(19) P. Chaudhuri, E. Rentschler, F. Birkelbach, C. Krebs, E. Bill, T. Weyhermüller and U. Flörke, *Eur. J. Inorg. Chem*., 2003, 541

(20) (a) M. Alexiou, C. Dendrinou-Samara, C. P. Raptopoulou, A. Terzis, V. Tangoulis and D. P. Kessisoglou, *Eur. J. Inorg. Chem*., 2004, 3822; (b) V. V. Pavlischuk, S. V. Kolotilov, A. W. Addison, M. J. Prushan, D. Schollmeyer, L. K. Thompson and E. A. Goreshnik, *Angew. Chem. Int. Ed*., 2001, **40**, 4734; (c) H. Miyasaka, T. Nezu, K. Sugimoto, K-i. Sugiura, M. Yamashita and R. Clerac, *Inorg. Chem*. 2004, **43**, 5486; (d) R. Clerac, H. Miyasaka, M. Yamashita, and C. Coulon, *J. Am. Chem. Soc*., 2002, **124**, 12837; (e) J. Fans, F. Lloret, M. Julve, J. M. Clemate-Juan, M. Munoz, X. Solans and M. Font-Bardia, *Angew. Chem. Int. Ed*., 1996, **35**, 1485

CHAPTER-3

MIXED-VALENCE LINEAR HOMO AND HETERO-TETRANUCLEAR $B^{III}Mn^{II}Mn^{II}B^{III}$, $Mn^{III}Mn^{II}Mn^{II}Mn^{III}$, $Mn^{IV}Mn^{II}Mn^{II}Mn^{IV}$, $Fe^{III}Mn^{II}Mn^{II}Fe^{III}$, $Cr^{III}Mn^{II}Mn^{II}Cr^{III}$ COMPLEXES : A MAGNETOSTRUCTURAL STUDY.

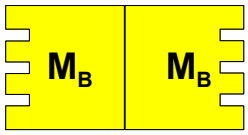

A Dinucleating Ligand Containing
Two Metal Centres

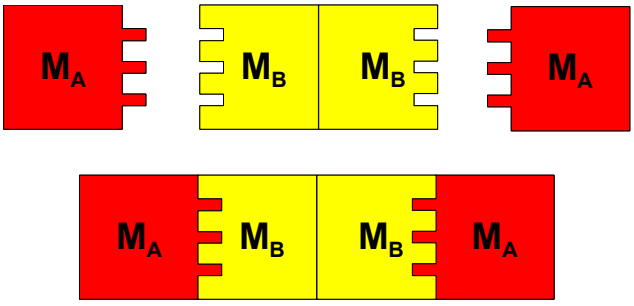

$M_AM_BM_BM_A$

3.1 Introduction:

This chapter presents homo and hetero-tetranuclear complexes. Synthetic methods to such species started with salen like ligands as binucleating agents, developed to acyclic dicompartmental macrocyclic ligands and finally flourished at the beginning of the 90's, with the baukasten or modular approach. Pathways to such complex molecular entities are based on step-by-step strategies. This provides an efficient means to control both nuclearity and dimensionality of the polymetallic systems. They are formed by two modules e.g. $[M(tmtacn)]^{n+}$ synthons, bridged by a coordinated oxime. The same features are valid for heterotetranuclear complexes. As a result the complexes formed follow the frames $[M_AM_AM_AM_A]$ and $[M_AM_BM_BM_A]$.

At present the study of exchange interaction between paramagnetic metal centers through various bridging ligands is an active research field in coordination chemistry with the aim of understanding fundamental factors governing the magnetic properties of transition metal compounds. Relatively few magnetic studies dealing with tetranuclear systems have been reported in contrast to the large number of studies dealing with tri- and bi-nuclear systems, primarily due to lack of fully structurally characterized compounds and to the increased complexity involved with the theoretical treatments of large spin systems. Most of the studies are concerned with homotetranuclear complexes, although a few have treated heterometallic systems. New exchange pathways can be expected for heteropolynuclear complexes,[1-12] where unusual sets of magnetic orbitals can be brought in close proximity; hence investigations of heteropolynuclear complexes might be more informative in comparison to those of homopolynuclear complexes.

As part of the investigation into the magnetostructural studies of the binucleating dioxime ligand 2,6-diformyl-4 methyl phenol dioxime (H_3dfmp), and various homo and heteropolynuclear complexes have been synthesized and designed to gain insight into magnetostructural studies. Formation of binuclear transition metal complexes with oxime ligands has been observed previously, notably with Cu^{II} and Ni^{II}. There have been relatively few reports dealing with the coordination chemistry of 2,6-diformyl-4 methyl phenol dioxime and its derivatives.[13-15, 23] In 1973 Okawa[13] et al., reported the reaction of 2,6-diformyl-4 methyl phenol with NH_2OH in the presence of $Cu(CH_3COO)_2.H_2O$ and $NiCl_2.6H_2O$ respectively. Recently Thompson[14] and co-workers have reported magnetochemical and structural data on related a nickel(II) oxime complex, Busch[15] and co-workers have prepared asymmetric iminooxime compartmental species, while Krebs et al., reported[4] magnetostructural study on heterometallic Fe_2Ni_2 cluster. But magnetostructural studies on manganese based systems have not been explored, which motivated us to design manganese based homo and heteropolynuclear complexes with an emphasis towards magnetostructural studies.

3.2 Synthesis:

This synthesis of the tetranuclear complexes involves five main steps. The first step is the synthesis of the macrocyclic amine 1,4,7-triazacyclononane(Tacn), it's derivative 1,4,7-trimethyl-1,4,7-triazacyclononane(Me_3Tacn) and the synthon $[M_A(Me_3Tacn)Cl_3]^0$ with the triamine facially coordinated and M_A = Fe(III), Mn(III), and Cr(III). These syntheses are well documented in the literature and therefore details are not given in this

work. The organic precursor H_3dfmp is synthesized as discussed previously and used for the synthesis of the dinuclear precursors $[(M_A)_2(dfmp)_3]^{5-}$ and $[(M_B)_2(dfmp)_3]^{5-}$ and finally the $M_AM_AM_AM_A$ and $M_AM_BM_BM_A$ complexes are synthesized.

A general schematic diagramme is given below:

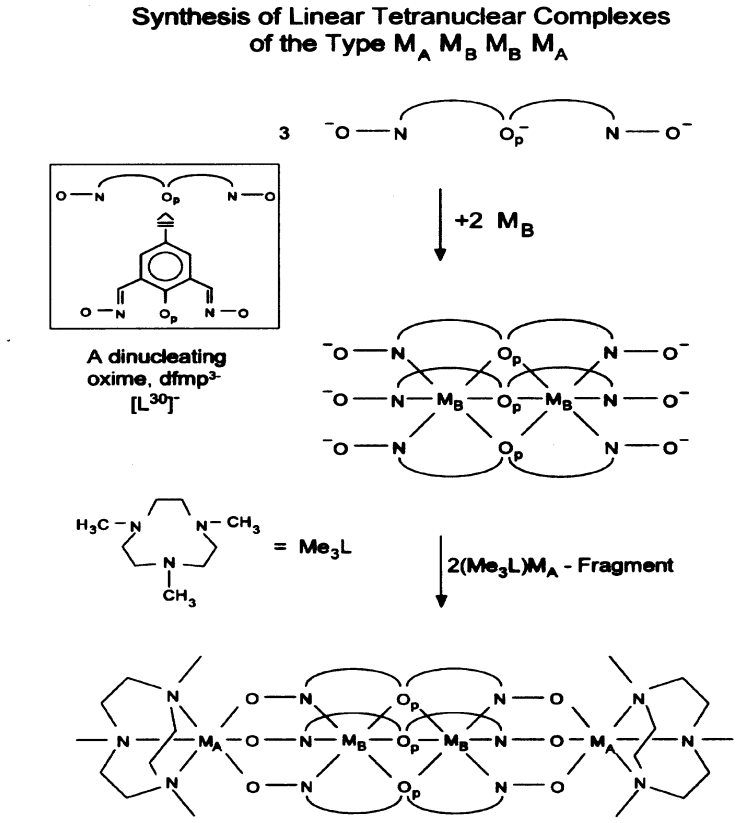

Figure 3.1: Schematic diagram for the synthesis of linear tetranuclear complexes

3.2A Linear homo and hetero-tetranuclear complexes:

The following complexes were synthesized and characterized:

4. **$[(MeB)_2Mn^{II}_2(dfmp)_3](Et_3NH)$** where MeB came from methylboronic acid[$MeB(OH)_2$].

5. **$[(Me_3Tacn)_2\ Mn^{III}_2Mn^{II}_2(dfmp)_3](ClO_4)$**

6. **$[(Me_3Tacn)_2\ Mn^{IV}_2Mn^{II}_2(dfmp)_3](ClO_4)_3$**

7. **$[(Me_3Tacn)_2\ Fe^{III}_2Mn^{II}_2(dfmp)_3](ClO_4)$**

8. **$[(Me_3Tacn)_2\ Cr^{III}_2Mn^{II}_2(dfmp)_3](ClO_4)$**

and will be identified in the following section by their metallic cores, namely **$B^{III}Mn^{II}Mn^{II}B^{III}$(4)**, **$Mn^{III}Mn^{II}Mn^{II}Mn^{III}$(5)**, **$Mn^{IV}Mn^{II}Mn^{II}Mn^{IV}$(6)**, **$Fe^{III}Mn^{II}Mn^{II}Fe^{III}$(7)** and **$Cr^{III}Mn^{II}Mn^{II}Cr^{III}$(8)**

This family of complexes illustrates how two simple tools such as the metal to phenol dioximate molar ratio and the coordination properties of the terminal coligand allow the synthetic chemist to design a great diversity of nuclearity tailored polynuclear species. Each of these compounds was characterized by IR spectroscopy and elemental analysis (C, H, N, metals). Mössbauer spectroscopy and temperature dependent magnetic behavior were studied and the complexes were also characterized by crystallographic techniques.

3.3 Infrared and Mass Spectroscopy:

The band in the IR spectra of the complex **4** at 2950 cm^{-1} corresponds to the C-H stretching of the Et_3NH group which present as a counteraction in the $B^{III}Mn^{II}Mn^{II}B^{III}$ core. A moderately intense C=N stretching band for the ligand was observed at 1608 cm^{-1}. Notable features are the sharp NO stretching bands at 1109, 1066 cm^{-1}.

Complexes **5**, **6, 7** and **8** also show C=N stretching bands for the ligand at 1608 cm^{-1}. Strong peaks at 2918-2920 cm^{-1} correspond to the C-H stretching mode of the Me_3Tacn group present as the terminal ligand in the $Mn^{III}Mn^{II}Mn^{II}Mn^{III}$, $Mn^{IV}Mn^{II}Mn^{II}Mn^{IV}$, $Fe^{III}Mn^{II}Mn^{II}Fe^{III}$, $Cr^{III}Mn^{II}Mn^{II}Cr^{III}$ core congeners. The NO stretching bands for all the linear tetranuclear complexes are observed at 1120, 1109 and1079 cm^{-1}. Strong bands at 1080 and 624 cm^{-1} corresponds to the ClO_4 unit which is the counteranion in all four linear tetranuclear complexes. Though it is not possible to distinguish the stretching frequencies for NO and ClO_4 around 1080 cm^{-1} but the peak at 624 cm^{-1} confirms the presence of ClO_4 group.

Electrospray-ioniziation mass spectrometry (ESI-MS) in the negative ion mode has been proved to be very successful in characterizing $B^{III}Mn^{II}Mn^{II}B^{III}$ which shows the mononegatively charged species $[M\text{-}Et_3NH]^-$ as the base peak. On the other hand, electrospray-ioniziation mass spectrometry (ESI-MS) in the positive ion mode is successful in characterizing $Mn^{III}Mn^{II}Mn^{II}Mn^{III}$ (**5**), $Fe^{III}Mn^{II}Mn^{II}Fe^{III}$ (**7**) and $Cr^{III}Mn^{II}Mn^{II}Cr^{III}$ (**8**) which show monopositively charged species $[M\text{-}ClO_4]^+$ as the base peaks, on the contrary the signal for $[M\text{-}3ClO_4]^{3+}$ of **6** is not found, but the base peak for the fragment $[M\text{-}2ClO_4]^{2+}$ was observed.

3.4 Solid state Structure

3.4.1 Solid-State Molecular Structure of $[(MeB)_2Mn^{II}_2(dfmp)_3](Et_3NH) \cdot C_2H_5OH$ (4)

The lattice consists of discrete tetranuclear monoanions, triethylammonium cations and ethanol molecules of crystallization. The X-ray structure clearly illustrates the formation of the cage ligand. The X-ray structure confirms that a linear (180°) tetranuclear complex has indeed been formed in such a way that each transition metal ion shows octahedral geometry with two terminal B(III) ions and two Mn(II) as the central ions are present in the lattice. The central tris(oximato)dimanganese(II) ion, $[Mn_2(dfmp)_3]^{5-}$, bridges two terminal B(III) centers through the deprotonated oxime oxygen atoms. All phenoxy oxygen atoms are μ_2-bridging yielding the Mn(2).....Mn(3) separation of 2.909 Å.

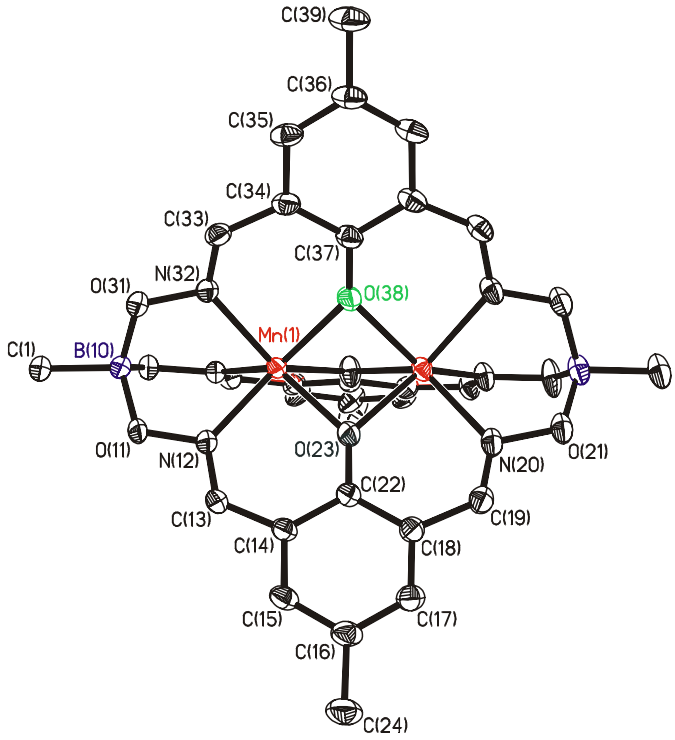

Figure 3.2: ORTEP and labeling scheme for $B^{III}Mn^{II}Mn^{II}B^{III}$ (4)

The terminal B(III) ions, B(1) and B(4) have distorted tetrahedral geometry and are bonded to one carbon atom from the methyl group and three oxygen atoms from the bridging oximate oxygen groups. The B-O bond length is 1.50Å. An intramolecular B(1).....B(4) separation of 8.864 Å has been found. The phenolate oxygen atoms O (23),

O (38) , O (23) of three ligand sets $dfmp^{3-}$, bridge two central manganese ions, Mn(2) and Mn(3) giving rise to a face sharing bioctahedral core structure. The coordination geometry around Mn(2) and Mn(3) are strongly trigonally distorted. Selected bond lengths and angles of the $B(O\text{-}N)_3$ $Mn(\mu_2\text{-}O)_3$ $Mn(N\text{-}O)_3B$ core in **4** are given in Table3.1. The Mn-O and Mn-N bond lengths for both manganese sites are not significantly different (average 2.127 Å and 2.174 Å respectively), indicating the equivalency of the sites. The three Mn(2)-O-Mn(3) bond angles are 86.67°, 86.04°, and 86.04°.

Table 3.1: *Selected Bond Lengths (Å) and Angles (deg)* for ***[(MeB)$_2$Mn$^{II}_2$(dfmp)$_3$](Et$_3$NH)*** **(4)**

Mn(2)•••Mn(3)	2.909(5)	B(1)•••B(4)	8.664
Mn(2)-O(38)	2.119(2)	Mn(2)-O(23)-Mn(3)	86.03(6)
Mn(2)-O(23)≠1	2.122(2)	Mn(2)-O(23)-Mn(3)≠1	86.03(6)
Mn(2)-O(23)	2.142(2)	Mn(2)-O(38)-Mn(3)	86.68(8)
Mn(2)-N(32)	2.173(2)		
Mn(2)-N(12)	2.174(2)		
Mn(2)-N(20)≠1	2.175(2)		

3.4.2 Solid-State Molecular Structure of [(Me$_3$Tacn)$_2$ Mn$^{III}_2$Mn$^{II}_2$(dfmp)$_3$](ClO$_4$) •CH$_3$CN • C$_2$H$_5$OH (5)

The molecular geometry and atom labeling scheme of the trication in **5** are shown in Figure 3.3. The structure of the complex molecule consists of a discrete monocationic tetranuclear unit, one perchlorate anion with a molecule of acetonitrile and methanol as solvents of crystallization. Selected bond lengths and angles are listed in Table 3.2. The X-ray structure confirms that a linear (178°) tetranuclear complex has indeed been formed in such a way that a tetrapseudooctaheral geometry containing four metal atoms, two terminal Mn(III) and two Mn(II) as the central atoms are present in the lattice. The central tris(oximato)dimanganese(II) ion, $[Mn_2(dfmp)_3]^{5-}$, bridges two terminal Mn(III) centers through the deprotonated oxime oxygen atoms. All phenoxy oxygen atoms are μ_2-bridging yielding a Mn(2).....Mn(3) separation of 3.043 Å. The terminal Mn(III) ions, Mn(1) and Mn(4), are in distorted octahedral geometry with three nitrogen atoms form

the facially coordinated tridentate macrocyclic amine and three oxygen atoms from the bridging oxygen groups. The terminal Mn-O (average 1.944 Å) and the terminal Mn-N (average 2.19 Å) bond lengths are consistent with those of implying a d^4 high spin electronic configuration of the terminal Mn(III) centers, Mn(1) and Mn(4). The N(7)-Mn(1)-O(8) bond defines an elongated Jahn-Teller axis of a high-spin d^4 ion in a distorted octahedral ligand field. The average N-Mn-N angle is 85.2°, whereas O-Mn-O angle is 98.46°. The Mn(1).....Mn(4) separation of 10.129 Å has been found.

The phenolate oxygen atoms O (53), O (73) , O (93) of the three $dfmp^{3-}$ ligands bridge the two central manganese ions, Mn(2) and Mn(3) giving rise to a face sharing bioctahedral core structure. The metrical details of the $N_3Mn(\mu_2\text{-}O)_3MnN_3$ core in the central part of **5** are briefly discussed in the following Table 3.2. The average Mn-N and Mn-O bond distances are 2.218 Å and 2.183 Å respectively, correspond nicely to those reported earlier. The coordination geometry of Mn(2) and Mn(3) are strongly trigonally distorted. The bond lengths are in agreement with the high spin Mn(II) description of the central Mn(2) and Mn(3) atoms. The three Mn(2)-O-Mn(3) bond angles are 88.1°, 88.3°, and 88.7°. The three dioxime molecules are nearly planar. The dihedral angles between the different planes comprising Mn^{III}-O-N-Mn^{II} atoms lie in the ranges 29.95-34.07°

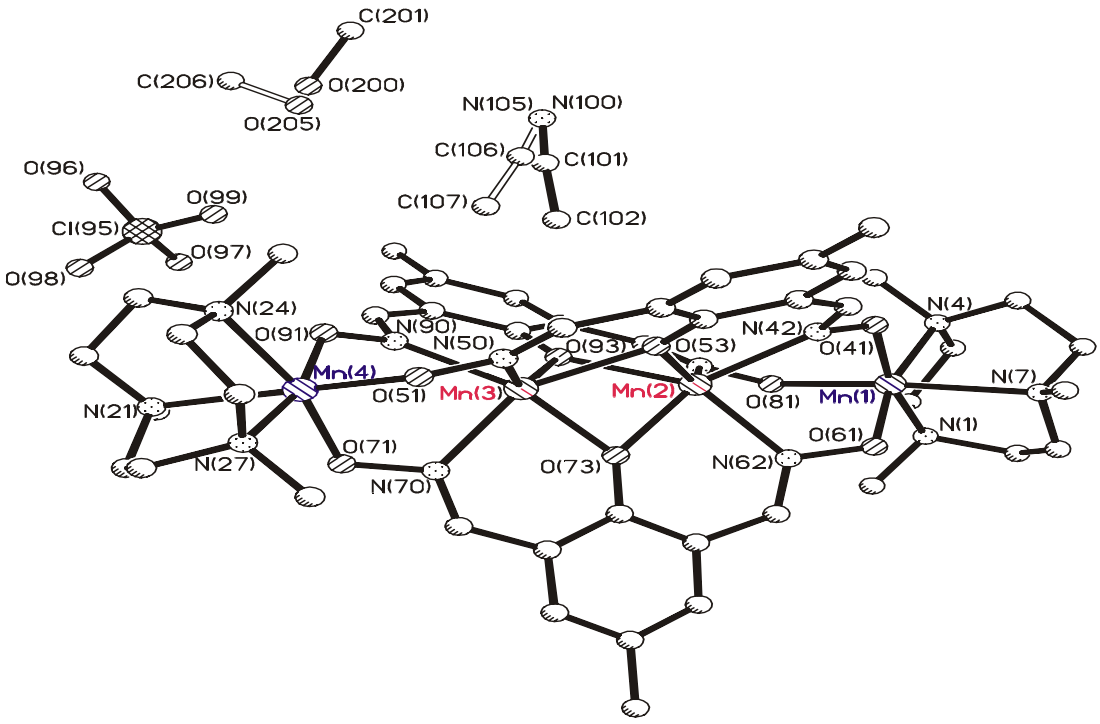

Figure 3.3: ORTEP and labeling scheme for $Mn^{III}Mn^{II}Mn^{II}Mn^{III}$ (5)

Table 3.2: *Selected Bond Lengths (Å) and Angles (deg) for* **[$(Me_3Tacn)Mn^{III}\{(dfmp)_3Mn^{II}Mn^{II}\}Mn^{III}(Me_3Tacn)](ClO_4) \cdot CH_3CN \cdot CH_3OH$ 5**

Mn(1)•••Mn(2)	3.541	Mn(2)•••Mn(3)	3.043(3)
Mn(3)•••Mn(4)	3.547	Mn(1)•••Mn(4)	10.129
Mn(1)-N(1)	2.134(7)	Mn(4)-N(21)	2.248(9)
Mn(1)-N(4)	2.119(8)	Mn(4)-N(24)	2.229(8)
Mn(1)-N(7)	2.315(8)	Mn(4)-N(27)	2.121(8)
Mn(1)-O(41)	1.888(6)	Mn(4)-O(51)	1.976(7)
Mn(1)-O(61)	1.894(6)	Mn(4)-O(71)	1.977(7)
Mn(1)-O(81)	2.063(7)	Mn(4)-O(91)	1.866(7)
Mn(2)-N(42)	2.214(8)	Mn(3)-N(50)	2.225(8)
Mn(2)-N(62)	2.231(8)	Mn(3)-N(70)	2.23(8)
Mn(2)-N(82)	2.196(8)	Mn(3)-N(90)	2.214(8)
Mn(2)-O(73)	2.20(6)	Mn(3)-O(73)	2.17(6)
Mn(2)-O(93)	2.176(6)	Mn(2)-O(93)	2.176(6)
		Mn(2)-O(53)-Mn(3)	88.1(2)
		Mn(2)-O(73)-Mn(3)	88.3(2)
		Mn(2)-O(93)-Mn(3)	88.7(2)

3.4.3 Solid-State Molecular Structure of $[(Me_3Tacn)_2 Mn^{IV}_2Mn^{II}_2(dfmp)_3](ClO_4)_3 \cdot 0.5\ CH_3CN \bullet 1.5\ H_2O$ (6)

The molecular geometry and atom labeling scheme of the trication in **6** are shown in Figure 3.4. The structure of the molecule consists of a discrete tricationic tetranuclear unit, three perchlorate anions, 0.5 of the acetonitrile and 1.5 of water molecules as solvent of crystallisation. Selected bond lengths and angles are listed in Table3.3. The X-ray structure confirms that a linear 179° tetranuclear complex has indeed been formed and similar with complex **5**. The central tris(oximato)dimanganese(II) ion, $[Mn_2(dfmp)_3]^{5-}$, bridges two terminal Mn(IV) centers through the deprotonated oxime oxygen atoms. All phenoxy oxygen atoms are μ_2-bridging yielding the Mn(2).....Mn(3) separation of 2.947 Å. The terminal Mn(IV) ions, Mn(1) and Mn(4), are in distorted octahedral geometry with three nitrogen atoms form the facially coordinated tridentate macrocyclic amine and three oxygen atoms from the bridging oximate oxygen groups. The terminal Mn-O

(average 1.848 Å) and the terminal Mn-N (average 2.09 Å) bond lengths are consistent with d^3 high spin electronic configuration of the terminal Mn(IV) centers, Mn(1) and Mn(4). The N-Mn-N angle is 83.39°, whereas O-Mn-O angles fall between 98.49°. An intramolecular Mn(1).....Mn(4) separation of 10.023 Å has been found.

The metrical details of the $N_3Mn(\mu_2\text{-}O)_3MnN_3$ core in the central part of **6** is similar to that of **4** and **5** and briefly discussed previously, so refraining from further elaboration. The three Mn(2)-O-Mn(3) bond angles are 86.49°, 86.54°, and 86.14°. The three dioxime molecules are nearly planar. The dihedral angles between the different planes comprising Mn^{IV}-O-N-Mn^{II} atoms lie in the ranges 20.8-39.8°

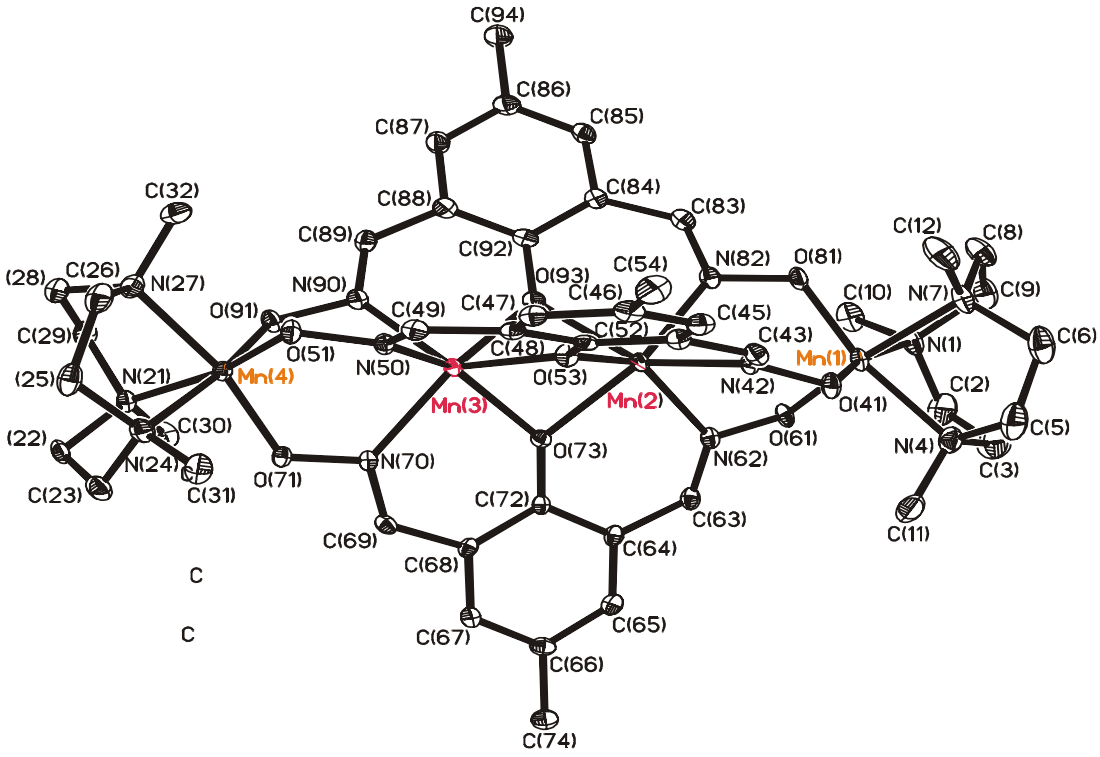

Figure 3.4: ORTEP and labeling scheme for $Mn^{IV}Mn^{II}Mn^{II}Mn^{IV}$ (6)

Table 3.3: *Selected Bond Distances (Å) and Angles (deg) for* **$[(Me_3Tacn)Mn^{IV}\{(dfmp)_3Mn^{II}Mn^{II}\}Mn^{IV}(Me_3Tacn)](ClO_4)_3$. 0.5 CH_3CN. 1.5H_2O 6**

Mn(1)•••Mn(2)	3.538	Mn(2)•••Mn(3)	2.947(10)
Mn(3)•••Mn(4)	3.537	Mn(1)•••Mn(4)	10.023
Mn(1)-N(1)	2.092(4)	Mn(4)-N(21)	2.090(4)
Mn(1)-N(4)	2.096(5)	Mn(4)-N(24)	2.087(4)
Mn(1)-N(7)	2.084(4)	Mn(4)-N(27)	2.093(4)

Mn(1)-O(41)	1.847(3)	Mn(4)-O(51)	1.837(3)
Mn(1)-O(61)	1.857(4)	Mn(4)-O(71)	1.846(3)
Mn(1)-O(81)	1.841(4)	Mn(4)-O(91)	1.862(3)
Mn(2)-N(42)	2.191(4)	Mn(3)-N(50)	2.202(4)
Mn(2)-N(62)	2.192(4)	Mn(3)-N(70)	2.204(4)
Mn(2)-N(82)	2.20(4)	Mn(3)-N(90)	2.188(4)
Mn(2)-O(53)	2.156(3)	Mn(3)-O(53)	2.146(3)
Mn(2)-O(73)	2.158(3)	Mn(3)-O(73)	2.142(3)
Mn(2)-O(93)	2.141(3)	Mn(2)-O(93)	2.175(3)
		Mn(2)-O(53)-Mn(3)	86.49(12)
		Mn(2)-O(73)-Mn(3)	86.54(12)
		Mn(2)-O(93)-Mn(3)	86.14(12)

3.4.4 Solid-State Molecular Structure of $[(Me_3Tacn)_2\ Fe^{III}_2Mn^{II}_2(dfmp)_3](ClO_4) \bullet 0.5\ CH_2Cl_2 \bullet CH_3CN$ (7)

The molecular geometry and atom labeling scheme of the trication in **7** is shown in Figure 3.5. The structure of the molecule consists of a discrete monocationic tetranuclear unit, one perchlorate anions, 0.5 of the dichloromethane and one acetonitrile molecules as solvent of crystallization. Selected bond lengths and angles are listed in Table 3.4. The X-ray structure confirms that a linear 179° tetranuclear complex has been formed and similar with complexes **5** and **6**, except two terminal Fe(III) ions instead of terminal Mn(III) or Mn(IV) ions. The central tris(oximato)dimanganese(II) ion, $[Mn_2(dfmp)_3]^{5-}$, bridges two terminal Fe(III) centers through the deprotonated oxime oxygen atoms. All phenoxy oxygen atoms are μ_2-bridging yielding the Mn(2).....Mn(3) separation of 3.029 Å. The terminal Fe(III) ions, Fe(1) and Fe(4), are in distorted octahedral geometry with three nitrogen atoms form the facially coordinated tridentate macrocyclic amine and three oxygen atoms from the bridging oxygen atoms. The terminal Fe-O (average 1.925 Å) and the terminal Fe-N (average 2.231 Å) bond lengths are consistent with d^5 high spin electronic configuration of the terminal Fe(III) centers, Fe(1) and Fe(4). The average N-Fe-N angle is average 78.93°, whereas average O-Fe-O angle is 98.89°. An intramolecular Fe(1).....Fe(4) separation of 10.034 Å has been found.

The central $N_3Mn(\mu_2\text{-}O)_3MnN_3$ core in the **7** is similar with complexes **4**, **5** and **6.** Selected bond lengths and angles are shown in Table 3.4. The three Mn(2)-O-Mn(3) bond

angles are 87.92°, 88.12°, and 87.82°. The three dioxime molecules are nearly planar. The dihedral angles between the different planes comprising Fe^{III}-O-N-Mn^{II} atoms lie in the ranges 29.02-33.98°

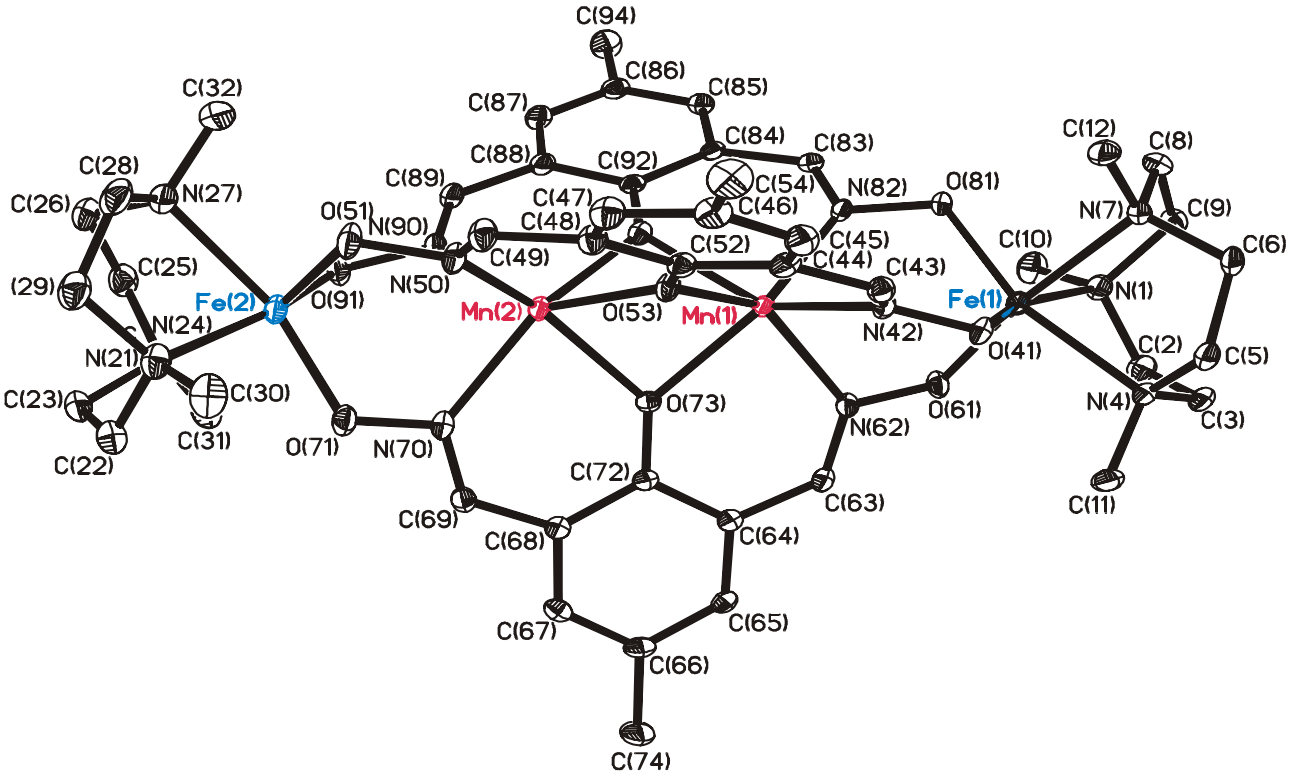

Figure 3.5: ORTEP and labeling scheme for $Fe^{III}Mn^{II}Mn^{II}Fe^{III}$ (7)

Table 3.4: *Selected Bond Lengths (Å) and Angles (deg)* for **$[(Me_3Tacn)Fe^{III}\{(dfmp)_3Mn^{II}Mn^{II}\}Fe^{III}(Me_3Tacn)](ClO_4)\ .0.5CH_2Cl_2\ .\ 1CH_3CN$ 7**

Fe(1)•••Mn(2)	3.507	Mn(2)•••Mn(3)	3.029(5)
Mn(3)•••Fe(4)	3.498	Fe(1)•••Fe(4)	10.034
Fe(1)-N(1)	2.239(3)	Fe(4)-N(21)	2.226(2)
Fe(1)-N(4)	2.232(2)	Fe(4)-N(24)	2.234(3)
Fe(1)-N(7)	2.226(2)	Fe(4)-N(27)	2.230(3)
Fe(1)-O(41)	1.938(2)	Fe(4)-O(51)	1.907(2)
Fe(1)-O(61)	1.935(2)	Fe(4)-O(71)	1.927(2)
Fe(1)-O(81)	1,917(2)	Fe(4)-O(91)	1.923(2)

Mn(2)-N(42)	2.228(2)	Mn(3)-N(50)	2.206(2)
Mn(2)-N(62)	2.245(2)	Mn(3)-N(70)	2.224(2)
Mn(2)-N(82)	2.192(2)	Mn(3)-N(90)	2.229(2)
Mn(2)-O(53)	2.170(2)	Mn(3)-O(53)	2.193(2)
Mn(2)-O(73)	2.179(2)	Mn(3)-O(73)	2.177(2)
Mn(2)-O(93)	2.194(2)	Mn(2)-O(93)	2.174(2)
		Mn(2)-O(53)-Mn(3)	87.92(7)
		Mn(2)-O(73)-Mn(3)	88.12(7)
		Mn(2)-O(93)-Mn(3)	87.82(7)

3. 5 Mössbauer spectroscopy:

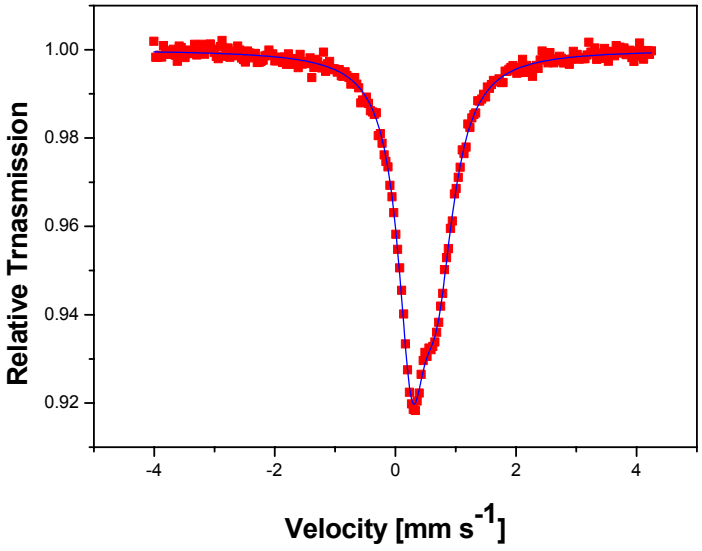

Figure 3.6 : Mössbauer spectrum of $Fe^{III}Mn^{II}Mn^{II}Fe^{III}$ (7)

The +3 oxidation state and the high spin electronic configuration of the iron centers in complex **7** are confirmed by a Mössbauer spectrum recorded at 80 K and zero field. The isomer shift (δ) and quadrupole splitting (E_Q) obtained are 0.48 mms^{-1} and 0.42 mms^{-1} respectively. The isomer shift δ_{Fe} around 0.5 mms^{-1} is of the magnitude expected for the high spin ferric state and is close to the values reported for similar compounds.[8,17]

3.6 Electrochemistry:

Cyclic voltamograms of complexes **4** and **5** were recorded in CH_3CN solution containing 0.1 M nBu_4PF_6 in the potential range -2.25 to +1.25 V vs. Fc^+/Fc. The CV of **4** afforded one 2e reversible oxidation process at nearly same potential of 0.55V vs. Fc^+/Fc, which is shown in Figure 3.7. The oxidation is metal centred and represents the Mn^{II}/Mn^{III} couple of both central Mn(II) ions.

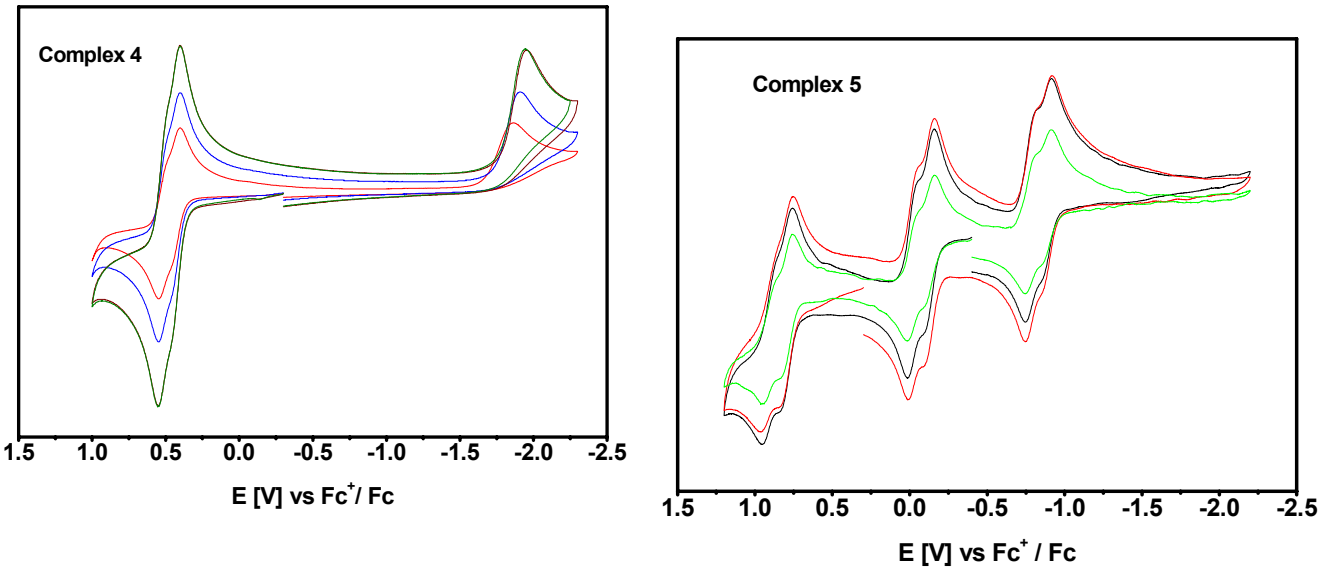

Figure 3.7: Cyclic Voltammogram for $B^{III}Mn^{II}Mn^{II}B^{III}$ (4) and $Mn^{III}Mn^{II}Mn^{II}Mn^{III}$ (5)

The CV of complex **5** afforded two consecutive reversible 2e oxidation processes in the potential range 0.0V and 1.0 V vs. Fc^+/Fc respectively and one 2e reversible reduction at - 0.75V vs. Fc^+/Fc. The first pair of oxidation may be assigned to a Mn^{III}/Mn^{IV} couple and the unambiguous evidence for this is the isolation of complex **6** in aerobic conditions where the terminal manganese centers are at the +4 oxidation state compared to the +3 oxidation state of complex **5**. The very similar oxidation potential for Mn^{III}/Mn^{IV} indicates very negligible electrostatic interaction. The second pair of oxidations can be assigned to the central ions and it reflects that in aerobic conditions this process is highly unfavourable due to the high oxidation potential. So the oxidation processes can be expressed as:

$$Mn^{III}Mn^{II}Mn^{II}Mn^{III} \overset{Ox_1}{\rightleftharpoons} Mn^{IV}Mn^{II}Mn^{II}Mn^{IV} \overset{Ox_2}{\rightleftharpoons} Mn^{IV}Mn^{III}Mn^{III}Mn^{IV}$$

Analysis of cyclic voltammograms in the more negative potential range (- 0.75V) with varying scan rates revealed one 2e reduction step attributable to the following equilibria:

$$Mn^{III}Mn^{II}Mn^{II}Mn^{III} \overset{Red_1}{\rightleftharpoons} Mn^{II}Mn^{II}Mn^{II}Mn^{II}$$

All attempts to isolate the mixed valence complex of the form $Mn^{IV}Mn^{II}Mn^{II}Mn^{III}$ proved to be unsuccessful. The comproportionation constant K_c for the equilibrium

$$Mn^{III}Mn^{II}Mn^{II}Mn^{III} + Mn^{IV}Mn^{II}Mn^{II}Mn^{IV} \overset{K_c}{\rightleftharpoons} 2\ Mn^{IV}Mn^{II}Mn^{II}Mn^{III}$$

is calculated to be 22, which is too low for the isolation of the mixed valence species.

3.7 Magnetic Properties:

Magnetic susceptibility data for polycrystalline samples of the complexes were collected in the temperature range 2-290 K in an applied magnetic field of 1T in order to characterize the sign and magnitude of the magnetic exchange interaction in the modular homo and hetero-tetranuclear systems. The analysis of the magnetic data was performed using the Heisenberg-Dirac-Van Vleck (HDVV) model. The least squares fitting computer programme JULIUS-F with a full matrix diagonalization approach was employed to fit the temperature and field dependent magnetization. The programme uses the spin -Hamiltonian operator, $H_{total} = H_z + H_{zfs} + H_{HDVV,}$ where the exchange coupling is described by $H_{HDVV} = -2JS_{1.}S_2$, the Zeeman interactions are given by $H_z = \mu_B B g_i S_i$ and the axial single ion zero field splitting interaction is described by $H_{zfs} = DS_z^2$. Here we use the Heisenberg spin Hamiltonian in the form, $H = -2JS_1S_2$ for an isotropic exchange coupling with $S_1 = S_2 = S_{Mn\ (II)} = 5/2$ in case of complex **4** and a "two J" model was applied to analyze the magnetic properties of this linear tetranuclear complexes and $E = -2J(S_1S_2 + S_3S_4) - 2J'S_2S_3$ are employed where $J = J_{12} = J_{34}$ and $J' = J_{23}$ for **5**, **6**,**7** and **8**.

In the model, $J = J_{12} = J_{34}$ represents the exchange coupling between adjacent metal ions i.e., the terminal manganese and the central divalent manganese ions in case of complexes **5** and **6**, terminal iron and the central divalent manganese ions for complex **7** and terminal chromium and the central divalent manganese ions for complex **8**, where as $J' = J_{23}$ describes the interaction between the central manganese nuclei within the linear tetranuclear complex. Table 3.5 summarizes the intratetramer exchange parameters.

The experimental effective magnetic moments (μ_{eff}) versus temperature (T) are displayed in Figures 3.8 and 3.10. The magnetic moment per molecule of B_2Mn_2 (**4**) at 290 K is 7.12 μ_B (χ_M•T = 6.35 $cm^3.K.mol^{-1}$) and decreases monotonically with decreasing temperature until it reaches 5.11 μ_B (χ_M•T = 3.27 $cm^3.K.mol^{-1}$) at 90 K and then starts to decrease further but rapidly and reaches a value of 0.74 μ_B at 2 K.

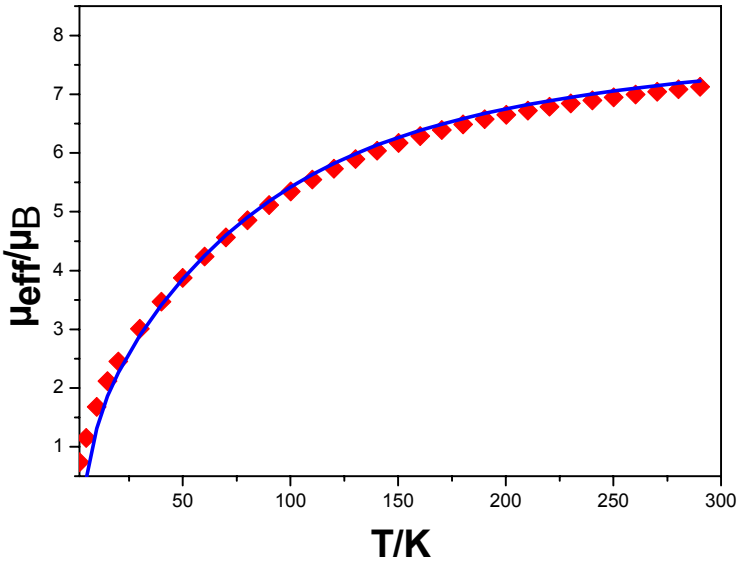

Figure 3.8: Magnetic data for $B^{III}Mn^{II}Mn^{II}B^{III}$ (4) as a plot of μ_{eff} vs. T. The bold points represent the experimental data while the solid line represents the simulation

This temperature dependence magnetic moment is in agreement with antiferromagnetic coupling between the neighbouring Mn(II) centers, resulting in a diamagnetic $S_T = 0$ ground state for **4**. A simulation shown as a solid line in Figure 3.8 results in J = -8.4 cm^{-1}, g_{Mn} = 1.98. The observed antiferromagnetic coupling agrees well with the comparable exchange coupling constant reported earlier.[24-26] The exchange coupling constant J between the manganese ions where exchange coupling is mediated through μ_2-phenoxo group will be used in deriving the exchange interaction parameters for the complexes **5-8**.

The magnetic behaviour of $Mn^{III}_2Mn^{II}_2$ (**5**) in the form of the effective magnetic moments (μ_{eff}) versus temperature (T) is displayed in Figure 3.10a. The magnetic moment of 9.41 μ_B (χ_M•T = 11.07 $cm^3.K.mol^{-1}$) at 290 K decreases monotonically with decreasing temperature and until it reaches a value of 7.3 μ_B (χ_M•T = 6.65 $cm^3.K.mol^{-1}$)

at 40 K and then starts to decrease further but rapidly and reaches a value of 2.51 μ_B at 2K. This temperature dependence magnetic moment is in agreement with antiferromagnetic coupling.

To analyze the magnetic data at the beginning the model for a linear tetranuclear complex with two terminal species $S_1 = S_4 = S_{Mn(III)} = 2$ and two central spins $S_2 = S_3 = S_{Mn(II)} = 5/2$ were considered, as depicted in the following coupling scheme. The parameter set, $g_1 = g_4 = g_{Mn(III)} = 1.85$ and $g_2 = g_3 = g_{Mn(II)} = 2.0$ and $J_{12} = +2.8$ cm^{-1} and $J_{23} = -8.2$ cm^{-1}(comparable with the coupling constant obtained from the complex **4**) were obtained from the best simulation. The agreement between the calculated magnetic moments is good as is evident from Figure 3.10a. The complex exhibit extremely complicated low-lying structure with a non diamagnetic ground state which is not well separated from the upper-lying states, is in full conformity with the non zero magnetic moment at 2 K. The fit parameters were also checked by the 2D-contour plot (Figure 3.9a) of the exchange coupling constants and the global minima observed in the plot of J_{12} and J_{23} show the value of J_{12} is undefined in the ferromagnetic scale and $J_{23} = -8.0$ cm^{-1} is also quite satisfactory.

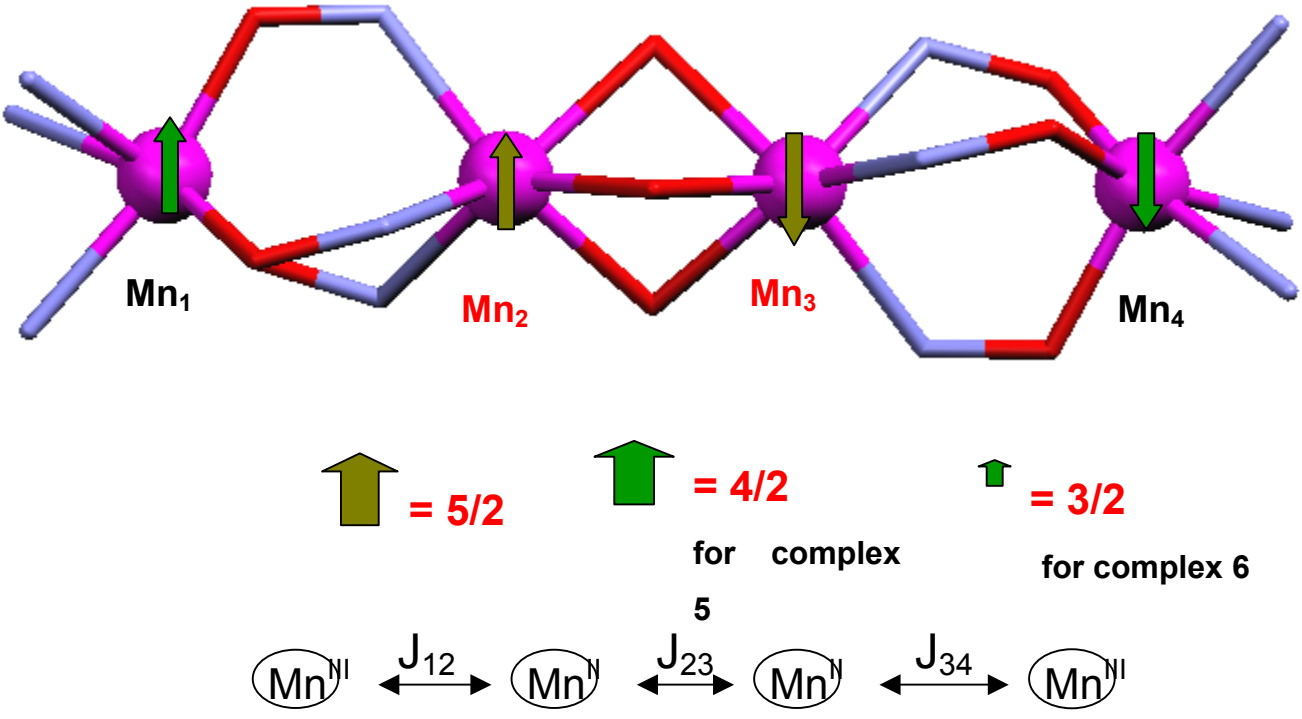

Scheme 1: Representation of the coupling scheme in complexes 5 and 6.

Exchange interaction between neighbouring manganese (III) and (II) ions for nioximate, glyoximate and also acetophenoximate complexes were reported[18-20] to be weak ferromagnetic (J~ +2 to +5 cm^{-1}) in nature.

The magnetic behaviour of $Mn^{IV}_2Mn^{II}_2$ (**6**) is shown in Figure 3.10a in the form of the effective magnetic moments (μ_{eff}) versus temperature (T). The magnetic moment of 10.37 μ_B ($\chi_M \bullet T$ = 13.43 $cm^3.K.mol^{-1}$) at 290 K decreases monotonically with decreasing temperature and reaches a value of 3.12 μ_B ($\chi_M \bullet T$ = 1.22 $cm^3.K.mol^{-1}$) at 2 K. The experimental magnetic data were simulated using a least squares fitting computer programme with a full-matrix diagonalization approach and the solid line in Figure 3.10 represents the simulation. To analyze the magnetic data at the beginning the model for a linear tetranuclear complex with two terminal species $S_1 = S_4 = S_{Mn(IV)} = 3/2$ and two central spins $S_2 = S_3 = S_{Mn(II)} = 5/2$ were considered, as depicted in the following coupling scheme. The parameter set, $g_1 = g_4 = g_{Mn(IV)} = 2.0$ and $g_2 = g_3 = g_{Mn(II)} = 2.2$ and $J_{12} = 0.8$ cm^{-1} and $J_{23} = -4.1$ cm^{-1} were obtained from the best simulation. The agreement between the calculated magnetic moments is good as is evident from Figure 3.10a. The experimental results were also simulated with $J_{12} = +0.8$ cm^{-1}, $J_{23} = -4.1$ cm^{-1}, and $J_{13} = +0.1$ cm^{-1} but J_{13} is neglected as it is very small and by neglecting J_{13} a good fit was obtained except some irrational g-values for the Mn(II) centers. This complex also exhibits extremely complicated low-lying structure with a non-diamagnetic ground state, which is not well separated from the upper-lying states, is in full conformity with the non-zero magnetic moment at 2K

The fit parameters were also checked by the 2D-contour plot (Figure 3.9b) of the exchange coupling constants and the global minima observed in the plot of J_{12} and J_{23} show the value of J_{12} is undefined in the ferromagnetic scale and $J_{23} = -4.2$ cm^{-1} is also quite satisfactory. It is to be noted here the exchange interaction between the central manganese(II) ions is reduced compared two the same interaction in case of complex **4**, can be attributed in terms of decreasing separation between Mn(2)....Mn(3) [2.95 Å] compared to the Mn(2)....Mn(3) [2,90 Å] in case of complex **4**.

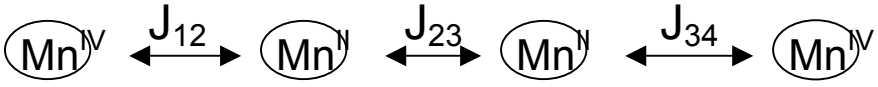

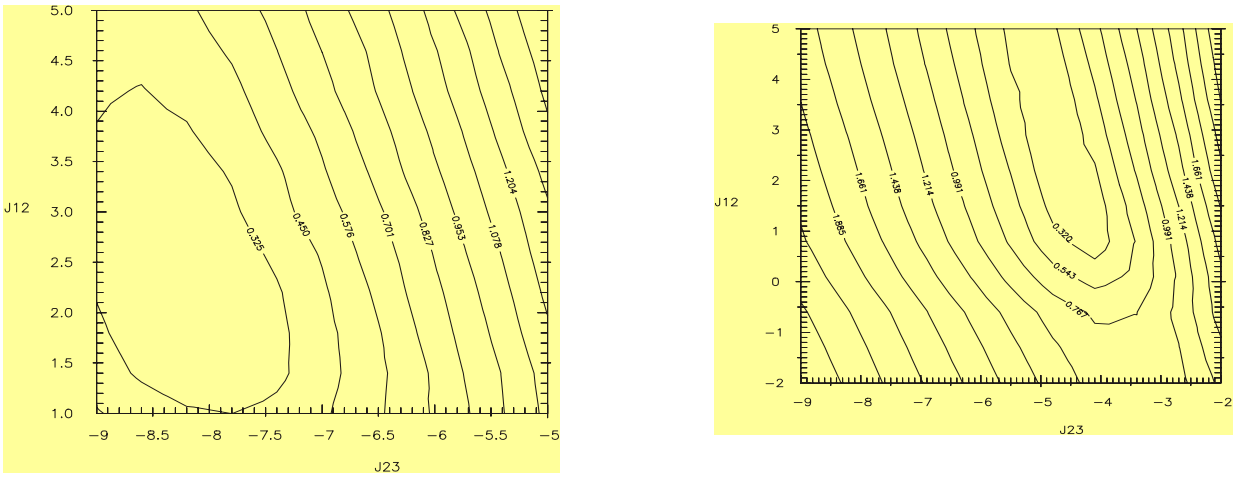

(a) **(b)**

Figure 3.9: Error surface plot for exchange coupling parameters in $Mn^{III}Mn^{II}Mn^{II}Mn^{III}$ and $Mn^{IV}Mn^{II}Mn^{II}Mn^{IV}$ core congeners

Exchange interactions between the neighbouring manganese (IV) and - (II) ions for nioximate, glyoximate complexes were reported to be ferromagnetic (J~ +18 to +25 cm^{-1}) previously by our group.[18a,21-22]

The magnetic behaviour of $Fe^{III}_2Mn^{II}_2$ (**7**) in the form of the effective magnetic moments (μ_{eff}) versus temperature (T) are displayed in Figure 3.10b. The magnetic moment of 10.66 μ_B ($\chi_M \bullet T$ = 14.21 $cm^3.K.mol^{-1}$) at 290 K decreases monotonically with decreasing temperature and until it reaches a value of 7.02 μ_B ($\chi_M \bullet T$ = 6.17 $cm^3.K.mol^{-1}$) at 20 K and then starts to decrease further but rapidly and reaches a value of 3.26 μ_B at 2K. This temperature dependence magnetic moment is in agreement with antiferromagnetic coupling between the spin carriers. To analyze the magnetic data at the beginning the model for a linear tetranuclear complex with two terminal species $S_1 = S_4 = S_{Fe(III)} = 5/2$ and two central spins $S_2 = S_3 = S_{Mn(II)} = 5/2$ were considered, as depicted in the following coupling scheme. The parameter set, $g_1 = g_4 = g_{Fe(III)} = 2.0$ and $g_2 = g_3 = g_{Mn(II)} = 2.0$ and J_{12} = -1.8 cm^{-1} and J_{23} = - 8.0 cm^{-1}(comparable with the coupling constant obtained from the complex **4**) were obtained from the best simulation. The agreement between the calculated magnetic moments is good as is evident from Figure 3.10b.

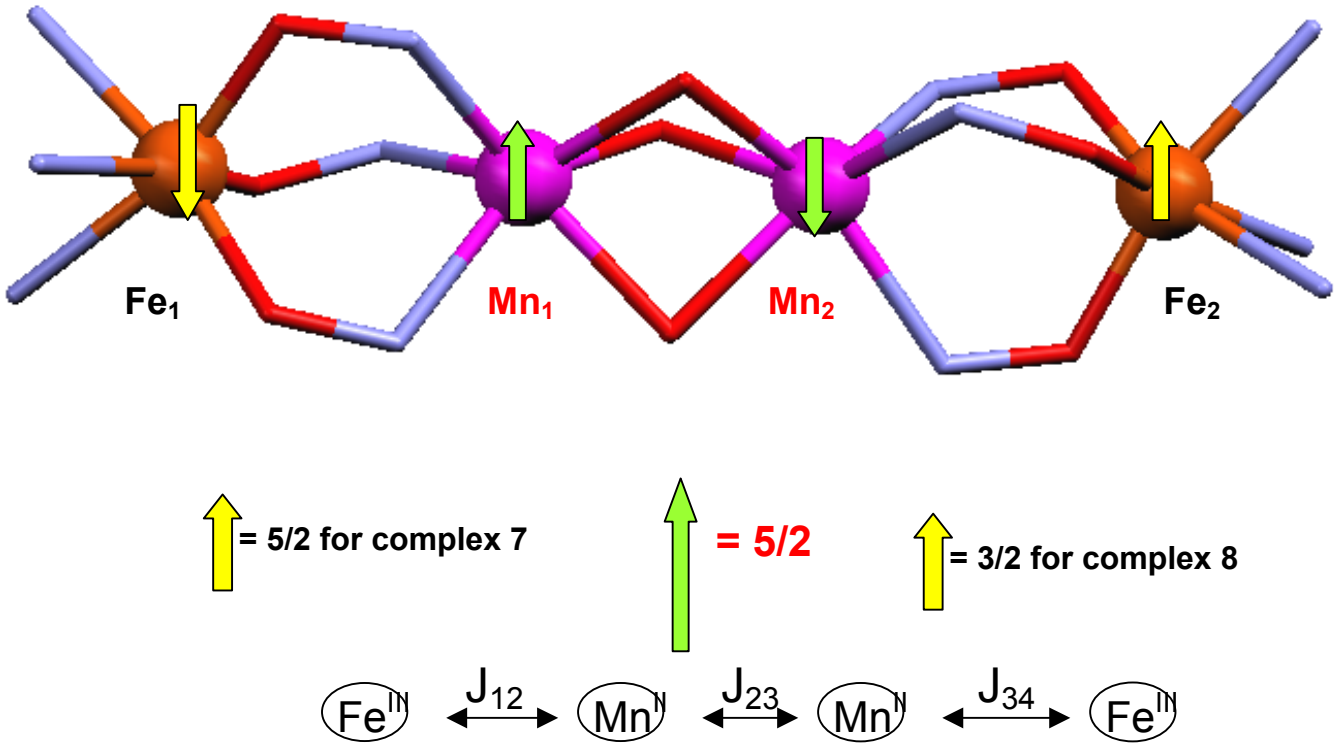

Scheme 2: Representation of the coupling Scheme in complexes 7 and 8.

The magnetic behaviour of $Cr^{III}_2Mn^{II}_2$ (**8**) is shown in Figure 3.10b in the form of the effective magnetic moments (μ_{eff}) versus temperature (T). The magnetic moment of 8.25 μ_B ($\chi_M \bullet T$ = 8.53 $cm^3.K.mol^{-1}$) at 290 K decreases monotonically with decreasing temperature and reaches a value of 2.18 μ_B ($\chi_M \bullet T$ = 0.593 $cm^3.K.mol^{-1}$) at 1.95 K. The experimental magnetic data were simulated using a least squares fitting computer programme with a full-matrix diagonalization approach and the solid line in Figure 3.10b represents the simulation. To analyze the magnetic data at the beginning the model for a linear tetranuclear complex with two terminal species $S_1 = S_4 = S_{Cr(III)} = 3/2$ and two central spins $S_2 = S_3 = S_{Mn(II)} = 5/2$ were considered, as depicted in the following coupling scheme. The parameter set, $g_1 = g_4 = g_{Cr(III)} = 1.9$ and $g_2 = g_3 = g_{Mn(II)} = 2.0$ and J_{12} = - 2.4 cm^{-1} and J_{23} = - 8.75 cm^{-1}(comparable with the coupling constant obtained from the complex **4**) were obtained from the best simulation. The agreement between the calculated magnetic moments is good as is evident from Figure 3.10b.

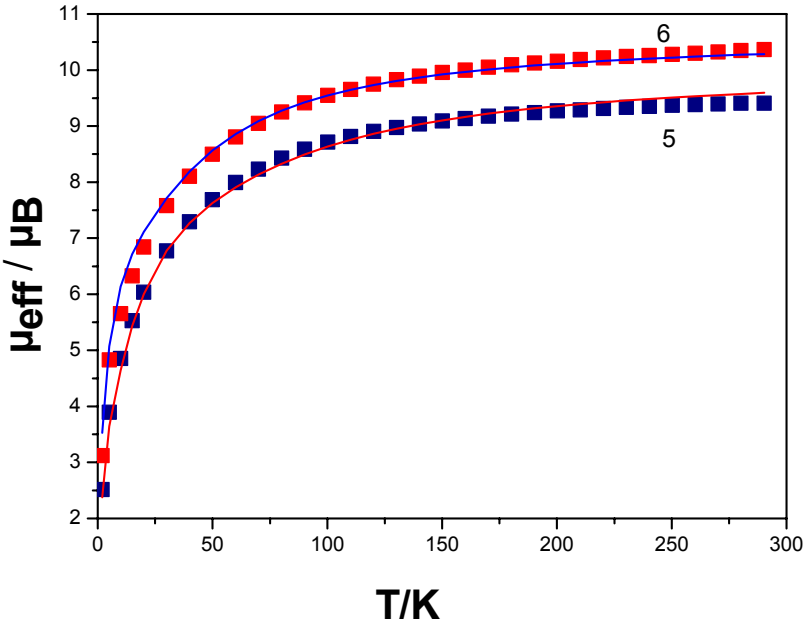

(a)

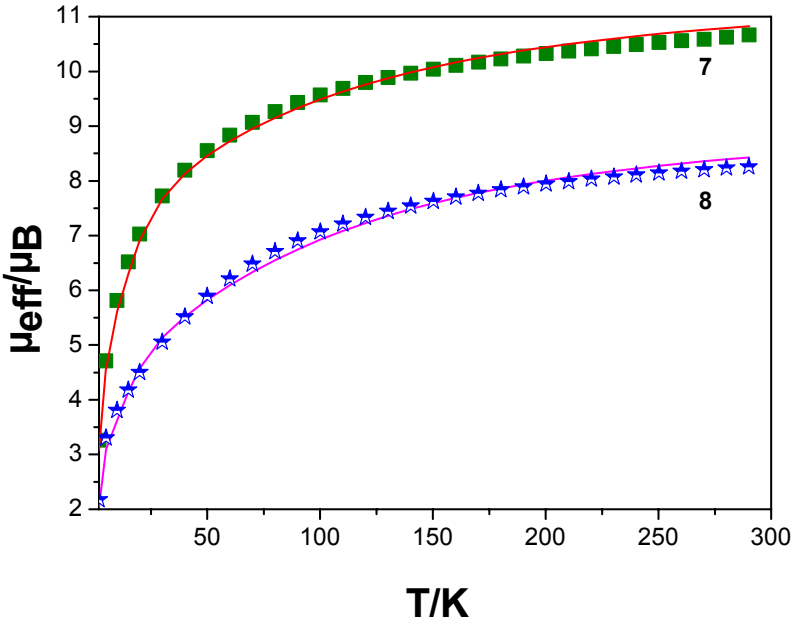

(b)

Figure 3.10: (a) Magnetic data for $Mn^{III}Mn^{II}Mn^{II}Mn^{III}$ (5) and $Mn^{III}Mn^{II}Mn^{II}Mn^{III}$ (6), as a plot of μ_{eff} vs T. (b) Magnetic data for $Fe^{III}Mn^{II}Mn^{II}Fe^{III}$ (7) and $Cr^{III}Mn^{II}Mn^{II}Cr^{III}$ (8) as a plot of μ_{eff} vs. T. The bold points represent the experimental data while the solid line represents the simulation

It is interesting to note that the related isoelectronic $Mn^{IV}Mn^{II}Mn^{II}Mn^{IV}$ complex exhibits ferromagnetic interaction between the $Mn^{IV}...Mn^{II}$ center and this can be attributable to the higher charge on the Mn(IV) center than that on the Cr(III) center. Thus, the higher covalent character of the Mn(IV)-ligand bond leads to stronger electronic interactions. Weak antiferromagnetic coupling between Cr(III) and Mn(II) ions obtained is in contrast to the ferromagnetically coupled oximate complexes with $Cr^{III}Mn^{II}Cr^{III}$ and $Cr^{III}Mn^{II}$ core congeners.[9,27]

Table 3.5: Intratetramer magnetic parameters for homo-and heterotetranuclear complexes.

Compounds	Magnetic core		J_{12} [cm^{-1}]	J_{23}[cm^{-1}]	$g_{Mn(II)}$	$g_{Fe(III)}$	$g_{Cr(III)}$	$g_{Mn(III)}$ or $g_{Mn(IV)}$
4	$Mn^{II}Mn^{II}$			**- 8.4**	**1.98**			
5	$Mn^{III}Mn^{II}Mn^{II}Mn^{III}$	$J_{12} = J_{34}$	**+ 2.8**	**- 8.2**	**2.00**			**1.85**
6	$Mn^{IV}Mn^{II}Mn^{II}Mn^{IV}$	$J_{12} = J_{34}$	**+ 0.8**	**- 4.1**	**2.00**			**2.00**
7	$Fe^{III}Mn^{II}Mn^{II}Mn^{III}$	$J_{12} = J_{34}$	**- 1.8**	**- 8.0**	**2.00**	**2.00**		
8	$Cr^{III}Mn^{II}Mn^{II}Cr^{III}$	$J_{12} = J_{34}$	**- 2.4**	**- 8.75**	**2.00**		**1.90**	

The nearest neighbour interaction, J is ferromagnetic in complexes **5** and **6,** and antiferromagnetic in complexes **7** and **8**, while J' is antiferromagnetic in all the complexes. Because of the competing influence of J and J' upon spin coupling in the complexes **5-8**, the ground state properties are determined by their ratios.

A qualitative rationale for the trend will now be provided and the nature of the exchange interactions between neighboring $Mn^{III}Mn^{II}$, $Fe^{III}Mn^{II}$, $Mn^{IV}Mn^{II}$ and $Mn^{II}Mn^{II}$ spin carriers on the basis of the established Goodenough-Kanamori rules for superexchange. The evaluated exchange coupling constants can be factored into two opposing contributions from antiferromagnetic and ferromagnetic interactions with J_{AF} expressed as a negative term and J_F as a positive term.

$$J_T = J_{AF} + J_F$$

Considering the O and N atoms of the bridging oxime groups as sp^2 hybridized in the network $M(O\text{-}N)_3Mn$ and sp^2 hybridization $Mn(O)_3Mn$, the interaction parameters evaluated from the magnetic data will be analyzed. Hence, the different possible interactions of the sp^2 orbitals on either side of the bridging oximate ligands with the different orbitals in idealized D_{3h} symmetry of the whole network $M_A(O\text{-}N)_3Mn(O)_3Mn(O\text{-}N)_3M_A$ will be considered

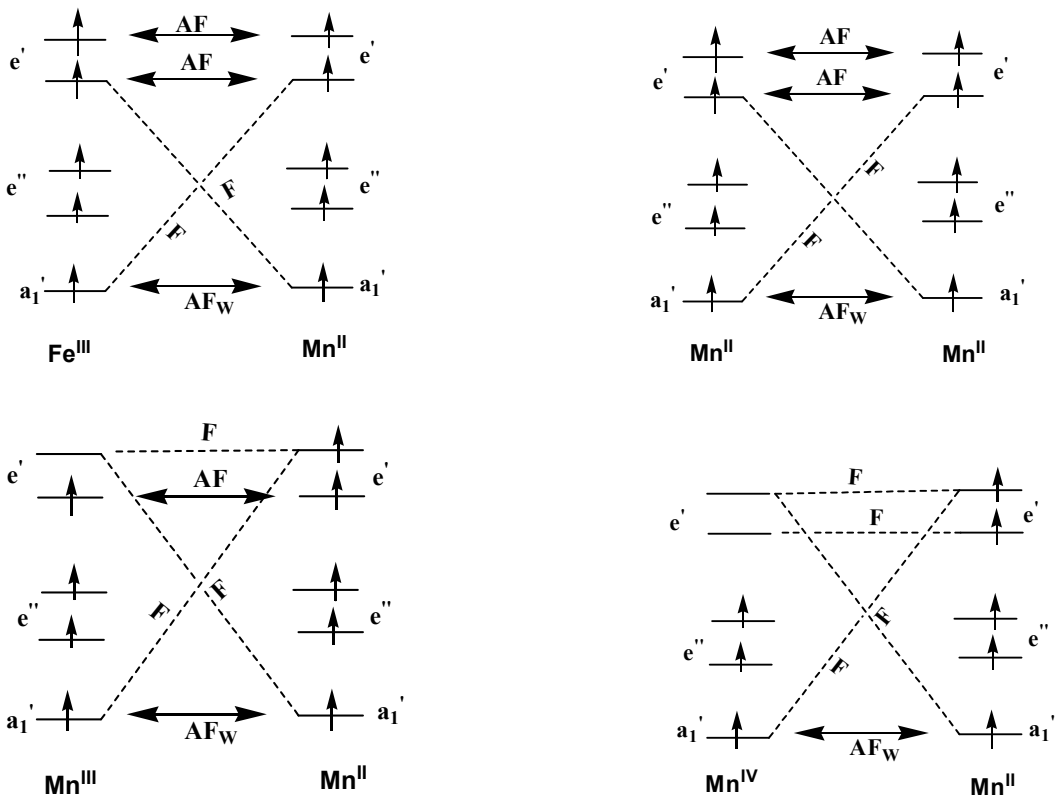

Figure 3.11: Schematic diagram for magnetic exchange interaction

The five metal d orbitals with the 3-fold axis as the z-axis along the M...Mn vector transform in D_{3h} symmetry as a_1' (d_z^2), e''(d_{xz},d_{yz}) and e'(d_x^2-$_y^2$,d_{xy}). Dominant exchange paths are schematically represented, it is obvious from the above scheme that for the $Fe^{III}Mn^{II}Mn^{II}Fe^{III}$ compound the antiferromagnetic path involving $e' \,||\, sp^2 \,||\, e'$ interactions dominates over all other interactions, resulting in overall antiferromagnetic interactions. Whereas in the $Mn^{III}Mn^{II}Mn^{II}Mn^{III}$ compounds interaction between the Mn^{II}....Mn^{II} is involving dominating $e' \,||\, sp^2 \,||\, e'$ antiferromagnetic pathways, and the antiferromagnetic pathways in Mn^{II}...Mn^{III} is over compensated by the presence of several ferromagnetic Mn^{III}.....Mn^{II} paths($e' \perp a_1'$) and are important in determining the strength of the overall exchange interactions. It is also to note that in the case of Mn^{III}.....Mn^{II} with the missing electron in the e' orbital the AF path present in Fe^{III}.....Mn^{II} vanished, resulting in stronger parallel coupling in d^4(HS)d^5 system. Now on going to the Mn^{IV}...Mn^{II}, in which Mn^{IV} has an empty 2e orbital, the overall interaction changes its nature from antiferromagnetic in Fe^{III}...Mn^{II} to weak ferromagnetic in Mn^{IV}...Mn^{II} (J = + 0.8 cm^{-1}). Thus the contribution of the path $e' \,||\, sp^2 \,||\, e'$ to the overall interaction becomes very important since the 2e orbitals centred on

manganese(IV) and manganese(II) are empty and half-filled respectively leading to ferromagnetic interaction. The π conjugated system of the 2,6-diformyl 4-methyl phenoldioximato ligand delocalized over the bridging groups and perpendicular to the plane of the oxime ligands, appears also to have a role, although small, in tuning the exchange interactions in this series of compounds.

Tables 3.6 and 3.7 summarize exchange coupling constants reported in $Mn^{II}Mn^{III}$, $Mn^{II}Mn^{IV}$, $Mn^{II}Fe^{III}$ and $Mn^{II}Cr^{III}$ core congeners, where exchange coupling mediated through oximate (NO) ligands.

Table 3.6: Magnetic parameters for exchange coupled polynuclear oximate complexes

Compounds	Magnetic core	$J_{Mn(II)...Mn(III)}$ [cm^{-1}]	$J_{Mn(II)...Mn(IV)}$ [cm^{-1}]	$g_{Mn(III)}$	$g_{Mn(II)}$	$g_{Mn(IV)}$	References
$[(Me_3Tacn)Mn^{III}\{(dmg)_3Mn^{II}\}Mn^{III}(Me_3Tacn)](ClO_4)_2$	$Mn^{III}Mn^{II}$	+ 4.7	+ 19. 6				18a
$[(Me_3Tacn)Mn\{(dmg)_3Mn\}Mn(Me_3Tacn)](ClO_4)_2$	$Mn^{IV}Mn^{II}$						18a
$[L_2Mn^{II}_2(\mu\text{-}O_2COMe)(MeOH)Mn^{III}](ClO_4)_2$	$Mn^{III}Mn^{II}$	+ 2.0		1.98	2.05		18b
$[(Me_3Tacn)MnMn(PyA)_3](ClO_4)_2$	$Mn^{III}Mn^{II}$	+ 1.8					19
$[(Me_3Tacn)Mn^{III}\{(niox)_3Mn^{II}\}Mn^{III}(Me_3Tacn)](ClO_4)_2$	$Mn^{III}Mn^{II}$	+ 4.7		1.99	1.99		11
$[(Me_3Tacn)Mn\{(niox)_3Mn\}Mn(Me_3Tacn)](ClO_4)_2$	$Mn^{IV}Mn^{II}$		+ 25.2		2.00	2.00	11
$[Mn_3(MeO)_2(pko)_4(SCN)_2]$	$Mn^{IV}Mn^{II}$		+ 3.06		2.09	2.09	21a
$[Mn_3(MeO)_2(pko)_4Cl_2]$	$Mn^{IV}Mn^{II}$		+ 3.9		2.07	2.07	21b
$[Mn_3(MeO)_2(pko)_4(OCN)_2]$	$Mn^{IV}Mn^{II}$		+ 4.05		2.08	2.08	21b
$(Me_4N)_2[Mn_4O_2(cao)_4(MeCN)_2(H_2O)_6](NO_3)_4$	$Mn^{III}Mn^{II}$	- 2.5		1.88	1.88		29
$[Mn_3(mcoe)_6](NO_3)$	$Mn^{III}Mn^{II}$	- 1.3 ± 0.3		2.00	2.00		29

Table 3.7: Magnetic parameters for exchange coupled polynuclear oximate complexes

Compounds	Magnetic core	$J_{Fe(III)...Mn(II)}$ [cm^{-1}]	$J_{Cr(III)...Mn(II)}$ [cm^{-1}]	References
$[(Me_3Tacn)Fe^{III}Mn^{II}(PyA)_3](ClO_4)_2$	$Fe^{III}Mn^{II}$	- 6.0		8
$[(Me_3Tacn)Cr^{III}Mn^{II}(PyA)_3](ClO_4)_2$	$Cr^{II}Mn^{II}$		+ 1.5	9
$[(Me_3Tacn)Fe^{III}\{(dmg)_3Mn^{II}\}Fe^{III}(Me_3Tacn)](ClO_4)_2$	$Fe^{III}Mn^{II}Fe^{III}$	- 6.7		28
$[(Me_3Tacn)Cr^{III}\{(dmg)_3Mn^{II}\}Cr^{III}(Me_3Tacn)](ClO_4)_2$	$Cr^{II}Mn^{II}Cr^{III}$		+ 4.5	27

3.8 References:

(1) O. Kahn, *Molecular Magnetism*, VCH Publishers, Weinheim, 1993

(2) (a) O. Kahn. *Adv. Inorg. Chem.,* 1995, **43**, 179; (b) K. S. Murray. *Adv. Inorg. Chem.*, 1995, **43**, 261

(3) F. Birkelbach, M.Winter, U. Flörke, H-J. Haupt, C. Butzlaff, M. Lengen, E. Bill, A. X. Trautwein, K. Wieghardt and P. Chaudhuri, *Inorg. Chem.,* 1994, **33**, 3990

(4) C. Krebs, M.Winter, T. Weyhermüller, E. Bill, K.Wieghardt and P.Chaudhuri, *J. Chem. Soc., Chem. Commun.,* 1995, 1913

(5) P. Chaudhuri, M.Winter, P. Fleischhauer, W. Hasse, U. Flörke and H-J. Haupt, *J. Chem. Soc., Chem. Commun.,* 1990, 1728

(6) C. N. Verani, E. Rentschler, T. Weyhermüller, E. Bill and P. Chaudhuri, *J. Chem. Soc.,Dalton Trans.,* 2000, 4263

(7) C. N. Verani, T. Weyhermüller, E. Rentschler, E. Bill and P.Chaudhuri, *J. Chem. Soc., Chem. Commun.,* 1998, 2475

(8) S. Ross, T. Weyhermüller, E. Bill, E. Bothe, U. Flörke, K. Wieghardt and P.Chaudhuri, *Eur. J. Inorg. Chem.,* 2004, 984

(9) S. Ross, T. Weyhermüller, E. Bill, K. Wieghardt and P. Chaudhuri, *Inorg. Chem.,* 2001, **40**, 6656

(10) C. N. Verani, E. Rentschler, T. Weyhermüller, E. Bill and P. Chaudhuri, *J. Chem. Soc., Dalton Trans* ., 2000, 251

(11) F. Birkelbach, T. Weyhermüller, M. Lengen, M. Gerdan, A. X. Trautwein, K. Wieghardt and P.Chaudhuri, *J. Chem. Soc.,Dalton Trans.,* 1997, 4529

(12) A few selected examples: (a) S. Mohanta, K. K. Nanda, L. K. Thompson, U. Flörke and K. Nag, *Inorg. Chem.,* 1998, **37**, 1465; (b) E. Colacio, J. M. Dominguez-Vera, M.Ghazi, R. Kivekäs, M. Klinga and J. M. Moreno, *Inorg. Chem.,* 1998, **37**, 3040; (c) K. E. Vostrikova, D.Luneau, W.Wernsdorfer, P. Rey and M.Verdauger, *J. Am. Chem. Soc.,* 2000, **122**, 718

(13) H. Okawa, T. Tokii, Y. Muto and S. Kida, *Bull. Chem. Soc. Jpn.,* 1973, **46**, 2624

(14) K. K. Nanda, A. W. Addison, N. Paterson, E. Sinn, L. K. Thompson and U. Sakaguchi, *Inorg. Chem.,* 1998, **37**, 1028

(15) E. V. Rybak-Akimova, D. H. Busch, P. K. Kahol, N. Pinto, N. W. Alcock and H. J. Clase, *Inorg. Chem.,* **1997**, **36**, 510

(16) (a) Q. Zeng, S. Gou, L. He,Y. Gong and X.You, *Inorg. Chim. Acta.,* 1999, **287**,14; (b) P. Chakraborty and S. K. Chandra, *Polyhedron.,* 1994, **13**, 684

(17) C. N. Verani, E. Bothe, D. Burdinsky, T. Weyhermüller, U. Flörke and P. Chaudhuri, *Eur. J. Inorg. Chem*., 2001, 2161

(18) (a) F. Birkelbach, U. Flörke, H-J. Haupt, C. Butzlaff, A. X. Trautwein, K. Wieghardt and P. Chaudhuri, *Inorg. Chem.,* 1998, **37**, 2000; (b) V.Pavlischuk, F. Birkelbach, T. Weyhermüller, K. Wieghardt and P. Chaudhuri, *Inorg. Chem.,* 2002, **41**, 4405

(19)P. Chaudhuri, *Coord. Chem. Rev.,* 2003, **243**, 143

(20) P. Chaudhuri, E. Rentschler, F. Birkelbach, C. Krebs, E. Bill, T. Weyhermüller and U. Flörke *Eur. J. Inorg. Chem.,* 2003, 541

(21) M. Alexiou, C. Dendrinou-Samara, A. Kasagianni, S. Biswas, C. M. Zeleski, J. Kampf, D. Yoder, J. E. Penner-Hahn, V. L. Pecoraro, D.P. Kessissoglou, *Inorg. Chem.,* 2003**, 42**, 2185

(22) T. Afrati, C. Dendrinou-Samara, C. P. Raptopoulou, A. Terzis, V. Tangoulis and D. P. Kessissoglou, *Angew. Chem.Int.Ed.Engl.,* 2002, **41**, 2148

(23) D. Black, A. J. Black, K. P. Dancy, A. Harrison, M. Mcpartin, S. Parsons, P. A. Tasker, G. Whittakar and M. Schroder, *J. Chem. Soc.,Dalton Trans.,* 1998, 3953

(24) L. Dubois, Da-Feng.Xiang, Xian-Shi. Tan, J. Pecant, P. Jones, S. Bandron, L. Le. Pape, J-M. Latour, C. Baffert, S. Chardon-Noblat, M. N. Coulomb and A. Deronzier, *Inorg. Chem.,* 2003**, 42**, 750

(25) S. Blanchard, G. Blondin, E. Riviere, M. Nierlich, J-J. Gireard, *Inorg. Chem.,* 2003**, 42**, 4568

(26) K. B. Jenson, E. Johanson, F. B. Larson, C. J. Mckenzie, *Inorg. Chem.,* 2004**, 43**, 3801

(27) D. Burdinski, F. Birkelbach, T. Weyhermüller, U. Flörke, H-J. Haupt, M. Lengen, A. X. Trautwein, E. Bill, K. Wieghardt and P. Chaudhuri, *Inorg. Chem.,* 1998**, 37**, 1009

(28) P. Chaudhuri and U. Flörke, unpublished result.

(29) D. J. Price, S. R. Batten, K. J. Berry, B. Moubaraki and K. S. Murray, *Polyhedron*, 2003, **22**, 165

CHAPTER - 4

HETEROTETRANUCLEAR $[Fe^{III}_2Cu^{II}_2]$, $[Cr^{III}_2Cu^{II}_2]$ BUTTERFLY CORE CONGENERS

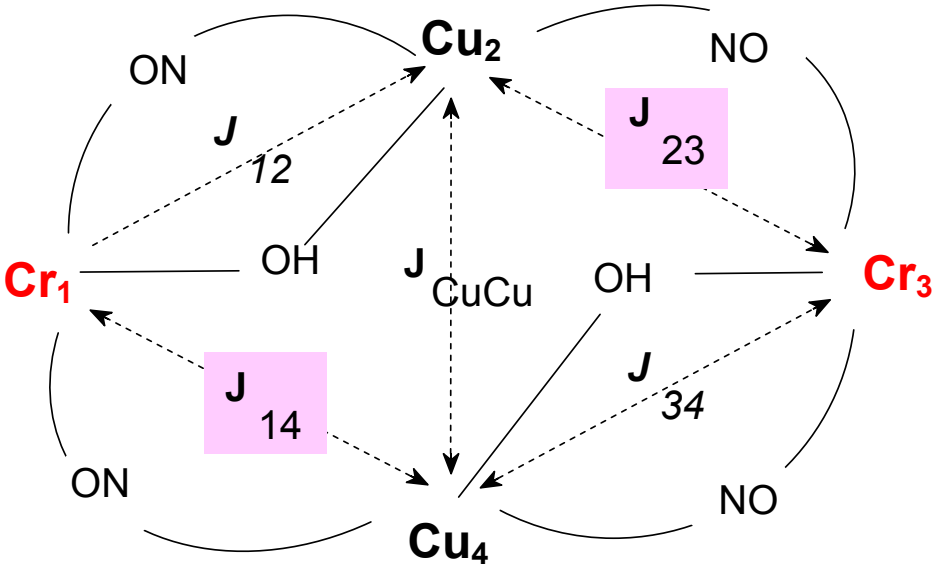

4.1 Introduction

Tetranuclear oxide bridged metal assemblies are pertinent to several areas including bioinorganic modelling and magnetochemistry. In the field of iron chemistry, the pursuit of model complexes[1-4] for the iron proteins has yielded several interesting tetranuclear complexes amongst other polynuclear iron complexes with unusual electronic structures.[5] The knowledge that in PSII the site of water oxidation, is a tetranuclear manganese aggregate in which four manganese atoms are essential for activity. This appears to be in close proximity to one another, has augmented the search for tetranuclear manganese complexes. Thus tetramanganese butterfly complexes with the $[Mn_4O_2]^{8+}$ core have emerged as the most intensely studied oxide bridged carboxylate clusters.[4,7-10]

But there are few studies of the heterometallic butterfly complexes,[11-13] despite the fact, that such studies might be more informative in comparison to those of homometal complexes. Because new exchange pathways can be expected for heteronuclear complexes[14-26] where unusual sets of magnetic orbitals can be brought into close proximity. For instance, the strict orthogonality of the magnetic orbitals resulting in the stabilization of the spin state of highest multiplicity is much easier to realize in heterometallic systems than in homometallic species.

There are several intriguing features associated with polynuclear clusters. Firstly, these complexes can have unusual electronic structures and may serve as sources of fundamental information about exchange coupling in multinuclear assemblies. A second general reason to study polynuclear metal complexes is that, they may be building blocks for molecular based magnetic materials. Because of their topology, molecules that have large numbers of unpaired electrons should serve as good starting points for constructing molecular magnetic materials.[27] Though the pairwise exchange interactions in these complexes are found almost always to be antiferromagnetic, spin frustration,[28] or competing spin interactions, can result in polynuclear complexes having relatively large number of unpaired electrons in the ground state.

Additionally, designing molecular entities with interesting spin topologies becomes easier with spin carriers of different kinds. Since the pioneering work of Olivier Kahn in the magnetism of heterometallic systems, the field has developed tremendously, as will be evident from the following discussion on the oximato-bridged tetranuclear heterometallic molecules.

4.2 Synthesis:

The most successful synthetic strategy for heterometallic complex is the use of metal complexes as ligands which can act as a building block for polynuclear complexes, Therefore, metal complexes containing potential donor atoms can act as a bridging ligand for another metal ion or metal complex with empty or available coordination sites. The following strategy is an attempt to obtain heterometal complex, in which the oxime ligand acting as a bridge between two different metal ions e.g. iron (III), copper(II) and chromium(III), copper(II)

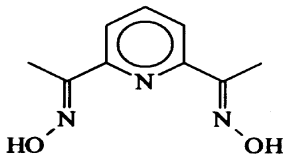

(a) dapdoH_2

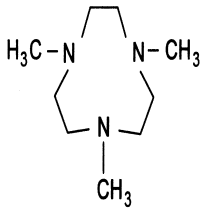

(b)Me_3Tacn

Ligands

The protonated oxime containing mononuclear complex[32] $[Cu(dapdoH_2)_2](ClO_4)_2$ has been reacted with either $[Me_3TacnFe^{III}]^{3+}$ or $[Me_3TacnCr^{III}]^{3+}$ unit in presence of triethylamine. The assembly of these two building blocks(oxime complex as bridging ligand and $[Me_3TacnM^{III}]^{3+}$ as capping ligand) in 1:2 molar ratio lead to the formation of heterotetranuclear clusters $[(Me_3Tacn)Fe^{III}_2(dapdo)_2Cu^{II}_2(O...H...O)(\mu_2\text{-}Cl)](ClO_4)_2$ **9** and $[(Me_3Tacn)Cr^{III}_2(dapdo)_2Cu^{II}_2(\mu_2\text{-}OH)_2Br_2](ClO_4)_2$ **10.**

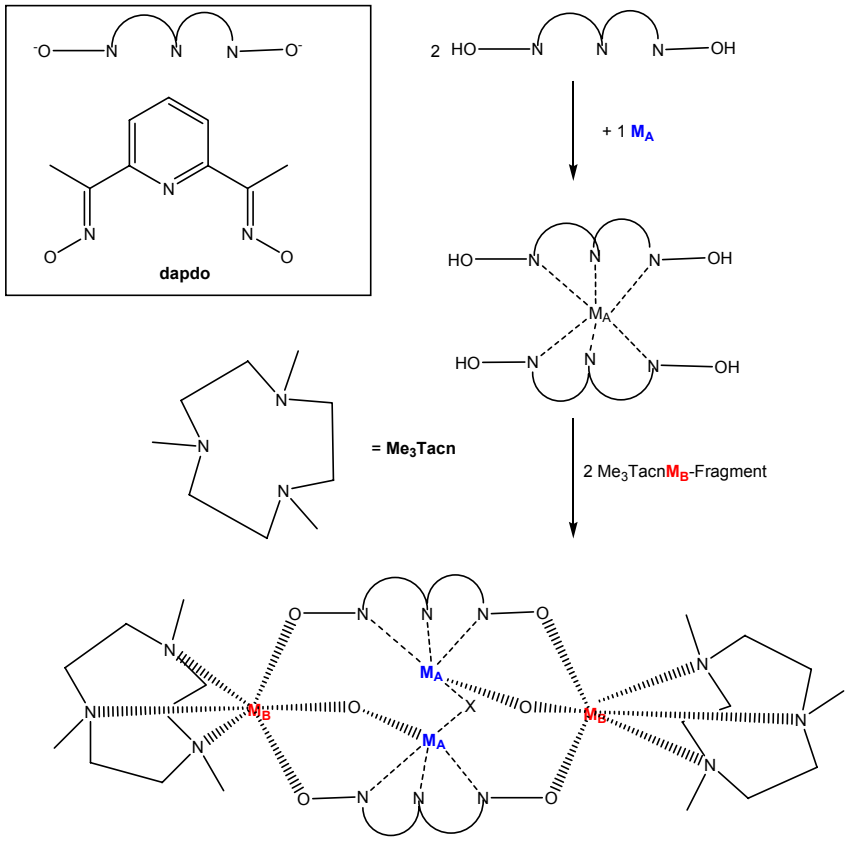

Figure 4.1: Schematic diagram for the synthesis of "butterfly" core congeners 9-10

4.3 Infrared and Mass Spectroscopy:

Complexes **9** and **10** show the C=N stretching bands for the ligand at 1593 and 1595 cm^{-1} respectively. Strong peaks at 2916-2920 cm^{-1} correspond to the C-H stretching of the Me_3Tacn group, in the $Fe^{III}_2Cu^{II}_2$ (**9**) and $Cr^{III}_2Cu^{II}_2$ (**10**) core congeners. The NO stretchings for these two tetranuclear complexes are observed at 1163 and 1080 cm^{-1}. Strong stretching bands at 1077, 624 cm^{-1} and 1090, 624 cm^{-1} respectively correspond to the counteranion ClO_4 unit in the tetranuclear $Fe^{III}_2Cu^{II}_2$ and $Cr^{III}_2Cu^{II}_2$ complexes.

Electrospray-ionaziation mass spectrometry (ESI-MS) in the positive ion mode has been proved to be very successful in characterizing $Fe^{III}_2Cu^{II}_2$ (**9**) which shows the dipositively charged species $[M\text{-}2ClO_4]^{2+}$ as the base peak. The peak due to $[M\text{-}ClO_4]^{+}$ is also observed. On the contrary, the signal for $[M\text{-}2ClO_4 + 0.5\ H_2O]^{2+}$ of **10** has been found as the base peak.

4.4 Solid state molecular structure:

4.4.1 X-ray Structure of $[(Me_3Tacn)_2Fe^{III}_2(dapdo)_2Cu^{II}_2(O...H...O)Cl](ClO_4)_2 .2CH_3OH$ (5)

The lattice is built of discrete tetranuclear dication; two noncordinatively bound perchlorate anions and two methanol molecules of crystallization. The molecular geometry and atom labeling scheme of the cation **9** are shown in Figure 4.3. The cation possesses a "*butterfly*" $[Fe_2(\mu_2\text{-}O...H...O\text{-}\mu_2)Cu_2]$ core. Cu(1) and Cu(1A) occupy "body" positions of the "*butterfly*" while Fe(1) and Fe(1A) occupy the "wing-tip" positions. The O(1) and O(1A) are acting as double bridging oxo groups in each FeCu unit respectively. The structure, thus, can be considered as two edge sharing $FeCu_2O$ triangular units as shown below.

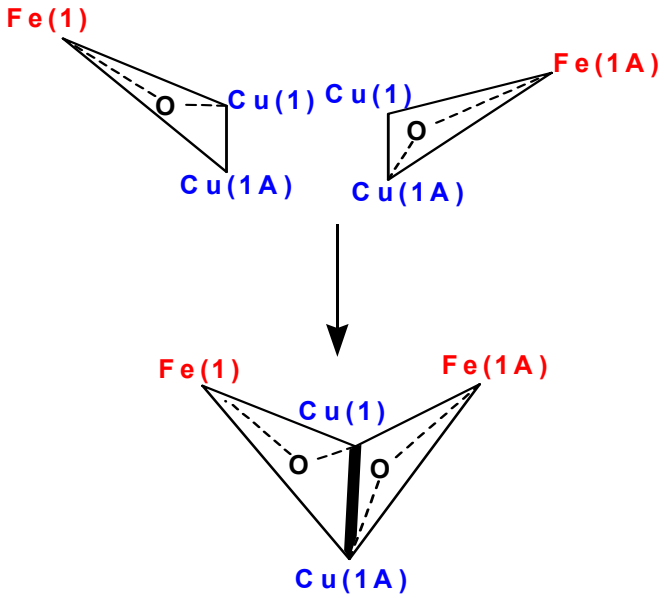

In addition to two μ_2-Oxo groups, there is one μ_2-Cl ion which acts as a bridge between the "body" copper ions. Both the μ_2-oxo groups are strongly hydrogen bonded with a distance of 2.24 Å where H is detected crystallographically and gives rise to (O...H...O) core. The 2,6-diacetylpyridine dioximate dianion ligands coordinate "*body*" Cu ions through its pyridine N(32) and two oximate nitrogen N(22) and N(30) atoms. So the

"*body*" Cu(II) ions are five coordinated with N_3OCl distorted square pyramidal geometry with the basal plane comprising two oximato nitrogen atoms, one pyridine nitrogen atom and one μ_2-oxo oxygen atom. The crystal structure gives τ value of 0.054 indicating an essentially square-pyramidal (4 + 1) coordination geometry of the "*body*" copper ions.[43] In a five coordinate system, ideally square pyramidal geometry is associated with $\alpha = \beta = 180°$ for A is the axial ligand (where α and β are the basal angles). In the great majority of real square pyramidal systems, metal is displaced out of the equatorial plane toward the axial ligand. The geometric parameter τ is defined as $[(\beta - \alpha) / 60]$ which is applicable to five coordinate environment as an index of degree of trigonality, within the structural continuum between trigonal bipyramidal and square pyramidal geometries. τ is zero for a perfectly square pyramidal geometry, while it becomes unity for a perfect trigonal bipyramidal geometry. The average N_{ox}-Cu bond length is 2.056(15) Å, is significantly longer than the N_{py}-Cu bond distance of 1.94(15) Å. The Cu-Cl bond distance is 2.539(5) Å and gives rise to Cu(1)-Cl(1)-Cu(1A) angle 87.91°,whereas the bond distance between Cu(1) and O(1) is 1.913(12) Å.

The coordination geometry of the "wing-tip" ferric ion Fe(1) is distorted octahedral, with the three nitrogen atoms N(1), N(4) and N(7) from the facially coordinated tridentate macrocyclic amine(Me_3Tacn) and three oxygen atoms [O(21) and O(31) from the deprotonated oxime group, O(1) from the μ_2-bridging oxo group] resulting in a *fac*-FeN_3O_3 coordination sphere. The Fe-N(average 2.24 Å) and Fe-O(average 1.99 Å) distances are in agreement with a d^5 high-spin electronic configuration for the iron center. The Fe(1)-μ_2-oxo distance is [1.856(12) Å], as expected, the shortest among metal-ligand bond lengths. The Fe(1) is displaced by 0.046 Å from the mean basal plane comprising N(4)N(7)O(21)O(31) toward the apical μ_2-oxygen atom O(1). Selected bond lengths and angles for the $Fe^{III}_2Cu^{II}_2O_2$ core are given in Table 4.1. The Fe-N distance trans to the μ_2-oxo group [Fe(1)-N(1) = 2.259(15) Å] is longer than the other Fe-N distances. A deviation from idealized octahedral geometry at the metal center is found for the capping ligand Me_3Tacn; the N-Fe-O angles lying in the ranges 77.72° to 78.71°, whereas O-Fe-O angles fall between 93.25 and 102.23°. The Fe(1)...Cu(1) and Fe(1A).....Cu(1A) separations of 3.29 Å are significantly shorter than the Fe(1)....Cu(1A) and Cu(1)....Fe(1A) separations of 4.020 Å. The "body" Cu(1).....Cu(1A) separation is about 3.526 Å, while the separation between the "wing-tip" Fe(1).....Fe(1A) is 5.442 Å.

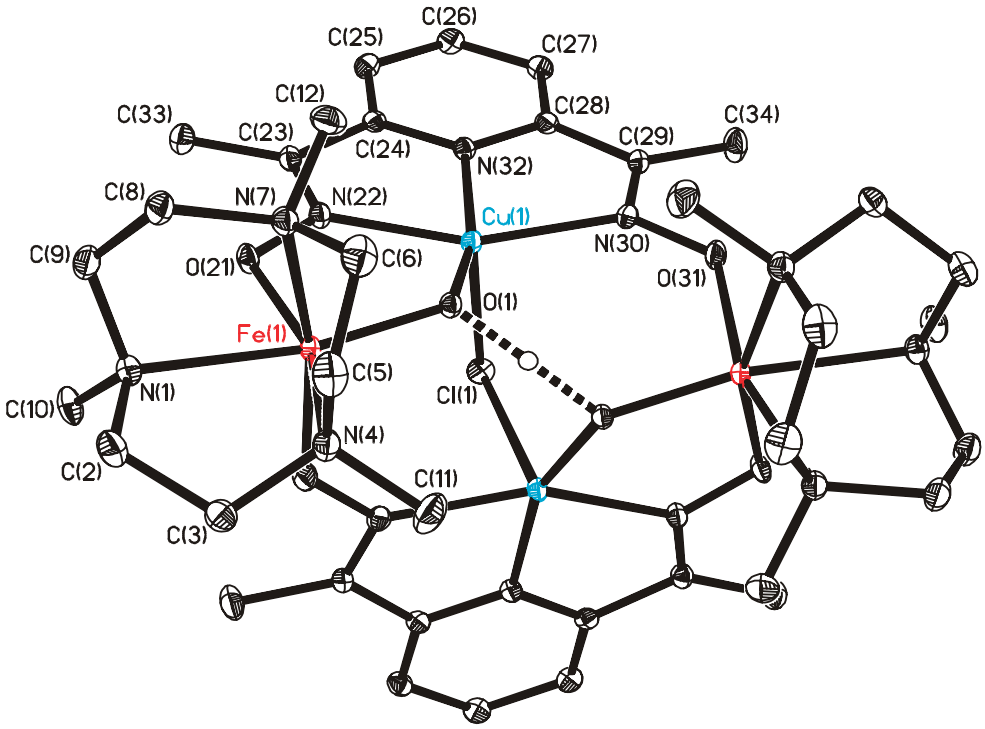

Figure 4.3: ORTEP and labeling scheme for the dication $Fe^{III}_2Cu^{II}_2$ (9)

Table 4.1: *Selected Bond Lengths (Å) and Angles (deg) for* **[$(Me_3Tacn)Fe^{III}\{(dapdo)_2Cu^{II}_2$ $\}(O....OH)ClFe^{III}(Me_3Tacn)](ClO_4)_2$ .2 CH_3OH 9**

Fe(1)•••Cu(1)	3.239	Cu(1A)•••Fe(1A)	4.020
Fe(1A) •••Cu(1)	3.239	Fe(1)•••Fe(1A)	5.442
Fe(1)•••Cu(1A)	4.020	Cu(1A)•••Cu(1)	3.526
Cu(1)-N(22)	2.009(15)	Cu(1)-N(22)	2.009(15)
Cu(1)-N(30)	2.112(15)	Cu(1A)-N(30)	2.112(15)
Cu(1)-N(32)	1.936(15)	Cu(1A)-N(32)	1.936(15)
Cu(1)-O(1)	1.913(12)	Cu(1A)-O(1)	1.913(12)
Cu(1)-Cl(1)	2.539(5)	Cu(1A)-Cl(1)	2.539(5)
Fe(1)-N(1)	2.259(15)	Fe(1A)-N(1)	2.259(15)
Fe(1)-N(4)	2.228(16)	Fe(1A)-N(4)	2.228(16)
Fe(1)-N(7)	2.250(15)	Fe(1A)-N(7)	2.250(15)
Fe(1)-O(1)	1.856(12)	Fe(1A)-O(1)	1.856(12)
Fe(1)-O(21)	2.014(13)	Fe(1A)-O(21)	2.014(13)
Fe(1)-O(31)	1.966(13)	Fe(1A)-O(31)	1.966(13)
		Fe(1)-O(1)-Cu(1)	118.46(7)

	Cu(1)-Cl(1)-Cu(1A)	87.91(2)
	O(1)-Fe(1)-N(1)	168.8(6)
	O(21)-Fe(1)-N(4)	159.68(5)
	O(31)-Fe(1)-N(7)	161.59(6)

4.4.2 X-ray Structure of $[(Me_3Tacn)_2Cr^{III}_2(dapdo)_2Cu^{II}_2(OH)_2Br_2](ClO_4)_2 \cdot 3CH_3CN \cdot 0.5\ H_2O$ (10)

The lattice is built of discrete tetranuclear dication, two noncordinatively bound perchlorate anions, three acetonitrile molecules and half water molecule of crystallization. The molecular geometry and atom labeling scheme of the cation **10** are shown in Figure 4.4. The cation possesses a "butterfly" $[Cr_2(\mu_2\text{-}OH)_2Cu_2]$ core. Cu(1) and Cu(2) occupy "body" positions while Cr(1) and Cr(2) occupy the "wing-tip" positions of the "*butterfly*". The O(100) and O(200) atoms are acting as double bridging hydroxo groups in each CrCu unit respectively. The structure, thus, can be considered as two edge sharing $CrCu_2OH$ triangular units as shown below.

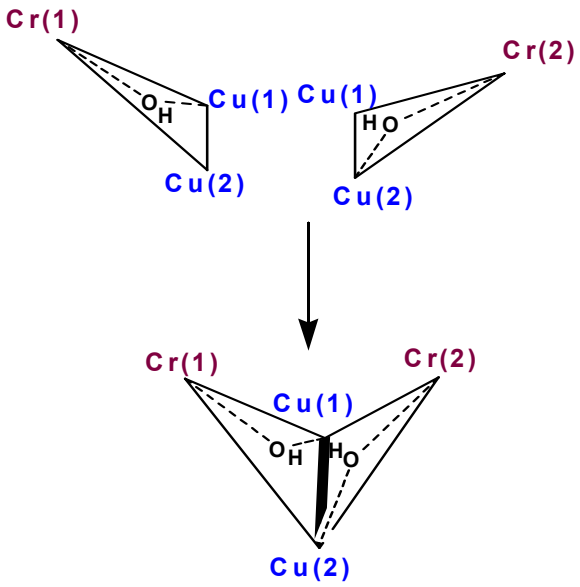

Both the μ_2-hydroxo groups are strongly hydrogen bonded with a distance of 2.9 Å, and gives rise to (O...HO) core. The 2,6-diacetylpyridine dioximate dianion coordinate to Cu(1) through its pyridine N(52) and two oximate nitrogen atoms N(42) and N(50) atoms, the average N_{ox}-Cu bond length is 2.07(2) Å is significantly longer than the N_{py}-Cu bond distance of 1.93(2) Å, whereas the bond distance between Cu(1) and O(200) is

1.976(13) Å. The fifth position of the copper ion is satisfied by axial Br(1) and thus "*body*" Cu ions Cu(1) and Cu(2) are in N_3OBr coordination sphere with square pyramidal geometry (τ value is calculated to be 0.09) around the copper centers.

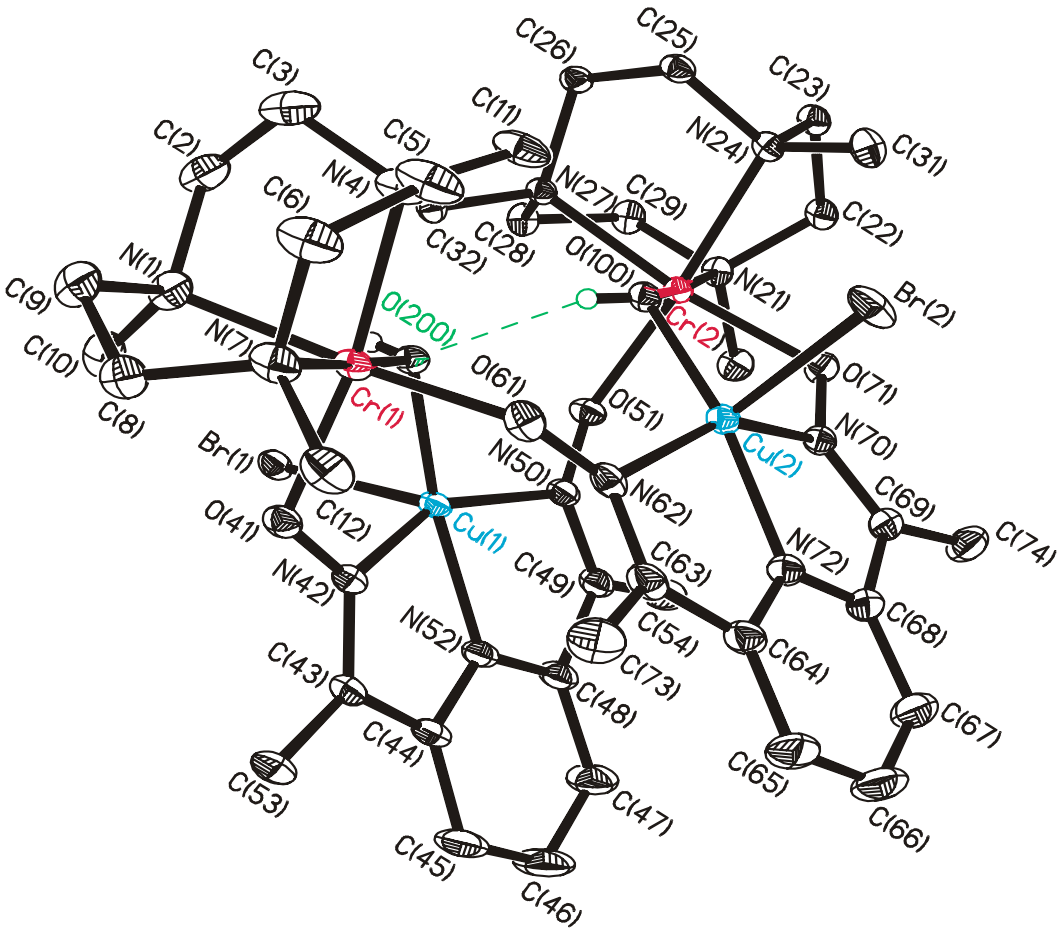

Figure 4.4: ORTEP and labeling scheme of the dication of $Cr^{III}_2Cu^{II}_2$ (10)

The coordination geometry of the "*wing-tip*" chromium ion Cr(1) is distorted octahedral, with the three nitrogen atoms N(1), N(4) and N(7) from the facially coordinated tridentate macrocyclic amine(Me_3Tacn) and three oxygen atoms [O(41) and O(61) from the deprotonated oxime groups, O(200) from the μ_2-bridging hydroxo group] resulting in a *fac*-CrN_3O_3 coordination sphere. The Cr-N [average 2.212(2) Å) and Cr-O_{ox}(average 1.95 Å) distances are in agreement with a d^3 high-spin electronic configuration for the chromium center. The Cr(1)-μ_2- hydroxo distance is 1.98(13) Å, as expected for chromium-hydroxo bond length. The Cr(1) is displaced by 0.688 Å from the mean basal

plane comprising N(4)N(7)O(41)O(61) toward the apical μ_2-oxygen atom O(200). Selected bond lengths and angles for the $Cr^{III}_2Cu^{II}_2(OH)_2$ core for the cation are given in Table 4.2. A deviation from idealized octahedral geometry at the metal center is found for the capping ligand Me_3Tacn; the N-Cr-O angles are lying in the ranges 82.02° to 82.96°, whereas O-Cr-O angles are found to be in the ranges 93.18 and 94.13°. The Cr(1)...Cu(1) separation of 3.3 Å is significantly shorter than the Cr(1)....Cu(2) separation of 4.377 Å. The "*body*" Cu(1).....Cu(2) separation is about 3.453 Å, while the separation between the "*wing-tip*" Cr(1).....Cr(2) is 5.948 Å.

Table4.2: *Selected Bond Lengths (Å) and Angles (deg) for* **$[(Me_3Tacn)Cr^{III}\{(dapdo)_2Cu^{II}_2\}(OH)_2Br_2Cr^{III}(Me_3Tacn)](ClO_4)_2\ 3CH_3CN\ .\ 0.5H_2O$ 10**

Cr(1)•••Cu(1)	3.313	Cu(2)•••Cr(2)	3.296
Cr(1)•••Cu(2)	4.377	Cr(1)•••Cr(2)	5.948
Cu(1) •••Cu(2)	3.453	Cu(1) •••Cr(2)	4.332
Cu(1)-N(42)	2.012(15)	Cu(2)-N(62)	2.139(2)
Cu(1)-N(50)	2.133(15)	Cu(2)-N(70)	2.020(2)
Cu(1)-N(52)	1.926(15)	Cu(2)-N(72)	1.932(2)
Cu(1)-O(200)	1.976(13)	Cu(2)-O(100)	1.946(14)
Cu(1)-Br(1)	2.6013(3)	Cu(2)-Br(2)	2.587(3)
Cr(1)-N(1)	2.125(2)	Cr(2)-N(21)	2.125(2)
Cr(1)-N(4)	2.117(2)	Cr(2)-N(24)	2.114(2)
Cr(1)-N(7)	2.115(2)	Cr(2)-N(27)	2.128(2)
Cr(1)-O(200)	1.976(13)	Cr(2)-O(100)	1.958(13)
Cr(1)-O(41)	1.956(14)	Cr(2)-O(51)	1.956(14)
Cr(1)-O(61)	1.951(14)	Cr(2)-O(71)	1.956(14)
		Cu(2)-O(100)-Cr(2)	115.17(7)
		Cu(1)-O(200)-Cr(1)	113.9(6)
		O(61)-Cr(1)-N(1)	172.83(6)
		O(41)-Cr(1)-N(4)	169.94(9)
		O(200)-Cr(1)-N(7)	176.67(7)

4.5 Magnetic Properties:

Magnetic susceptibility data for polycrystalline samples of the complexes were collected in the temperature range 2-290 K in an applied magnetic field of 1 T. We use the Heisenberg spin Hamiltonian in the form $H = -2J_A(S_1S_2 + S_3S_4) - 2J_B (S_1S_4 + S_2S_3) - 2J_CS_2S_4$ (for complex **9**) and $H = -2J_A(S_1S_2 + S_3S_4) - 2J_B (S_1S_4 + S_2S_3)$ (for complex **10**) for an isotropic exchange coupling with $S_1 = S_3 = S_{Fe} = 5/2$, $S_2 = S_4 = S_{Cu} = 1/2$ for **9**, and $S_1 = S_3 = S_{Cr} = 3/2$, $S_2 = S_4 = S_{Cu} = 1/2$ for **10**. The experimental data as the effective magnetic moments (μ_{eff}) versus temperature (T) are displayed in Figures 4.6 and 4.8 respectively. The experimental magnetic data are simulated using a least squares fitting computer program with a full-matrix diagonalization approach and the solid lines in Figures 4.6 and 4.8 represent the simulations. Table 4.5 summarizes intratetramer exchange parameters

The magnetic moment μ_{eff}/molecule for **9**, $Fe^{III}_2Cu^{II}_2$, of 7.24 μ_B ($\chi_M \bullet T$ = 6.55 $cm^3 \bullet K \bullet mol^{-1}$) at 290 K, is smaller than the spin only value of $\chi_M \bullet T$ (g = 2) for a unit composed of noninteracting $[Fe^{III}_2Cu^{II}_2]$ ions is 10.25 $cm^3 \bullet K \bullet mol^{-1}$ and increases monotonically with decreasing temperature until it reaches a value of 8.2 μ_B ($\chi_M \bullet T$ = 8.41 $cm^3 \bullet K \bullet mol^{-1}$) at 5 K and then starts to decreases and reaches a value of 7.02 μ_B ($\chi_M \bullet T$ = 6.15 $cm^3 \bullet K \bullet mol^{-1}$) at 2 K. Hence the molecule appears to have a high-spin ground state, with the low temperature decrease assigned to some contribution from zero-field splitting (D). This temperature dependence behavior is in agreement with a non diamagnetic ground state, is evidenced from the μ_{eff} value at 2 K.

From the temperature dependence of the magnetic behavior of complex **9,** it can be thought of ferromagnetic exchange interaction between the spin carriers but this kind of nature is also possible due to the presence of different competing spin interactions. The total spin (S_T) values of the different resultant states range from 0 to 6. For a molecule such as **9** with very low symmetry, different exchange parameters J_{ij} are theoretically required for each possible pairwise exchange interactions between $Fe^{III}...Cu^{II}$, $Cu^{II}...Cu^{II}$ and $Fe^{III}...Fe^{III}$ centers. In such a case, the determination of different J parameters would yield unreliable and correlating values. The exchange parameters between the "*wing-tip*" Fe(III) is assumed to be zero given the large distance between Fe(1) and Fe(1A) [5.442 Å]. There are two different kinds of exchange interactions between the "*wing-tip"* Fe(III) and "*body*" Cu(II) centers. Inspection of the molecular structure of **9** reveals that there are three main exchange pathways.

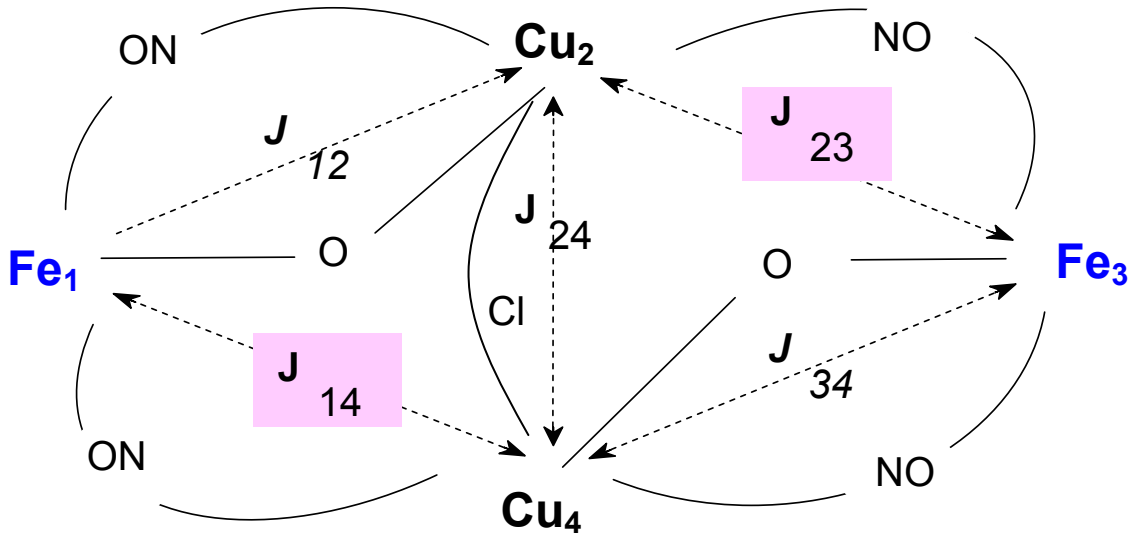

Figure 4.5: Perspective view of coupling scheme. ($J_A = J_{12} = J_{34} = J_{wb}$, $J_B = J_{23} = J_{14} = J_{wb'}$, $J_C = J_{24} = J_{bb}$)

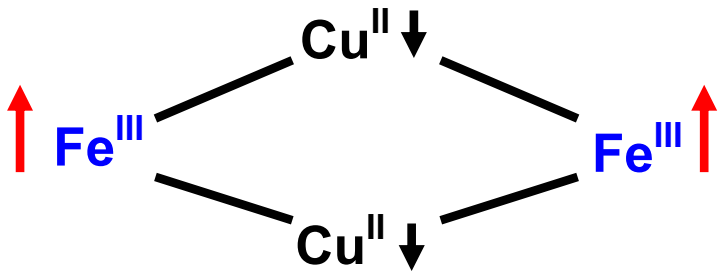

Scheme 1

The first exchange pathway $J_A = J_{12} = J_{34}$ (J_{wb}) refers to the $Fe^{III}(O)(NO)Cu^{II}$ interaction, second one, $J_B = J_{14} = J_{23}$ ($J_{wb'}$) refers to the $Fe^{III}(NO)Cu^{II}$ interaction and the third pathway $J_C = J_{24}$ (J_{bb}) refers to the $Cu^{II}(Cl)Cu^{II}$ interaction. So the magnetic exchange coupling (J_A) between iron (III) and copper(II) is mediated through different bridges [a two atom N-O bridge and through oxo bridge], on the other hand the magnetic exchange coupling (J_B) between iron (III) and copper(II) is mediated through a two atom N-O bridge. It is to be noted here that the dominated exchange interaction pathways are via the μ_2-O^{2-} groups not the oximate (N-O) transmitters. So from the magnetochemical view point, only three J values are required: $J_A = J_{wb} = J_{12} = J_{34}$, $J_B = J_{wb'} = J_{14} = J_{23}$ and $J_C = J_{bb} = J_{24}$; where w = wing-tip and b = body. The full-matrix diagonalization of the spin

Hamiltonian matrix produced best fit parameters: $J_A = J_{12} = J_{34} = -125\ cm^{-1}$; $J_B = J_{14} = J_{23} = -6\ cm^{-1}$ and $J_{24} = -50\ cm^{-1}$ with $g_1 = g_3 = 2.01$ and $g_2 = g_4 = 2.04$. So, the data for complex **9** is analyzed with a "three-J" model. The exchange coupling between the high spin iron(III) and copper(II) is antiferromagnetic on the basis of Goodenough-Kanamori[33] rules. In the analysis, two different iron(III)-copper(II) magnetic exchange interactions are taken into consideration. The exchange coupling is expected to be much stronger in case of J_A compared to J_B, due to the presence of an oxo transmitter. In the past some authors have proposed an oxide ligand as possibly mediating the antiferromagnetic coupling in the heme-copper site for the fully oxidized enzyme. It has been reported[34] that all oxo-and hydroxo bridged $Fe^{III}Cu^{II}$ adducts exhibit strong antiferromagnetic coupling. In general, oxo bridged dinuclear $Fe^{III}Cu^{II}$ core of compounds exhibit near linear Fe-O-Cu linkage, which makes favourable overlap between the magnetic orbitals and is reflected in strong antiferromagnetic exchange interactions. Magnetic exchange interaction parameters of these kind of complexes are listed in Table 4.3.

Table 4.3: Magnetic parameter of some $Fe^{III}(O)Cu^{II}$ cores

Compounds	Magnetic core	$J_{Fe(III)...Cu(II)}$ [cm^{-1}]	Fe-O-Cu (bond angle in deg.)	References
[(F_8TPP)Fe-O-Cu(TMPA)]$^+$	**$Fe^{III}Cu^{II}$**	**- 174.0**	**178**	**34c**
[(OEP)Fe-O-Cu(Me_6tren)]$^+$	**$Fe^{III}Cu^{II}$**	**≥ - 200.0**	**180**	**34f**
[(L)Fe-O-Cu]$^+$	**$Fe^{III}Cu^{II}$**	**> - 200.0**	**171**	**34g**
[(F_8TPP)Fe-OH-Cu(TMPA)]$^{2+}$	**$Fe^{III}Cu^{II}$**	**- 144.0**	**157**	**34b**
[(OEP)Fe-O-Cu(Me_5tren)(ClO_4)]$^+$	**$Fe^{III}Cu^{II}$**	**- 170.0**	**157**	**34d**

The environment around the Cu(II) ions in complex **9** is square pyramidal which is observed from the structural parameters, with an unpaired electron in the $d_{x^2-y^2}$ orbital. Thus the strong magnetic interactions can be interpreted as the symmetry allowed $Fe(d_{x^2-y^2}) \,||\, (O) \,||\, Cu(d_{x^2-y^2})$ (using Ginsberg symbols) σ-superexchange pathway. The $d_{x^2-y^2}$ magnetic orbitals of Fe^{III} and Cu^{II} ions also interact through the oximato (NO) group, and the strong magnetic interaction is expected as the symmetry allowed $Fe(d_{x^2-y^2}) \,||\, \sigma_{NO} \,||\, Cu(d_{x^2-y^2})$ pathway. The overall exchange coupling constant J results from individual antiferromagnetic and ferromagnetic exchange interactions: $J = J_{AF} + J_F$. The

ferromagnetic contributions provided by the $d_{x^2-y^2} \perp \sigma_{NO} || t_{2g}$ exchange paths can not balance the dominant antiferromagnetic interaction, leading to an effective antiparallel spin coupling between Fe^{III} and Cu^{II} centers. The following diagram shows the orientation of the relevant orbitals for the mechanism of interaction.

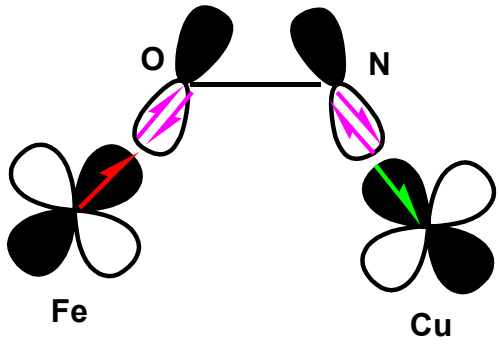

The reported antiferromagnetic exchange coupling between iron (III) and copper(II) through oxo transmitter in case of synthetic models for heme copper oxidases[34]lie in the ranges of - 80 to - 200 cm^{-1}(based on $H = -2JS_iS_j$ model). In these heterobinuclear iron(III)-copper(II) complexes exchange interaction which mediates through oxo transmitter is found to be stronger due to the near linear arrangement, which makes the Fe-O-Cu angle of nearly 180°. In case of complex **9,** it is observed that the Fe-O-Cu bond angle is 118.46(7)°, thus the exchange coupling constant is expected to be lower compared to the values obtained in the complexes reported by Holm[34d,e] and Karlin.[34a,b,c] The oximate (N-O) group also contributes in the exchange coupling constant ($J_{wb} = J_A$) and this contribution is also antiferromagnetic in nature and thus, makes the overall exchange coupling (J_A) to be stronger in magnitude. The investigation of exchange interactions as a function of d^n- electronic configuration where a two atom N-O bridge is the transmitter, reported[11,21,31] to be in the ranges of - 40 to - 60 cm^{-1}. Some literature values of the exchange interactions mediated through oximato (NO) transmitter between high-spin Fe(III) and Cu(II) ions is listed in Table 4.4. It has been observed that, exchange coupling constant between high spin Fe(III) and Cu(II) (through N-O transmitter) is - 20 cm^{-1} in the $Fe^{III}Cu^{II}Ni^{II}$ complex[20] and even is lesser in magnitude (- 5 cm^{-1}) in the $Fe^{III}Cu^{II}Cu^{II}$ complex reported by Verani et.al.[19] So in case of complex **9** strong antiferromagnetic coupling ($J_A = J_{12} = J_{34}$) between Fe^{III}-Cu^{II} (through oxo and oximate bridges) predominates over antiferromagnetic exchange coupling ($J_B = J_{14} = J_{23}$), and the values obtained from simulation is comparable to the values reported earlier.

Table 4.4: Magnetic parameters of $Fe^{III}Cu^{II}$ oximate complexes

Compounds	Magnetic core	$J_{Fe(III)...Cu(II)}$ [cm^{-1}]	References
$[(Me_3Tacn)Fe^{III}\{(dmg)_3Cu^{II}\}Fe^{III}(Me_3Tacn)](ClO_4)_2$	$Fe^{III}Cu^{II}Fe^{III}$	- 42.0	18
$[(Dopn)Cu^{II}(OH_2)Fe^{III}(Cl)(Me_3Tacn)](ClO_4)_2$	$Cu^{II}Fe^{III}$	- 38.8	16
$[(Me_3Tacn)Fe^{III}(Cl)Cu^{II}(MeOH)Ni^{II}(MeOH)_2L_{ox}](ClO_4)_2$	$Fe^{III}Cu^{II}Ni^{II}$	- 20.0	20
$[(Me_3Tacn)Fe^{III}(Cl)Cu^{II}(H_2O)Cu^{II}(H_2O)L_{ox}](ClO_4)_2$	$Fe^{III}Cu^{II}Cu^{II}$	- 5.0	19
$[(Me_3Tacn)Fe^{III}Cu^{II}(PyA)_3](ClO_4)_2$	$Fe^{III}Cu^{II}$	- 53.0	21

The exchange coupling between the "body" copper (II) ions was evaluated to be - 50 cm^{-1}, mediated through μ_2-Cl bridge. The magnetic properties of a number of bis (μ-chloro) copper(II) dimers have been studied and most of them exhibit antiferromagnetic spin coupling. For the dichloride bridged dicopper(II) system, an empirical relationship has been developed between the exchange coupling constant and φ / R (φ is the Cu-Cl-Cu angle and R is the longer Cu-Cl separation). According to the relationship, the antiferromagnetic interaction would become more significant with increasing φ / R (when φ / R > 33).[41] However copper(II) compounds with a monochloride ion bridge are very few and there is no magnetostructural relationship developed. In the present case the two body copper atoms bridged by a chloride ion (φ / R = 34.6), are in axial position and due to the square pyramidal environment of copper(II) ions, the unpaired electron resides in copper ions mainly in the $d_{x^2-y^2}$ orbital. According to the orbital overlap between copper ions and the bridging chloride ligand, a weak coupling is expected. Weak ferromagnetic to strong antiferromagnetic exchange coupling interactions through μ-chloro bridge ligand are reported in literature.[42] Hendrickson and co-workers pointed out that the value of J_{wb} can be well determined, but the value of J_{bb} not. Since J_{wb} is much stronger than J_{bb} and there are four "*wing-body*" interactions (two J_{wb} and two $J_{wb'}$) and only one J_{bb}, the spin-manifold energies are primarily determined by "*wing-body*" interactions, making the precise value of J_{bb} indeterminate. Tetranuclear $Fe^{III}_2Cu^{II}_2$ "*butterfly*" complex is regarded as an example exhibiting spin frustration. The strong antiferromagnetic "*wing-body*" interactions frustrate the weaker "*body-body"* interaction leading to the S_T = 4 ground state via the spin alignments shown pictorially in scheme1 i.e., the Cu^{II}(body) spins are polarized ferromagnetically, although the intrinsic interaction between these ions is antiferromagnetic. Competing interactions are evidently not limited to triangular

topologies. They occur in all cases where there is a competition between different exchange interactions. In a certain sense the uncertainty in body-body interaction is the mathematical response to this competition between antagonist factors. It should be remembered that the topology sometimes creates a ferromagnetic polarization between two antiferromagnetically coupled spin carriers. The competition between these two opposite forces may lead to ground states that can not be described in the simple fashion of combining the local spins assimilated to classical vectors.

To determine the spin ground state, magnetization data were collected at 1, 4 and 7 T in the temperature range 2-290 K and plotted as reduced magnetization (M/Ngβ) vs (βH/kT) (*vide infra*), where N is the avogadro's number, β is the Bohr magneton and k is the Boltzmann's constant. For a system occupying only the ground state and experiencing no zero-field splitting (D), the various isofield lines would be superimposed and M/Ngβ would saturate at a value S_T. The non-superposition of the variable temperature variable field (VTVH) plots at low temperature clearly indicates the presence of zero-field splitting (ZFS or D). Reduced magnetization measurement yielded a ground state $S_T > 3$ but < 4. According to the spin coupling scheme ground state $S_T = 4$ could be expected, but $S_T < 4$ could be due to the intermolecular interaction or zero-field splitting (D) of the ground state.

Attempts to fit the data by using the method of full-matrix diagonalization of the spin Hamiltonian matrix including axial ZFS, with the pairwise exchange interactions, produced best fit parameters: $J_{wb} = J_A = J_{12} = J_{34} = -125.0$ cm^{-1}, $J_{wb'} = J_B = J_{14} = J_{23} = -5.0$ cm^{-1}, $J_{bb} = J_C = -50$ cm^{-1} with $D_{Fe} = +2.7$ cm^{-1}. With $D_{Fe} = -2.7$ cm^{-1} (fixed) a fit with poorer quality than that with positive D was obtained. The values of zero field splitting, $D_{Fe} = +2.7$ cm^{-1} from the best fit, is also quite similar to the value obtained ($D_{Fe} = |2.2|$ cm^{-1}) in case of $Fe^{III}Cu^{II}$ complex reported by Ross et al.[21] For comparison it is to be mentioned, that for a dinucler $Fe^{III}Cu^{II}$ complex reported[40] by Kahn et. al, observed spin Hamiltonian parameters are, $J_{Fe\text{-}Cu} = -78$ cm^{-1}, $D_{Fe} = +11.8$ cm^{-1} and $D_{S=2} = +7.8$ cm^{-1}.

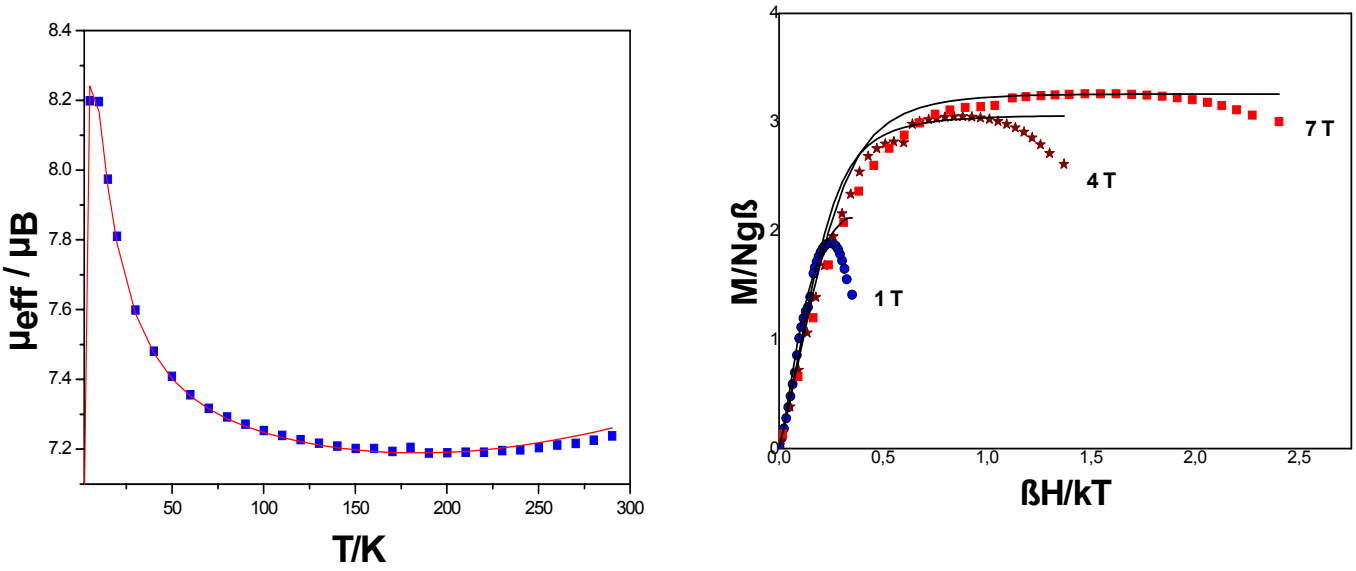

Figure 4.6: Magnetic data for $Fe^{III}_2Cu^{II}_2$ (9) plot of μ_{eff} vs T and M/Ngß vs ßH/kT. The bold points represent the experimental data while the solid line represents the simulation.

It has been shown in detail by Hendrickson[2,7-8] and co-workers that, in the case of spin frustration, subtle changes in the ratios of competing exchange interactions in a polynuclear transition metal complexes can have dramatic effects on the exact nature of the ground and low-lying states. It is the ratio of competing exchange interactions and not so much their absolute magnitudes which characterizes the electronic structure of these complexes. The ground state of the present complex represents $S_T = 4$. This result is in accord with the analysis made by Hendrickson that, when competing exchange interactions are antiferromagnetic and are of similar magnitude, the complex will have a ground state with the smallest S_T value. In the case of $Fe^{III}_2Cu^{II}_2$ "butterfly" core congener Fe...Cu and Cu...Cu interactions are not of similar magnitudes and that stabilizes a high-spin ground state, as is evidenced from the VTVH magnetic measurement.

The magnetic moment μ_{eff}/molecule for **10**, $Cr^{III}_2Cu^{II}_2$, of 4.9 μ_B ($\chi_M \bullet T$ = 3.0 $cm^3 \bullet K \bullet mol^{-1}$) at 290 K decreases monotonically with decreasing temperature until it reaches a value of 4.39 μ_B ($\chi_M \bullet T$ = 8.41 $cm^3 \bullet K \bullet mol^{-1}$) at 100 K and then starts to increases and reaches a value of 4.84 μ_B ($\chi_M \bullet T$ = 2.92 $cm^3 \bullet K \bullet mol^{-1}$) at 15

K and then finally decreases to a value of 4.58 μ_B. This temperature dependence is in agreement with a non diamagnetic ground state. This kind of temperature dependence behavior is due to irregular spin state structure. The relative energies of the low-lying states can be calculated by using obtained exchange coupling constants. The spin state structure, i.e., the energy versus spin diagram is no longer regular; the spin does not vary monotonically versus the energy. On the contrary, for J< 0, the ground state has the spin $S_T = 2$ which is presented schematically in the scheme 2. This irregularity of the spin state structure has quite drastic consequences on the magnetic behavior. The high-temperature limit of μ_{eff} is equal to the sum of the contributions of the isolated ions. When the temperature is lowered from high-temperature, the first excited state to be thermally depopulated and μ_{eff} decreases. In the low-temperature range, when only a few excited states are significantly populated, further cooling depopulates states with a spin lower than that of the ground state, and μ_{eff} increases. At very low temperature, when only the ground state is populated, μ_{eff} reaches a plateau. These high- and low temperature behaviors result in a minimum for the μ_{eff} vs. T plot. The more pronounced the antiferromagnetic interactions, the higher is the temperature of this minimum.

For a molecule such as **10** with different exchange parameters J_{ij} are theoretically required for each possible pairwise exchange interactions between $Cr^{III}...Cu^{II}$, and $Cr^{III}...Cr^{III}$ centers. The exchange parameter between the "*wing-tip*" Cr(III) is assumed to be zero given the large distance between Cr(1) and Cr(2) [5.948 Å]. Inspection of the molecular structure of **10** reveals that there are two main exchange pathways between the "*wing-tip"* Cr(III) and "*body*" Cu(II) centers. The first exchange pathway $J_A = J_{12} = J_{34}$ (J_{wb}) refers to the $Cr^{III}(O)(NO)Cu^{II}$ interaction, second one, $J_B = J_{14} = J_{23}$ ($J_{wb'}$) refers to the $Cr^{III}(NO)Cu^{II}$ interactions. So the magnetic exchange coupling (J_A) between chromium (III) and copper(II) is mediated through different bridges [a two atom N-O bridge and through oxo bridge], on the other hand the magnetic exchange coupling (J_B) between chromium(III) and copper(II) is mediated through a two atom N-O bridge. It is to be noted here that the dominated exchange interaction pathways are via the μ_2-OH^- groups not the oximate (N-O) transmitters.

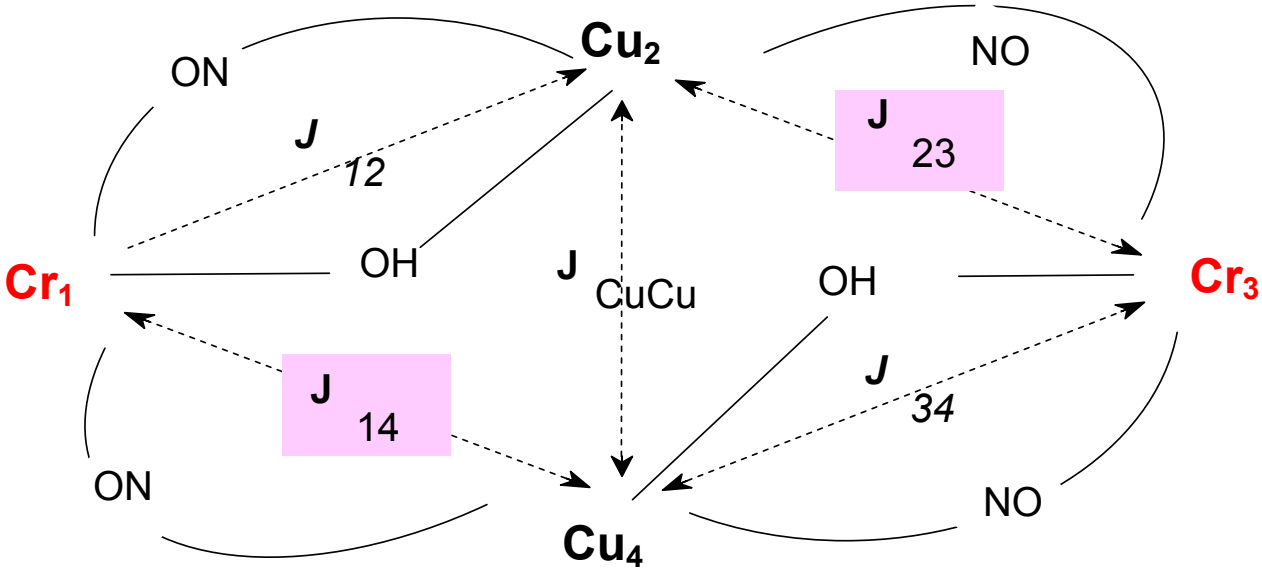

Figure 4.7: Perspective view of coupling scheme. ($J_A = J_{12} = J_{34} = J_{wb}$, $J_B = J_{23} = J_{14} = J_{wb'}$)

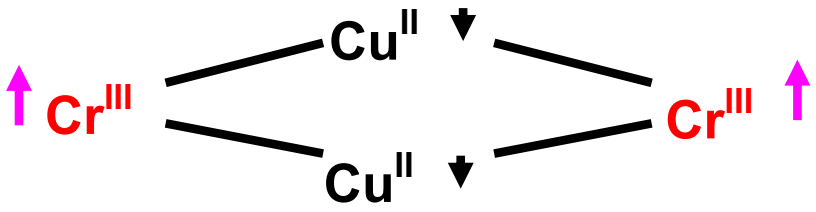

Scheme 2

So from the magnetochemical view point, only two J values are required: $J_A = J_{wb} = J_{12} = J_{34}$, $J_B = J_{wb'} = J_{14} = J_{23}$; where w = wing-tip and b = body. A good fit was obtained with $J_A = J_{12} = J_{34} = -79\ cm^{-1}$; $J_B = J_{14} = J_{23} = -17\ cm^{-1}$ with $g_1 = g_3 = 1.98$ and $g_2 = g_4 = 2.03$. So, the data for complex **10** was analyzed with a "two-J" model. The higher value of J_A compared to J_B can be explained on the basis of spin transmitter. In the model, J_A coupling transmitted through the diatomic N-O bridge and also μ_2-hydroxo group while J_B coupling transmitted only through the diatomic N-O bridge. In case of J_B the bond distance between Cr...Cu (4.38Å) is much longer compared to the J_A, where Cr...Cu bond distance is 3.3Å and gives rise to higher interaction in case of J_A compared to J_B.

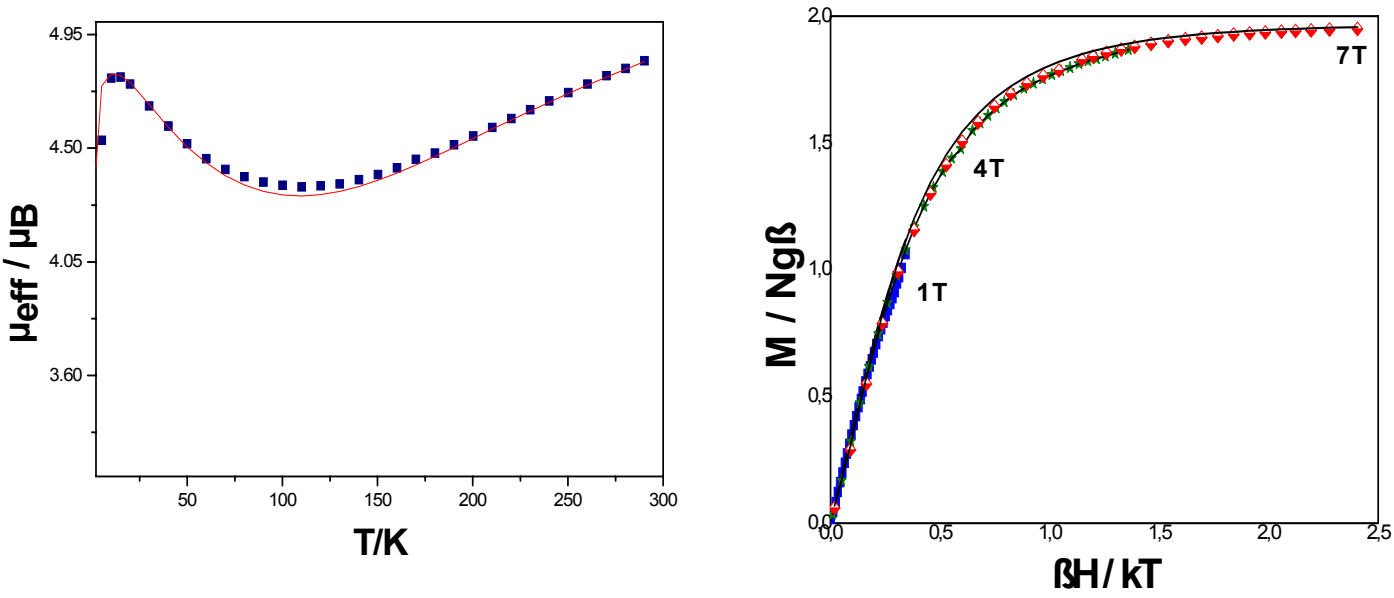

Figure 4.8: Magnetic data for $Cr^{III}_2Cu^{II}_2$ (10) plot of μ_{eff} vs T and M/Ngß vs ßH/kT. The bold points represent the experimental data while the solid line represents the simulation.

The exchange coupling between the chromium(III) and copper(II) is ferromagnetic on the basis of Goodenough-Kanamori rules. The occurrence of an antiferromagnetic interaction in **10** is unexpected on the basis of Goodenough-Kanamori rules, since a survey of the literature,[16,35-36,38-39] shows that most generally, the Cu^{II}-Cr^{III} pair has a ferromagnetic interaction with J values ranging from + 1.8 to + 52cm^{-1}(based on $H = - 2JS_iS_j$). In these complexes the equatorial coordination planes are coplanar and ferromagnetism results from strict orthogonality of the magnetic orbitals. The complex $Cr^{III}_2Cu^{II}_2$ may adopt a very low symmetry which could relax the symmetry requirements for effective overlap of the magnetic orbitals, allowing the AF contribution to be predominant. Moreover the average Cu-O-Cr angles are 114.5° which reduce the orthogonality of the magnetic orbitals and can cause a better overlap, gives rise to antiferromagnetic coupling. On the contrary to the ferromagnetic interaction between Cr^{III}-Cu^{II} pair antiferromagnetic spin interaction J = - 19.5 cm^{-1} was reported for a Cr^{III}-Cu^{II} complex based on oxime ligand.[37]

Variable temperature variable field magnetic measurements confirm the molar magnetization (M/Ngß) at 7T, is 1.95, very close to the expected saturation value of S_T = 2. The VTVH magnetic measurement was also simulated by using the method of full matrix diagonalization and from the best fit the values obtained are $J_A = J_{12} = J_{34}$ = - 79

cm^{-1}, $J_B = J_{14} = J_{23} = -17\ cm^{-1}$ with $g_1 = g_3 = 1.98$ and $g_2 = g_4 = 2.03$. These "J" and g values are exactly the same values evaluated from the susceptibility measurements at 1 T described earlier and thus confirm the credibility of the simulated parameters. The superposition of the variable temperature variable field (VTVH) plots clearly indicates the absence of zero-field splitting (ZFS or D). So unambiguously the exchange coupling parameters for this $Cr^{III}_2Cu^{II}_2$ complex are evaluated

The energy of the ground state $S_T = 2$, has arbitrarily set at zero and which is 42 cm^{-1} below the first excited state $S_T = 1$, and $S_T = 0$ state is about 67 cm^{-1} well above the ground state $S_T = 2$. Since the total spin of the first and the second excited states are $S_T = 1$ and $S_T = 0$, their population with increasing temperature reduces the effective magnetic moment of complex **10**. Population of the third excited state, $S_T = 3$ occurs around ~ 100 K, which accounts for the increase in μ_{eff} at higher temperatures. As a result a minimum is observed in the magnetic moment curve. The ground state with $S_T = 2$ results from spin frustration in a broad sense. The term spin frustration describes as an effect where the interplay of various exchange interactions in a polynuclear complex causes a net spin-vector alignment which is different from that expected upon coordination of pairwise exchange interactions.

Table 4.5: Intratetramer exchange parameters for complexes 9-10

Compounds	Magnetic core		J_{12} [cm^{-1}]	J_{23}[cm^{-1}]	J_{24}[cm^{-1}]	g_{Fe}	g_{Cr}	$g_{Cu(II)}$
9	$Fe^{III}_2Cu^{II}_2$	$J_{12} = J_{34}$	- 125.0	- 6.0	- 50.0	2.01		2.04
		$J_{14} = J_{23}$						
10	$Cr^{III}_2Cu^{II}_2$	$J_{12} = J_{34}$	- 79.0	- 17.0			1.98	2.03
		$J_{14} = J_{23}$						

336 cm^{-1} - - - - - - $S_T = 3$

66 cm^{-1} - - - - - - $S_T = 0$

42 cm^{-1} - - - - - - $S_T = 1$

0 - - - - - - $S_T = 2$

Low-lying states of the $Cr^{III}_2Cu^{II}_2$ complex 10

4.6 References:

(1) W. H. Armstrong, M. E. Roth and S. J. Lippard, *J. Am. Chem. Soc*., 1987, **109**, 6318

(2) J. M. McCusker, J. B. Vincent, E. A. Schmitt, M. L. Mino, K. Shin, D. K. Coggin, P. M. Hagen, J. C. Huffman, G. Christou and D. N. Hendrickson, *J. Am. Chem. Soc*., 1991, **113**, 3012

(3) P. Chaudhuri, M. Winter, P. Fleischhauer, W. Hasse, U. Flörke and H. J. Haupt, *Inorg. Chim. Acta.,* 1993, **212**, 241

(4) M. W. Wempel, D. K. Coggin, J. B. Vincent, J. M. McCusker, W. E. Streib, J. C. Huffman, D. N. Hendrickson and G. Christou, *J. Chem. Soc., Dalton Trans.,* 1998, 719

(5) (a) K. Wieghardt, K. Pohl, I. Jibril and G. Huttner, *Angew. Chem. Int. Ed. Engl.,* 1984, **23**, 77; (b) C. Delfs, D. Gatteschi, L. Pardi, R. Sessoli, K. Wieghardt and D. Hanke, *Inorg Chem*., 1993, **32**, 3099

(6) (a) V. L Pecoraro, *Ed. Manganese Redox Enzymes*, VCH verlagsgesellschaft, Weinheim, 1992; (b) H. Siegel, A. Siegel, *Ed. Metal Ions in Biological Systems*, Marcel Dekker, New York, 2000 vol **37**

(7) J. B. Vincent, C. Christmas, H-R. Chang, Q. Li, P. D. Boyd, J. C. Huffman, D. N. Hendrickson and G. Christou, *J. Am. Chem. Soc*., 1989, **111**, 2086

(8) E. Libby, J. M. McCusker, E. A. Schmitt, K. Folting, D. N. Hendrickson and G. Christou, *Inorg. Chem*., 1991, **30**, 3486

(9) E. Bouwman, M. A. Bolcar, E. Libby, J. C. Huffman, K. Folting and G. Christou, *Inorg Chem*., 1992, **31**, 5185

(10) M. W. Wempel, H-L. Tsai, S. Wang, J. B. Claude, W. E. Streib, J. C. Huffman, D. N. Hendrickson and G. Christou, *Inorg. Chem*., 1996, **35**, 6437

(11) P. Chaudhuri, F. Birkelbach, M. Winter, P. Fleischhauer, W. Hasse, U. Flörke and H-J. Haupt, *J. Chem. Soc., Chem. Commun.,* 1993, 566

(12) P. Chaudhuri, F. Birkelbach, M. Winter; V. Staemmler, P. Fleischhauer; W. Hasse, U. Flörke and H-J. Haupt, *J. Chem. Soc., Dalton Trans.,* 1994, 2313

(13) P. Chaudhuri, E. Rentschler, F. Birkelbach, C. Krebs, E. Bill, T. Weyhermüller and U. Flörke, *Eur. J. Inorg. Chem.,* 2003, 541

(14) O. Kahn, *Molecular Magnetism*, VCH Publishers, Weinheim, 1993

(15) F. Birkelbach, U. Flörke, H-J. Haupt, C. Butzlaff, A. X. Trautwein, K. Wieghardt, andP. Chaudhuri, *Inorg. Chem.,* 1998, **37**, 2000

(16) F. Birkelbach, M. Winter, U. Flörke, H-J. Haupt, C. Butzlaff, M. Lengen, E. Bill, A. X. Trautwein, K. Wieghardt and P. Chaudhuri, *Inorg. Chem.,* 1994, **33**, 3990

(17) C. Krebs, M. Winter, T. Weyhermüller, E. Bill, K. Wieghardt and P. Chaudhuri, *J. Chem. Soc., Chem. Commun.,* 1995, 1913

(18) P. Chaudhuri, M. Winter; P. Fleischhauer; W. Hasse, U. Flörke andH-J. Haupt, *J. Chem. Soc., Chem. Commun.,* 1990, 1728

(19) C. N. Verani, E. Rentschler, T. Weyhermüller, E. Bill and P. Chaudhuri, *J. Chem. Soc.,Dalton Trans.,* 2000, 4263

(20) C. N. Verani, T. Weyhermüller, E. Rentschler, E. Bill and P. Chaudhuri, *J. Chem. Soc., Chem. Commun.,* 1998, 2475

(21) S. E. Ross, T. Weyhermüller, E. Bill, E. Bothe, U. Flörke, K.Wieghardt and P. Chaudhuri, *Eur. J. Inorg. Chem.,* 2004, 984

(22) S. E Ross, T. Weyhermüller, E. Bill, K. Wieghardt and P. Chaudhuri, *Inorg. Chem.,* 2001, **40**, 6656

(23) C. N. Verani, E. Rentschler, T. Weyhermüller, E. Bill and P. Chaudhuri, *J. Chem. Soc.,Dalton Trans.,* 2000, 251

(24) (a) O. Kahn, *Adv. Inorg. Chem.,* 1995, **43**, 179; (b) K. S. Murray, *Adv. Inorg. Chem.,* 1995, **43**, 261

(25) F. Birkelbach, T. Weyhermüller, M. Lengen, M. Gerdan, A. X. Trautwein, K. Wieghardt and P. Chaudhuri, *J. Chem. Soc.,Dalton Trans.,* 1997, 4529

(26) A few selected examples: (a) S. Mohanta, K. K. Nanda, L. K. Thompson, U. Flörke and K. Nag, *Inorg. Chem.,* **1998**, **37**, 1465; (b) E. Colacio, J. M. Dominguez-Vera, M. Ghazi, R. Kivekäs, M. Klinga and J. M. Moreno, *Inorg. Chem.,*1998, **37**, 3040; (c) K. E. Vostrikova, D. Luneau, W. Wernsdorfer, P. Rey and M. Verdauger, *J. Am. Chem. Soc.,* 2000, **122**, 718

(27) (a) P. D. W. Boyd, Q. Li, J. B. Vincent, K. Folting, H. R. Chang, W. E. Streib, J. C. Huffman, G. Christou and D. N. Hendrickson, *J. Am. Chem. Soc.,* 1988, **110**, 8537; (b) R. Sessoli, H. L. Tsai, A. R. Schake, S. Wang, J. B. Vincent, K. Folting, D. Gatteschi, G. Christou and D. N. Hendricson, *J. Am. Chem. Soc.,* 1993, **115**, 1804; (c) D. Gatteschi, A. Caneschi, L. Pardi and R. Sessoli, *Science* 1994, **265**, 1054; (d) A. L Barra, A. Caneschi, A. Cornia, D. Fabrizi de Biani, D. Gatteschi, C. Sanggregorio, R. Sessoli and L. Sorace, *J. Am. Chem. Soc.,* 1999, **121**, 5302

(28) O. Kahn, *Chem. Phys. Let.,* 1997, **265**, 109

(29) P. Chaudhuri, *Coord. Chem. Rev*., 2003, **343**, 143

(30)V. Pavlischuk, F. Birkelbach, T. Weyhermüller, K. Wieghardt and P. Chaudhuri, *Inorg. Chem.,* 2002, **41**, 4405

(31) P. Chaudhuri, M. Winter, H. J. Kuppers, K. Wieghardt, B. Nuber and J. Weiss, *Inorg. Chem.,* 1987, **26**, 3302

(32) C. W. Glynn and M. M. Turnbull, *Transition. Met. Chem.,* 2002, **27**, 822

(33) (a) J. B. Goodenough, *Phy. Rev* 1955, **100**, 564; (b) J. Kanamori, *J. Phys. Chem. Solids,* 1959, **10**, 87

(34) (a) E. Kim, E. E. Chufan, K. Kamraj and K. D. Karlin, *Chem. Rev.,* 2004, **104**, 1077; (b) S. Fox, A. Nanthakumar, M. Wikstrom, K. D. Karlin and N. J. Blackburn, *J. Am. Chem. Soc.,* 1996, **118**, 24; (c) K. D. Karlin, A. Nanthakumar, S. Fox, N. N. Murthy, N. Ravi, B. H. Huynh, R. D. Orosz and E. P. Day, *J. Am. Chem. Soc.,* 1994, **116**, 4753 ; (d) M. J. Scot, H. H. Zhang, S. C. Lee, B. Hedman, K. O. Hodgson and R. H. Holm, *J. Am. Chem. Soc.,* 1995**, 117**, 568; (e) S. C. Lee and R. H. Holm, *J. Am. Chem. Soc.,* 1996, **115**, 11789; (f) K. E. Kaufmann, C. A. Goddard, Y. Zang, R. H. Holm and E. Münck, *Inorg. Chem.,*1997, **36**, 985; (g) H. V. Obias, G. P. F. Van Strijdonk, D-H. Lee, M. Ralle, N. J. Blackburn and K. D. Karlin, *J. Am. Chem. Soc.,* 1998, **120**, 9696; (35) M. Ohba, H. Tamaki, N. Matsumoto and H. Okawa, *Inorg. Chem.,*1993, **32**, 5385

(36) (a) H. Okawa, J. Nishio, M. Ohba, M. Todokoro, N. Matsumoto, M. Koikawa, S. Kida and D. E. Fenton, *Inorg. Chem.,*1993, **32**, 2949; (b) Z. J. Zhong, N. Matsumoto, H. Okawa and S. Kida, *Inorg. Chem.,*1991, **30**, 436; (c) Z. J. Zhong, N. Matsumoto, H. Okawa and S. Kida, *Chem. Lett.,*1990, 87; (d) Z. J. Zhong, H. Okawa, N. Matsumoto, H. Sakiyama and S. Kida, *J. Chem. Soc.,Dalton Trans.,* 1991, 497

(37) J. P. Costes, F. Dahan, A. Dupuis and J. P. Laurent, *J. Chem. Soc.,Dalton Trans.,* 1998, 1307

(38) (a) M. Ghiladi, K. B. Jensen, J. Jiang, C. J. Mckenzie, S. Morup, I. Sotofte, and J. Ulstrup, *J. Chem. Soc.,Dalton Trans.,* 1999, 2675; (b) C. Stadler, J. Daub, J. Kohler, R. W. Saalfrank, V. Coropceanu, V. Schunemann, C. Ober, A. X. Trautwein, S. F. Parker, M. Poyraj, T. Inomata and R. D. Cannon, *J. Chem. Soc.,Dalton Trans.,* 2001, 3373

(39) D. Burdinsky, F. Birkelbach, T. Weyhermüller, U. Flörke, H-J. Haupt, M. Lengen, A. X. Trautwein, E. Bill, K. Wieghardt and P. Chaudhuri, *Inorg. Chem.,*1998, **37**, 1009

(40) Y. Journaux, O. Kahn, J. Zarembowitch, J. Galy and J. Jaud, *J. Am. Chem. Soc.,* 1983, **105**, 7585

(41) (a) W.E. Marsh, K.C. Patel, W.E. Hatfield and D.J. Hodgson, *Inorg. Chem.,* 1983*,* **22**, 511; (b) S. O'Brien, R. M. Gaura, C. P. Landee, B. L. Ramakhrishna and R. D. Willett. *Inorg. Chim. Acta*., 1988, **141**, 83 and references therein.

(42) (a) F. Bentiss, M. Lagrenee, O. Mentre, P. Conflant, H. Vezin, J. P. Wignacourt and E. M. Holt, *Inorg. Chem.,* 2004*,* **43**, 1865; (b) S. K. Hoffmann, D. K. Towle, W. E. Hatfield, P. Chaudhuri and K. Wieghardt, *Inorg. Chem.,* 1985*,* **24**, 1307; (c) J. A. Carrabine and M. Sunderlingam, *J. Am. Chem. Soc.,* 1970, **92**, 369; (d) R. F. Drake, V. H. Crawford, N. W. Laney and W. E. Hatfield, *Inorg. Chem.,* 1974*,* **13**, 1246

(43) A. W. Addison, T. N. Rao, J. Reedijk and G. C. Vershcoor, *J. Chem. Soc., Dalton Trans.*, 1984, 1349

CHAPTER 5

STAR SHAPED Mn^{II}_4 AND TETRAHEDRAL Mn^{III}_4 HIGH-SPIN MOLECULES.

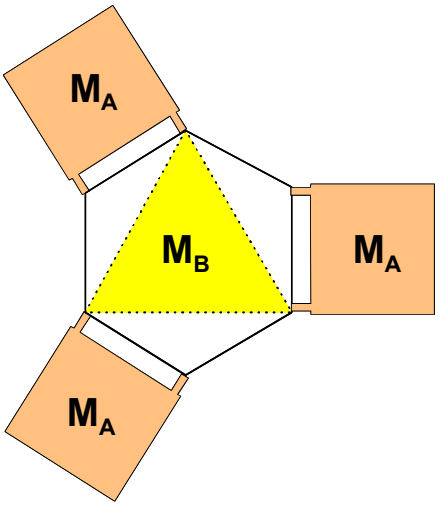

5.1 Introduction:

Polynuclear manganese clusters have received considerable interest in recent years. The interest arises, mainly due to the interesting magnetochemical properties of polynuclear complexes. One of the focuses in this respect is to achieve molecular systems with high-spin ground states via intramolecular ferromagnetic coupling or ferromagnetic-like effects, which are attractive as potential precursors to molecular magnetic materials or as single-molecule magnets (SMMs).[1-4] Another important impetus for investigating polynuclear Mn clusters lies in their biological relevance. It has become accepted that the water-oxidizing complex (WOC) of Photosystem II contains a tetranuclear manganese aggregate, although the structure has not yet been fully understood.[5] Thus far, numerous Mn_4 clusters have been reported, the core structure varying from butterfly-like, cubane-like, adamantane-like, tetrahedral, rhomboidal, linear to "pair-of-dimer", and others.[4-7] Surprisingly, the trigonal Mn_4 structure with a Mn atom at the center (centered trigonal cluster) is rare. Although the topology is rather simple and may exhibit interesting magnetic properties: the ferromagnetic interaction between the central metal ion and the apical ones would lead to an $S_T = 10$ ground state with the spin structure illustrated in Scheme 1a, while the antiferromagnetic interaction would lead to an $S_T = 5$ ground state with the spin structure illustrated in Scheme 1b. A tetranuclear Fe(III) cluster with this

simple topology and double methoxo bridges [$Fe_4(OCH_3)_6(dpm)_6$, where Hdpm = dipivaloylmethane] has been reported to behave as a single-molecule magnet[8] in which the double methoxo bridges mediate antiferromagnetic interaction to give rise to the expected S_T = 5 ground state (Scheme 1b). Herein, the structural and magnetic characterization of a Mn4 cluster that exhibits this interesting topology will be discussed. The compound, $[Mn_4(ppi)_6](BF_4)_2$ (Hppi is the Schiff base derived from 2-pyridylaldehyde and 2-aminophenol), contains the trigonal Mn(II)[(μ_2-phenoxo)$_2$Mn(II)]$_3$ cluster core in which very weak ferromagnetic interactions are operative through the double phenoxo bridges, leading to a S_T = 10 ground state not well isolated from other low-lying states.

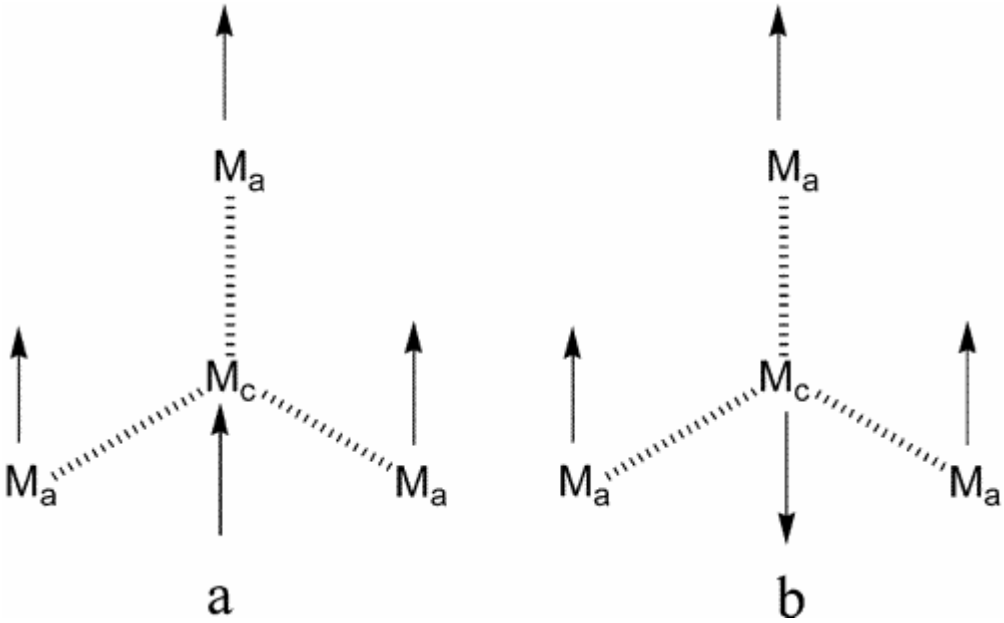

Scheme 1

5.2 Synthesis:

Synthetic clusters containing three or four or more metal centers are often obtained by *self assembly* reactions. Small variations of the reaction conditions may have a great influence on the resulting structure. Therefore well directed design is of high interest for preparative inorganic chemistry to open new ways for the synthesis of polynuclear complexes. The use of precursor complexes as building blocks establishes an accessible way to design multinuclear compounds with a defined structural arrangement. The

complex $[Mn^{II}_4(ppi)_6](BF_4)_2$ was synthesized by using the precursor complex $[Mn(ppi)_2]$, where $[Mn(ppi)_2]$ is the mononuclear neutral Mn^{II} complex, in which two ppi ligands chelate the manganese atom and both the phenoxo oxygen atom occupy the cis position. In the tetranuclear $[Mn^{II}_4(ppi)_6]^{2+}$ complex dication Mn(1), Mn(1A) and Mn(3) are equivalently coordinated by two deprotonated Hppi ligands leading to N_4O_2 donor set. The environment of the central Mn(2) is formed by coordination of the three $[Mn(ppi)_2]$ fragments resulting in a phenoxo bridged *star-shaped* Mn_4O_6 core motif.

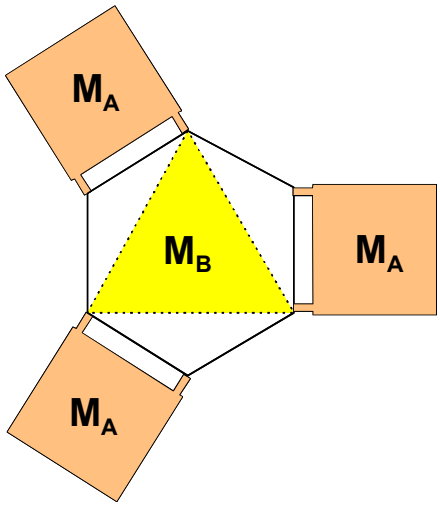

Figure 5.1: Perspective view of the star-shaped core motif

The complex $[Mn^{III}_4(salox)_4(salox\ H)_4]$ was synthesized by using the ligand salicylaldoxime ($saloxH_2$), $MnCl_2.4H_2O$ and Et_3N in 2:1:4 ratio.

5.3 Infrared and Mass Spectroscopy:

The C=N stretching band in the Mn^{II}_4 (**11**) complex is observed at 1585 cm^{-1}, while the strong N_{py} stretching band is observed at 1457 cm^{-1}. The bands at 1083 and 1061 cm^{-1} corresponds to the stretching frequency of B-F, confirms the presence of BF_4 anion as the counteranion in the molecule.

The C=N stretching band in the Mn^{III}_4 (**12**) complex is observed at 1598 cm^{-1}, while the sharp O-H stretching band is observed at 3422 cm^{-1} and the band at 2900 cm^{-1} confirms the hydrogen bonded OH...O core, which is also evidenced from the single-crystal X-ray structure. The NO stretchings for the "*tetrahedral*" Mn^{III}_4 complex are observed at 1152 and 1122 cm^{-1}.

The manganese containing complex Mn^{II}_4 (**11**) provide signals in the ESI mass spectrum which allow unambiguous characterization of the complex. The base peak at 701 is due to the dipositively charged species $[M\text{-}2BF_4]^{2+}$. The peak due to monocation $[M\text{-}BF_4]^+$ (10% intensity) is also observed. Similarly for the Mn^{III}_4 (**12**) complex the peak due to [M-2(salox H)]$^+$ corresponds to the base peak and the peak due to $[Mn^{III}_4(salox)_4(salox\ H)_4]$ is also observed with 10% intensity.

5.4 Solid State Molecular Structure:

5.4.1 Structure of tetranuclear "High Spin Molecule" with a Star-Shaped Mn_4O_6 core motif (11)

The molecular geometry and atom labeling scheme of the dication are shown in Figure 5.2. The crystallographic analysis of the complex revealed that the structure of **11** consists of a dicationic tetranuclear Mn(II) cluster with $[Mn_4(ppi)_6]^{2+}$, with tetrafluoroborate ions as counteranions, two acetonitrile molecules and one water molecule as solvents of crystallization. A perspective view of the cluster is shown in Figure 5.2 with selected bond distances and angles listed in Table 5.1.

The tetramanganese cluster contains a $Mn^{II}[(\mu_2\text{-}O)_2Mn^{II}]_3$ trigonal core with a Mn atom (Mn2) at the center and three Mn atoms (Mn1, Mn1A, Mn3) at the apexes and lies on a crystallographic 2-fold axis that passes through Mn2 and Mn1. Each of the apical Mn(II) ions is ligated by two deprotonated ppi ligands, which are tridentate via the pyridyl nitrogen, imine nitrogen, and phenolate oxygen atoms, to complete a highly distorted octahedral MnN_4O_2 coordination sphere. Although Mn1 and Mn3 are crystallographically independent, their bond distances and angles are more or less similar. As expected, the Mn-N distances [2.214(2)-2.337(2) Å] are longer than the Mn-O distances [2.138(14)-2.144(14) Å]. The pyridine nitrogen atoms N(1) and N(21) exhibit the longest distances to Mn(1) [2.288(2)-2.313(2) Å]. The three donor atoms of each ligand occupy the meridional positions around the metal ion and form two five-membered chelate rings, imposing very large angular distortions upon the coordination environments: the N(pyridyl)-Mn-N(azomethine) and O(phenoxo)-Mn-N(azomethine) bite angles of the ligands are restricted to values smaller than 74°. The bond angles of cis O(15)-Mn1-N(8), N(8)-Mn(1)-N(1), and O(15)-Mn(1)-N(1) with values 74.26(6)°, 72.14(6)° and 142.33(6)° are indicative of a distortion of the octahedral coordination

environment of Mn(1). This can be attributed to the ligand structure that only allows for the formation of five membered chelate rings. Despite their conjugated π system, both the ligands show a distortion from planarity.

All the six ligands in the cluster are further coordinated to the central Mn(2) atom via their phenolate oxygen atoms, completing a pseudo-octahedral MnO_6 coordination environment around Mn(2), and hence, each apical Mn^{II} ion is linked to the central one through a double phenoxo bridging moiety. The distortion of the Mn(2) sphere is much less significant than that of the apical Mn^{II} spheres. The cis O-Mn(2)-O angles are in the ranges of 79.81-94.9°, and the trans angles are about 170°. The Mn(2)-O distances fall in a narrow range of 2.1695(14)-2.186(14) Å and are slightly longer than the Mn(apical)-O bond distances. Detailed examination of the bond parameters around Mn2 shows the coordination environment approaches 3-fold symmetry very closely.

The independent double μ_2-phenoxo bridging moieties in the cluster show only minor differences. The Mn-O-Mn, O-Mn(apical)-O, and O-Mn(2)-O angles are in the narrow ranges of 98.75-100.8°, 79.81-82.40°, and 78.55-80.1°, respectively, while all the Mn···Mn distances spanned by the phenoxo bridges are equal within experimental error, taking the value 3.3 Å. The structural parameters are similar to those of $[Mn^{II}_4L_6](BPh_4)_2$ and $[Mn^{II}_4L_6](ClO_4)_2$ complexes reported recently.[37]

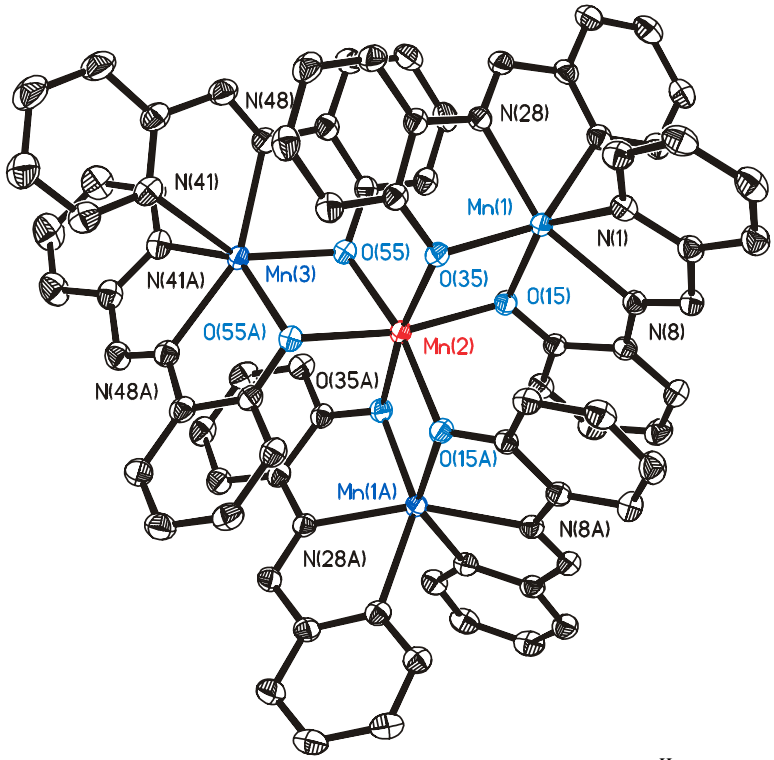

Figure 5.2: ORTEP and labeling scheme for Mn^{II}_4 (11)

Due to the presence of the 2-fold axis through the cluster, the four Mn atoms are strictly coplanar and form a centered isosceles triangle. The apical angle Mn1···Mn3···Mn1A is 61.19°, and the basal and side edge lengths are, respectively, 5.78 Å (Mn1···Mn1A) and 5.68 Å (Mn1···Mn3). The Mn(1)-O(15)-Mn(2)-O(35) bridging ring is strictly planar, which is imposed by the 2-fold symmetry, and the Mn(2)-O(55)-Mn(3)-O(55)≠ ring is also planar with the constituent atoms deviating from the mean plane by only ±0.001 Å, negligible within experimental error. The Mn(2)-O(55)-Mn(3)- O(55)≠ ring forms dihedral angles of 91.9 and 95.4 with the Mn(2)-O(55)-Mn3-O(35) ≠ and Mn(1)-O(15)-Mn(2)-O(35) rings, respectively. Therefore, the tetranuclear molecule has a propeller shape and is chiral. Neighboring molecules are related by rotations to give a heterochiral but noncentrosymmetric structure. The molecules in the crystal are well separated from each other with the shortest Mn···Mn distance between neighboring clusters being 10.34 Å.

Table 5.1*: Selected Bond Lengths (Å) and Angles (deg)* **$[Mn^{II}_4(ppi)_6](BF_4)_2 .2CH_3CN . H_2O$**

Mn(1)•••Mn(2)	3.286	Mn(3)•••Mn(2)	3.322
Mn(1)-O(15)	2.139(14)	Mn(2)-O(55)	2.17(14)
Mn(1)-O(35)	2.144(14)	Mn(2)-O(55)	2.17(14)
Mn(1)-N(28)	2.214(2)	Mn(2)-O(15)	2.181(14)
Mn(1)-N(8)	2.223(2)	Mn(2)-O(15)	2.181(14)
Mn(1)-N(1)	2.288(2)	Mn(2)-O(35)	2.186(14)
Mn(1)-N(21)	2.313(2)	Mn(2)-O(35)	2.186(14)
Mn(3)-O(55)	2.141(14)	N(50)-Mn(3)-N(42)	143.56(11)
Mn(3)-O(55)	2.247(14)	N(10)-Mn(1)-N(2)	141.7(12)
Mn(3)-N(48)	2.226(2)	O(15)-Mn(1)-O(35)	82.00(5)
Mn(3)-N(48)	2.226(2)	O(55)-Mn(3)-O(55)	79.81(8)
Mn(3)-N(41)	2.337(2)	O(55)-Mn(2)-O(55)	78.55(7)
Mn(3)-N(41)	2.337(2)	O(15)-Mn(2)-O(15)	93.68(8)
		O(55)-Mn(2)-O(15)	168.54(5)
		Mn(1)-O(15)-Mn(2)	99.07(6)
		Mn(1)-O(35)-Mn(2)	98.75(11)
		Mn(3)-O(55)-Mn(2)	100.82(6)

Mn(3)-O(55)-Mn(2)	100.82(6)

5.4.2 X-ray Structure of $[Mn^{III}_4(salox)_4\ (salox\ H)_4]\ 2.5\ CH_3OH$ (12)

The lattice is built of discrete neutral tetranuclear units and two and half methanol molecules of crystallization. The molecular geometry and atom labeling scheme of the tetranuclear unit is shown in Figure 5.3. The tetranuclear unit possesses a tetrahedral Mn^{III}_4 core. The N_{ox}-O bond lengths of average 1.343 +0.003 Å are nearly identical to those for other comparable structures and significantly shorter than 1.40 Å in general for free oxime ligands. The bond distance $C=N_{ox}$ (average 1.28Å) are expected, identical for other reported complexes.

The X-ray crystal structure depicts a cluster containing four Mn^{III} centers, each of which has a distorted octahedral coordination environment with four O and two cis N donor atoms. Each Mn^{III} center is ligated by a terminal bidentate saloxH N and O donor [those containing N(19), N(39), N(59), N(79) and four atoms (1N and 3O) of ligand [[those containing N(19), N(39), N(59), N(79)] Each of these bridging ligand joins two Mn^{III} centers through its oximate oxygen atom (μ-O); the attached nitrogen atom links this Mn-O-Mn moiety to a third Mn^{III} center (μ-ON) and the phenolate oxygen atom is bound to this Mn^{III} ion to form a six membered MnNCCCO chelate ring. The structure of the cluster is further stabilized by four intramolecular hydrogen bonds between a terminal oxime NOH group of the bidentate salox H ligand and the adjacent phenolate oxygen atom of another such ligand. The X-ray structure clearly shows that all the manganese ions are Jahn-Teller distorted, high-spin d^4 Mn^{III} ions; the axially elongated sites are occupied by the oximate nitrogen atom and oximate oxygen in μ_2-fashion with Mn(1)-N(19) = 2.261(5)Å, Mn(1)-O(70) = 2.248(4)Å, and O(70)-Mn(1)-N(19) = 168.84(18)°; Mn(2)-N(39) = 2.276(6)Å, Mn(2)-O(90) = 2.213(5)Å, and O(90)-Mn(2)-N(39) = 166.06(18)°; similarly Mn(3)-N(59) = 2.226(6)Å, Mn(3)-O(30) = 2.232(4)Å , and O(70)-Mn(3)-N(19) = 166.07(19)° ; Mn(4)-N(19) = 2.261(5)Å, Mn(4)-O(70) = 2.248(4)Å , and O(70)-Mn(4)-N(19) = 172.26(18)°. Although in oximate based polynuclear systems a two atom (N-O) bridging group between two metal centers is virtually the universal bonding mode for oximes, a monoatomic oximate-O bridging is also not very uncommon, and once again it is also supported from the X-ray structure of the Mn^{III}_4 tetrahedron core. All the oximate oxygen of the ligands are not deprotonated, four oximate oxygen atoms O(20,40,60,80) remain protonated and hydrogen bonded with the phenolate oxygen atom

of the adjacent ligand. The remaining four oximate oxygen atoms O(30,50,70,90) act as a bifurcated ligands, O(30), O(50), O(70), O(90) act as a bridge between Mn(3) and Mn(2); Mn(3) and Mn(4); Mn(4) and Mn(1); Mn(1) and Mn(2) respectively. The Mn-O_{ox} bond lengths lie in the ranges 1.96 to 2.278Å. The average Mn-$O_{phenoxo}$ bond length is 1.885(4) Å and is shorter than the Mn-O_{ox} bond distances, whereas the average Mn-N bond length is 2.135(5)Å. So the metrical parameters for the trivalent manganese ions are significantly shorter than the metrical parameters of the divalent manganese ions.

The four Mn^{III} centers of the tetranuclear cluster have a distorted tetrahedral arrangement with average Mn....Mn distances of about 3.5Å for linkage by one μ-O and one μ-ON, and about 4.1 Å for linkage by two μ-ON groups. A tetranuclear Mn^{III} cluster, albeit with a different structure, was identified in $[L_2Mn^{III}_2(\mu_3\text{-}O)_2(salox)_2(\mu_2\text{-}OOCR)_3Mn^{III}_2](ClO_4)$; the cation of which contains a butterfly arrangement of the four Mn^{III} centers formed by two edge sharing $Mn^{III}_3(\mu_3\text{-}O)$ triangular units in which deprotonated NO groups bridge the "wing" and "body" position of manganese atoms.[35d] A similar isostructural Fe^{III}_4 cluster with a tetrahedral core is also known.[20]

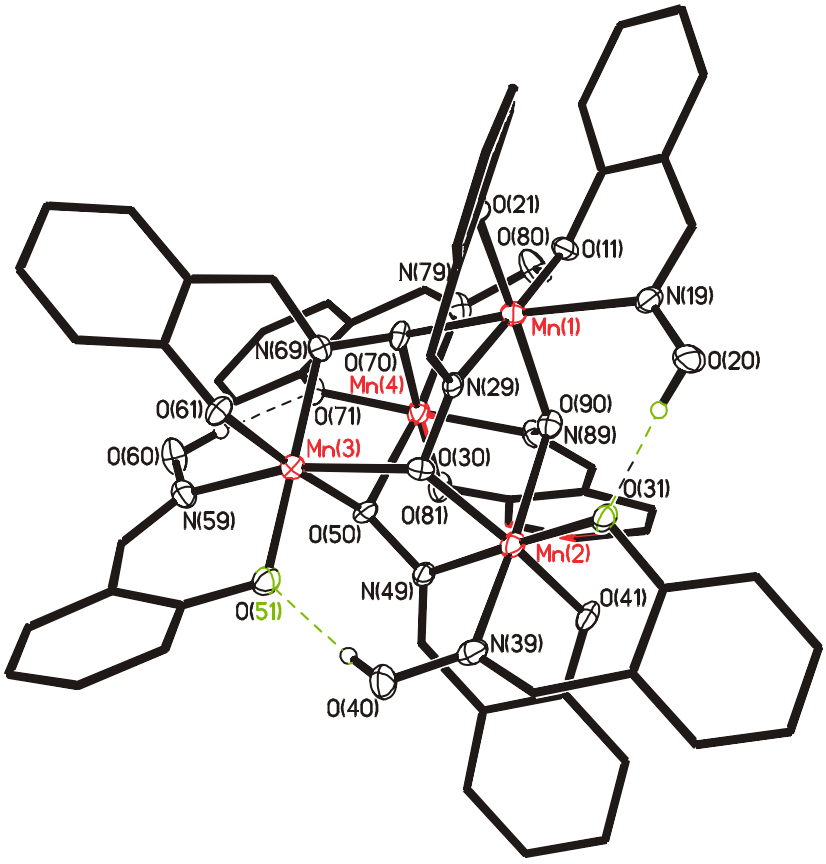

Figure 5.3: ORTEP and labeling scheme for Mn^{III}_4 (12)

There are six strong hydrogen bondings prevailing between the oximate oxygen atoms, phenoxo oxygen atoms and methanol oxygen atoms and is shown as dotted lines in the Figure 5.3. The OH...O bond distances lie in the ranges of 2.656-2.889 Å and are listed in Table 5.2A. These chemically significant hydrogen bondings are responsible for the stabilization of the tetranuclear core in cluster **12.**

Table 5.2: *Selected Bond Lengths (Å) and Angles (deg) for* **$[Mn^{III}_4(salox)_4(salox\ H)_4]$ 2.5 CH_3OH (12)**

Mn(1)•••Mn(2)	3.531	Mn(2)•••Mn(3)	3.574
Mn(3)•••Mn(4)	3.578	Mn(4)•••Mn(1)	3.584
Mn(1)-O(21)	1.869(4)	Mn(3)-O(61)	1.869(4)
Mn(1)-O(11)	1.900(5)	Mn(3)-O(51)	1.901(5)
Mn(1)-O(90)	1.967(4)	Mn(3)-O(50)	1.976(4)
Mn(1)-O(70)	2.248(4)	Mn(3)-O(30)	2.232(4)
Mn(1)-N(29)	2.035(6)	Mn(3)-N(69)	2.022(6)
Mn(1)-N(19)	2.261(5)	Mn(3)-N(59)	2.226(6)
Mn(2)-O(41)	1.867(4)	Mn(4)-O(81)	1.875(4)
Mn(2)-O(31)	1.912(4)	Mn(4)-O(71)	1.896(4)
Mn(2)-O(90)	2.213(5)	Mn(4)-O(50)	2.278(5)
Mn(2)-O(30)	1.960(4)	Mn(4)-O(70)	1.968(4)
Mn(2)-N(49)	2.012(5)	Mn(4)-N(89)	2.009(5)
Mn(2)-N(39)	2.276(6)	Mn(4)-N(79)	2.220(6)
O(70)-Mn(1)-N(19)	168.84(18)	Mn(2)-O(30)-Mn(3)	116.9(2)
O(90)-Mn(2)-N(39)	166.06(18)	Mn(3)-O(50)-Mn(4)	114.4(2)
O(30)-Mn(3)-N(59)	166.07(19)	Mn(4)-O(70)-Mn(1)	116.31(18)
O(50)-Mn(4)-N(79)	172.26(18)	Mn(1)-O(90)-Mn(2)	114.3(2)

Table 5.1A: *Selected Bond Lengths (Å) for the hydrogen bonding in the Mn^{III}_4 cluster.*

O(51)•••HO(40)	2.685	O(31)•••HO(20)	2.656
O(81)•••HO(100)	2.889	O(71)•••HO(60)	2.696

O(41)•••HO(300)	2.887	O(11)•••HO(80)	2.670

5.5 Magnetic Properties:

5.5.1 Magnetic Properties of Mn^{II}_4:

The magnetic behavior of Mn^{II}_4 is shown in Figure 5.4 in the form of the effective magnetic moments (μ_{eff}) versus temperature (T). The magnetic susceptibility was measured at 1T in the 1.95-290 K temperature range. The magnetic moment of 11.74 μ_B (χT = 17.24 emu mol^{-1} K) at 290 K is lower than the spin only value of χT = 17.5 emu mol^{-1} K expected for four isolated high-spin Mn(II) ions. The effective magnetic moment (μ_{eff}) increases monotonically with decreasing temperature until it reaches a value of 12.42 μ_B (χT = 19.31) emu mol^{-1} K at 10 K and then starts to decreases and reaches a value of 7.98 μ_B (χT = 7.99 emu mol^{-1} K) at 1.95K. This temperature dependence magnetic behavior suggests that a ferromagnetic interaction is operative through the double phenoxo bridges.

To further verify the weak ferromagnetic interaction, variable temperature variable field (VTVH) measurements have been performed at 1.95 -290K at 1, 4 and 7 T. The molar magnetizations per Mn^{II}_4 cluster in the field range of 1, 4 and 7 T are shown in Figure 5.4. When ferromagnetic coupling exists between the central and peripheral Mn(II) ions, the magnetization will saturate more rapidly than that in the uncoupled system. On the other hand, if the coupling were antiferromagnetic, the magnetization would increase less rapidly than that in the uncoupled system. In the present case of **11**, the magnetization increases more rapidly than that of the uncoupled system and saturates at 20Ngβ, confirming the ferromagnetic interaction

The analysis of the magnetic data was performed using Heisenberg-Dirac-Van Vleck (HDVV) model. The least squares fitting computer program JULIUS-F with a full matrix diagonalization approach was employed to fit the temperature and field dependent magnetization. The program uses the spin-Hamiltonian operator, $H_{total} = H_z + H_{zfs} + H_{HDVV,}$ where the exchange coupling is described by $H_{HDVV} = -2JS_{i.}S_j$, the Zeeman interactions are given by $H_z = \mu_B B g_i S_i$ and the axial single ion zero field interaction is described by $H_{zfs} = DS_z^2$. Here we use the Heisenberg spin Hamiltonian in the form $E = -2J(S_1S_2 + S_1S_3) - 2J'S_1S_4$ where $J = J_{12} = J_{13}$ and $J' = J_{14}$.

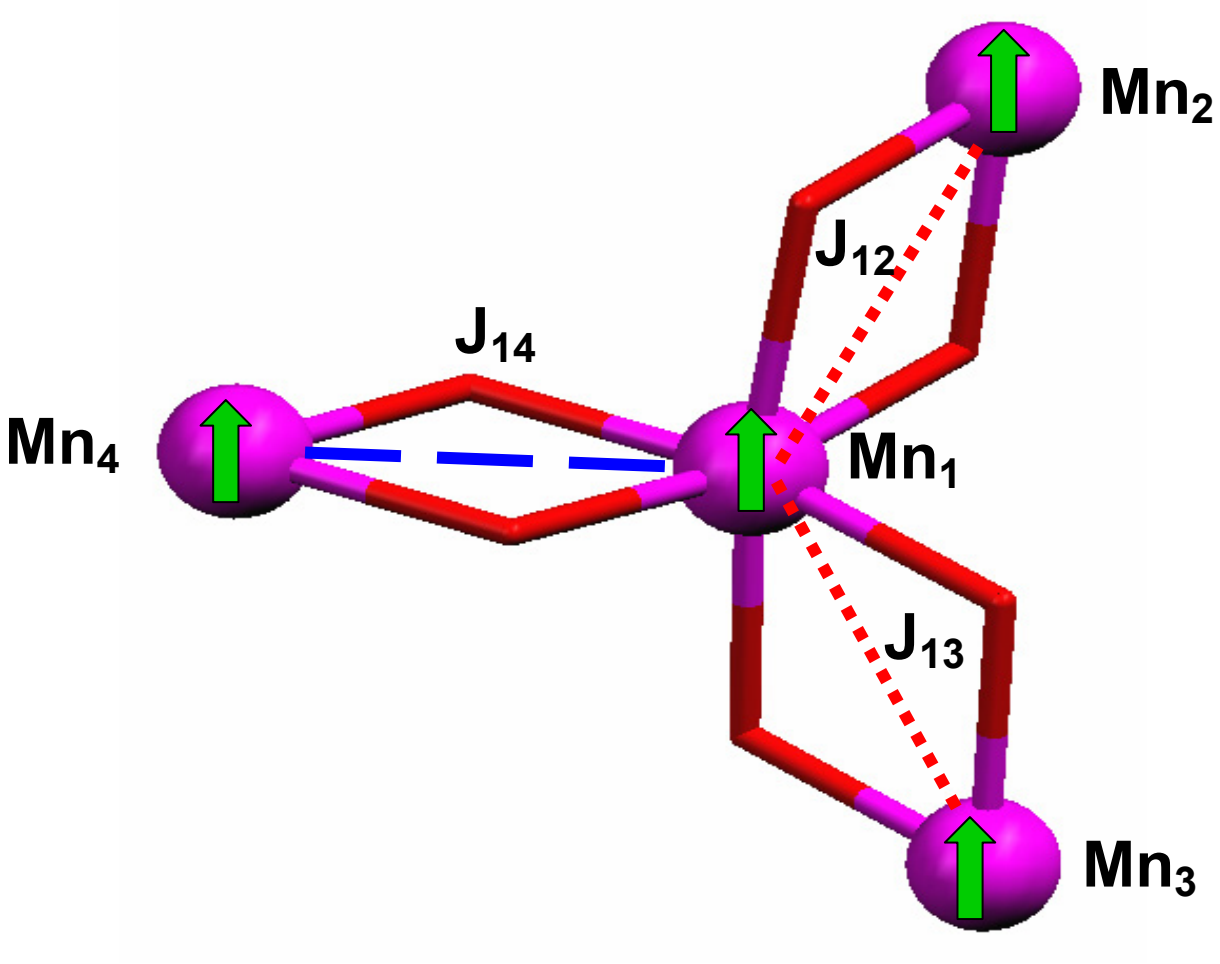

Schematic representation of exchange coupling model in the star-shaped Mn^{II}_4 core

A simulation shown as a solid line in Figure 5.4 results in $J = J_{12} = J_{13} = + 0.32$ cm^{-1} and $J' = J_{14} = - 0.2$ cm^{-1}, with $g_1 = g_2 = g_3 = g_4 = 1.98$. The experimental data can also be simulated by taking isotropic exchange interactions between the central Mn(2) and the apical Mn(1,1A, 3) centers with $J = J_{12} = J_{13} = J_{14}$ and the result obtained is $J = J_{12} = J_{13} = J_{14} = + 0.2$ cm^{-1}, $g_{Mn(II)} = 1.98$ and $\theta = - 0.2$. But the more physical solution of explaining the exchange interactions is to consider two different exchange couplings due to the variation in the average bond angles which are 98.9° [Mn(1)-O-Mn(2); Mn(1A)-O-Mn(2)] and 100.8°[Mn(3)-O-Mn(2)]. We have also extracted the exchange coupling constants by simulating VTVH measurements. The unambiguously determined parameters are $J = J_{12} = J_{13} = + 0.47$ cm^{-1} and $J' = J_{14} = - 0.19$ cm^{-1} $g_1 = g_2 = g_3 = g_4 = 1.98$. So the high-spin Mn(II) centers with S = 5/2 exhibit weak ferromagnetic coupling in the

Mn^{II}_4 molecule as is evidenced from both the magnetic susceptibility and VTVH measurements, yielding high-spin molecules with $S_T = 10$ ground state.

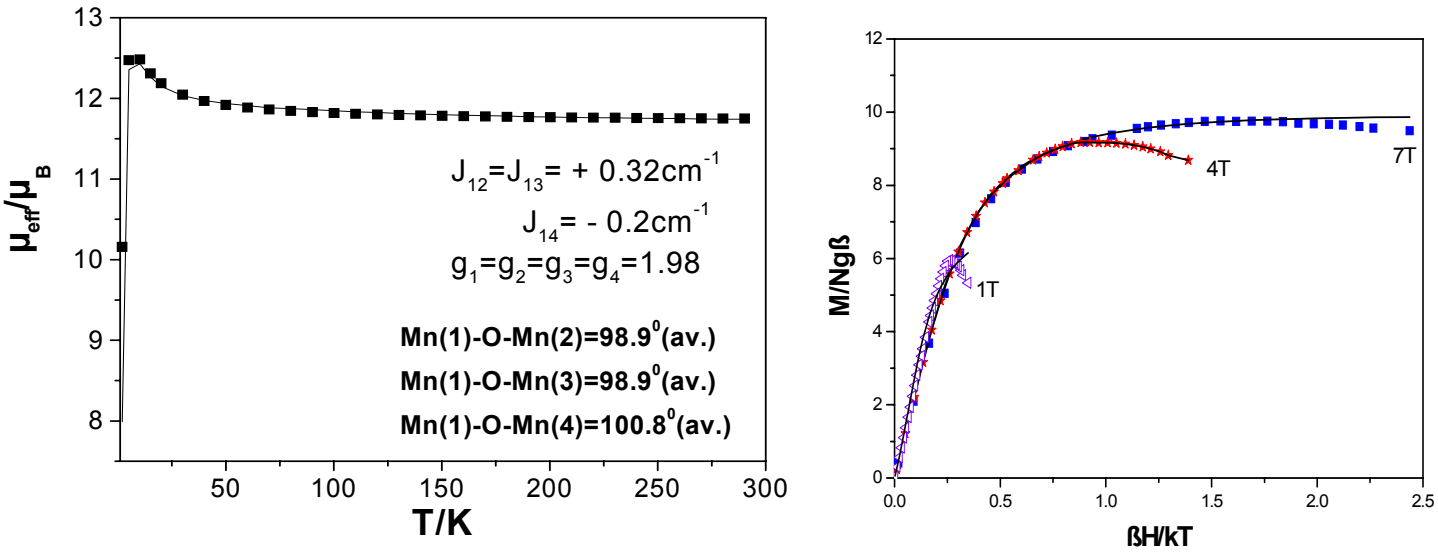

Figure 5.4: Magnetic data for Mn^{II}_4 (11) plot of μ_{eff} vs T and M/Ngß vs ßH/kT. The bold points represent the experimental data while the solid line represents the simulation.

So due to the weak exchange coupling between the Mn(II) ions, the molecule exhibits an extremely complicated low-lying structure which is not well separated from the upper-lying states, according to the Boltzmann distribution law all the excited states will be populated. Accordingly, the measured magnetization has more contributions from excited states of lower spins than from the ground spin. The above discussion is qualitatively valid, although we have ignored zero-field splitting effects. The negative value suggests that the zero-field splitting effects should cause a decrease in magnetization, so the phenomenon that the magnetization of Mn^{II}_4 increases more rapidly than that of a hypothetical uncoupled system should be due to ferromagnetic coupling between Mn(II) ions.

Sofar reported exchange interactions between high-spin Mn(II) ions are weakly antiferromagnetic, although ferromagnetic coupling between Mn(II) ions is known in one azide bridge in the -1,1 mode,[9] the ferromagnetic coupling between Mn(II) ions mediated by the phenoxo bridge in **11** is rare. For dimeric Cu(II) or Ni(II) complexes it is well known that bis(-phenoxo), bis(-alkoxo), and bis(-hydroxo) bridges can mediate overall antiferromagnetic coupling or, in the case that accidental orthogonality is achieved,

overall ferromagnetic coupling.[10-11] Good correlations between the exchange integral J and the M-O-M bridging angle have been established in case of Ni and Cu, and the magnetic interaction changes from antiferromagnetic to ferromagnetic at a certain angle (in most cases around 98°). However, magnetostructural analyses for coupled Mn(II) and Fe(III) complexes are far more difficult intrinsically due to complications arising from the larger numbers of magnetic orbitals and exchange pathways that have to be taken into account for high-spin d_5 ions.[12-13] Nevertheless, some semiempirical correlations between J and bridging parameters have been reported for diiron(III) complexes containing -phenoxo, -alkoxo, or -hydroxo bridges, suggesting that J correlates strongly with Fe-O distances whereas its dependence on the M-O-M bridging angle is very weak. It is interesting to note that nearly all these diiron(III) complexes display antiferromagnetic interactions, and only one has been reported to be ferromagnetic.[14] The authors ascribed ferromagnetic coupling mainly to the distortion of the coordination geometry based on extended Hückel MO calculations.

The number of oxygen-bridged dimanganese(II) complexes is much smaller than that of the Fe(III) analogues, probably due to the tendency of Mn(II) to be oxidized. A number of dimanganese(II) complexes with a phenoxo bridge and one or two other bridges (frequently carboxylato groups) have been reported,[15-16] among which all the magnetically characterized species were found to exhibit antiferromagnetic intramolecular interactions with $-J < 10$ cm^{-1}. For (μ-phenoxo)bis(μ-carboxylato)dimanganese(II) complexes, Dubois et al. established recently a rough linear magnetostructural correlation between the J value and the average Mn-O(phenoxo) distance (d_{Mn-O}), and the general trend is - J decreasing as d_{Mn-O} increases.[16a] Some dimanganese(II) complexes with the bis(μ_2-phenoxo), bis(μ_2-alkoxo), or bis(μ_2-hydroxo) bridge have also been reported.[17-19] While most of them exhibit antiferromagnetic coupling (- J <10 cm^{-1}) with d_{Mn-O} = 2.07-2.16 Å, only a bis(μ_2-alkoxo) complex and a bis(μ_2-phenoxo) complex, both with d_{Mn-O} = 2.15 Å, have been found to exhibit weak ferromagnetic interactions (J = + 1.0 and + 0.8 cm^{-1}, respectively).[19] In the present ferromagnetic bis(μ_2-phenoxo)-bridged Mn^{II}_4 complex, the Mn-O distances are between 2.14 and 2.19 Å. Apparently, with these limited data it is impossible to deduce a correlation between the nature of the coupling and d_{Mn-O} for these complexes. We also compared these complexes in terms of the Mn-O-Mn bridging angle (87-103°) and the Mn···Mn distance (2.98-3.37Å), and no simple magnetostructural correlation is evident concerning the nature and magnitude of the magnetic coupling. However, close

inspection into structural data reveals that the metal environments in the ferromagnetic species are highly distorted from octahedral. Similar distortion occurs for the ferromagnetic bis(μ_2-alkoxo)dimanganese(II) complex,[19a] while the ferromagnetic bis(μ_2-phenoxo)dimanganese(II) complex exhibits more significant distortion: the chelating carboxylato group dictates a very small cis angle of 55°, and the four largest angles lie in the narrow 133-140° range.[19b] It is difficult to distinguish the cis and trans angles in such a structure. On the other hand, the antiferromagnetic species exhibit relatively small distortion. The largest distortion was observed for $[Mn(SALPS)]_2$ {SALPS = N,N'-[1,l'-dithiobis-(phenylene)]bis(salicy1ideneaminato)}[18a] in which the largest cis and the smallest trans angles are 108 and 153°, respectively. Although the data available are limited, the above observation may suggest that the nature of magnetic coupling in this class of complexes correlates with the distortion of the coordination geometry. Perhaps the distortion, in conjunction with other factors, dictates a proper relative orientation for the interacting magnetic orbitals so that accidental orthogonality is achieved.

5.5.2 Magnetic Properties:

Magnetic susceptibility data for polycrystalline samples of the complex **12** were collected in the temperature range 2-290 K in an applied magnetic field of 1 T. The experimental data as the effective magnetic moments (μ_{eff}) versus temperature (T) are displayed in Figure 5.5. The experimental magnetic data were simulated using a least squares fitting computer program with a full-matrix diagonalization approach and the solid lines in Figures 5.5 represent the simulations.

The analysis of the magnetic data was performed using Heisenberg-Dirac-Van Vleck (HDVV) model. The least squares fitting computer program JULIUS-F with a full matrix diagonalization approach was employed to fit the temperature and field dependent magnetization. The program uses the spin-Hamiltonian operator, $H_{total} = H_z + H_{zfs} + H_{HDVV,}$ where the exchange coupling is described by $H_{HDVV} = -2JS_{1.}S_2$, the Zeeman interactions are given by $H_z = \mu_B B g_i S_i$ and the axial single ion zero field interaction is described by $H_{zfs} = DS_z^2$.

The magnetic moment μ_{eff}/molecule for Mn^{III}_4 (**12**) of 9.82 μ_B ($\chi_M \bullet T$ = 12.05 $cm^3 \bullet K \bullet mol^{-1}$) at 290 K increases monotonically with decreasing temperature until it reaches a value of 11.58 μ_B ($\chi_M \bullet T$ = 16.78 $cm^3 \bullet K \bullet mol^{-1}$) at 10 K and then starts to decrease with decreasing temperature and reaches a value of 6.8 μ_B ($\chi_M \bullet T$ = 5.72

$cm^3 \bullet K \bullet mol^{-1}$) at 1.95 K. This temperature dependence is in agreement with ferromagnetic interaction in the Mn^{III}_4 cluster.

The coupling model could probably require two J values, exchange pathways with "edge" coupling constants and "diagonal" coupling constants; the dominant one would be expected to be that associated with the Mn(μ-O)Mn fragment, since μ-oxo bridge Mn^{III} dimers are known to be weakly antiferromagnetic or ferromagnetic in nature.

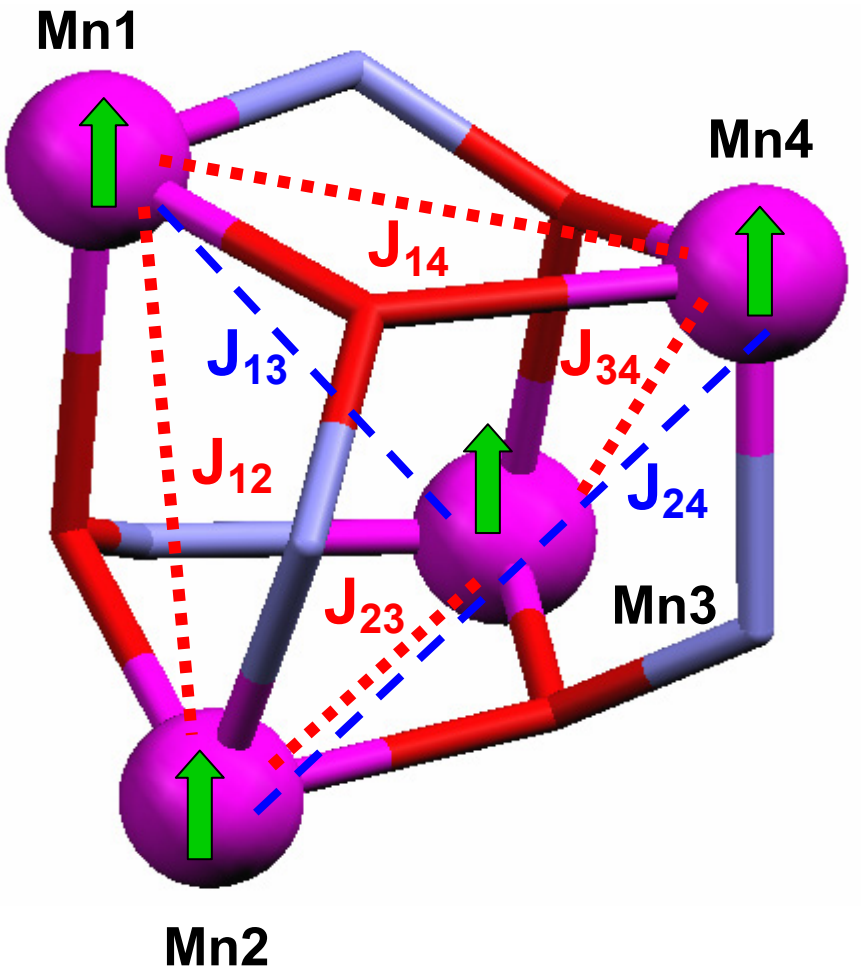

Schematic representation of exchange coupling model in the tetrahedral Mn^{III}_4 core.

Simulations of the experimental data for **12** yield two coupling constants of nearly same magnitude, but with opposite signs. In the model as shown below, J ($J_{12} = J_{23} = J_{34} = J_{14}$) represents the exchange interactions between adjacent metal ions, whereas J'($J_{13} = J_{24}$) describes interaction between the corner ions of the tetrahedral Mn^{III}_4 core. Here we use the Heisenberg spin Hamiltonian in the form $E = - 2J(S_1S_2 + S_2S_3 + S_3S_4 + S_1S_4)$ -

$2J'(S_1S_3 + S_2S_4)$. The J coupling is mediated through a combination of μ_2-NO and μ_2-O(N) groups, while the J' is mediated only through μ_2-NO group.

The nearest neighbour coupling i e., the exchange interactions between Mn(1)....Mn(2), Mn(2)....Mn(3), Mn(3)...Mn(4), Mn(4)....Mn(1) pairs, J is ferromagnetic in nature with a value of + 1.9 cm^{-1}, but the spin interactions between the diagonal Mn(III) ions, Mn(1)....Mn(3), Mn(2)....Mn(4) are antiferromagnetic with J' = - 1.6 cm^{-1}. To simulate the experimental data with an "one-J" model proved to be unsuccessful. To fit particularly the low temperature data for **12**, it is necessary to consider the single ion zero-field splitting parameter for Mn(III), $D(Mn^{III})$ during the fitting procedure. It is important to note that variations of μ_{eff} are not very sensitive to the sign of D and it is difficult, if not impossible, to determine unambiguously the sign of D from powder magnetic susceptibility measurement. From the best fit the parameters obtained are J = + 1.9 cm^{-1}, J' = - 1.6 cm^{-1}, $|D| = 3.00$ cm^{-1} and $g_{Mn}{}^{III} = 1.95$

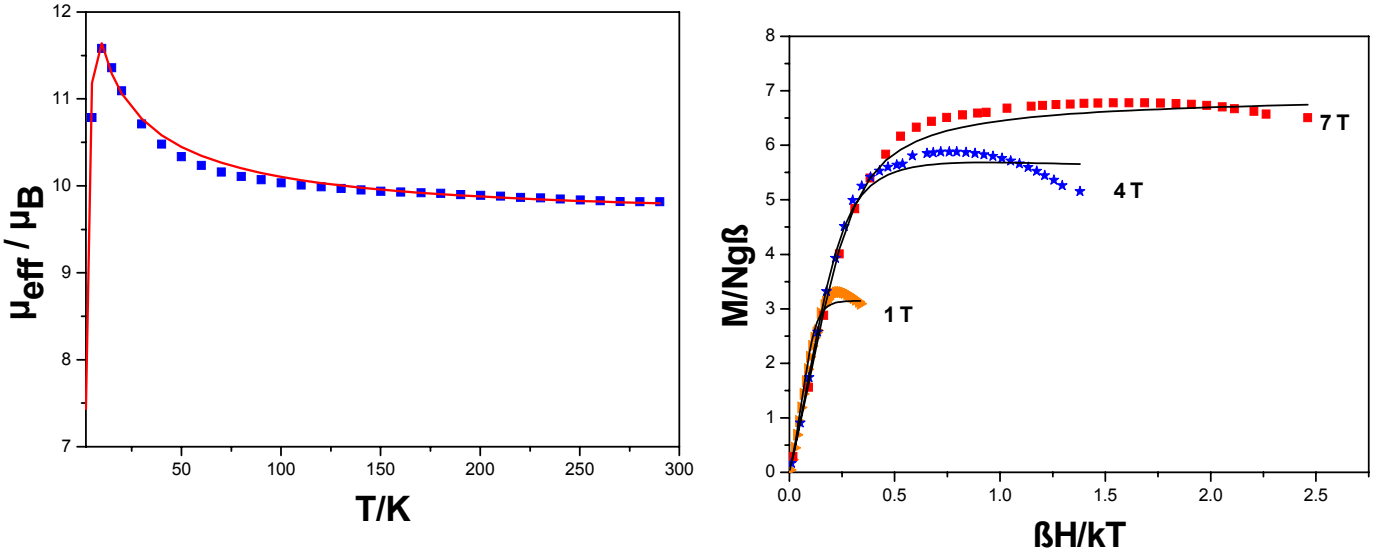

Figure 5.5: Magnetic data for $Mn^{III}{}_4$ (12) plot of μ_{eff} vs. T and M/Ngß vs. ßH/kT. The bold points represent the experimental data while the solid line represents the simulation.

To determine the spin ground state, magnetization data were collected at 1, 4 and 7 T in the temperature range 2-290 K and plotted as reduced magnetization (M/Ngβ) vs. (βH/kT) (*vide infra*), where N is the Avogadro's number, β is the Bohr magneton and k is the Boltzmann's constant. For a system occupying only the ground state and experiencing no zero-field splitting (D), the various isofield lines would be superimposed and M/Ngβ

would saturate at a value S. The non-superposition of the variable temperature variable field (VTVH) plots at low temperature clearly indicates the presence of zero-field splitting (ZFS or D). Reduced magnetization measurement yielded a ground state $S_T = 8$ Attempts to fit the data by using the method of full-matrix diagonalization of the spin Hamiltonian matrix including axial ZFS, with the pairwise exchange interactions, produced best fits with, $J = + 1.9\ cm^{-1}$, $J' = - 1.6\ cm^{-1}$, $g_{Mn} = 1.95$, $D_1 = D_3 = D_5 = D_6 = |D_{Mn(III)}| = 3.0\ cm^{-1}$. These "J" and g values are exactly the same values evaluated from the susceptibility measurements at 1 T described earlier and thus confirm the credibility of the simulated parameters. The variable temperature variable field (VTVH) plot is shown in the Figure 5.5. It should be pointed that the main source of the molecular anisotropy is due to the presence of four Jahn-Teller distorted Mn^{III} ions. The projections of these single-ion anisotropies onto the molecular anisotropy axis will determine the molecular parameter D. This above result suggests that unambiguous determination of the sign of D is not precisely possible from VTVH measurements.

A consideration of intermolecular interactions is relevant to the discussion that follows of the magnetic properties of this complex. Magnetochemical characterization reveals that the tetrahedral Mn^{III}_4 complex possesses small intramolecular ferromagnetic and antiferromagnetic interactions manifested through this μ_2-NO and μ_2-O(N) bridges. The smaller magnitude of the exchange interactions derived for **12** may result from the fact that the O-atom bridge is a μ-ON rather than a μ-oxo. It must be stressed again that when two spin carriers are bridged by several groups, identical or different, it is not possible to analyze the interaction parameter deduced from magnetic data without taking into account the phase relations between the bridges. In other terms, what is crucial for predicting the nature of the interaction is not the symmetry of each of the bridges, but the symmetry of the bridging network as a whole.

Ferromagnetic interactions between Mn^{III} ions found in a tetranuclear manganese complex reported by Christou et.al.[21] Weak ferromagnetic interaction ($J = + 1.9\ cm^{-1}$) between Mn^{III} centers are also found in an approximately square Mn^{III}_4 clusters reported by Boskovic et al,[22] and in a dinuclear manganese(III) oximate complex reported by Verani et al.[35e]

The pertinent point of the magnetic analysis and a survey of the series of Mn^{III}-polynuclear clusters are given below. It led to the combination of similarly sized antiferromagnetic and ferromagnetic interactions as shown in Figure 5.5. With the sparse data presented to date, it is not obvious why the J values have different signs, although it

is known, that J can be just positive or just negative. The Mn...Mn separation in these complexes is in the range from 3.08 to 3.26Å , while the Mn-O-Mn angles vary between 117.9 and 130.9°. Variable temperature magnetic measurement of these complexes indicate both weakly ferromagnetic and antiferromagnetic interactions between manganese(III) centers.[34](see Table 5.3). Observed weak ferromagnetic exchange coupling constant in the complex **12** with average Mn-O-Mn angle of 115° is in well accord. Table 5.4 summarizes magnetic parameters of exchange coupled manganese oximate complexes.[36]

Table 5.3: Structural and magnetic properties of Mn^{III}....Mn^{III} core congeners

Compounds	Magnetic core	Mn-O-Mn angle(in deg)	$J_{Mn(III)..Mn(III)}$ [cm^{-1}]	References
$[Mn_2O(OAc)(tmima)_2](ClO_4)_2 \cdot 2CH_3CN$	Mn^{III}-Mn^{III}	130.9	+ 1.33	23
$[Mn_2O(OAc)(bispicen)_2](ClO_4)_3$	Mn^{III}-Mn^{III}	130.8	+ 19.5	24
$[Mn_2O(O_2CC_6H_5)_2(N_3)_2(bpy)_2](ClO_4)_3$ $CH_3CN \cdot 4H_2O$	Mn^{III}-Mn^{III}	122.0	+ 8.8	25
$[Mn_2O(OAc)_2Cl_2(bpy)_2]$	Mn^{III}-Mn^{III}	124.3	- 4.1	26
$[Mn_2O(OAc)_2((HB(pz)_3)]_2 \cdot 4CH_3CN$	Mn^{III}-Mn^{III}	125.1	- 0.2	27
$[Mn_2O(OAc)_2((HB(pz)_3)]_2 \cdot CH_3CN$	Mn^{III}-Mn^{III}	125.0	- 0.7	27
$[Mn_2O(OAc)_2(tacn)_2](ClO_4)_2$	Mn^{III}-Mn^{III}	117.9	+ 9.0	28
$[Mn_2O(5\text{-}NO_2\text{-}saldien)]$	Mn^{III}-Mn^{III}	168.4	- 120.0	29
$[Mn_2O(OAc)_2(Me_3Tacn)_2](ClO_4)_2 \cdot H_2O$	Mn^{III}-Mn^{III}	120.9	+ 9.0	28
$[Mn_2O(OAc)(tppn)]_2(ClO_4)_4 \cdot 4CH_3CN$	Mn^{III}-Mn^{III}		+ 11.0	31
$[Mn_2O(OAc)(tmip)_2](ClO_4)_2$	Mn^{III}-Mn^{III}	124.4	- 0.2	30
$[Mn_2O(OAc)(ttco)_2](PF_6)_2$	Mn^{III}-Mn^{III}	122.2	+ 4.6	32
$[Mn_2O(OAc)(mpepma)_2](PF_6)_2$	Mn^{III}-Mn^{III}		+ 1.0	33
$[(Me_3Tacn)_2Mn_4(salox)_2(\mu_3\text{-}O)_2(Ph_2C(OH)COO)_3](ClO_4)$	Mn^{III}-Mn^{III}	92.8	- 7.73	35d
$[(Me_3Tacn)_2Mn_4(salox)_2(\mu_3\text{-}O)_2(Ph_3CCOO)_3](ClO_4)$	Mn^{III}-Mn^{III}		- 6.71	35d

Table 5.4: Magnetic parameters in exchange coupled manganese oximate complexes

Compounds	Magnetic core	$J_{Mn(III)..Mn(III)}$ [cm^{-1}]	References
$[(Me_3Tacn)Mn^{III}\{(dmg)_3Mn^{II}\}Mn^{III}(Me_3Tacn)](ClO_4)_2$	Mn^{III}-Mn^{III}	- 3.0	35a
$[(Me_3Tacn)Mn^{III}\{(dmg)_3Mn^{II}\}Mn^{III}(Me_3Tacn)]$	Mn^{III}-Mn^{III}	+ 2.7	35a

$(ClO_4)_2$			
$[(Me_3Tacn)Mn^{III}\{(dmg)_3Mn^{II}\}Mn^{III}(Me_3Tacn)]$	Mn^{III}-Mn^{III}	- 2.8	35a
$(ClO_4)_2$			
$[Mn_3(mcoe)_6]$ (NO_3)	Mn^{III}-Mn^{III}	- 0.6	35b
$[Mn_3(\mu_3\text{-}O)(bamen)_3]$ (ClO_4)	Mn^{III}-Mn^{III}	+ 22.3	35c
$[(Me_3Tacn)_2Mn_4(salox)_2(\mu_3\text{-}O)_2(Ph_2C(OH)COO)_3](ClO_4)$	Mn^{III}-Mn^{III}	- 0.47	35d
$[(Me_3Tacn)_2Mn_4(salox)_2(\mu_3\text{-}O)_2(Ph_3CCOO)_3](ClO_4)$	Mn^{III}-Mn^{III}	- 1.63	35d
$[(Me_3Tacn)Mn^{III}Mn^{III}(salox)_3]$	Mn^{III}-Mn^{III}	+ 6.5	35e

It is anticipated that further characterization of the system to determine more precisely the values of S_T and D and to fully elucidate the sign of the ZFS(D), alternating current susceptibility (AC) measurement or high-frequency EPR (HFEPR) techniques will be needed.

Verification of the S_T = 8 ground state and the sign and magnitudes of ZFS parameters for complex 12 • 2.5 MeOH needs to obtain by means of high-frequency EPR (HFEPR) method. This technique is ideally suited for complexes that have appreciable zero-field splitting and/or an integer spin ground state. Since the microwave energies employed (> 100 GHz) are relatively large, it is possible to observe direct transitions between the zero-field split components of the large spin ground state. HFEPR has been used to characterize the ground state of several high-spin complexes. An analysis of HFEPR spectra can give the sign and precise value for the ZFS parameters. In an ideal case, the spin ground state can be determined by simply counting the number of peaks in the fine structure, and the zero-field splitting can be evaluated from the spacing between successive peaks in the structure.

5.6 References:

1. (a) O. Kahn, *Molecular Magnetism*; VCH: New York, 1993. (b) *Magnetism: Molecules to Materials*, J. S. Miller, M. Drillon, Eds. Wiley-VCH: Weinheim, 2002.

2. (a) R. Sessoli, H-L. Tsai, A. R. Schake, S. Wang, J. B. Vincent, K. Folting, D. Gatteschi, G. Christou, D. N. Hendrickson, *J. Am. Chem. Soc*. 1993, **115**, 1804. (b) R. Sessoli, D. Gatteschi, A. Caneschi, M. A. Novak, *Nature* 1993, **365**, 141.

3. (a) C. Boskovic, E. K. Brechin, W. E. Streib, K. Folting, J. C. Bollinger, D. N. Hendrickson and G. Christou, *J. Am. Chem. Soc*., 2002, **124**, 3725 and references therein. (b) D. J. Price, S. R. Batten, B. Moubaraki and K. S. Murray, *J. Chem. Soc., Chem. Commun*. 2002, 762; (c) E. K. Brechin, C. Boskovic, W. Wernsdorfer, J. Yoo, A.

Yamaguchi, E. C. Sañudo, T. R. Concolino, A. L. Rheingold, H. Ishimoto, D. N. Hendrickson and G. Christou, *J. Am. Chem. Soc*. 2002, **124**, 9710

4. (a) E. C. Sañudo, V. A Grillo, M. J. Knapp, J. C. Bollinger, J. C. Huffman, D. N. Hendrickson, and G. Christou, *Inorg. Chem*. 2002, **41**, 2441 (b) S. M. J. Aubin, N. R. Dilley, L. Pardi, J. Krzystek, M. W. Wemple, L. C. Brunel, M. B. Maple, G. Christou, and D. N. Hendrickson, *J. Am. Chem. Soc.* 1998, **120**, 4991 (c) S. M. J Aubin, M. W. Wemple, D. M. Adams, H-L. Tsai, G. Christouand D. N. Hendrickson, *J. Am. Chem. Soc.* 1996, **118***,* 7746 (d) S. Wang, M. S. Wemple, H-L. Tsai, K. Folting, J. C. Huffman, K. S. Hagen, D. N. Hendrickson and G. Christou, *Inorg. Chem.* 2000, **39**, 1501 (e) H. Andres, R. Basler, H-U. Gudel, G. Aromi, G. Christou, H. Buttner and B. Ruffle, *J. Am. Chem. Soc.* 2000, **122**, 12469 (f) J. Yoo, E. K. Brechin, A. Yamaguchi, M. Nakano, J. C. Huffman, A. L. Maniero, L-C. Brunel, K. Awaga, H. Ishimoto, G. Christou and D. N. Hendrickson. *Inorg. Chem.* 2000, **39**, 3615

5. (a) K. N. Ferreira, T. M. Iverson, K. Maghlaoui, J. Barber and S. Iwata, *Science* 2004, **303**, 1831. (b) A. W. Rutherford, A. Boussac, *Science* 2004, **303**, 1782.(c) S. Mukhopadhyay, S. K. Mandal, S. Bhaduri, W. H. Armstrong, *Chem. Rev.,* 2004, **104***,* 3981 (d) A. Zouni, H-T. Witt, J. Kern, P. Fromme, N. Krauss, W. Saenger, and P. Orth, *Natur*e 2001, **409**, 739. (e) J. Nugent, Ed. *Photosynthetic Water Oxidation*. *Biochim. Biophys. Acta: Bioenerg*. 2001, **1503** (1-2), Special Dedicated Issue.

6. (a) T. Afrati, C. Dendrinou-Samara, C. P. Raptopoulou, A. Terzis, V. Tangoulis and D. P. Kessissoglou, *Angew. Chem., Int. Ed. Engl*. 2003, **42**, 2148 and references therein. (b) S. Mukhopadhyay, R. J. Staples, W. H. Armstrong, *J. Chem. Soc.,Chem*. *Commun*. 2002, *864* and references therein. (c) Y. Sanakis, N. Ioannidis, G. Sioros and V. Petrouleas, *J. Am. Chem. Soc.* 2001, **121**, 10766.

7. K. S. Murray, *Adv*. *Inorg*. *Chem*., 1996, **43**, 261 and references therein.

8. A. L. Barra, A. Caneschi, A. Cornia, F. F. De. Biani, D. Gatteschi, C. Sangregorio, R. Sessoli, And L. Sorace, *J. Am. Chem. Soc.* 1999, **121**, 5302

9. (a) J. Ribas, A. Escuer, M. Monfort, R. Vicente, R. Cortés, L. Lezama, T. Rojo, *Coord. Chem. Rev*., 1999, **193-195**, 1027 and references therein. (b) E.-Q. Gao, S.-Q Bai, Y.-F.Yue, Z.-M. Wang and C.-H. Yan, *Inorg. Chem*. 2003, **42**, 3642; (c) T. Karmakar, B. K. Ghosh, A. Usman, H-K. Fun, E. Riviere, T. Mallah, G. Aromi and S. K. Chandra, *Inorg. Chem*. 2005, **44**, 2391

10. (a) V. H Crawford, H. W. Richardson, J. R. Wasson, D. J. Hodgson and W. E. Hatfield, *Inorg. Chem.* 1976, **15**, 2107. (b) L. Merz and W. Haase, *J. Chem. Soc., Dalton*

Trans. 1980, 875. (c) M. Handa, N. Koga and S. Kida, *Bull. Chem. Soc. Jpn.* 1988, **61**, 3853. (d) L. K Thompson, S. K. Mandal, S. S. Tandon, J. N. Bridson and M. K.Park, *Inorg. Chem.* **1996**, **35**, 3117

11. (a) P. J. Hay, J. C. Thibeault and Hoffmann, *J. Am. Chem. Soc.* 1975, **97**, 4884. (b) J. Lorösch, U. Quotschalla and W. Haase, *Inorg. Chim. Acta.,* 1987, **131**, 229. (c) D. J. Hodgson, *Prog. Inorg. Chem.* 1975, **19**, 173. (d) K. K. Nanda, L. K. Thompson, J. N. Bridson, and K. Nag, *J. Chem. Soc., Chem. Commun.* 1994, 1337.

12. A. P. Ginsberg, *Inorg. Chim. Acta Rvu.* 1971, **5**, 45.

13. (a) R. Werner, S. Ostrovsky, K. Griesar, and W. Haase, *Inorg. Chim. Acta.,* 2001, **326**, 78 and references therein. (b) S. M. Gorun, and S. J. Lippard, *Inorg. Chem.*1991, **30**, 1625.

14. B. S. Snyder, G. S. Patterson, A. J. Abrahamson and R. H. Holm, *J. Am. Chem. Soc.* 1989, **111**, 5214.

15. (a) M. Suzuki, M. Mirukiya, S. Murata, A. Uehara, H. Oshio, S. Kida and K. Saito, *Bull. Chem. Soc. Jpn.* 1987, **60**, 4305. (b) M. Mikuriya, T. Fuji, S. Kamisawa, Y. Kawasaki, T. Tokii, and H. Oshi, *Chem. Lett.* 1990, 1181. (c) H. Sakiyama, H. Tamaki, M. Kodera, N. Matsumoto, and H. Okawa, *J. Chem. Soc., Dalton Trans.* 1993, 591. (d) M. Mikuriya, T. Fujii, T. Tokii and A. Kawamori, *Bull. Chem. Soc. Jpn.* 1993, *66*, 1675.

16. (a) L. Dubois, D-F. Xiang, X-S. Tan, J. Pecaut, P. Jones, S. Baudron, L. L. Pape, J-M. Latour, C. Baffert, S. Chardon-Noblat, M-N. Collomb and A. Deronzier, *Inorg. Chem.* 2003, **42**, 750 (b) C. Higuchi, H. Sakiyama, H. Okawa, and D. E. Fenton, *J. Chem. Soc., Dalton Trans.* 1995, 4015. (c) H. Sakiyama, A. Sugawara, M. Sakamoto, K. Unoura, K. Inoue and M. Yamasaki, *Inorg. Chim. Acta.,* 2000, **310**, 163 (d)C. Higuchi, H. Sakiyama, H. Okawa, R. Isobe, D. E: Fenton, *J. Chem. Soc., Dalton Trans.* 1994, 1097.

17. (a) M. Calligaris, D. Minichell, G. Nardin and L. Randaccio, *J. Chem. Soc. A* 1971, 2720. (b) B. Mabad, P. Cassoux, J-P. Tuchagues and D. N. Hendrickson, *Inorg. Chem.* 1986, **25**, 1420. (c) C. J. Sanders, P. N. O'Shaughnessy and P. Scott, *Polyhedron* 2003, **22**, 1617 (d) B. J. Kennedy, and K. S. Murray, *Inorg. Chem.* **1985**, **24**, 1552.

18. (a) D. P. Kessissoglou, W. M. Butler and V. L. Pecoraro, *Inorg. Chem.* 1987, **26**, 495. (b) D. J. Hodgson, B. J. Schwartz, and T. N. Sorrell, *Inorg. Chem.* 1989, **28**, 2226. (c) T. Aono, H. Wada, M. Yonemura, M. Ohba, H. Okawa, and D. E. Fenton. *J. Chem. Soc.*, *Dalton Trans*. 1997, 1527. (d) D. Coucouvanis, K. Greiwe, A. Salifoglou, P. Challen, A. Simopoulos and A. Kostikas, *Inorg. Chem.* 1988, **27**, 593. (e) , S.-B. Yu, C-P. Wang, E. P. Day and R. H. Holm, *Inorg. Chem*. 1991, **30**, 4067-4074.

19. (a) A. Gelasco, M. L. Kirk, J. W. Kampf and V. L. Pecoraro, *Inorg. Chem.* 1997, **36**, 1829 (b) H. Wada, K. Motoda, M. Ohba, H. Sakiyama, N. Matsumoto and H. Okawa, *Bull. Chem. Soc. Jpn*. 1995, **68**, 1105.

20. J. M. Thorpe, R. L. Beddoes, D. Collison, C. D. Garner, M. Helliwell, J. M. Holmes and P. A. Tasker, *Angew. Chem. Int. Ed*., 1999, **38**, 119

21. M. W. Wemple, D. M. Adams, K. S. Hagen, K. Folting, D. N. Hendrickson and G. Christou, *J. Chem. Soc., Chem. Commun*. 1995, 1591

22. C. Boskovic, R. Bircher, P. L. W. Tregenna-Piggott, H. U. Güdel, C. Paulsen, W. Wernsdorfer, A. L. Barra, E. Khatsko, A. Neels and H. Stoeckli-Evans, *J. Am. Chem. Soc*., 2003, **125**, 14046

23. K. J. Oberhausen, R. J. O'Brien, J. F. Richardson, R. M. Buchanon, R. Costa, H. L. Tsai and D. N. Hendrickson, *Inorg. Chem*, 1993, **32**, 4561

24. N. Arulsamy, J. Glerup, A. Hazell, D. J. Hodgson, C. J. Mckenzie and H. Toftlund, *Inorg. Chem*, 1994, **33**, 3023

25. J. B. Vincent, K. Foting, J. C. Huffmann and G. Christou, *Biochem. Soc. Trans.* 1988, **16**, 822

26. J. B. Vincent, H. L. Tsai, A. G. Blackmann, S. Wang, P. W. D. Boyd, K. Folting, J. C. Huffmann, E. B. Labkovsky, D. N. Hendrickson and G. Christotu, *J. Am. Chem. Soc*., 1993, **115**, 12353

27. J. E. Sheats, R. S. Czernuszewicz, G. C. Dismukes, A. L. Rheingold, V. Petrouleas, J. Stubbe, W. H. Armstrong, R. H. Beer and S. J. Lippard, *J. Am. Chem. Soc*., 1987, **109**, 1435

28. K. Wieghardt, U. Bossek, D. Ventur and J. Weiss, *J. Chem. Soc., Chem. Commun*. 1985, 347

29. C. A. Kipke, M. J. Scott, J. W. Gohdes and W. H. Armstrong, *Inorg. Chem*, 1990, **29**, 2193

30. F. J. Wu, Jr. D. M. Kurtz, K. S. Hagen, P.D. Nyman, P. G. Debrunner and V. A. Vankai, *Inorg. Chem*, 1990, **29**, 5174

31. H. Toftlund, A. Markiewicz and K. S. Murray, *Acta Chem. Scand*., 1990, **44**, 443

32. C. Bolm, N. Meyer, G. Raabe, T. Weyhermuller and E. Bothe, *Chem. Commun*. 2000, 2435

33. S. Mahapatra, T. K. Lal and R. Mukherjee, *Inorg. Chem*, 1994, **33**, 1579

34. S. Mukhopadhayay, S. K. Mandal, S. Bhaduri and W. H. Armstrong. *Chem. Rev*. 2004, **104**, 3981

35 (a) F. Birkelbach, U. Flörke, H-J. Haupt, C. Butzlaff, A. X. Trautwein, K. Wieghardt and P. Chaudhuri, *Inorg. Chem.,* 1998, **37**, 2000, (b) D. J. Price, S. R. Batten, K. J. Berry, B. Moubaraki and K. S. Murray, *Polyhedron*, 2003, **22**, 165; (c) S. Gupta and S. Pal, *Inorg. Chem*. 2002, **41**, 4843; (d) P. Chaudhuri, E. Rentschler, F. Birkelbach, C. Krebs, E. Bill, T. Weyhermüller and U. Flörke *Eur. J. Inorg. Chem.,* 2003, 541; (e) C. N. Verani, E. Bothe, D. Burdinsky, T. Weyhermüller, U. Flörke and P. Chaudhuri *Eur. J. Inorg. Chem.,* 2001, 2161

36. P. Chaudhuri, *Coord. Chem. Rev.,* 2003, **243**, 143

37 (a) N. Reddig, M. U. Triller, D. Pursche, A. Rompell and B. Krebs, *Z. Anorg. Allg. Chem*. 2002, **628**, 2458; (b) E-Q. Gao, S-Q. Bai, Z. He and C-H. Yan, *Inorg. Chem*. 2005, **44**, 677

CHAPTER-6

MIXED-VALENCE HEXANUCLEAR MANGANESE COMPLEXES OF $[Mn^{II}_2Mn^{III}_4O_2]^{12+}$ AND HEXANUCLEAR COPPER COMPLEX OF $[Cu^{II}_3O...H...OCu^{II}_3]^{9+}$ CORE CONGENERS.

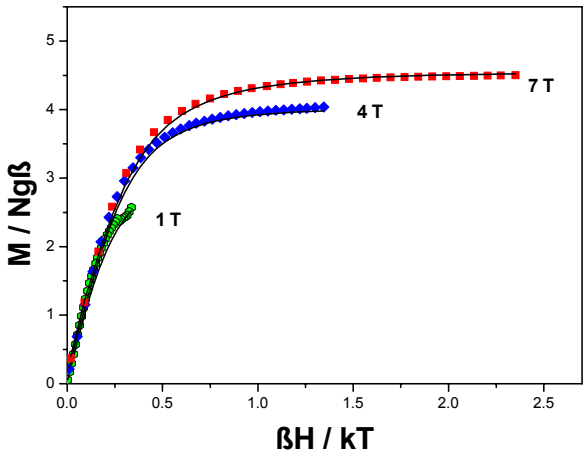

6.1 Introduction:

It has been shown previously that the oxime ligands can connect two transition metal ions, generating oxime bridged polynuclear complexes. Also the ability of the oxime functionality to efficiently transmit magnetic coupling has been well documented. A number of complexes with Cu_3O or Cu_3OH cores held by peripheral bridging ligands have been reported.[1-4] Synthetic and magnetic properties of high nuclearity (≥ 4) manganese compounds have been the focus of intense interest of research efforts in recent years. Impetus for studying the structural and physical properties of this class of molecules has come from a variety of sources including the need for bioinorganic models of the polynuclear manganese core in Photosystem II, interest in polynuclear compounds of iron, manganese, nickel as possible molecular units for the construction of magnetic materials. Large clusters of this kind also represent a new phase of magnetism that lies between the simple paramagnetism of isolated molecules and the bulk magnetism of extended lattices.

With the above areas of interest in mind some groups have synthesized a variety of polynuclear magnanese complexes and characterized them crystallographically and by several other physical techniques. Several Mn_4 compounds have been prepared, which

exhibit either a "*butterfly*" or "*distorted cubane*" structural motif and which form the basic unit of many of the higher nuclearity assemblies. Discrete complexes containing more than four metal centers are considerably fewer in number.

Continuous interest in polynuclear oxime based complexes enabled the discover yet uncommon hexanuclear mixed valence $Mn^{III}_4Mn^{II}_2$ complexes containing the structural core $[Mn^{III}_4Mn^{II}_2(\mu_4\text{-}O)_2]$. Hexanuclear compound containing the $[Mn^{II}_4Mn^{III}_2(\mu_4\text{-}O)_2]^{10+}$ core[5] which have $S_T = 0$ ground state is known, but the core in the fashion $[Mn^{III}_4Mn^{II}_2(\mu_4\text{-}O)_2]^{12+}$ is unusual and thus it's magnetic behavior is of interest and comparisons of its properties to those of the $[Mn^{III}_4Mn^{II}_2(\mu_4\text{-}O)_2]^{12+}$ core can be made.

Recent report indicates that the pathway used to obtain polynuclear arrays are based essentially on the following synthetic strategies: (i) the self-assembly method, (ii) the use of polynucleating ligands and (iii) the use of "*complexes as ligands*". On the basis of these principles, a large variety of polynuclear complexes have been synthesized and magnetostructurally characterized. So on the basis of the self assembly and using polydentate oxime two manganese hexanuclear and one copper hexanuclear complexes were isolated and magnetostructurally characterized.

6.2 Synthesis:

Complexation of the trinuclear precursor $[Mn_3O(CH_3COO)_6(H_2O)_3](CH_3COO)$ by 2,6-diacetylpyridine dioxime ligand in methanolic solution yields hexanuclear complex $[Mn^{II}_2Mn^{III}_4(\mu_4\text{-}O)_2(\mu_2\text{-}OMe)_2(dapdo)_2(dapdoH)_4](ClO_4)_2$ (**13**) and $[Mn^{II}_2Mn^{III}_4(\mu_4\text{-}O)_2(\mu_2\text{-}OH)_2(dapdo)_2(dapdoH)_4](ClO_4)_2$ (**14**) was synthesized by the complexation of $Mn(ClO_4)_2 .6H_2O$ by 2,6-diacetylpyridine dioxime where $dapdoH_2$ = 2,6-diacetylpyridine dioxime. The mechanism likely involves reaction of a $[Mn_3O]^{7+}$ unit of trinuclear complex to a $[Mn_3O]^{6+}$ species which spontaneously aggregates to **13** and **14** containing the $[Mn_6O_2]^{12+}$ core. On the other hand by using another oxime ligand (b), a hexanuclear copper (II) complex which is also composed of two Cu^{II}_3O triangular cores synthetically and magnetostructurally explored and will be discussed briefly in this chapter. The different oximes used for these hexanuclear complexes are shown on next page:

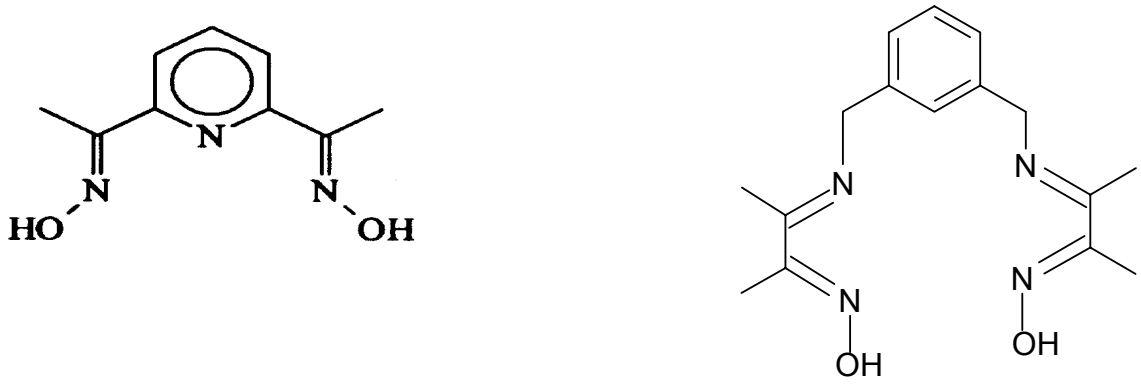

Figure 6.1: Ligands used for the hexanuclear complexes, (a) dapdoH_2, (b) LH_2

6.3 Infrared and Mass Spectroscopy:

The relevant bands in IR spectra of the complex **13** and **14** at 3425 and 2950 cm^{-1} correspond to the O-H and C-H stretching respectively in the $Mn^{III}_4Mn^{II}_2$ core. A moderately intense C=N stretching band for the ligand is observed at 1597 cm^{-1}. A notable feature of the NO stretching for **13** and **14** are the sharp bands at 1141, 1121 cm^{-1}. A sharp band around 1052 cm^{-1} is due to bridging OMe groups. Stretching bands at 624 cm^{-1} correspond to the ClO_4 unit which is the counteranion in all the two hexanuclear magnanese complexes.

Complexes **15** also shows the C=N stretching band for the ligand at 1628 cm^{-1}. Moderate peaks at 3421 cm^{-1} corresponds to the presence of O-H stretching. While the NO stretching bands for the Cu^{II}_6 complex are observed at 1121, 1089 cm^{-1}, strong peak at 1080 is due to the BF_4 counteranion.

Electrospray-ionaziation mass spectrometry (ESI-MS) in the positive ion mode has been proved to be very successful in characterizing the hexanuclear manganese and copper complexes, which show the dipositively charged species $[M\text{-}2ClO_4]^{2+}$ as the base peak for the hexanuclear manganese complexes (**14** and **15**), and the tripositively charged species $[M\text{-}3BF_4]^{3+}$ for **15.**

6.4 X-ray structure:

6.4.1 Solid State Molecular Structure of $[Mn^{II}_2Mn^{III}_4(\mu_4\text{-}O)_2(\mu_2\text{-}OH)_2(dapdo)_2(dapdoH)_4](ClO_4)_2 .6CH_3CN$ (14) :

The molecular structures of the complexes **13** and **14** are depicted in the Figures 6.3 and 6.4 respectively. Approximately equivalent views are presented to aid comparison. The labeling schemes are similar but not identical. Selected bond lengths and angles for **14**

and **13** are given in full detail in Tables 6.1 and 6.2 respectively. The structure of **14** is identical with that of **13** except for small differences in ligation for example μ-OH in **14** and μ-OMe in **13,** herein molecular structure of the complex **14** will be discussed briefly.

The structure of the complex molecule consists of a discrete dicationic hexanuclear unit; two noncordinatively bound perchlorate anions and six acetonitrile molecules as solvents of crystallization. The structure of **14** consists of six Mn atoms arranged as two "edge-sharing" tetrahedra. At the center of each tetrahedron lies a μ_4-O^{2-} ion. Peripheral ligation includes two dioxime dianions, four dioxime monoanions and two exogenous methoxide ligands for **13**, and two exogenous hydroxide ligands for **14**. Oxidation states for the manganese ions in these hexanuclear complexes are readily assigned by examining the bond distances in each manganese ion. Many compounds containing Mn(III) ions exhibit the classic Jahn-Teller distorted geometry expected for a high-spin d^4 ion, making the identification of this oxidation state for manganese straightforward. All the manganese(III) ions are six coordinate and possess distorted octahedral geometry. Charge considerations indicate a mixed valence $Mn^{III}_4Mn^{II}_2$ description and the Mn^{III} centers are assigned as Mn(1), Mn(6), Mn(3) and Mn(5) . The Mn^{II} centers are assigned as central Mn(2) and Mn(4), both the Mn^{II} centers being seven coordinate and are crystallographically equivalent as can be seen in Figure 6.3. As shown in Table 6.1, the Mn(1)-O(100), Mn(3)-O(100), Mn(3)-O(110) distances are noticeably shorter by 0.40Å than the Mn(2)-O(100) and Mn(2)-O(110) distances consistent with the higher oxidation state in Mn(1) and Mn(3). As the core structure can be thought of two similar triangular $Mn^{III}_2Mn^{II}$ units joined through μ_4-O ligation, only one triangular unit will be discussed. The Mn^{III} pair [Mn(1) and Mn(3)] are bridged by oximate-O(11) and through μ_4-O(100), whereas the $Mn^{II}Mn^{III}$ pairs [Mn(2) and Mn(3)] and [Mn(2) and Mn(1)] are bridged by [μ_4-O(100) and μ_2-OH(110)] and [[μ_4-O(100) and oximate-O(31)] respectively. In each triangular $Mn^{III}_2Mn^{II}$ unit, the Mn^{III} ions [Mn(1) and Mn(3)] have a distorted N_3O_3 coordination sphere, whereas the Mn^{II} ion [Mn(2)] has distorted N_3O_4 ligands mode. The usual coordination number of Mn(II) is 6, and since high-spin Mn(II) obtains no ligand field stabilization in either octahedral or tetrahedral environment, the geometry about the Mn is dictated by the ligand constraints. In this case, we observe a seven-coordinated Mn(II) with close to pentagonal bipyramidal geometry. The average Mn^{III}-N_{ox} bond distance is 2.245(3)Å, significantly longer than the Mn^{III}-N_{py} bond distance of 2.166(3)Å. The average Mn^{III}-O_{ox} distance of 1.938(3) Å is significantly shorter than the divalent manganese oxygen distances lying in the range 2.1-2.3 Å

(average), whereas the Mn^{III}-O(oxo or hydroxo) bond lengths are also significantly shorter ([1.875(2)Å] compared to the divalent manganese oxygen distance of 2.247(2)Å. The Mn(1)-O(100)-Mn(3) bond angle is 109.67(12)°. The X-ray structure clearly shows that the Mn^{III} ions [Mn(1) and Mn(3)] are Jahn-Teller distorted, high spin d^4 ions, the axially elongated sites are occupied by the imine nitrogen atoms of the oximate, with Mn(1)-N(2) 2.28(3) Å, Mn(1)-N(10) 2.22(3) Å and N(2)-Mn(1)-N(10) 141.7(12)°, Mn(3)-N(42) 2.37(3) Å , Mn(3)-N(50) 2.17(3) Å and N(42)-Mn(3)-N(50) 143.56(11)°.

The average Mn^{II}-N_{ox} bond distance lies in the range of 2.302(3)- 2.384(3) Å, is longer than the Mn^{III}-N_{py} bond distance of 2.313(3) Å. The average Mn^{II}-O_{ox} distance of 2.265(2) Å is significantly longer than the Mn^{III}-O_{ox} distances of 1.938(3)Å. The μ_4-O-Mn^{II} bond distance 2.247(2) Å is also significantly longer than the average μ_4-O-Mn^{III}[1.944(2)Å] bond distance. The μ_2-OH(110) which acts as a bridge between divalent Mn(2) and trivalent Mn(3), showed that the Mn(2)-O(110) bond distance of 2.203(3)Å is significantly larger than the Mn(3)-O(110) bond distance of 1.875(2)Å. The Mn(1)-O(100)-Mn(2), The Mn(3)-O(100)-Mn(2), The Mn(3)-O(110)-Mn(2), bond angles are 116.78(11)°, 98.88(10)°, 102.69(11)° respectively.

In addition to the "*edge-sharing tetrahedra*" description of the Mn_6O_2 core, two alternative ways of describing it can be presented that emphasize the structural relationship to smaller nuclearity Mn/O units: (i) The Mn_6O_2 unit can be considered as two $[Mn_3O]^{6+}$ units, joined together by each of the μ_3-O^{2-} atoms becoming μ_4 by ligation to the Mn^{II} center of the adjacent Mn_3O unit. This also relates to the synthetic procedure for making complex **14** from$[Mn_3O]^{7+}$, for reduction of the $[Mn_3O]^{7+}$ unit yields the $[Mn_3O]^{6+}$ core and it could be argued that lowering the average metal oxidation state increases, the basicity of the μ_3-O^{2-} and allows ligation to an additional metal center. The two $[Mn^{III}_2Mn^{II}O]^{6+}$ units comprising the Mn_6O_2 core of **14** are conceptually representing its parentage, are Mn(1,2,3)O(100) and Mn(4,5,6)O(100) or, alternatively Mn(1,3,4)O(100) and Mn(2,5,6)O(100). (ii) The Mn_6O_2 core can be considered to contain the $[Mn^{III}_2Mn^{II}_2O_2]$ core of $[Mn_4O_2(OH)(L)_2(LH)_2]^+$. This unit possesses a planar Mn_4 rhombus with two μ_3-O bridge, one above and one below the plane. This unit has been found within **14** [Mn(1,2,3,4)O(100,100)] or [Mn(5,2,6,4)O(100,100)], and completion of the Mn_6O_2 core then requires merely the conversion of the two μ_3-O^{2-} to μ_4-O^{2-} by ligation to an additional Mn^{II} center. Also it is to be noted that the Mn_6O_2 core contains the nonplanar "butterfly" like Mn_4O_2 unit in complex **14**. Such a unit in **14** would be formed by Mn(1,2,4,6)O(100,100) or Mn(3,2,4,5)O(100,100) with Mn(2,4) representing

the "body" or "backbone" positions and completion of the Mn_6O_2 again requires conversion of the two μ_3-O^{2-} to μ_4-O^{2-} by ligation to an additional Mn^{II} sites. Thus, the planar and butterfly like Mn_4O_2 units represent the products from two possible ways of removing two Mn atoms from the Mn_6O_2 core as shown:

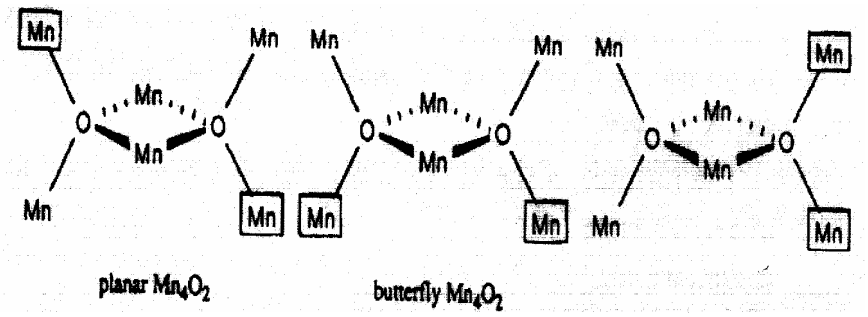

Figure 6.2: Schematic view of the hexamanganese core structure

It should also be noted that the Mn^{III}...Mn^{III} [Mn(1) and Mn(3)] separation in the $[Mn^{III}_2Mn^{II}O]^{6+}$ triangular unit is 3.122(9)Å, and the Mn^{II}...Mn^{III} [Mn(1)...Mn(2), Mn(3)...Mn(2)] separations are 3.516(9)Å and 3.19(9)Å respectively, whereas the separation between the Mn^{II}...Mn^{II} [Mn(2)...Mn(4)] is 3.36(9)Å .

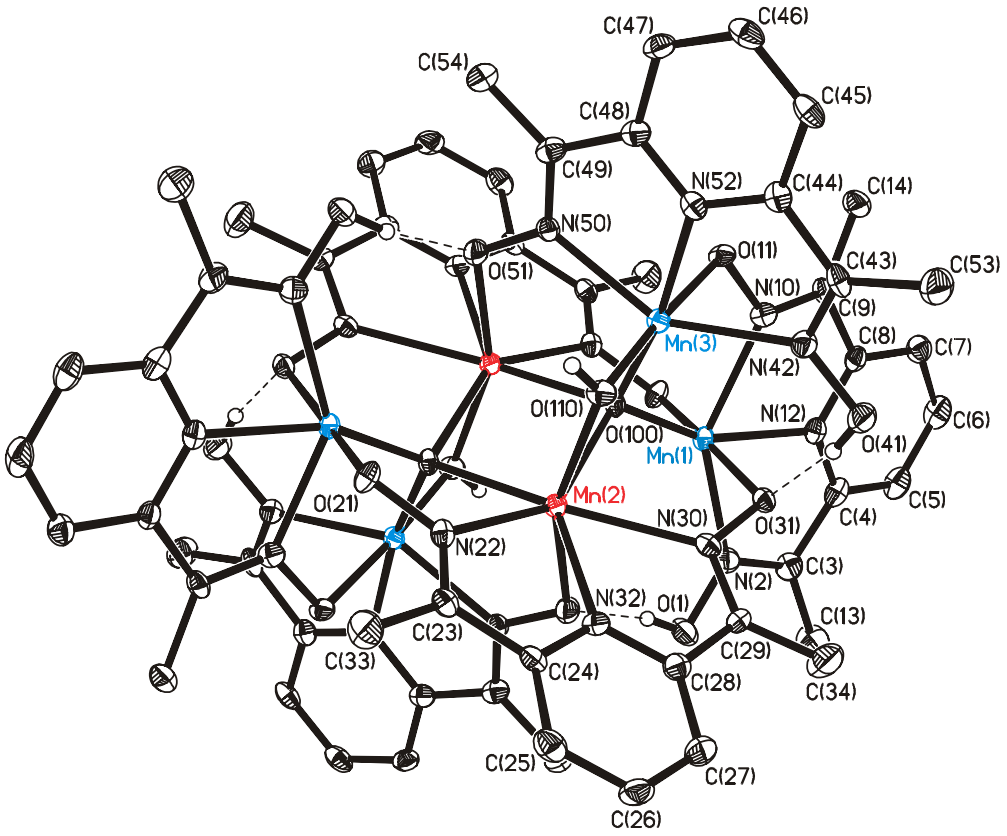

Figure 6.3: ORTEP plot of the dication in complex 14

Table 6.1: *Selected Bond Lengths (Å) and Angles (deg)* **$[Mn^{II}_2Mn^{III}_4(\mu_4\text{-}O)_2(\mu_2\text{-}OH)_2(dapdo)_2(dapdoH)_4](ClO_4)_2 .6CH_3CN$ (14)**

Mn(1)•••Mn(2)	3.516	Mn(2)•••Mn(3)	3.1903(9)
Mn(1)•••Mn(3)	3.122	Mn(2)•••Mn(4)	3.36
Mn(1) •••Mn(4)	3.616	Mn(3) •••Mn(4)	3.547
Mn(1)-O(100)	1.875(2)	Mn(3)-O(100)	1.944(2)
Mn(1)-O(21)	1.890(3)	Mn(3)-O(11)	1.925(3)
Mn(1)-O(31)	1.938(3)	Mn(3)-O(110)	1.874(3)
Mn(1)-N(12)	2.163(3)	Mn(3)-N(52)	2.149(3)
Mn(1)-N(10)	2.215(3)	Mn(3)-N(50)	2.170(3)
Mn(1)-N(2)	2.282(3)	Mn(3)-N(42)	2.365(3)
Mn(2)-O(110)	2.203(3)	N(50)-Mn(3)-N(42)	143.56(11)
Mn(2)-O(100)	2.247(2)	N(10)-Mn(1)-N(2)	141.7(12)
Mn(2)-O(51)	2.265(2)	Mn(1)-O(100)-Mn(3)	109.67(12)
Mn(2)-O(100)	2.293(3)	Mn(1)-O(100)-Mn(2)	116.78(11)
Mn(2)-N(22)	2.302(3)	Mn(3)-O(100)-Mn(2)	98.88(10)
Mn(2)-N(32)	2.313(3)	Mn(1)-O(100)-Mn(4)	119.99(12)
Mn(2)-N(30)	2.384(3)	Mn(3)-O(100)-Mn(4)	113.39(11)
		Mn(2)-O(100)-Mn(4)	95.66(9)
		Mn(3)-O(110)-Mn(2)	102.69(11)

6.4.2 Solid State Molecular Structure of $[Mn^{II}_2Mn^{III}_4(\mu_4\text{-}O)_2(\mu_2\text{-}OMe)_2(dapdo)_2(dapdoH)_4](ClO_4)_2 .2C_2H_5OC_2H_5$ (13) :

The structure of the complex **13** consists of a discrete dicationic hexanuclear unit, two perchlorate anions and two diethyl ether molecules as solvents of crystallization. The structure of **13** also consists of six Mn atoms arranged as two "*edge-sharing*" tetrahedra. The structure of complex **13** is essentially similar with that of **14** except the difference in ligation between Mn(3) and Mn(2). In the complex **14** one of the bridging unit is μ_2-OH, which is replaced by μ_2-OMe in complex **13**. Except this difference the core structure is identical with that of **14**. A view of the dication is shown in the Figure 6.4. Selected bond lengths and angles are given in Table 6.2.

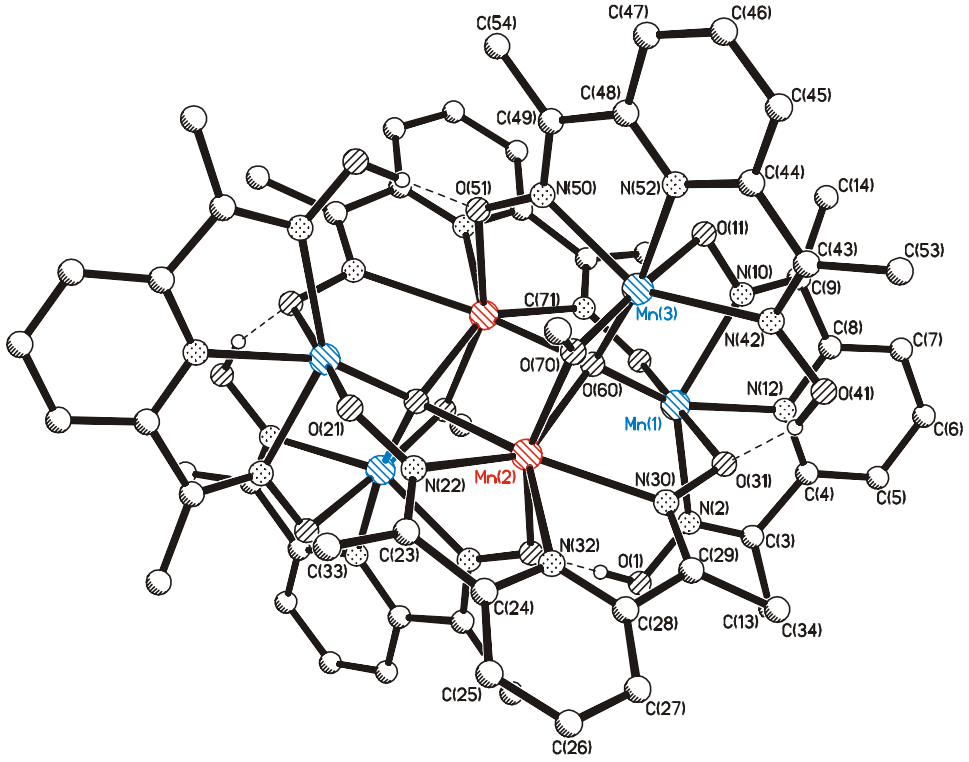

Figure 6.4: ORTEP plot of the dication in complex 13

Table 6.2: *Selected Bond Lengths (Å) and Angles (deg)* **$[Mn^{II}_2Mn^{III}_4(\mu_4\text{-}O)_2(\mu_2\text{-}OMe)_2(dapdo)_2(dapdoH)_4](ClO_4)_2 .2C_2H_5OC_2H_5$ (13)**

Mn(1)•••Mn(2)	3.477	Mn(2)•••Mn(3)	3.2073(15)
Mn(1)•••Mn(3)	3.1147(13)	Mn(2)•••Mn(4)	3.396
Mn(1) •••Mn(4)	3.613	Mn(3) •••Mn(4)	3.554
Mn(1)-O(60)	1.877(2)	Mn(3)-O(60)	1.944(3)
Mn(1)-O(21)	1.883(3)	Mn(3)-O(11)	1.931(4)
Mn(1)-O(31)	1.938(3)	Mn(3)-O(70)	1.876(4)
Mn(1)-N(12)	2.153(4)	Mn(3)-N(52)	2.137(4)
Mn(1)-N(10)	2.224(4)	Mn(3)-N(50)	2.168(4)
Mn(1)-N(2)	2.283(5)	Mn(3)-N(42)	2.385(4)
Mn(2)-O(70)	2.207(3)	N(50)-Mn(3)-N(42)	143.4(2)
Mn(2)-O(60)	2.222(2)	N(10)-Mn(1)-N(2)	142(2)
Mn(2)-O(51)	2.242(4)	Mn(1)-O(60)-Mn(3)	109.2(2)
Mn(2)-O(60)	2.306(3)	Mn(1)-O(60)-Mn(2)	115.88(2)
Mn(2)-N(22)	2.288(4)	Mn(3)-O(60)-Mn(2)	100.46(14)

Mn(2)-N(32)	2.305(4)	Mn(1)-O(100)-Mn(4)	119.1(2)
Mn(2)-N(30)	2.370(4)	Mn(3)-O(100)-Mn(4)	113.21(15)
		Mn(2)-O(100)-Mn(4)	97.18(13)
		Mn(3)-O(70)-Mn(2)	103.2(2)

6.4.3 Solid State Molecular Structure of $[Cu^{II}_6(\mu_3\text{-}O)(\mu_3\text{-}OH)L_3(H_2O)_6](BF_4)_3$ (15)

The lattice is built of discrete hexanuclear trications, three tetrafluoroborate counteranions. The molecular geometry and atom labeling scheme of the complex **15** is shown in the Figure 6.5. The hexanuclear Cu^{II} cluster consists of two linked $[Cu_3O]$ cores. The metal ions lie at the corners of an equilateral triangle and are at an average distance of 3.204 Å and 3.235 Å respectively in both the two $[Cu_3O]$ core. The association of two parallel triangular Cu_3 species is through two μ_3-bridging oxo ligands and three deprotonated oximate dianion (L^{2-}) moieties. Both the two $[Cu_3O]$ units are strongly hydrogen bonded with the formation of $[Cu_3O...H...OCu_3]$ core, and the bond distance in the O...H...O core is 2.518Å. There are two oximate groups in each ligand, one oximate binds one triangular unit while the other part binds the other trinuclear unit, making the hexanuclear complex. The N_{ox}-O bond lengths of average 1.34 Å are nearly identical to those for other comparable structures and significantly shorter than 1.40 Å in general for free oxime ligands. The bond distance $C=N_{ox}$ (average 1.28Å) are expected, identical for other reported complexes.[54]

Each copper ion is five coordinate and has a distorted square pyramidal N_2O_3 environment. The average Cu-N bond distance is 1.976(3)Å, whereas the average Cu-O_{ox} bond length is 1.937(2)Å. The average Cu-O (oxo or hydroxo) bond length is 1.919(10)Å. The fifth position of each copper ion is filled by an apical water molecule and this longer Cu-O bond length is 2.467(5) Å and is very much similar to the bond distance of the water molecules ligated to the copper ions in reported compounds. In the $[Cu_3O]$ core the trans N(2)-Cu(1)-O(1) bond angle is 176.86°(10), where as the N(5)-Cu(1)-O(30) bond angle is 168.68°(9), thus the τ parameter[55] for each copper in this trinuclear unit is 0.14 and explains that is in square pyramidal environment, [τ = 0 for ideal square pyramidal and τ = 1 for ideal trigonal bipyramidal geometry]. Similarly in the other $[Cu_3O]$ core the trans N(17)-Cu(2)-O(8) bond angle is 169.17°(15), whereas the N(14)-Cu(2)-O(40) bond angle is 166.37°(10), thus the τ parameter for each copper in this trinuclear unit is 0.045

and is in a nearly ideal square pyramidal environment. The Cu^{II}_6 unit can be thought of as dimer of Cu^{II}_3 units.

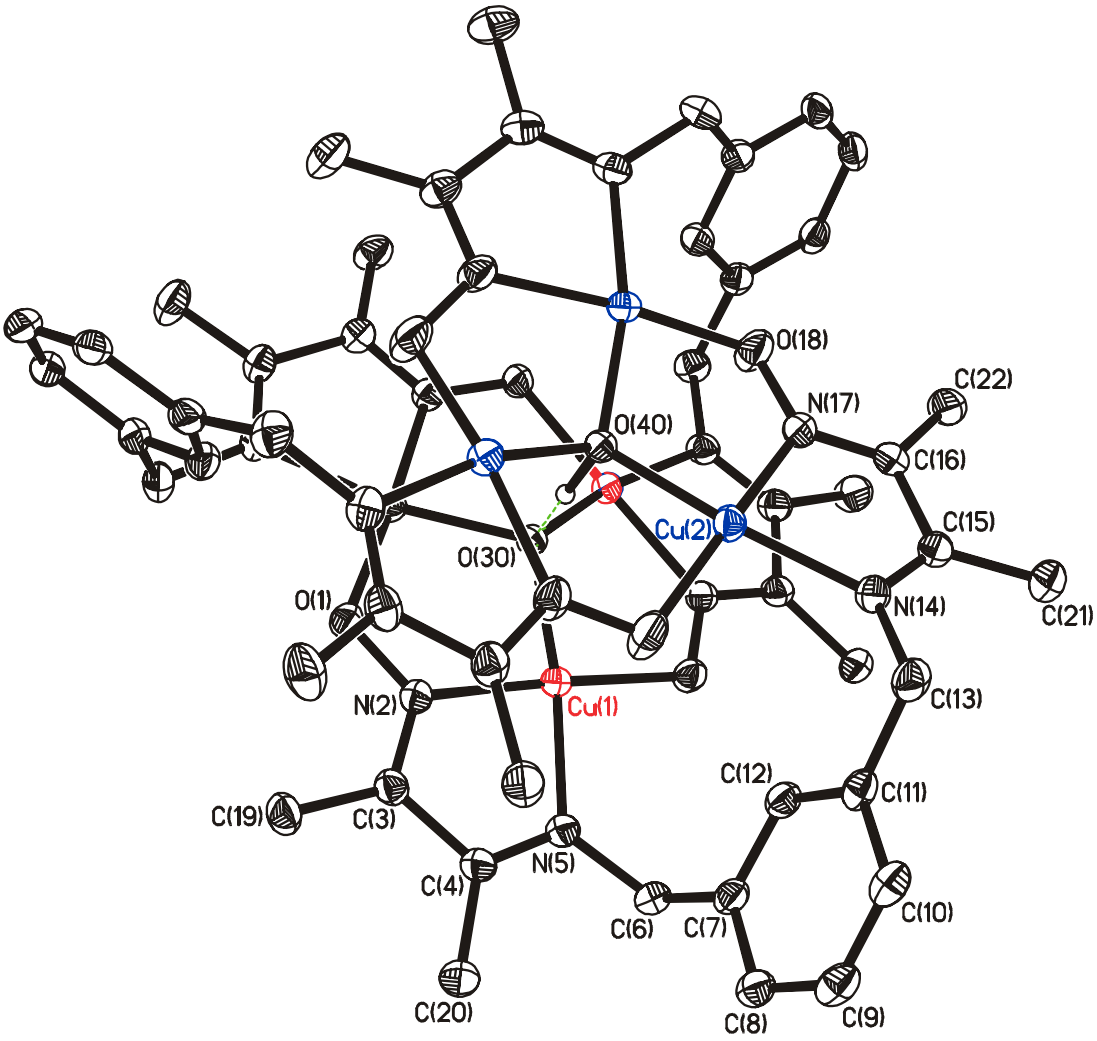

Figure 6.5: ORTEP plot of the trication in complex 15

Three different kinds of non-bonded Cu...Cu separation (3.686Å, 4.239Å, 5.042Å) in the inter dimer unit is observed, whereas the observed Cu-O-Cu angles in each triangular unit are 113.65(9)° and 114.32(8)° respectively. The core structure of the hexacopper(II) cluster is shown below in Figure 6.5A.

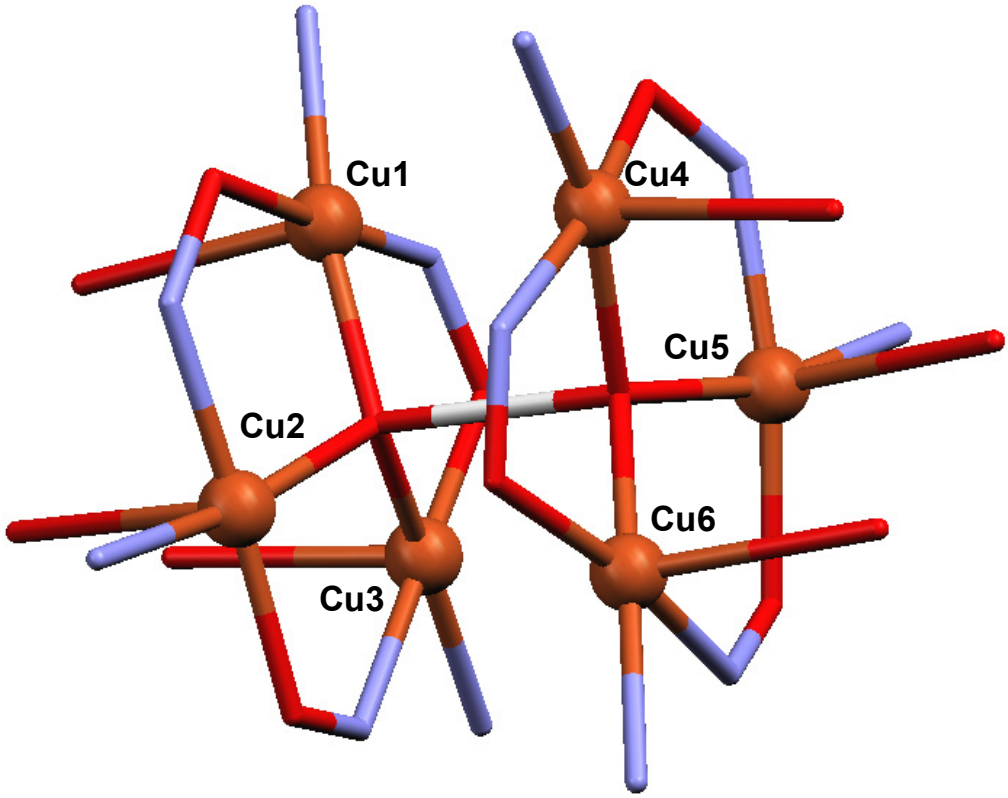

Figure 6.5A: Core structure of the hexacopper(II) cluster 15

Table 6.3: *Selected Bond Lengths (Å) and Angles (deg)* **$[Cu^{II}_6(\mu_3\text{-}O)(\mu_3\text{-}OH)L_3(H_2O)_6](BF_4)_3$ (15)**

Cu(1)•••Cu(1)	3.204	Cu(2)•••Cu(2)	3.235
Cu(1)•••Cu(2)	3.686	Cu(1)•••Cu(2B)	5,042
Cu(1)•••Cu(2A)	4.239	O(30)...HO(40)	2.518
Cu(1)-O(30)	1.9138(10)	Cu(2)-O(40)	1.9251(10)
Cu(1)-O(1)	1.937(2)	Cu(2)-O(18)	1.943(3)
Cu(1)-N(2)	1.967(3)	Cu(1)-N(17)	1.968(3)
Cu(1)-N(5)	1.999(3)	Cu(1)-N(14)	1.989(3)
Cu(1)-O(60)	2.469(5)	Cu(1)-O(70)	2.465(5)
Cu(1)-O(30)-Cu(1)	113.65(9)	Cu(1)-O(30)-Cu(1)	114.32(8)
N(2)-Cu(1)-O(1)	176.86(10)	N(17)-Cu(1)-O(18)	169.17(15)
N(5)-Cu(1)-O(30)	168.68(9)	N(14)-Cu(1)-O(40)	166.37(10)

6.5 Magnetic Properties:

6.5.1 Magnetic Properties of Hexanuclear Manganese Complexes

Magnetic susceptibility data for polycrystalline samples of the complexes were collected in the temperature range 2-290 K in an applied magnetic field of 1T. The Heisenberg spin Hamiltonian in the form $H = -2J_A(S_1S_3 + S_5S_6) - 2J_B (S_1S_2 + S_4S_6) - 2J_C(S_2S_3+S_4S_5)-2J_DS_2S_4$ (for complexes **13** and **14**) for an isotropic exchange coupling with $S_1 = S_3 = S_5 = S_6 = S_{Mn(III)} = 4/2$, $S_2 = S_4 = S_{Mn(II)} = 5/2$ for **13** and **14** are employed to analyze the magnetic properties. The experimental data as the effective magnetic moments (μ_{eff}) versus temperature (T) are displayed in Figure 6.7. Due to the similarity of the magnetic nature in complexes **13** and **14**, herein detailed magnetism of the complex **14** will be described in the following section.

The magnetic moment μ_{eff}/molecule for **14**, $Mn^{III}_4Mn^{II}_2$, of 11.44 μ_B ($\chi_M \bullet T$ = 16.35 $cm^3 \bullet K \bullet mol^{-1}$) at 290 K is less than expected for the spin only value of $\chi_M \bullet T$ = 20.75 $cm^3 \bullet K \bullet mol^{-1}$for 4 uncoupled Mn^{III} and 2 Mn^{II} ions and decreases monotonically with decreasing temperature until it reaches a value of 8.77 μ_B ($\chi_M \bullet T$ = 9.63 $cm^3 \bullet K \bullet mol^{-1}$) at 30 K and then starts to increase with decreasing temperature and reaches a value of 9.03 μ_B ($\chi_M \bullet T$ = 10.19 $cm^3 \bullet K \bullet mol^{-1}$) at 10 K and then again decreases to reach a value of 6.93μ_B ($\chi_M \bullet T$ = 5.99 $cm^3 \bullet K \bullet mol^{-1}$) at 1.95 K. This temperature dependence behavior is consistent with the presence of antiferromagnetic interactions between the spin carriers, with the low temperature value of μ_{eff} indicating that the molecule has a reasonably large spin ground state.

The magnetic moment μ_{eff}/molecule for **13**, $Mn^{III}_4Mn^{II}_2$, of 11.34 μ_B ($\chi_M \bullet T$ = 16.08 $cm^3 \bullet K \bullet mol^{-1}$) at 290 K decreases monotonically with decreasing temperature until it reaches a value of 8.68 μ_B ($\chi_M \bullet T$ = 9.42 $cm^3 \bullet K \bullet mol^{-1}$) at 30 K and then starts to increase with decreasing temperature and reaches a value of 8.83 μ_B ($\chi_M \bullet T$ = 9.73 $cm^3 \bullet K \bullet mol^{-1}$) at 10 K and then again decreases to reach a value of 6.76μ_B ($\chi_M \bullet T$ = 5.72 $cm^3 \bullet K \bullet mol^{-1}$) at 1.95 K.

By far the commonest way to model exchange coupling have been performed through Kambe's vector coupling method[30] and various extensions of Kambe's method have been used in specific cases. The Heisenberg Hamiltonian, $H = -2J \sum S_i S_j$ can be expressed in case of n number of paramagnetic spin carriers as equation,

$H = -2 \sum J_{ij} S_i S_j$ .....(1).

Substitution of the vector model into equation (1) as a general case has been given by the equation, $H = - 2 (\sum J_{ij} S_i S_j + 2 \sum J_{in} S_i S_n + 2 S_i S_n)$.....(2).

The eigen value equation from (2) can be written as: $E(S_T) = - \sum (J_{ij} - J_{in}) [S_{ij} (S_{ij} + 1) - S_i (S_i + 1) - S_j (S_j + 1)] - \sum (J_{ij} - J_{1n}) [S_{in} (S_{in} + 1) - S_i (S_i + 1) - S_n (S_n + 1)] - J_{1n} S_T (S_T + 1) + J_{1n} \sum S_i (S_i + 1)$.....(3).

In real situation, suitable simplifications of the problem can often be made from symmetry considerations in order to reduce equation (3) to an unambiguous and simple expression, from which the energy values of the spin states will be available and hence the magnetic susceptibility are readily obtained. However, in completely general case (none of the J_{ij} necessarily equal) not all the allowed values can be given unambiguously, and the problem can not be solved by the extended Kambe's approach. So except for very specialized cases, exchange interactions in a discrete trinuclear and tetranuclear clusters can not be described by the Kambe's method of vector coupling. Thus, difficulties increase as the number of interacting paramagnetic atoms increases. When the number of paramagnetic centers are greater than 5, suitable equation for $E(S_T)$ can be obtained by substituting in equation (3), but again, for nearly all physical probable arrangement of paramagnetic atoms. So due to the complexity in polynuclear complexes, Kambe's theory can not be applied to the general case and it is therefore desirable to evolve a completely general treatment which would permit complete freedom of choice in the magnitudes of the exchange integrals of J_{ij} between pair of spins S_i and S_j; where none of the J_{ij} or S_i, S_j need to be equal.

The total degeneracy of the spin levels for a cluster of n identical spins S is $(2S + 1)^n$, a number which grows very fast beyond the possibilities of handling with any computer. It is apparent that procedures are required which employ symmetry in order to reduce the dimensions of the matrices. These are essentially of two types, one which takes advantages of the total spin symmetry and the other which exploits the point symmetry of the cluster.

A theoretical model to interpret the magnetic susceptibility data for complexes **13** and **14** was sought. At the outset it has to be realized that this is a formidable task, for with four Mn^{III} (S = 2) and two Mn^{II} (S = 5/2) ions, there is a total degeneracy of $(2S_{Mn}^{III} + 1)^4 (2S_{Mn}^{II} + 1)^2 = 22400$. It is simple to realize that as a result of magnetic interactions, the hexanuclear complexes have total spin (S_T) values of the resultant states range from13, 12, 11,....., 0. So owing to the size and symmetry of the hexamanganese clusters, it is not possible to use Kambe approach to derive a theoretical equation to fit the $\chi_M T$ versus T

data. In addition this large number of spin states makes it effectively impossible to evaluate the pairwise exchange interactions in the spin Hamiltonian. However, it takes an appreciate amount of time with a computer program employing the mathematical treatment given below to identify all of the 22400 different electronic states for the hexanuclear manganese complexes. By using irreducible tensor operator (ITO) approach it is possible to drastically cut the requirement of memory storage and time needed for the diagonalization of the Hamiltonian matrices, making the calculations for medium size clusters possible even for work station type computers. So the exchange coupling model was considered for simulation of the experimental magnetic data using the irreducible tensor operator (ITO) mathematical method[58] with the Heisenberg Hamiltonian in the form $H = - 2JS_iS_j$

An examination of the structures of **13** and **14** shows that two central bis (μ-oxide)-bridged Mn^{II} (S = 5/2) ions are bridged to four Mn^{III} (S = 2) via single μ-oxide bridges. The bridging pathways connecting each of the Mn^{II} ions, Mn(2) or Mn(4), to one pair of the Mn^{III} ions, Mn(1,3) or Mn(5,6) are equivalent. The appropriate bridging angles in the structure of **13** and **14** are noticeably different, e.g., Mn(2)-O(100)-Mn(1) and Mn(2)-O(100)-Mn(3) are 115.88 and 100.46° respectively for **13** and Mn(2)-O(100)-Mn(1) and Mn(2)-O(100)-Mn(3) are 116.78 and 98.88° respectively. At the same time there is another μ_2-OMe and μ_2-OH bridge between the Mn(2) and Mn(3) ions respectively for **13** and **14**, giving the Mn(2)-O(110)-Mn(3) angle around 103.2° and102.69° respectively. A general spin-spin interaction model allowing for dissimilar coupling between the Mn^{II}-Mn^{III} pairs could not be constructed by using the Kambe vector coupling method.

To simplify the problem, a "three-J" model was taken into consideration and the assumption was made that all of the Mn^{II}-Mn^{III} exchange interactions are equal; i.e the Mn_6O_2 core has the idealized symmetry (D_{2h}) of the two "*edge-sharing*" tetrahedra. Least squares computer program was used to fit the observed temperature dependence of μ_{eff} / Mn_6 cluster as a function of the three exchange parameters, J_1, J_2, J_3, and an isotropic g value. A proposed model for the exchange interactions in the $Mn^{III}_4Mn^{II}_2$ cluster is shown below in the scheme 1 and we used the spin Hamiltonian in the form, $H = - 2J_1(S_1S_3 + S_5S_6) - 2J_2(S_1S_2 + S_2S_3 + S_5S_4 + S_6S_4) - 2J_3S_2S_4$; where $S_1 = S_3 = S_5 = S_6 = 2$ and $S_2 = S_4 = 5/2$

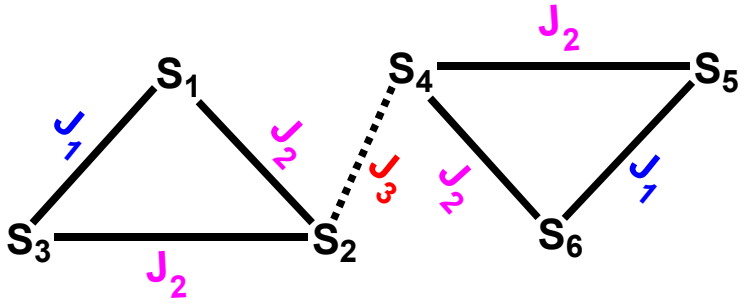

Scheme 1

During the fitting, it was observed that there was little correlation between the nature of the experimental susceptibility plot and the simulated curve. In this procedure the simulation does not show any minimum, which is observed in the experimental data at the lower temperature region. Possible reasons for this deviation include the neglect of single ion zero-field splitting or the assumption that all the $Mn^{III}..Mn^{II}$ interactions are equal. To test the latter possibility a "four J" model was employed to fit the experimental data instead of the "three J" model. A schematic view of the spin topology of the cluster is given below in scheme 2.

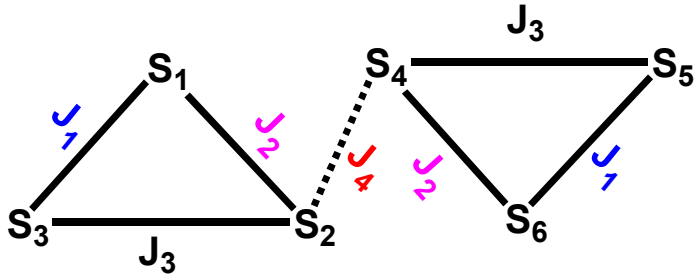

Scheme 2

We used the spin Hamiltonian in the form, $H = - 2J_1(S_1S_3 + S_5S_6) - 2J_2(S_1S_2 + S_6S_4) - 2J_3(S_2S_3 + S_5S_4) - 2J_4S_2S_4$; where $S_1 = S_3 = S_5 = S_6 = 2$ and $S_2 = S_4 = 5/2$. Since the value of the parameter g is best determined by the high-temperature data, only the data above 20 K were fit at first, and by doing so from the best fit the parameters obtained are $g = 1.98$, $J_1 = - 12.6$ cm^{-1}, $J_2 = - 4.6$ cm^{-1}, $J_3 = + 2.4$ cm^{-1} and $J_4 = + 1.9$ cm^{-1}. From this simulation the nature of the curve is similar to that of the experimental one but below 20 K the simulated curve does not fit perfectly with the experimental one. Zero field splitting effects are likely to influence the data in this temperature range. The parameter J_1 represents the coupling constant between the Mn(III) atoms, the coupling between Mn(II) and Mn(III) atoms in each triangular unit are labeled with J_2 and J_3, while J_4 represents the coupling between the Mn(II) atoms. The μ_4-oxo bridges are assumed to be the dominant pathways of magnetic exchange

interactions between the Mn ions. Although the oximate (N-O) and μ_2-OH or μ_2-OMe ligands could theoretically transmit the exchange coupling, the fact that the magnetic data are nearly similar for complexes **13** and **14** support the assumption that the μ_4-oxo bridges dominate the exchange interactions. The values of the Mn^{III}-Mn^{III}, Mn^{II}-Mn^{III} and Mn^{II}-Mn^{II} exchange coupling parameters can be compared with those found for the oxo-bridged manganese complexes[5-6,8-10,20,22,24-26,29,31-38,41] with attention towards the exchange coupling, which is mediated through oximate(=N-O) also.[29,54,59-60] Interaction through the oximate bridge are antiferromagnetic in nature as usually observed. The exchange coupling between the Mn^{II}-Mn^{III} pair is weak, in case of J_3 the weak ferromagnetic coupling between the mixed valence manganese ions compared to the weak antiferrmagnetic exchange interaction (J_2) between another set of mixed valence manganese ions can be explained in terms of the Mn-O-Mn bond angles. The J_2 coupling mediates through the Mn-O-Mn angle of 116.78°, whereas the J_3 exchange coupling mediates through average Mn-O-Mn angle of 101.7°, means, a better overlap between the magnetic orbitals expected in case of J_2 and can give rise to better antiferromagnetic exchange interactions compared to J_3. The system may be envisaged as ferromagnetically coupled two AF triangles and the fact $J_1 >> J_3$ clearly stabilizes a local S = 5/2 ground state in each triangular unit. The ferromagnetic pathway (J_4) leads to an S = 5 ground state of the hexanuclear cluster (*vide infra*). From the above data set for the exchange coupling constant, it has been observed that S_T = 5 has minimum energy compared to other possible spin states and being the ground state. Similar weak ferromagnetic exchange coupling constant for $Mn^{II}(\mu_4\text{-O})Mn^{II}$ was found in a oximate based manganese complex reported recently.[60a] Mn(II)...Mn(II) exchange coupling constant mediated through μ_4-O, with a Mn-O-Mn angle of 94.4° is reported to be + 2.5 cm^{-1}. Similarly exchange interaction between Mn^{III} centers with a combination of μ_3-O and oximate (N-O) bridge is reported to be - 12.6 cm^{-1} in a hexanuclear manganese complex.[10]

In order to provide a theoretical basis for the observed magnetic properties of the complexes **13** and **14**, especially to offer a rationale for the high-spin ground state S_T = 5 the proposed model for the exchange interactions in the $Mn^{III}_4Mn^{II}_2$ clusters, schematic view of the spin topology is given below.

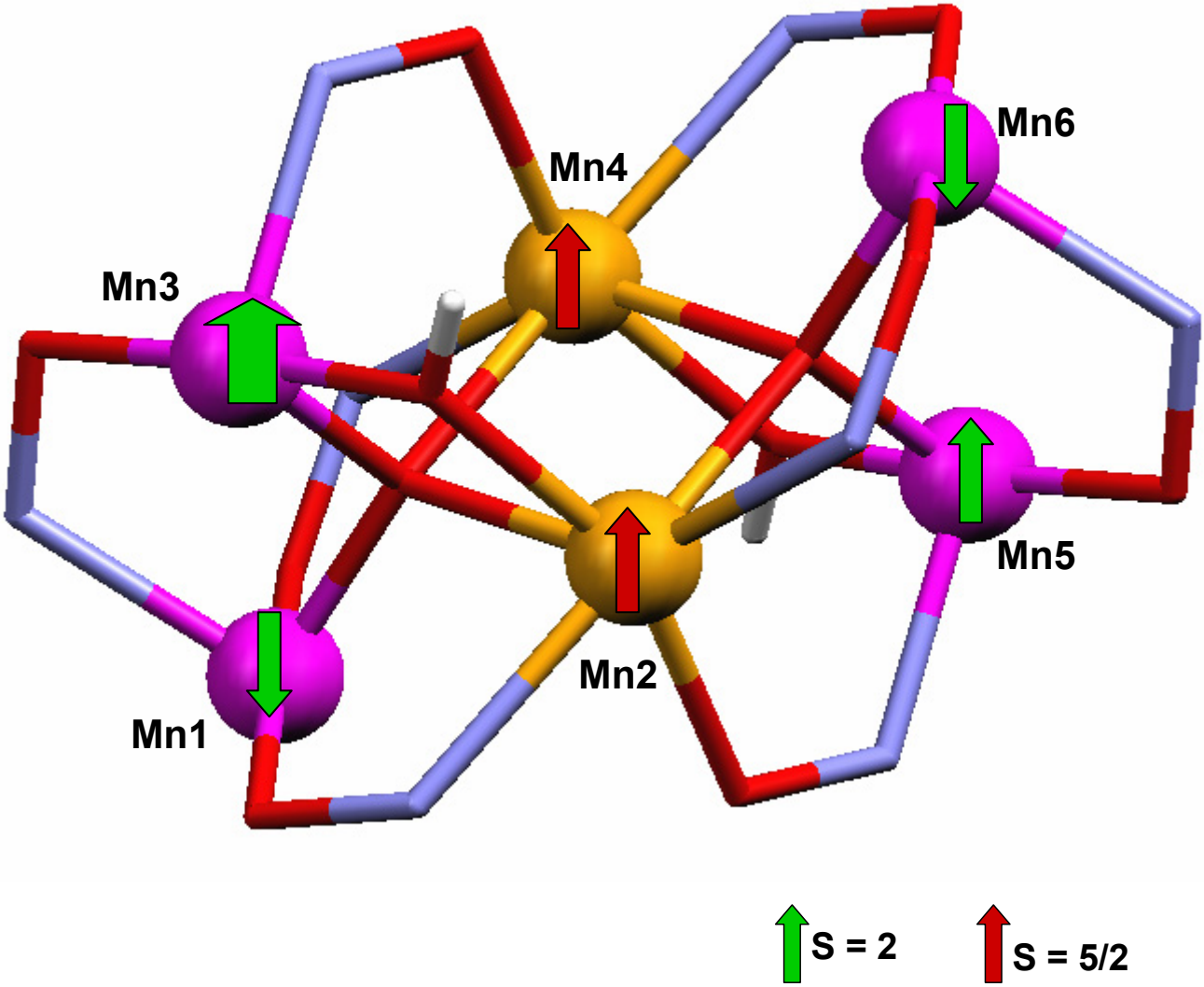

Figure 6.6: Spin coupling model for the $Mn^{II}_2Mn^{III}_4$ clusters

Detailed rationale of the exchange interaction of the different spin carriers will be given and compared with the reported literature. The sign of the intramolecular exchange coupling constant results from the sum of antiferromagnetic and ferromagnetic contributions given in the equation $J = J_{AF} + J_F$. From the structures of the hexanuclear clusters the Mn^{III}_2O unit in both complexes may be described as resulting from two octahedrally coordinated manganese(III) ions sharing an edge comprised of a μ-oxo bridge. The manganese(III) centers (high spin, d^4) are tetragonally distorted as is evidenced in the X-ray structure, the electronic configuration of the localized metal orbitals being $(d_{xz}, d_{yz})^2$, $(d_{xy})^1$, $(d_z^2)^1$, $(d_x^2{-}y^2)^0$ in order of increasing energy. It is then obvious that the interaction between the $(d_{xz}, d_{yz})^2$ orbitals of the two manganese(III) ions and the bridging oxygen atom provide antiferromagnetic π-pathways; similarly

antiferromagnetic σ-paths are available between the $(d_{xy})^1$ pairs via s and p orbitals of oxygen. The path $d_z^2 \,||\, d_z^2$ involves weakly delocalized in the molecular plane, and its contribution is expected to be rather weak, irrespective of its magnetic nature, with Mn-O overlap being of the σ-type. As the Mn^{III}-O-Mn^{III} angle is about 110°, d_z^2 electrons interact via an antiferromagnetic pathway involving a non-orthogonality of the bridging oxygen atom. A negetive J i.e., a net antiferromagnetic interaction is thus expected and is observed.[5-6,9-10,20,22,24-26,29,31-32,35-38,41] This picture is consistent with the predictions made by Kahn for dinuclear complexes. When Mn^{III}-O-Mn^{III} angle is close to 90°, a ferromagnetic exchange interaction is also observed.[8,24-25,33-34]

The Mn^{II}...Mn^{III} interactions obtained in this work for complexes **13** and **14** are weakly antiferromagnetic as have been found in most molecules, that have been reported to have such interactions. Taking literature data into account the calculated J value ($J_{Mn^{II}..Mn^{III}}$) is reasonable. The sign and the strength of the exchange interaction between the Mn^{III} centers in compounds containing the $\{Mn^{III}_2(\mu\text{-OR})\}^{4+}$ subunit, where the oxygen atoms occupy Jahn-Teller positions at each metal ion, are influenced by subtle geometric and electronic factors which create a subtle balance between different exchange pathways, as predicted by Goodenough and Kanamori. One important point is that the complex[34] $[Mn^{III}_2(\mu_2\text{-O})(\mu\text{-}O_2CR)_2(Me_3Tacn)_2]^{2+}$ exhibits ferromagnetic exchange interaction (J = + 9 cm^{-1}) between the Mn^{III} centers. Chaudhuri[56] et al., showed the terminal ligand has a significant effect on the sign and magnitude of J. Recently Solomon et. al showed[25] such a influence on the sign and magnitude of J, e.g, replacement of the terminal ligand Me_3Tacn by bpy and H_2O in one complex and bpy and azide in another complex with the core of $[Mn^{III}_2(\mu_2\text{-O})(\mu\text{-}O_2CR)_2(bpy)_2(H_2O)_2]^{2+}$ and $[Mn^{III}_2(\mu_2\text{-O})(\mu\text{-}O_2CR)_2(bpy)_2(N_3)]^{2+}$ the value of the exchange coupling constant shifts to - 3.4 cm^{-1} and + 8.8 cm^{-1} respectively. Careful study of the literatures[8, 24, 27, and 33] reveals that the Mn^{III}-O(R)-Mn^{III} angles smaller than ≈ 102° tend to favor weak ferromagnetic exchange interactions. Thus from the viewpoint of this structural parameter only, the antiferromagnetic nature of J_1 in complexes **13** and **14** with Mn^{III}-O(R)-Mn^{III} angle of 110° is understandable whereas the interaction between Mn^{III}(3) and Mn^{II}(2) is also expected to be weak whatever in nature taking into account all the cross interaction between the said spin carriers and from the viewpoint of the structural parameter with average Mn^{III}(3)-O(R)-Mn^{II}(2) angle of 100.5°, a weak positive exchange coupling constant is more likely. Although there is no magnetostructural correlations between the Mn^{III}-O-Mn^{II} angle and the sign/magnitude of the exchange constant, it has been shown that for Mn^{III}-O-Mn^{II} angle of ≈ 120° the

interaction is antiferromagnetic,[5-6,9-10,12-15,17-21,26,31-32,35,38,41] while for ≈ 105° the interaction is ferromagnetic.[5,11,16-19,21,33,39-40] The ferromagnetic nature of exchange coupling interactions can be explained by assuming prevalent e_g-e_g contributions. Given the elongated nature of the distortion from octahedral symmetry, the $d_{x^2-y^2}$ orbital is empty. Due to the arrangement of local elongation axes in the structure, the d_{z^2} magnetic orbitals of Mn^{III} have a nonzero overlap with the half-filled $d_{x^2-y^2}$ orbitals of the Mn^{II} through μ_2-OH or μ_2-OMe ligands.

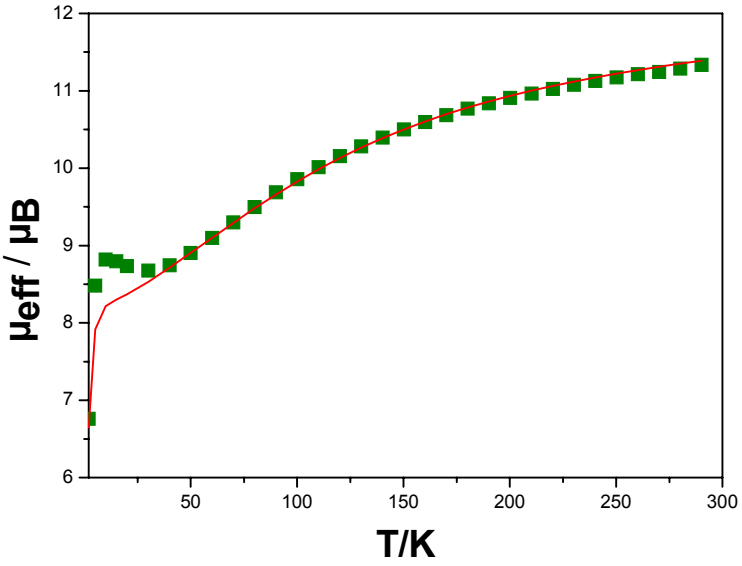

Figure 6.7: Magnetic data for $Mn^{III}_4Mn^{II}_2$ (14), plot of μ_{eff} vs. T. The bold points represent the experimental data while the solid line represents the simulation

The weak interaction found between $Mn^{III}(3)$ and $Mn^{II}(2)$ may be rationalized on the basis of the empty $d_{x^2-y^2}$ orbital of the Mn^{III} ions and due to the elongated Jahn-Teller distortion, the electronic configuration of the metal orbitals being $(d_{xz}, d_{yz})^2$, $(d_{xy})^1$, $(d_{z^2})^1$, $(d_{x^2-y^2})^0$ in order of increasing energy and presumably the different cross interactions between the Mn(II) and Mn(III) orbitals cancels each other, and can be anticipated from $J = J_{AF} + J_F$. This $d_{x^2-y^2} \,||\, d_{z^2}$ pathway is expected to provide a ferromagnetic contribution towards overall exchange coupling constant and is nicely explained by Ginsberg. Thus the observed exchange coupling constant (J_3 = + 2.4 cm^{-1}) is well justified. On the contrary the $Mn^{III}(1)$-O(R)-$Mn^{II}(2)$ angle of 116° leads to a better overlap between the magnetic orbitals giving rise to a net weak antiferromagnetic exchange interaction (J_2)

and the obtained value in this case is quite reasonable enough. This is consistent with the literature values reported for binuclear and polynuclear transition metal complexes containing Mn^{II} and Mn^{III} ions

To determine the spin ground state, magnetization data were collected at 1, 4 and 7 T in the temperature range 2-290 K and plotted as reduced magnetization (M/Ngβ) vs. (βH/kT) (*vide infra*), where N is the Avogadro's number, β is the Bohr magneton and k is the Boltzmann's constant. For a system occupying only the ground state and experiencing no zero-field splitting (D), the various isofield lines would be superimposed and M/Ngβ would saturate at a value S. The non-superposition of the variable temperature variable field (VTVH) plots at low temperature clearly indicates the presence of zero-field splitting (ZFS or D). Reduced magnetization measurement yielded a ground state $S_T = 5$.

Attempts to fit the data by using the method of full-matrix diagonalization of the spin Hamiltonian matrix including axial ZFS, with the pairwise exchange interactions, produced best fits with, $J_1 = -12.6$ cm^{-1}, $J_2 = -4.6$ cm^{-1}, $J_3 = +2.4$ cm^{-1}, $J_4 = +1.9$ cm^{-1}, $g_{Mn} = 1.98$, $D_1 = D_3 = D_5 = D_6 = D_{Mn(III)} = 4.0$ cm^{-1}. These "J" and g values are exactly the same values evaluated from the susceptibility measurements at 1 T described earlier and thus confirm the credibility of the simulated parameters. The variable temperature variable field (VTVH) plot is shown in the Figure 6.8. It should be pointed that the main source of the molecular anisotropy is due to the presence of four Jahn-Teller distorted Mn^{III} ions. The projections of these single-ion anisotropies onto the molecular anisotropy axis will determine the molecular parameter D. With $D_1 = D_3 = D_5 = D_6 = D_{Mn(III)} = -4.0$ cm^{-1} a fit of poorer quality than that with positive D was obtained.

It is anticipated that further characterization of the system to determine more precisely the values of S_T and D and to fully elucidate the sign of the ZFS(D), alternating current susceptibility (AC) measurement or high-frequency EPR (HFEPR) techniques will be needed.

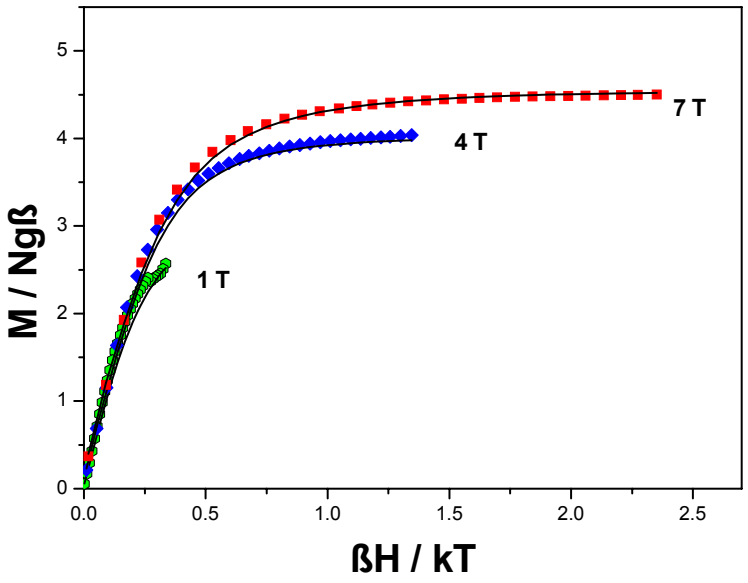

Figure 6.8: Variable temperature variable field (VTVH) magnetic data for $Mn^{III}_4Mn^{II}_2$ (14), plot of M/Ngß vs. ßH/kT. The bold points represent the experimental data while the solid line represents the simulation

In order to offer a rationale for the high-spin ground-state where ferromagnetically coupled two AF [$Mn^{III}_2Mn^{II}$] triangular units give rise to S_T = 5 ground state is shown below in Figure 6.9

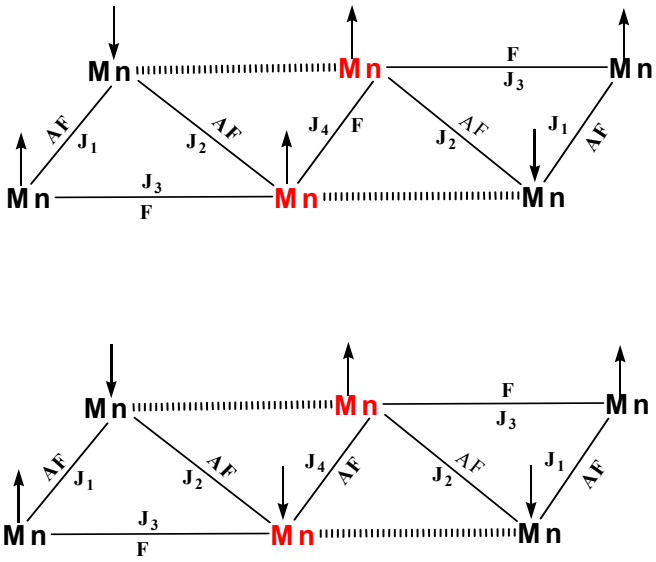

Figure 6.9: Pictorial representation of exchange coupling for the two possibilities for the ground states, the above diagram shows the S_T = 5 ground state (above) and S_T = 0 ground state (below).

The main lesson from these study is that high nuclearity Mn_x complexes can be prepared which have either pairwise ferromagnetic $Mn^{II}...Mn^{III}$ or $Mn^{III}...Mn^{III}$ interactions or a combination of pairwise antiferromagnetic interactions or in the third possibility a combination of pairwise ferromagnetic-antiferromagnetic interactions that lead to molecules with $S_T \neq 0$ ground state. Combinations of pairwise exchange interactions or competing exchange interactions and topology stabilize the high spin ground states of these polynuclear manganese complexes.

Although no simple straightforward magnetostructural correlation has been established based on either Mn....Mn separation or Mn-O-Mn angles (except in case of J vs Mn^{IV}-O-Mn^{IV}),[57] with the availability of more structural data for closely related complexes displaying suitable variation over the structural parameters, qualitative magnetostructural correlations for exchange coupling in manganese complexes can be provided. But based on Goodenough-Kanamori, Ginsberg[42] and Kahn[7] it can be concluded that $Mn^{II}...Mn^{III}$ and $Mn^{III}...Mn^{III}$ interactions are weakly ferromagnetic or weakly antiferromagnetic in nature depending on the Mn-O-Mn angle, when it is close to 90°, orthogonality of the magnetic orbitals would be expected and thus provides ferromagnetic exchange, while deviations from 90°, causes the net exchange interaction to be antiferromagnetic.

6.5.2 Magnetic Properties of Cu^{II}_6:

Magnetic susceptibility data for polycrystalline samples of the complexes were collected in the temperature range 2-290 K in an applied magnetic field of 1 T. The experimental data as the effective magnetic moments (μ_{eff}) versus temperature (T) are displayed in Figure 6.10. The experimental magnetic data were simulated using a least squares fitting computer program with a full-matrix diagonalization approach and the solid lines in the Figure 6.10 represent the simulations. The magnetic moment μ_{eff}/molecule for **15**, Cu^{II}_6, of 2.77 μ_B ($\chi_M \bullet T = 0.96 cm^3 \bullet K \bullet mol^{-1}$) at 290 K is smaller than the value of six uncoupled copper (II) ions ($\chi_M \bullet T = 2.25\ cm^3 \bullet K \bullet mol^{-1}$) assuming g = 2.00 and decreases monotonically with decreasing temperature until it reaches a value of 1.65 μ_B ($\chi_M \bullet T = 0.34\ cm^3 \bullet K \bullet mol^{-1}$) at 1.9 K . This temperature dependence is in agreement with a strong antiferromagnetic exchange interaction between the spin carriers.$[Cu^{II}_6(O)_2]^{8+}$ core has a strong antiferromagnetic interaction within both the $[Cu_3O]^{4+}$ subunit and leaves a single unpaired electron in each triangular unit. If the trimeric unit has each metal equivalent

and forms an equilateral triangle the spin Hamiltonian will describe in the form given as, $H = -2J_A(S_1S_2 + S_1S_3 + S_2S_3 + S_4S_5 + S_4S_6 + S_6S_5)$ for an isotropic exchange coupling with $S_1\ S_2 = S_3 = S_4 = S_5 = S_6 = S_{Cu(II)} = 1/2$. But for a better model the exchange interaction between the interdimer units was taken into consideration and hence by using a "two J" model the magnetic data of the hexacopper complex was analyzed and we used the Hamiltonian in the form; $H = -2J_A(S_1S_2 + S_1S_3 + S_2S_3 + S_4S_5 + S_4S_6 + S_6S_5) - 2J_B(S_1S_4 + S_1S_5 + S_1S_6 + S_2S_4 + S_2S_5 + S_2S_6 + S_3S_4 + S_3S_5 + S_3S_6)$

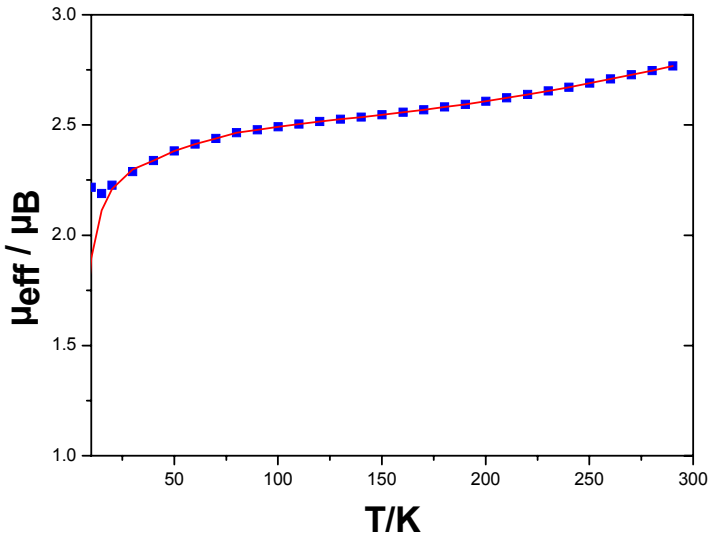

Figure 6.10: Magnetic data for Cu^{II}_6 (16), plot of μ_{eff} vs. T. The square points represent the experimental data while the solid line represents the simulation

So the magnetic susceptibility data was simulated by full matrix diagonalization of the appropriate isotropic spin Hamiltonian for a Cu^{II}_6 molecule with a dimer of trimers topology. The fit was carried out by the Irreducible Tensor Operator (ITO) formalism using the CLUMAG program and provides best fit with the following parameters : $J_A = -614.0\ cm^{-1}$, $J_B = -114.5\ cm^{-1}$ and $g = 2.00$.

As previously reported[43-48] the strong antiferromagnetic coupling is possible when the trinuclear entity is completely planar. The triangular Cu_3X (X = OH, O) core is known to be present in different copper(II) complexes with strong antiferromagnetic coupling. It has been observed that the Cu_3OH core has weaker magnetic exchange ($J \approx -200\ cm^{-1}$). The tetrahedral sp^3 hybridization forces the oxygen to be above the plane of the copper atoms and furthermore disrupts the coplanarity of the ligand bridging network due to

hindered $d_{x^2-y^2}$ overlap. The Cu_3O core on the other hand has nearly coplanar geometry; the Cu_3O oxygen is only slightly raised above the plane to form a weak trimer bond. As a result of the nearly coplanar configuration plus additional electrostatic effects, the Cu-O bonds are shorter for the Cu_3O core. Since the oxygen exhibits the more flat sp^2 character, overlap with the copper $d_{x^2-y^2}$ orbitals still permits the oxime ligands to retain their coplanar Cu_3O geometry. This overall coplanar Cu_3O structure permits larger magnetic coupling ($J \geq -300$ cm^{-1}), the magnetic exchange properties of triangular Cu^{II} species result from large antiferromagnetic interaction documented by a strong exchange coupling constant ranging up to - 1000 cm^{-1}.

That oximate ligands generally mediate very strong antiferromagnetic exchange interaction between two d^9 copper(II) ions to provide, in some cases, a nearly complete spin pairing at room temperature as was first authenticated in a trinuclear copper(II) complex of pyridine-2-aldoxime. The first diamagnetic copper(II) dimer, thus historically worth mentioning and ascribable to superexchange through the oxime bridged, was described by Bertrand[50] et al. with a centrosymmetric nearly planar six-membered ring formed by copper atoms and two oxime (NO) groups. Strong antiferromagnetic coupling between copper(II) ions ($J \approx -475$ cm^{-1})[51] was observed, revealing that the NO-group has a remarkable ability to mediate strong antiparallel spin coupling when it acts as a bridging ligand either through the nitrogen and oxygen atoms or only through oxygen atom. Trinuclear copper complexes are known with planar[52] or non planar[53] geometrical arrangements with the exchange coupling constants ($J < -300$ cm^{-1} and $J \approx -448$ cm^{-1}) respectively, which suggest that the unusually large spin exchange interaction is not the result of any special geometrical feature but is related to the electronic structures of the bridging dioximato ions. Detailed inspection of the magnetostructural data[54] of oximato bridged copper(II) complexes reveal that exchange interactions (J values) show no correlation with the distances Cu...Cu, Cu-N_{ox}, Cu-O_{ox} or with the nature of the basal skeleton $Cu(NO)_2Cu$ i.e. the magnitude of exchange coupling is independent of the degree of deviation from planarity, or deviation of the copper from the mean basal plane.

In summary it is concluded that due to the presence of oxo and oximate groups, the exchange coupling constants are really very strong in magnitude and antiferromagnetic in nature.

6.6 References:

(1) R. J. Buthcher, C. J. O'connor and E. Sinn, *Inorg. Chem.,* 1981, **20**, 537

(2) R. Beckett and B. F. Hoskins, *J. Chem. Soc., Dalton. Trans.,* 1992, 291

(3) J. G. Mohanty, S. Baral, R. P. Singh and A. Chakravorty, *Inorg. Nucl.Chem.Lett.,* 1974,**10**, 655

(4) Y. Agnus, L. B. Metz, C. Boudon, J. P. Gisselbrecht, and M. Gross *Inorg. Chem.,* 1991, **30**, 3155

(5) G. Rajaraman, M. Murugesu, E. C. Sanudo, M. Soler, W. Wernsdorfer, M. Helliwell, C. Muryn, J. Raftery, S. J. Teat, G. Christou and E. K. Brechin, *J.Am.Chem.Soc.,* 2004, **126**, 15445

(6) A. R. Schake, J. B. Vincent, Q. Li, P. D. W. Boyd, K. Folting, J. C. Huffman, D. N. Hendrickson and G. Christou, *Inorg. Chem.,* 1989, **28**, 1915

(7) O. Kahn, *Molecular Magnetism*, VCH Publishers, Weinheim, 1993

(8) G. L. Abbati, A. Cornia, A. C. Fabretti, A. Caneschi and D. Gatteschi, *Inorg. Chem* .,1998, **37**, 1430

(9) G. L. Abbati, A. Cornia, A. C. Fabretti, A. Caneschi and D. Gatteschi *Inorg. Chem.,* 1998, **37**, 3759

(10) C. J. Milos, C. P. Raptopoulou, A. Terzis, F. Floret, R. Vincent, S. P. Perlepes and A. Escuer, *Angew. Chem. Int.Ed. Engl.,* 2004, **43**, 210

(11) C. Dendrinou-Samara, G. Psomas, L. Iordanidis, V. Tangoulis and D. P. Kessissoglou, *Chem. Eur.J.,* 2001, **7**, 504

(12) D. P. Kessissoglou, M. L. Kirk, M. S. Lah, X. H. Li, C. P. Raptopoulou, W. E. Hatfield and V. L. Pecoraro, *Inorg. Chem.,* 1992, **31**, 5424

(13) D. A. Malamati, P. hitou, A. G. Hatzidimitrou, F. E. Inscore, A. Gourdon, M. L. Kirk and D. P. Kessissoglou, *Inorg. Chem.,* 1995, **34**, 2493

(14) V. Tangoulis, D. A. Malamati, K. Soulti, V. Stergiou, C. P. Raptopoulou, A. Terzis, T. A. Kabanos and D. P. Kessissoglou, *Inorg. Chem.,* 1996, **35**, 4974

(15) V. Tangoulis, D. A. Malamati, G. A. Spyrroulias, C. P. Raptopoulou, A. Terzis and D. P. Kessissoglou, *Inorg. Chem.,* 2000, **39**, 2621

(16) M. Hirotsu, M. Kojima and Y. Yoshikawa, *Bull.Chem.Soc.Jpn.,* 1997,**70**,649

(17) J. Yoo, E. K. Brechin, A. Yamaguchi, M. Nakano, J. C. Huffmann, A. L. Maniero, L. C. Brunel, K. Awaga, H. Ishimoto and G. Christou, *Inorg. Chem.,* 2000, **39**, 3615

(18) C. Puloploi, M. G. Siera, G. Robles, F. dahan, J. P. Tuchagues and S. Signorella, *J. Chem. Soc.,Dalton. Trans.,* 2002, 3813.

(19) V. Borne, A. Bencini, D. Gatteschi and F. Totti *Chem. Eur.J.,* 2002, **8**, 5019

(20) C. Christmas, J. B. Vincent, H-R. Chang, J. C. Huffman, G. Christou and D. N. Hendrickson, *J.Am.Chem.Soc.,* 1988, **110**, 823

(21) H. Diril, H-R. Chang, X. Zhang, S. K. Larsen, J. A. Potenza, C. G. Pierpont, H. J. Schugur, S. S Isied and D. N. Hendrickson, *J.Am.Chem.Soc.,* 1987, **109**, 6207

(22) C. A. Kipke, M. J. Scott, J. W. Gohdes and W. H. Armstrong, *Inorg. Chem.,* 1990, **29**, 2193

(23) D. P. Goldberg, A. Caneschi and S. J. Lippard, *J.Am.Chem.Soc.,* 1993, **115**, 9299

(24) H. L. Tsai, S. Wang, K. Folting, W. E. Streib, D. N. Hendrickson and G. Christou *J.Am.Chem.Soc.,* 1995, **117**, 2503

(25) T. C. Brunold, D. R. Gamelin, T. L. Stemmler, S. K. Mandal, W. H. Armstrong, J. E. Penner-Hahn and E. I. Solomon, *J.Am.Chem.Soc.,* 1998, **120**, 8247

(26) M. Mikuriya, K. Nakadera, T. Kotera, T. Tokii and W. Mori, *Bull.Chem.Soc.Jpn.,* 1995, **68**, 3077

(27) G. Aromi, M. J. Knapp, J. P. Claude, J. C. Huffman, D. N. Hendrickson and G. Christou, *J.Am.Chem.Soc.,* 1999, **121**, 5489

(28) A. Caneschi, D. Gatteschi, J. Laugier, P. Rey, R. Sessoli and C. Zanchini *J.Am.Chem.Soc.,* 1988, **110**, 2795

(29) P.Chaudhuri, E. Rentschler, F. Birkelbach, C. Krebs, E. Bill, T. Weyhermüller and U. Flörke, *Eur. J. Inorg. Chem.,* 2003, 541

(30) K. Kambe, *J. Phys. Soc. Jpn.,* 1950, **5**, 48

(31) W. W. Wemple; H. L-Tsai, S Wang, J. P. Claude, W. E. Streib, J. C. Huffman, D. N. Hendrickson, and G. Christou, *Inorg. Chem.,* 1996, **35**, 6437

(32) B. Albela, M. S. E. Fallah, J. Ribas, K. Folting, G. Christou and D. N. Hendrickson *Inorg. Chem.,* 2001, **40**, 1037

(33) L. M. Wittick, K. S. Murray, B. Moubaraki, S. R. Batten, L. Spiccia and K. J. Berry, *J. Chem. Soc., Dalton. Trans.,* 2004,1003

(34) R. Hotzelmann, K. Wieghardt, U. Flörke, H-J. Haupt, D. C. Weatherburn, J. Bonvoisin, G. Blondin and J-J. Girerd, *J.Am.Chem.Soc.,* 1992, **114**, 1681

(35) H-R. Chang, S. K. Larsen, P. D. W. Boyd, C. G. Pierpont and D. N. Hendrickson *J.Am.Chem.Soc.,* 1988, **110**, 4565

(36) J. B. Vincent, C. Christmas, H-R. Chang, Q. Li, P. D. W. Boyd, J. C. Huffman, D. N. Hendrickson and G. Christou, *J.Am.Chem.Soc.,*1989, **111**, 2086

(37) S-B. Yu, C-P. Wang, E. P. Day and R. H. Holm, *Inorg. Chem.,* 1991, **30**, 4067

(38) C. Boskovic, W. wernsdorfer, K. Folting, J. C. Huffman, D. N. Hendrickson and G. Christou, *Inorg. Chem.,* ASAP

(39) A. Yoshino, T. Miyagi, E. Asato, M. Mikuriya, Y. sakato, K-I. Sugiura, K. Iwasaki and S. Hino, *J. Chem. Soc., Chem. Commun.,* 2000, 1475

(40) J. S. baskin, A. R. Schake, J. B. Vincent, H-R. Chang, Q. Li, J. C. Huffman, G. Christou and D. N. Hendrickson, *J. Chem. Soc.,Chem. Commun* 1988, 700

(41) N. Hoshino, T. Ito, M. Nishi and H. Oshio, *Inorg. Chem. Commun.,* 2003, **6**, 377

(42) A. Ginsberg *Inorg. Chim. Acta. Rev.,* 1971, **5**, 45

(43) D. J. Hodgson *Prog. Inorg. Chem*.,1975, **19**, 173

(44) C. J. O'Connor, D. P. Freyberg and E. Sinn, *Inorg. Chem.,* 1979, **18**, 1077

(45) E. Sinn, *Inorg. Chem.,* 1976, **15**, 2698

(46) R. J. Buthcher, C. J. O'Connor and E. Sinn, *Inorg. Chem.,* 1979, **18**, 1913

(47) E. Sinn, *J. Chem. Soc., Chem. Commun* 1975, 665

(48) R. J. Butcher and E. Sinn, *Inorg. Chem.,* 1976, **15**, 1604

(49) P. Chaudhuri, F. Birkelbach, M. Winter, V. Staemler, P. Fleischhauer, W. Hasse, U. Flörke and H-J. Haupt, *J. Chem. Soc., Dalton. Trans.,* 1994, 2313

(50) J. A. Bertrand, J. H. Smith and P. G. Eller, *Inorg. Chem.,* 1974, **13**, 1649

(51) R. Ruiz, J. Sanz, B. Cervera, F, Lloret, M. Julve, C. Bois, J. Fans and M. C. Munoz ,*J. Chem. Soc., Dalton. Trans.,* 1993, 3035

(52) D. Luneau, H. Oshio, H. Okawa, and S. Kida, *Chem.Lett.,* 1989, 443

(53) P. Chaudhuri, M. Winter, B. P. C. D. Vedova, E. Bill, A. Trautwein, S. Gehring, P. Fleischhuer, B. Nuber and J. Weiss, *Inorg. Chem.,* 1991, **30**, 2148

(54) P. Chaudhuri, *Coord. Chem. Rev.,* 2003, **243**, 143

(55) A. W. Addison, T. N. Rao, J. Reedijk and G. C. Vershcoor, *J. Chem. Soc., Dalton Trans.*, 1984, 1349

(56) P. Chaudhuri, M. Guttmann, K. Wieghardt, B. Nuber and J. Weiss, *J. Chem. Soc., Chem. Commun.,* 1985, 1618

(57) N. A. Law, J. W. Kampf and V. L. Pecoraro, *Inorg. Chim. Acta*., 2000, **297**, 252

(58) D. Gatteschi and L. Pardi, *Gazz. Chim. Ita*., 1993, **123**, 231

(59) (a) V. Pavlischuk, F. Birkelbach, T. Weyhermüller, K. Wieghardt and P. Chaudhuri, *Inorg. Chem.,* 2002, **41**, 4405; (b) F. Birkelbach, U. Flörke, H-J. Haupt, C. Butzlaff, A. X. Trautwein, K. Wieghardt and P. Chaudhuri, *Inorg. Chem.,* 1998, **37**, 2000; (c) F. Birkelbach, T. Weyhermüller, M. Lengen, M. Gerdan, A. X. Trautwein, K. Wieghardt and P. Chaudhuri, *J. Chem. Soc., Dalton Trans.*, 1997, 4529

(60) (a) T. Afrati, C. Dendrinou-Samara, C. P. Raptopoulou, A. Terzis, V. Tangoulis and D. P. Kessissoglou, *Angew. Chem. Int. Ed*., 2002, **41**, 2148; (b) M. Alexiou, C. Dendrinou-Samara, A. Kasagianni, S. Biswas, C. M. Zeleski, J. Kampf, D. Yoder, J. E. Penner-Hahn, V. L. Pecoraro and D. P. Kessissoglou, *Inorg. Chem.,* 2003, **42**, 2185; (c) D. J. Price, S. R. Batten, K. J. Berry, B. Moubaraki and K. S. Murray, *Polyhedron*, 2003, **22**, 165

CHAPTER-7

TWO RARE EXAMPLES OF NONANUCLEAR NICKEL(II) AND COPPER(II) CLUSTERS.

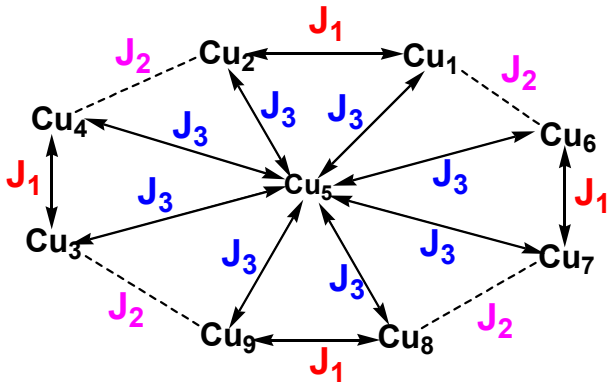

7.1 Introduction:

This chapter describes magnetostructural study of two rare examples of nonanuclear Ni(II) and Cu(II) complexes. One over-riding feature, that helps to create self-assembled clusters, is the presence of ligand binding sites that upon complexation form five-membered chelate rings. This helps to prevent the ligand chelating to a single metal ion center and forces it to look for additional Lewis acid species. There are classic examples using ligand where special arrangements of coordination pockets allow each subunit to interlock in a high yield self-assembly process to isolate polynuclear clusters. In essence, in this case the self-assembly involves a polynuclear subunit and, so, highlights a possibly useful strategy for generating even larger clusters. In recent years, self-assembly of nanoscale high-nuclearity metal clusters via methods of coordination chemistry has attracted increasing interest, because these supramolecules not only exhibit novel structural characteristics as well as important applications in both biology and materials chemistry, especially as potential precursors applied in magnetic, optical, electronic, and catalytic processes for their size-dependent physical properties. To obtain these high-nuclearity clusters, a common synthetic strategy has been applied to control the hydrolysis of metal ions in the presence of appropriate chelating ligands. Many classes of ligands are adequate to the task, including carboxylate, oxamate, oxamide, oximate and alkoxides. Hydrophilic groups, such as oxo and hydroxo, bridge the metal ions to make up a cluster core,

whereas the hydrophobic groups take up positions in the periphery, preventing the core from further aggregation and thus forming a finite-sized polynuclear complex.

It has been shown that oxime ligands can connect two transition metal ions due to their versatility in coordination modes. Also the ability of the oxime group to efficiently transmit magnetic coupling has been well doccumented.[14] There are only ten structurally characterized oximate bridged nickel(II) complexes reported in last 30 years, only seven of which have been subjected to magnetic susceptibility measurements. Thus no correlation between structural and magnetic properties for such complexes has yet been obtained and hence more oximate bridged paramagnetic complexes of nickel(II) are warranted. Since nickel(II) is known to have a large single-ion zero-field splitting and the geometrical parameters, which in Ni complexes are well understood, gives rise to ferromagnetic coupling, we wish to study the structure and magnetic properties of a nonanickel(II) cluster. The complexation of nickel(II) by pyridine-2-aldoxime in aqueous solution was studied by Orama et.al[1] and the structure of the nickel(II) complex of pyridine-2-aldoxime, a neutral tris complex was found in the solid state to consist of the monomeric $[Ni(PyAH)(PyA)_2]$ units held together by two OH...O hydrogen bonds between the oxygen atoms. This is an apparent contrast to the analogous complexes of copper(II), both of which in aqueous solution and in solid state are characterized by the presence of trinuclear complex species $[Cu_3(PyA)_3(OH)]^{2+}$ containing a Cu_3OH central core.[2] We herein present a new nonameric nickel(II) complex with syn-2-pyridine aldoxime ligand, $[Ni_9(PyA)_{10}(\mu_3\text{-}OH)_2(\mu_2\text{-}OH)_2(\mu_2\text{-}OH_2)_2(H_2O)_6](ClO_4)_4 \bullet 12H_2O$ underlining the versatility of this ligand to adopt a variety of coordination modes. Moreover there are very few nonanickel(II) complexes[3] known, one of which has been subjected to magnetically characterized.[4] The difficulties in analyzing large clusters magnetochemically prompted us to characterize the nonanuclear Ni(II) cluster magnetostructurally and compare the nature of exchange interaction through oximate and hydroxo bridging ligands reported earlier.

The magnetism of bis-(μ-hydroxo)- or (μ-alkoxo) dicopper(II) complexes has been the subject of extensive investigations for the last two decades.[5a] According to Hatfield and Hodgson, antiferromagnetic interactions between copper(II) ions become larger with increasing Cu-O-Cu angle in these complexes.[5] This was reasonably explained in terms of quantum-mechanical treatments by Hoffmann et al.[6a] and Kahn.[6b] However this rationale had been confined to doubly bridged systems with the Cu-O-Cu angle in the range 95-105° until Mckee et al.[7] and Kida et al.[8] reported the

synthesis and magnetism of copper(II) complexes with a single alkoxide bridge derived from 1,3-diamino-2-propanol. Since the Cu-O-Cu angle in such complexes is much larger (120-135°) than that of the other bridging ligands, substantially stronger antiferromagnetic interactions are expected in spite of the fact that the superexchange pathways due to the presence of other ligands might be expected to be different in magnitude and sign. It was also revealed that when another bridging group is added to the system, the antiferromagnetic interaction is substantially weakened or enhanced, depending on the second ligand. This fact was reasonably interpreted in terms of Hoffmann's theory that the matching of symmetries of the HOMOs of the bridging groups determines whether the two bridges work complementarily or countercomplementarily in the superexchange interaction. This theory is essentially important when the magnetism of a polynuclear complex possessing two different bridging groups is considered. This fact has been recognized in some other examples.[9] Moreover there are very few nonacopper(II) complexes[12] known. Thus a nonanuclear copper(II) complex was isolated and characterized magnetically where the spin exchange interaction was mediated through alkoxo, hydroxo and alkoxo-hydroxo bridge. Magnetic properties of this cluster follows the same trend reported earlier.[10,12]

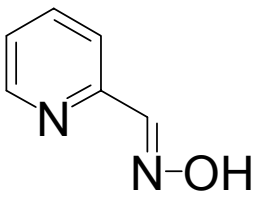

(a) (PyAH)

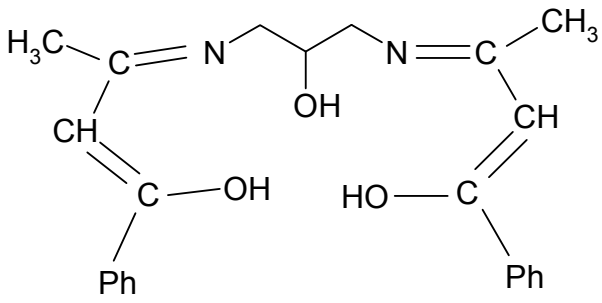

(b) L'H$_3$

Figure 7.1: (a) Ligand (PyAH) for the nonanuclear Ni(II) complex; (b) Ligand (L'H$_3$) for the nonanuclear Cu^{II} complex.

7.2 Synthesis:

Nonanuclear nickel(II) and copper(II) complexes respectively are isolated by self assembly, using tridentate oxime (PyAH) and pentadentate schiff base ligand(L'H$_3$). The schematic diagram of the synthesis is given below:

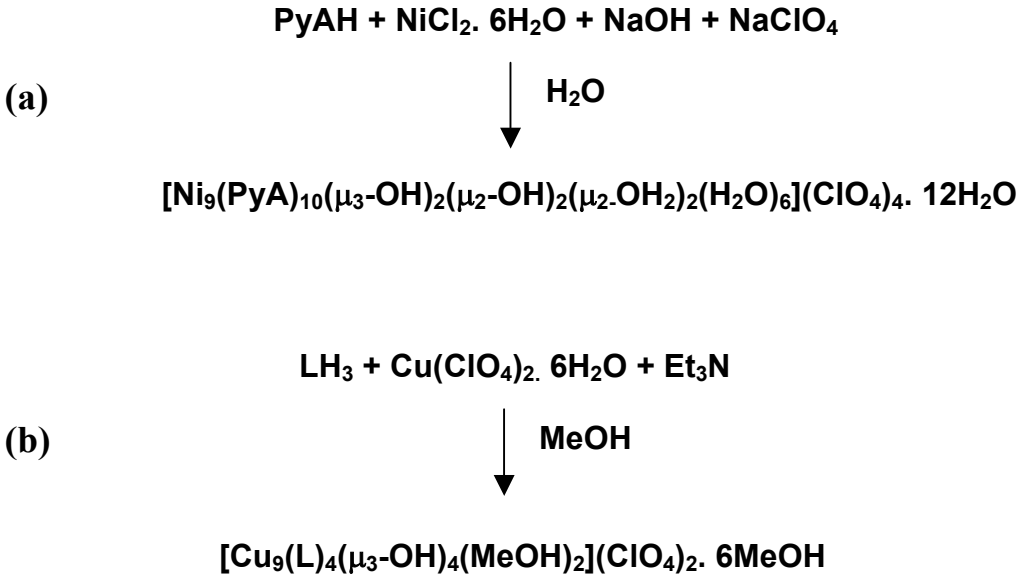

7.3 Infrared and Mass Spectroscopy:

The relevant bands in IR spectra of comparable pyridine-2-aldoximato containing heteronuclear $Cr^{III}M^{II}$ and $Fe^{III}M^{II}$ complexes have been reported earlier by Ross et al[16] and the spectra of **16** are also very similar. A notable feature for **16** are the sharp NO stretching bands at 1141, 1120, 1031 cm^{-1}. The presence of two different coordination modes of the oxime group in **16** is consistent with the splitting. A broad O-H stretching band around 3441 cm^{-1} indicates the presence of the OH groups in the compound while the stretching band for ClO_4 was also identified in the region of 1089 and 626 cm^{-1}. The IR spectrum of compound **17** revealed that the broad stretching band around 3463 cm^{-1} indicates the presence of the OH groups in the compound while the stretching bands for ClO_4 were also identified in the region of 1089 and 626 cm^{-1}.

Electrospray-ionaziation mass spectrometry (ESI-MS) in the positive ion mode does not provide signal for unambiguous characterization and shows only the monopositively charged species $[(PyA)_5Ni_3]^+$ as the base peak with the peak of $[(PyA)_6Ni_4(ClO_4)]^+$ (10%). On the other hand the signal for $[L_2Cu_4(OH)]^+$ of **17** is the base peak, together with the peak for the fragment $[L_3Cu_6(OH)]^+$ (50%) and $[L_4Cu_8(OH)_4]$ (15%).

7.4 X-ray Structure:

7.4.1 Solid State molecular structure of $[Ni_9(PyA)_{10}(\mu_3\text{-}OH)_2(\mu_2\text{-}OH)_2(\mu_2\text{-}OH_2)_2(H_2O)_6]\ (ClO_4)_4.\ 12H_2O$

The asymmetric unit contains of a discrete nonanuclear tetracation, four perchlorate anions and twelve water molecules of crystallization. There are two types of oximic groups, (i) a two atom -N-O bridging group O1, O11, O31, O41, O51, O81 and (ii) μ_2-O bridging oximate O21, O61, O71, and O91. The nonanuclear complex can be described as consisting of two $[Ni^{II}_4(PyA)_5(\mu_3\text{-}OH)(\mu_2\text{-}OH)(\mu\text{-}OH_2)(H_2O)_3]^+$moieties are connected to a centrally placed Ni(II) ion, Ni(7) through two μ_3-OH groups O(153), O(156) and four μ_2-O_{ox}, O(21), O(61), O(71) and O(91) of the ligands and yielding an $Ni(7)O_6$ core. As shown in Figure 7.2, all the nickel centers are 6-fold coordinate and the structure contains an octahedral NiO_6 central core and four different NiN_4O_2 and NiN_2O_4 environments. All of the oxime groups are deprotonated, and the nine nickel atoms are linked together via several bi-or trifurcated oximato, hydroxo and water bridges. Two nickel atoms (Ni1 and Ni3) display pseudo-octahedral geometry with NiN_4O_2 coordination spheres with two pyridine nitrogen atoms, two imine nitrogen atoms and one μ_2-OH and the 6th coordination mode is satisfied through μ-bridging water molecules O(151) and O(154). As shown in Table 7.1, the Ni-μ_2-O(151) and Ni-μ_2-O(154) bond lengths [2.129(6)-2.147(7) Å] are significantly longer than the bond distances of Ni-μ-O(152), Ni-μ-O(153), Ni-μ-O(155) and Ni-μ-O(156) [2.000(6)-2.032(6) Å] and thus O(151), O(154) are assigned as μ_2-bridging water molecules. The coordination mode around Ni(2)and Ni(9) are N_2O_4, one pyridine nitrogen, one imine nitrogen, one μ_3-OH, two oximate oxygen, and the 6th coordination is satisfied by μ-bridging water molecules. The coordination environment around Ni(4) and Ni(6) differs from that of Ni(2) and Ni(9) in that their is only one μ- bridging oxygen of the oximate instead two, μ_2-OH instead of μ_3-OH and terminally coordinated water. Whereas Ni(5) and Ni(8) are also in an N_2O_4 octahedral environment with one pyridine nitrogen, one imine nitrogen, one μ- bridging oxygen from the oximates, one μ_3-OH and two coordinated water molecules. The distortion from octahedral geometry for the nickel centers are more pronounced; the trans donor angles deviate from 180° by nearly 12°. Selected bond lengths and angles are given in Table 7.1.

The C=N and N-O distances of the oximate moieties are in the ranges of 1.28 and 1.36 Å respectively and nearly identical to the corresponding distances for other

comparable structures.[16d-e,17] The Ni-O distances lie in the range of 2.005 Å to 2.174 Å as expected, the Ni-μ_2-O_{ox} bond lengths are significantly longer than the Ni-O_{ox} bond distances. The Ni-N bond distances are consistent with normal covalent bonds for high-spin d^8 Ni(II) ions with oximate ligands. The Ni-N_{ox} bond lengths are shorter than the Ni-N_{py} bond lengths as is evidenced from the X-ray structure. The μ_3-OH(153) group acts as a bridge between Ni(2), Ni(7) and Ni(8) atoms, similarly μ_3-OH(156) group acts as a bridge between Ni(5), Ni(7) nd Ni(9). The μ_2-OH(152) and OH(155) groups are bridging ligands between Ni1 and Ni6; Ni3 and Ni4 respectively. In the cluster there are two different sets of Ni-O-Ni bond angles lying in the ranges 93.7-102.2 and 108.4-114.6°

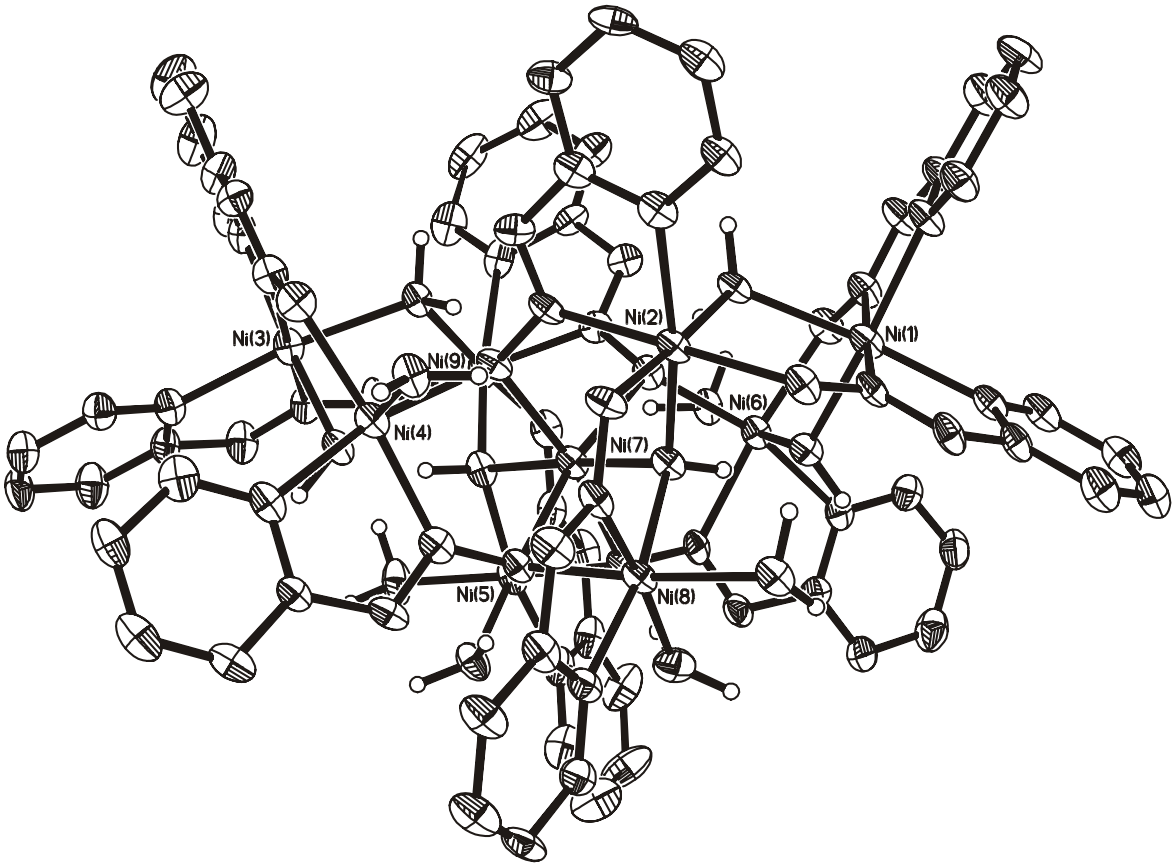

Figure 7.2: ORTEP and labeling scheme for Ni^{II}_9 (17)

There are eight strong hydrogen bondings prevailing between the oximate, hydroxo and water oxygen atoms and is shown as dotted lines in the Figure 7.3. The OH...O bond distances lie in the ranges of 2.625-2.757 Å and are listed in Table 7.1A. These chemically significant hydrogen bondings are responsible for the stabilization of the supramolecular metallocyclic core in cluster **16.**

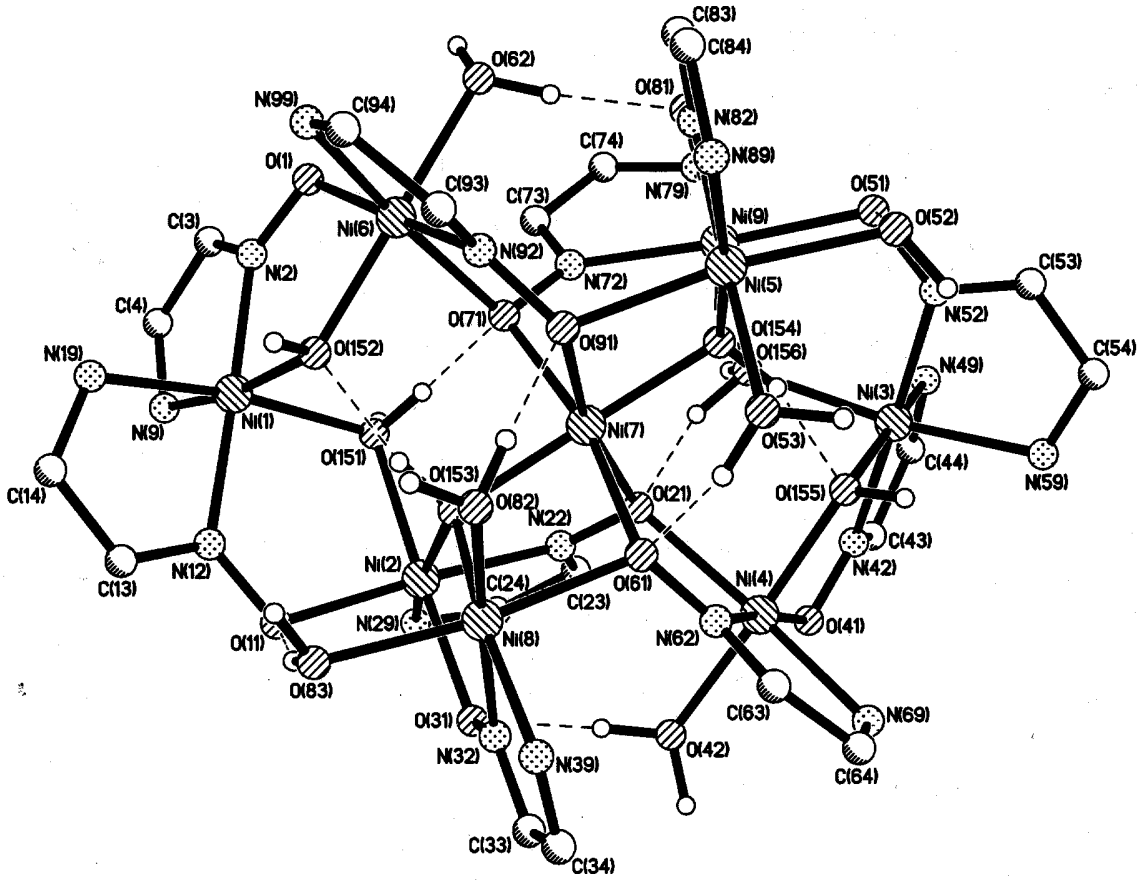

Figure 7.3: Schematic view of the hydrogen bonding in the Ni_9 core structure.

Table 7.1: *Selected Bond Lengths (Å) and Angles (deg)* **$[Ni^{II}_9(PyA)_{10}(\mu_3\text{-}OH)_2(\mu_2\text{-}OH)_2(H_2O)_6](ClO_4)_4 .12H_2O$ (16)**

Ni(1)•••Ni(2)	3.479	Ni(2)•••Ni(8)	3.351
Ni(3)•••Ni(4)	3.379	Ni(4)•••Ni(5)	3.396
Ni(5)•••Ni(9)	3.367	Ni(5)•••Ni(7)	3.117
Ni(3)•••Ni(9)	3.486	Ni(7)•••Ni(8)	3.125
Ni(7)•••Ni(9)	3.378	Ni(1)•••Ni(6)	3.486
Ni(1)-N(2)	2.019(7)	Ni(4)-N(62)	2.052(8)
Ni(1)-N(12)	2.044(7)	Ni(4)-N(69)	2.070(8)
Ni(1)-N(19)	2.056(8)	Ni(4)-O(21)	2.171(6)
Ni(1)-N(9)	2.056(7)	Ni(4)-O(41)	2.040(7)
Ni(1)-O(151)	2.147(7)	Ni(4)-O(42)	2.096(6)
Ni(1)-O(152)	2.008(6)	Ni(4)-O(155)	2.004(6)

Ni(2)-N(22)	2.068(7)	Ni(5)-N(82)	2.031(8)
Ni(2)-N(29)	2.083(8)	Ni(5)-N(89)	2.049(9)
Ni(2)-O(11)	2.071(6)	Ni(5)-O(52)	2.102(7)
Ni(2)-O(31)	2.043(6)	Ni(5)-O(53)	2.090(7)
Ni(2)-O(151)	2.142(6)	Ni(5)-O(91)	2.118(6)
Ni(2)-O(153)	2.032(6)	Ni(5)-O(156)	2.002(6)
Ni(3)-N(42)	2.038(7)	Ni(6)-N(92)	2.058(8)
Ni(3)-N(49)	2.070(8)	Ni(6)-N(99)	2.082(8)
Ni(3)-N(52)	2.036(7)	Ni(6)-O(1)	2.052(6)
Ni(3)-N(59)	2.075(7)	Ni(6)-O(62)	2.117(6)
Ni(3)-O(154)	2.129(6)	Ni(6)-O(71)	2.174(6)
Ni(3)-O(155)	2.005(6)	Ni(6)-O(152)	2.008(6)
Ni(7)-O(21)	2.110(6)	Ni(8)-N(32)	2.034(8)
Ni(7)-O(61)	2.160(6)	Ni(8)-N(39)	2.074(7)
Ni(7)-O(71)	2.132(6)	Ni(8)-O(61)	2.122(6)
Ni(7)-O(91)	2.137(6)	Ni(8)-O(82)	2.065(7)
Ni(7)-O(153)	2.001(6)	Ni(8)-O(83)	2.108(6)
Ni(7)-O(156)	2.004(6)	Ni(8)-O(153)	2.000(6)
Ni(9)-N(72)	2.055(7)	Ni(7)-O(21)-Ni(4)	112.7(3)
Ni(9)-N(79)	2.091(8)	Ni(8)-O(61)-Ni(7)	93.7(2)
Ni(9)-O(51)	2.068(6)	Ni(7)-O(71)-Ni(6)	112.4(3)
Ni(9)-O(81)	2.055(6)	Ni(7)-O(91)-Ni(5)	94.2(2)
Ni(9)-O(154)	2.131(6)	Ni(2)-O(151)-Ni(1)	108.4(3)
Ni(9)-O(156)	2.040(6)	Ni(1)-O(152)-Ni(6)	114.6(3)
		Ni(7)-O(153)-Ni(8)	102.7(3)
		Ni(8)-O(153)-Ni(2)	112.4(3)
		Ni(7)-O(153)-Ni(2)	113.9(3)
		Ni(3)-O(154)-Ni(9)	109.8(3)
		Ni(3)-O(155)-Ni(4)	114.5(3)

		Ni(7)-O(156)-Ni(5)	102.2(3)
		Ni(5)-O(156)-Ni(9)	112.8(3)
		Ni(7)-O(156)-Ni(9)	113.3(3)

Table 7.1A: *Selected Bond Lengths (Å) for the hydrogen bonding in the Ni^{II}_9 cluster.*

O(152)•••HO(153)	2.652	O(21)•••HO(154)	2.643
O(81)•••HO(62)	2.707	O(155)•••HO(154)	2.632
O(31)•••HO(42)	2.757	O(71)•••HO(151)	2.625
O(61)•••HO(53)	2.704	O(91)•••HO(82)	2.716

7.4.2 Solid State molecular structure of $[Cu_9(L')_4(\mu_3\text{-}OH)_4(MeOH)_2](ClO_4)_2 \bullet 6$ MeOH (17)

The asymmetric unit consists of one half of the nonanuclear dication which resides on a crystallographic inversion center, one perchlorate anion and three methanol molecules of crystallization. The X-ray structure clearly illustrates the formation of the nonanuclear cluster. An ORTEP view of the dication is shown in the Figure 7.4. Selected bond lengths and angles are listed in Table 7.2 The nonanuclear complex consists of four alkoxo bridged dinuclear units $\{Cu_2L\}^+$, that are covalently linked by μ_3-OH bridging ligands to form the nonacopper(II) metallocyclic core. The nonacopper cluster can be described as consisting of two $[Cu^{II}_4L_2(\mu_3\text{-}OH)_2(MeOH)]$ moieties connected to a centrally placed Cu(II) ion, Cu(5) through four μ_3-OH groups and two μ_3-alkoxo bridges of the ligands and yielding a $Cu(5)O_6$ core. Thus the centrosymmetric aggregate can be regarded as two irregular tetrahedral $[Cu^{II}_4L_2(\mu_3\text{-}OH)_2(MeOH)]^{2+}$ units linked via a central Cu^{II} ion, Cu(5), at its inversion center. As shown in the Figure 7.4, the structure contains an octahedral CuO_6 central core and all other copper(II) ions are in distorted $CuNO_4$ environments. All the ligands are deprotonated and the nine copper atoms are linked together via several bi-or trifurcated endogenous-alkoxo, exogenous-hydroxo groups and enolized oxygen atoms. In the $\{Cu_2L\}^+$ unit, the trianionic ligand displays N_2O_3-pentadentate coordination mode with alkoxide oxygen acting as the endogenous bridging ligand.

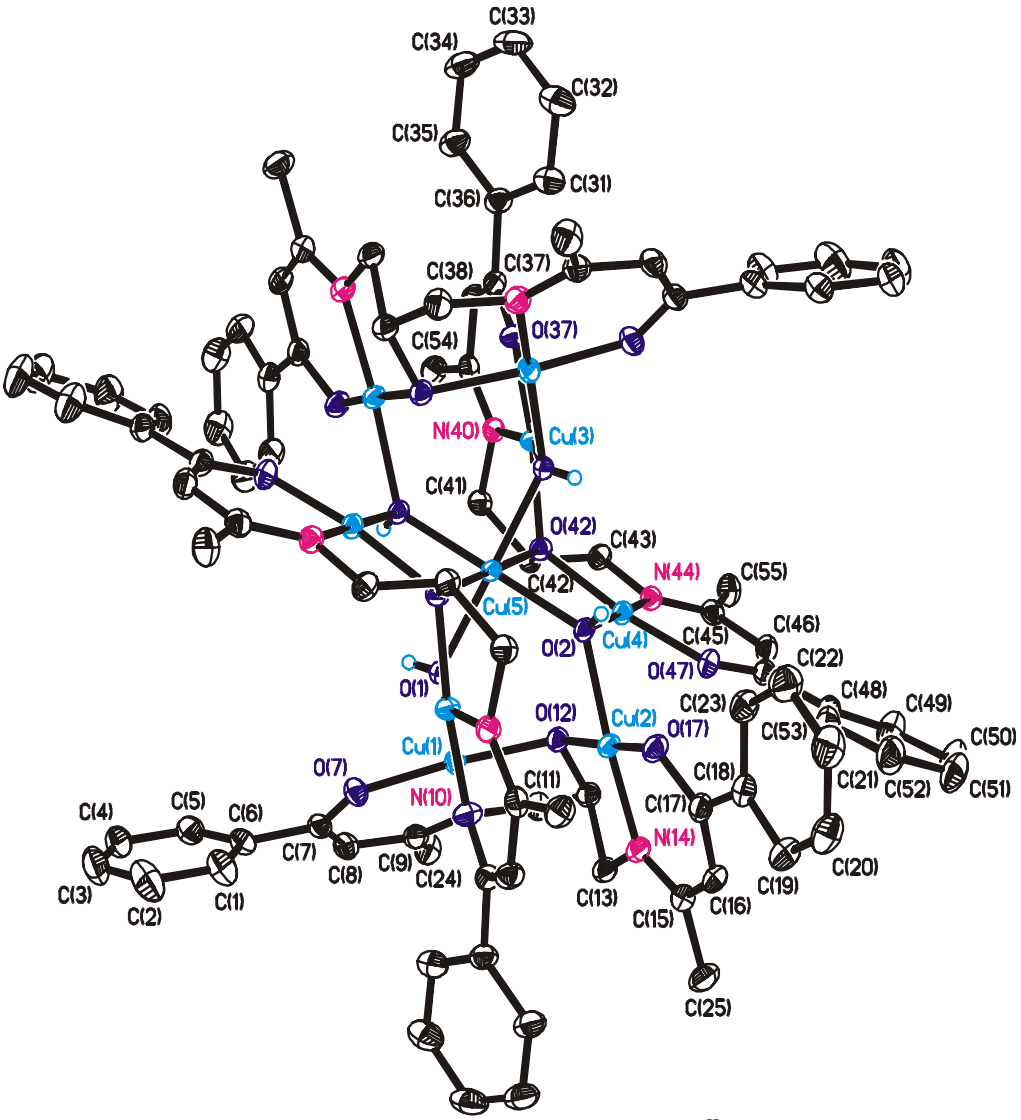

Figure 7.4: ORTEP and labeling scheme for Cu^{II}_9 (18)

All the five coordinated copper ions, Cu(1), Cu(2), Cu(3), Cu(4) and its symmetric equivalent centers are in distorted NO_4 square pyramidal geometry with an unpaired electron in the $d_{x^2-y^2}$ orbital. The basal planes around the copper centers are formed from the imine nitrogen, alkoxo oxygen, the enolized oxygen atom of the ligand moiety and the hydroxo oxygen atoms. The crystal structure gives τ values in the range 0.08-0.26 indicating an essentially square-pyramidal (4 + 1) coordination geometry of the metal in **17**.[18] In a five coordinate system, ideally square pyramidal geometry is associated with α = β = 180° for A is the axial ligand (where α and β are the basal angles). In the great majority of real square pyramidal systems, metal is displaced out of the equatorial plane toward the axial ligand. The geometric parameter τ is defined as [(β - α)/60] which is applicable to five coordinate environment as an index of degree of trigonality, within the structural continuum between trigonal bipyramidal and square pyramidal geometries. For

a perfectly square pyramidal geometry τ is zero, while it becomes unity for a perfect trigonal bipyramidal geometry. The Cu-N bond distances in all the eight copper ions, Cu(1), Cu(2), Cu(3), Cu(4) and its symmetric equivalent centers are 1.91 Å. A close look into the X-ray structure illustrates the presence of two different types of enolized oxygen atoms in the complex **17**; O(37) and O(47) are bifurcated, whereas O(7) and O(17) are monodentate. The O(12) and O(42) alkoxo groups are acting as a μ_3-bridge between {Cu(1), Cu(2) and Cu(4)} and {Cu(3), Cu(4) and Cu(5)} respectively. The Cu (1)-O(12) and Cu(2)-O(12) bond distance is 1.95 Å(basal plane), whereas the Cu(4)-O(12) bond distance of 2.5 Å is longer compared to the previous bond distance. Similarly the Cu(5)-O(42) bond distance of 2.4 Å is significantly larger compared to Cu(3)-O(42) and Cu(4)-O(42) bond distances of 1.94 Å. On the other hand O(37) and O(47) act as bridges between {Cu(1), Cu(3)} and {Cu(2),Cu(4)} respectively.

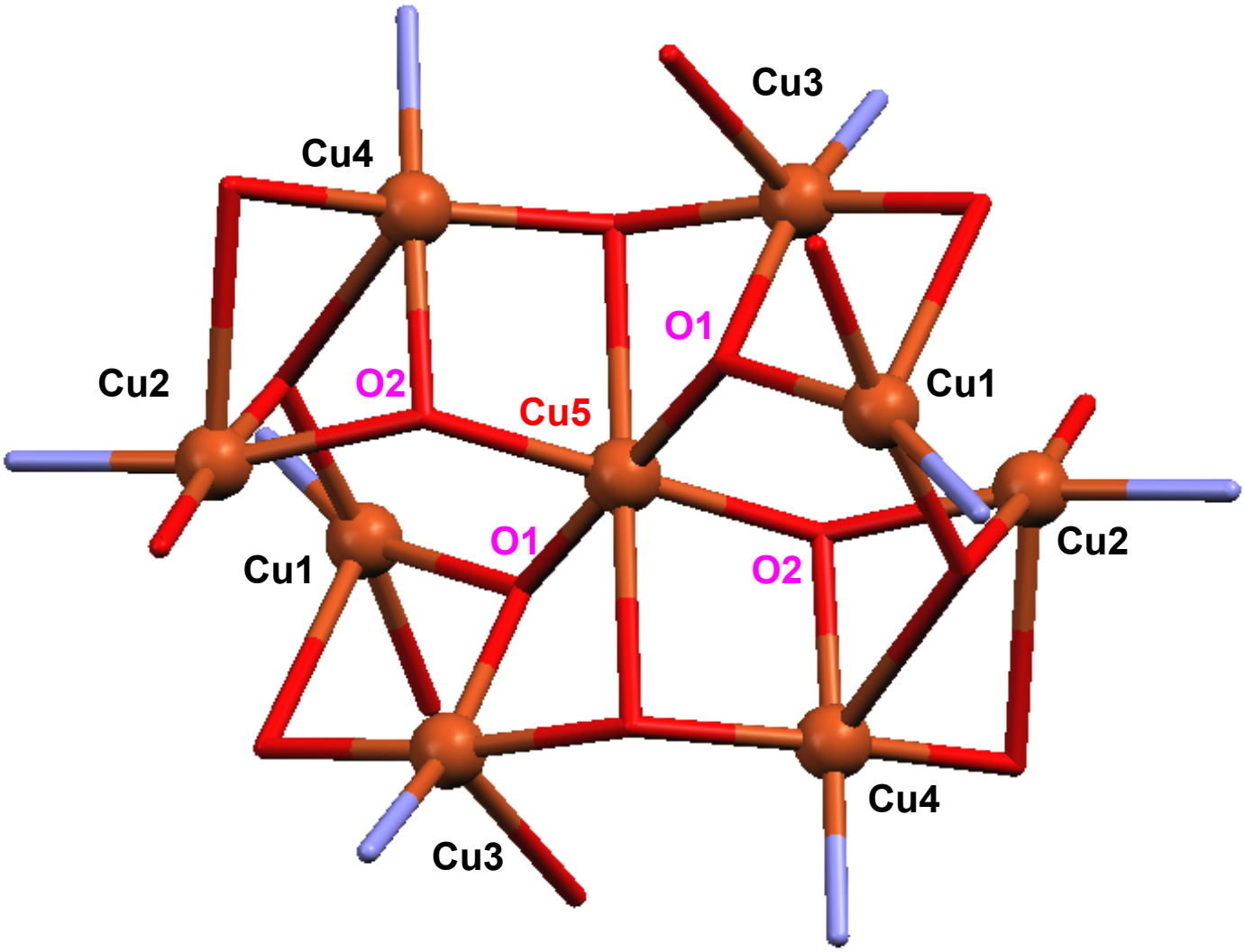

Figure 7.5A: Core structure of the nonacopper(II) cluster 17

The central copper ion Cu(5) has been subjected to Jahn-Teller distortion, as is evident from the two significantly larger Cu(5)-O(42) and Cu(5)-O(42A) bond distances of 2.4 Å compared to Cu(5)-O(1), Cu(5)-O(1A), Cu(5)-O(2), Cu(5)-O(2A) bond distances of ~ 1.97 Å . The bond distances of copper with oxygen atoms are also dissimilar ($Cu\text{-}O_{av}$ = 1.9 and 2.6 Å) in case of μ_2-alkoxo groups [O(37) and O(47)]. The μ_3-hydroxo groups O(1) and O(2) connect {Cu(1), Cu(3), Cu(5)} and {Cu(2), Cu(4), Cu(5)} respectively. The average Cu-OH(μ_3-) bond distance is 1.975 Å. The nonseparated Cu...Cu distances lie in the range from 2.88 Å to 7.3 Å in the nonanuclear cluster. The entire Cu...Cu separations are given in the table 6.2. A notable outcome of this cluster is the presence of different Cu-O-Cu bond angles which lie in the range 83.95 to 132°. It is to be mentioned that the Cu-O(H)-Cu angles are in the range 91.81 to 133.92°, whereas the Cu-μ_3-O(R)-Cu and Cu-μ_2-O(R)-Cu angles fall in the range 79.56 to 130.26°, and 77.65° respectively.

The dihedral angles (φ) between the basal planes are 72.8° within the $\{Cu_2L\}^+$ moiety. This suggests a significant deviation from the planarity of the two planes. The dihedral angles between the two interunit basal planes {Cu(1) and Cu(3)} and {Cu(2) and Cu(4)} having hydroxide bridging ligands are 107.8 and 113.2° respectively. Strong deviation from planarity may reduce the magnitudes of the exchange coupling considerably.

The crystal structure of **17** exhibits chemically significant hydrogen-bonding interaction between the complex and the lattice molecules, and also between oxygen atoms of the ligand and the coordinated methanol molecules. So the hydrogen bonding network may stabilize the core conformation. The O(2)...O(100), O(1)...O(100), O(7)...O(60), O(74)...O(80) distances of 2.73, 2.85, 2.84, and 2.83 Å respectively with O-H....O angle of ~ 160, 155, 160 and 168° respectively indicate the presence of strong hydrogen-bonding interactions.

The crystal structure of **17** is of importance as structurally characterized discrete molecular nonanuclear copper(II) complexes are limited in number.[11] Again the diversity of the core structures in these high-nuclearity copper(II) complexes means any meaningful comparison difficult.

Table 7.2: *Selected Bond Lengths (Å) and Angles (deg)* **$[Cu^{II}_9(L)_4(\mu_3\text{-}OH)_4(MeOH)_2](ClO_4)_2$ .6 MeOH (17)**

Cu(1)•••Cu(2)	3.2	Cu(1)•••Cu(5)	3.64
Cu(1)•••Cu(3)	3.25	Cu(2)•••Cu(3)	3.33
Cu(3)•••Cu(4)	3.4	Cu(3)•••Cu(5)	2.92
Cu(2)•••Cu(5)	3.64	Cu(2)•••Cu(4)	2.88
Cu(4)•••Cu(5)	3.03	Cu(4)•••Cu(4A)	6.06
Cu(2)•••Cu(2A)	7.25	Cu(3)•••Cu(3A)	6.94
Cu(1)-N(10)	1.920(2)	Cu(3)-N(40)	1.913(2)
Cu(1)-O(7)	1.914(1)	Cu(3)-O(37)	1.901(1)
Cu(1)-O(12)	1.947(1)	Cu(3)-O(42)	1.944(1)
Cu(1)-O(1)	1.980(1)	Cu(3)-O(1)	1.999(1)
Cu(1)-O(37)	2.579(6)	Cu(3)-O(60)	2.444(6)
Cu(2)-N(14)	1.911(2)	Cu(4)-N(44)	1.912(2)
Cu(2)-O(17)	1.877(1)	Cu(4)-O(47)	1.888(1)
Cu(2)-O(12)	1.949(1)	Cu(4)-O(42)	1.945(1)
Cu(2)-O(2)	1.993(1)	Cu(4)-O(2)	2.013(1)
Cu(2)-O(47)	2.612(1)	Cu(4)-O(12)	2.499(6)
Cu(5)-O(1)	1.971(1)	N(10)-Cu(1)-O(1)	158.82(8)
Cu(5)-O(1A)	1.971(1)	O(12)-Cu(1)-O(7)	174.75(7)
Cu(5)-O(2)	1.960(1)	N(14)-Cu(2)-O(2)	166.89(8)
Cu(5)-O(2A)	1.960(1)	O(17)-Cu(1)-O(12)	175.97(7)
Cu(5)-O(42)	2.395(1)	N(40)-Cu(3)-O(1)	161.64(8)
Cu(5)-O(42A)	2.395(1)	O(37)-Cu(3)-O(42)	172.56(7)
		N(44)-Cu(4)-O(2)	176.85(8)
		O(42)-Cu(4)-O(47)	172.15(7)
Cu(1)-O(12)-Cu(2)	111.43(8)	Cu(2)-O(47)-Cu(4)	77.65
Cu(1)-O(1)-Cu(5)	133.92(9)	Cu(2)-O(12)-Cu(4)	79.56

Cu(1)-O(1)-Cu(3)	109.59(8)	Cu(3)-O(1)-Cu(5)	94.73(7)
Cu(1)-O(12)-Cu(4)	130.26	Cu(3)-O(42)-Cu(4)	123.18(9)
Cu(1)-O(37)-Cu(3)	91.79	Cu(3)-O(42)-Cu(5)	83.95(6)
Cu(2)-O(2)-Cu(5)	132.92(9)	Cu(4)-O(42)-Cu(5)	88.00(6)
Cu(2)-O(2)-Cu(4)	91.81(7)	Cu(4)-O(2)-Cu(5)	99.49

7.5 Magntic Properties:

The magnetic susceptibility data for polycrystalline samples of **16** and **17** were collected in the temperature range 2-290 K in an applied magnetic field of 1T and are displayed in Figures 7.6 and 7.9 respectively as plots of the effective magnetic moment (μ_{eff}) versus temperature (T).

The plot of μ_{eff} vs. T for Ni^{II}_9 shows typical antiferromagnetic behavior, and the magnetic moment μ_{eff}/molecule of **17** is 8.2 μ_B ($\chi_M T$ = 8.4 emu mol^{-1}) at 290 K, smaller than the expected value for nine isolated Ni(II) ions S = 1 (9 x 1.00 = 9.00 emu mol^{-1}) assuming g = 2.00 (which is unrealistic for a Ni(II) ion, which always has g values > 2.00) decreases monotonically with decreasing temperature until it reaches a value of 2.51μ_B ($\chi_M T$ = 0.8 emu mol^{-1}) at 1.96 K. This temperature dependence is in agreement with antiferromagnetic behavior. Complex **17** contains 9 Ni(II) centers, with total spin from 0 to 9, owing to the size and low symmetry of the molecule, it is not possible to apply Kambe method.[19]

To fit and interpret the magnetic susceptibility data of complex **16**, first it is necessary to find all the possible magnetic pathways in the complicated but regular structure of the complex **16**. Close examination of the structure gives the pathways shown in scheme 7.5. From this scheme two different superexchange pathways can be identified, due to the different bridging modes, whereas the g value is considered to be isotropic and equal for all Ni(II) ions. A schematic core for the nonanickel(II) cluster is shown below.

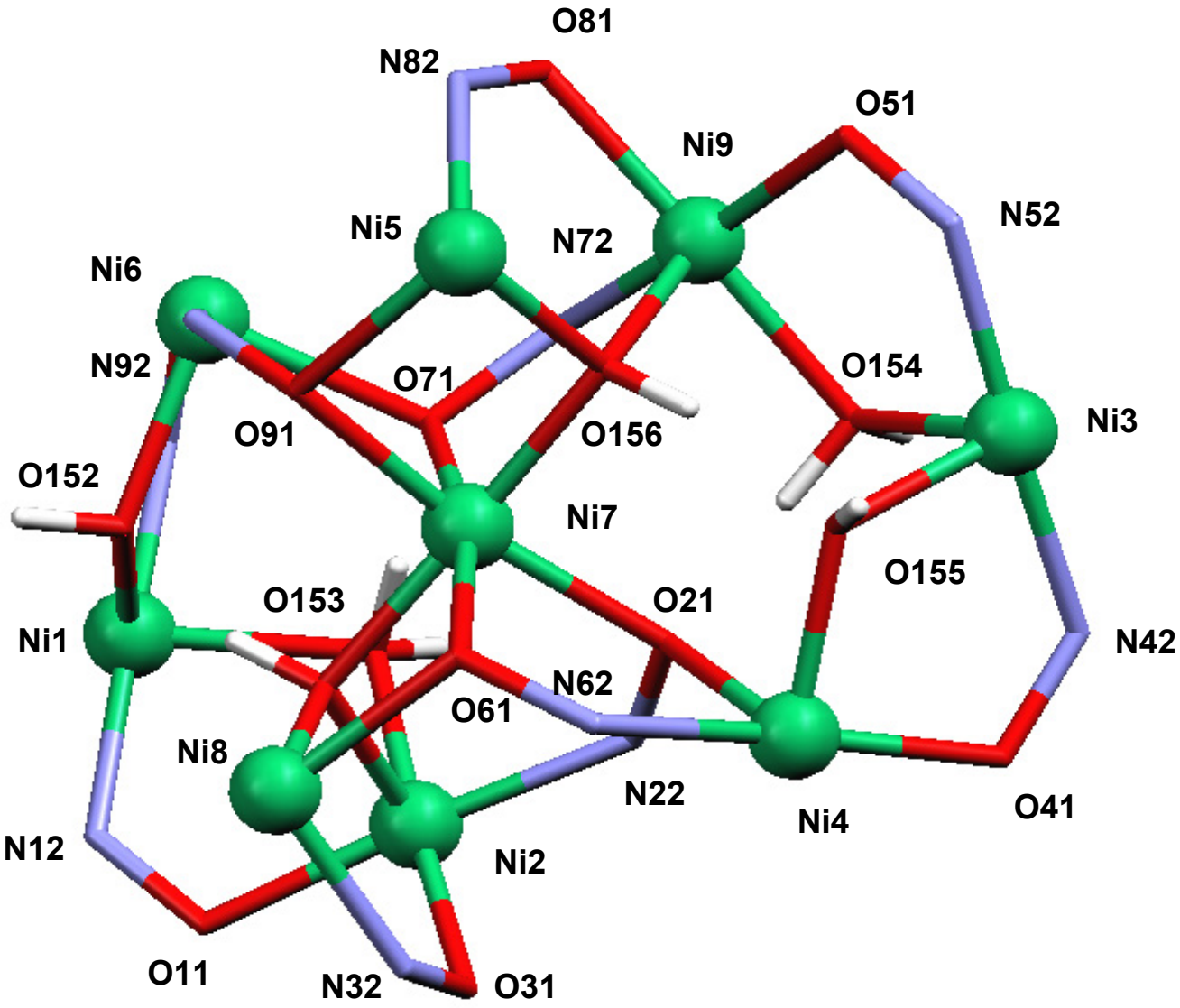

Perspective view of the coordination environment around each nickel centers in Ni^{II}_9 cluster

The exchange coupling model shown in Figure 7.5 was considered for simulation of the experimental magnetic data using irreducible tensor operator (ITO)[17] mathematical approach with the Heisenberg Hamiltonian in the form $H = -2JS_iS_j$. The experimental magnetic data have been fitted using the Hamiltonian, $H = -2J_1(S_1S_2 + S_1S_6 + S_3S_4 + S_3S_9) -2J_2(S_2S_7 + S_6S_7 + S_8S_7 + S_4S_7 + S_5S_7 + S_9S_7 +S_2S_8 + S_5S_9)$; where the numbering of the spins follows the numbering of the nickel atoms in Figure 7.5.

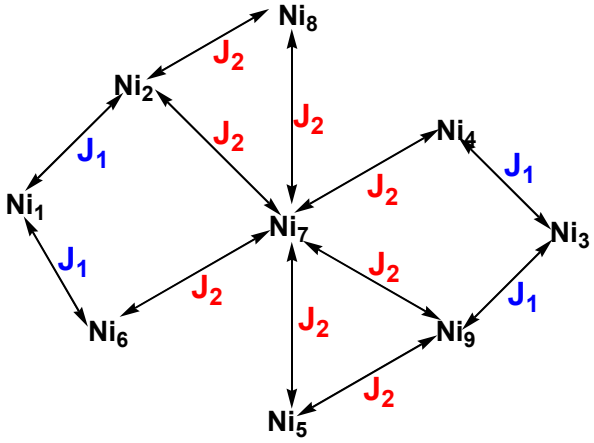

Figure 7.5: Coupling Scheme

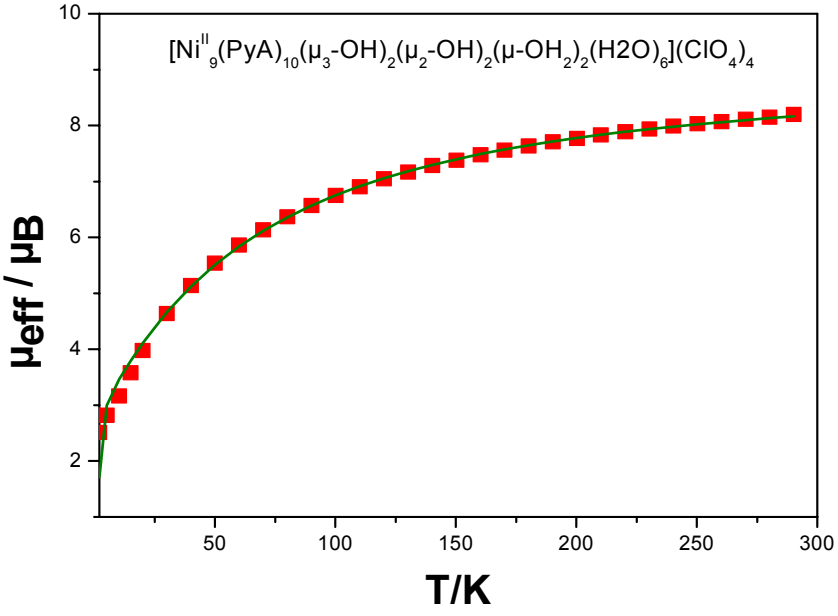

Figure 7.6: Plot of effective magnetic moment as a function of temperature. The solid line represents the best least-squares fit parameters given in the text.

Such a complicated magnetic structure represents an interesting challenge in order to fit and interpret the susceptibility data, J_1 and J_2 pathways seem to be most defined, where the J_1 pathway represents the exchange interaction between the nickel centers through (-N-O) and μ_2-hydroxo, whereas J_2 pathway represents the exchange interaction between the nickel centers through μ_2-oxygen atoms of the oximate ligands and μ_3-hydroxo ligands. In adopting this procedure we have reduced the overparametarization. The total

degeneracy of spin levels for nonanuclear nickel (II) with single ion S_{Ni} = 1 is 3^9, a number which grows very fast beyond the possibilities of handling with any computer. So it is really not a trivial task to diagonalize this 19683 X 19683 matrix. Thus it is apparent that procedures are required which employ symmetry in order to reduce the dimension of the matrices. Here in the approximation we have reduced the matrix by taking 5 nickel centers, as it was described earlier that two tetranuclear units are connected with the central nickel(II) ion. In doing so the total degeneracy is now 3^5 and now the matrix dimension is reduced to 243X243. The best fit parameters obtained where J_1 = - 26.54 cm^{-1} and J_2 = -7.02 cm^{-1} with g = 2.15. The bridging geometries between the nickel centers exhibit small variations, and this leads to variation in the exchange coupling constant.

It is known that the exchange interaction is ferromagnetic when the Ni-O-Ni angle falls below 98°, above which the exchange interaction is antiferromagnetic. Since in our case just two Ni-O-Ni angles are less than 98°, and all other Ni-O-Ni angles are greater than 98° and lie in the ranges 108-114°, the exchange interaction leads complex **16** is an antiferromagnetically coupled cluster. This can be explained in terms of interaction of the magnetic orbitals of Ni(II) with S_{Ni} = 1 which are singly occupied $(d_{x^2-y^2})^1$ and $(d_{z^2})^1$ orbitals and the dominant interactions prevailing are listed below,

$$d_{x^2-y^2} || \sigma_{sp}^2(NO) || d'_{x^2-y^2} \quad \text{antiferromagnetic}$$

$$d_{z^2} || \sigma_{sp}^2(NO) || d'_{z^2} \quad \text{antiferromagnetic}$$

$$d_{x^2-y^2} || \sigma_{sp}^2(NO) || d'_{z^2} \quad \text{ferromagnetic.}$$

All reported oximate bridged nickel(II) complexes[14-15] accordingly exhibit moderate to weak antiferromagnetic interactions, ranging from -7 cm^{-1} to - 40 cm^{-1}.

The antiferromagnetically coupled nonanuclear nickel(II) complex possesses S_T = 1 ground state, as is also evidenced from the variable temperature variable field (VTVH) magnetic measurement. From the best simulation we have evaluated the ZFS (D) parameter of the S_T = 1 ground state to be $D_{S=1}$ = 2.7 cm^{-1}

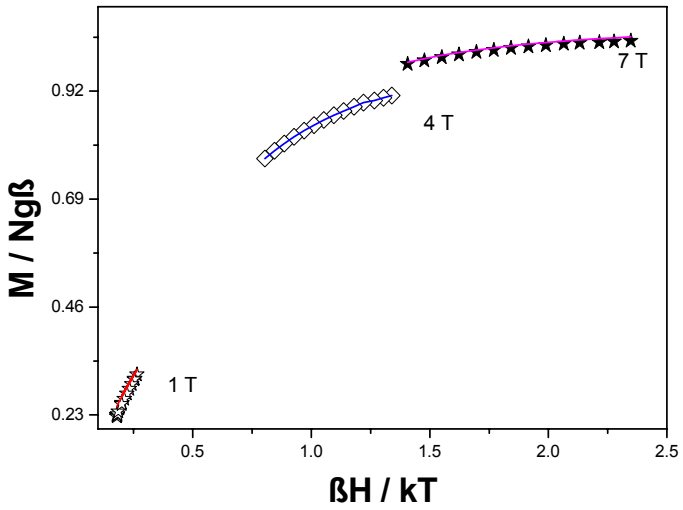

Figure 7.7: Plot of variable temperature variable field magnetic measurements (VTVH). The solid line represents the best least-squares fit parameters given in the text.

In conclusion we have been able to isolate the Ni^{II}_9 complex by using a tridentate oxime ligand. The metal ions are in a distorted octahedral coordination sphere. The complex exhibits moderate antiferromagnetic exchange interaction.

The magnetic moment μ_{eff}/molecule for **17**, Cu^{II}_9, of 4.59 μ_B ($\chi_M \bullet T$ = 2.63 $cm^3 \bullet K \bullet mol^{-1}$) at 290 K, is smaller than the typical value for nine isolated Cu(II) ions S = 0.5 (9 x 0.375 = 3.375 $cm^3 \bullet K \bullet mol^{-1}$) assuming g = 2.00 (which is unrealistic for a Cu(II) ion, which typically has g values > 2.00) decreases monotonically with decreasing temperature until it reaches a value of 3.34 μ_B ($\chi_M \bullet T$ = 1.39 $cm^3 \bullet K \bullet mol^{-1}$) at 70 K and then starts to increase slowly and reaches a value of 3.38 μ_B ($\chi_M \bullet T$ = 1.43 $cm^3 \bullet K \bullet mol^{-1}$) at 20 K and then finally decreases to a value of 2.7 μ_B ($\chi_M \bullet T$ = 0.91 $cm^3 \bullet K \bullet mol^{-1}$). This temperature dependence behavior agrees well with that expected for an antiferromagnetic exchange coupling between the copper(II) ions, leading to an irregular spin state structure. So in the μ_{eff} vs. T plot, the minima at 70-20 K indicating the presence of irregular spin levels in the compound.

Complex **17** contains 9 Cu(II) centers, with total spin from 0 to 4.5, owing to the size and low symmetry and also due to the complexity of the molecule, here also it is not possible to apply the Kambe method[19] of vector coupling to model the exchange coupling scheme. To fit and interpret the magnetic susceptibility data of complex **17**, firstly it is necessary to find all possible magnetic pathways in the complicated but regular structure of the complex **17**. Close examination of the structure gives the

pathways shown in scheme 7.8. From this scheme four different superexchange pathway can be identified, due to the different bridging modes, whereas the g value is considered isotropic and equal for all Cu(II) ions.

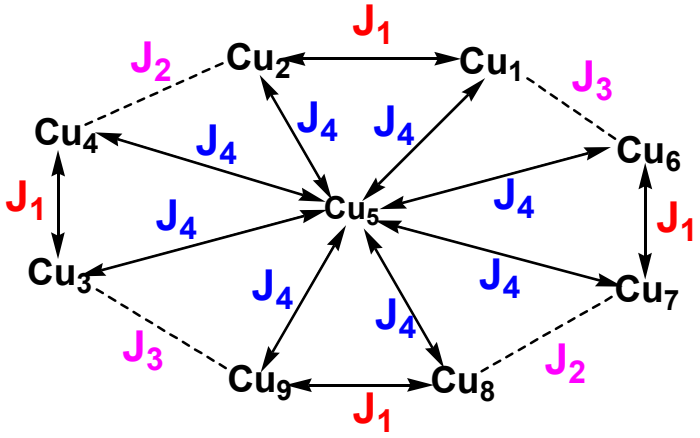

Figure 7.8: Coupling Scheme

The exchange coupling model shown in Figure 7.8 was considered for simulation of the experimental magnetic data using the irreducible tensor operator (ITO) mathematical approach with the Heisenberg Hamiltonian in the form $H = -2JS_iS_j$. The experimental magnetic data have been fitted using the Hamiltonian, $H = -2J_1(S_1S_2 + S_9S_8 + S_3S_4 + S_6S_7) - 2J_2(S_2S_4 + S_7S_8) - 2J_3(S_1S_6 + S_3S_9) - 2J_4(S_1S_5 + S_2S_5 + S_3S_5 + S_4S_5 + S_6S_5 + S_7S_5 + S_8S_5 + S_9S_5)$; where the numbering of the spins follows the numbering of the copper(II) atoms in Figure 7.8.

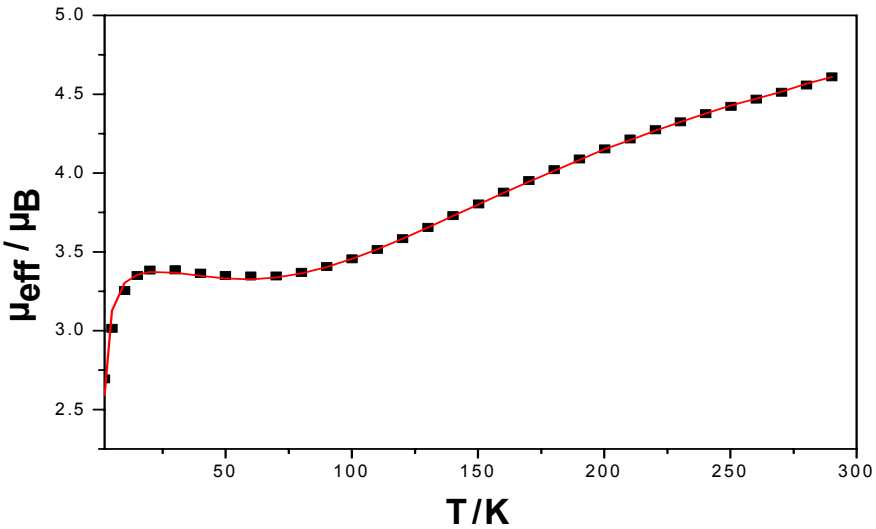

Figure 7.9: Magnetic data for Cu^{II}_9 (18) plot of μ_{eff} vs. T. The bold squares represent the experimental data while the solid line represents the simulation.

Such a complicated magnetic structure represents an interesting challenge in order to fit and interpret the susceptibility data. It is logical to consider J_1, J_2, J_3 and J_4 pathways where the J_1 pathway represents the interaction between the copper centers through alkoxo bridge in the binuclear $\{Cu_2L\}^+$ unit; whereas J_2 and J_3 pathway represent the interaction between the copper centers through (alkoxo, enolized μ_2-O and hydroxo) and enolized μ_2-O-hydroxo) groups respectively; on the other hand J_4 defines exchange interaction between the copper(II) ions through hydroxo bridge. The total degeneracy of spin levels for nonanuclear copper (II) with single ion $S_{Cu} = 0.5$ is 2^9, giving rise to a matrix of 512 X 512. From the best fit, the parameters obtained are $g_{Cu} = 2.30$, $J_1 = -193.3$ cm^{-1}; $J_2 = -27.4$ cm^{-1}; $J_3 = -6.4$ cm^{-1}; $J_4 = -53.1$ cm^{-1}, with a *R* agreement factor ($R = (\chi_M^{calc} - \chi_M^{exp})^2/(\chi_M^{exp})^2$) of 2.9×10^{-4}.

But to reduce the possible over parameterization another set of spin modeling was taken into consideration with the Heisenberg Hamiltonian; $H = -2J_1(S_1S_2 + S_9S_8 + S_3S_4 + S_6S_7) - 2J_2(S_2S_4 + S_7S_8 + S_1S_6 + S_3S_9) - 2J_3(S_1S_5 + S_2S_5 + S_3S_5 + S_4S_5 + S_6S_5 + S_7S_5 + S_8S_5 + S_9S_5)$, where J_1, J_2, and J_3 define the exchange interactions between the copper(II) ions through alkoxo, (alkoxo-hydroxo-enolized μ_2-O) and hydroxo bridges respectively. In the previous scheme two different exchange coupling constants through alkoxo-hydroxo-enolized μ_2-O and enolized μ_2-O-hydroxo bridges exchange interactions were considered. By using a "three-J" model overparametarization is reduced.

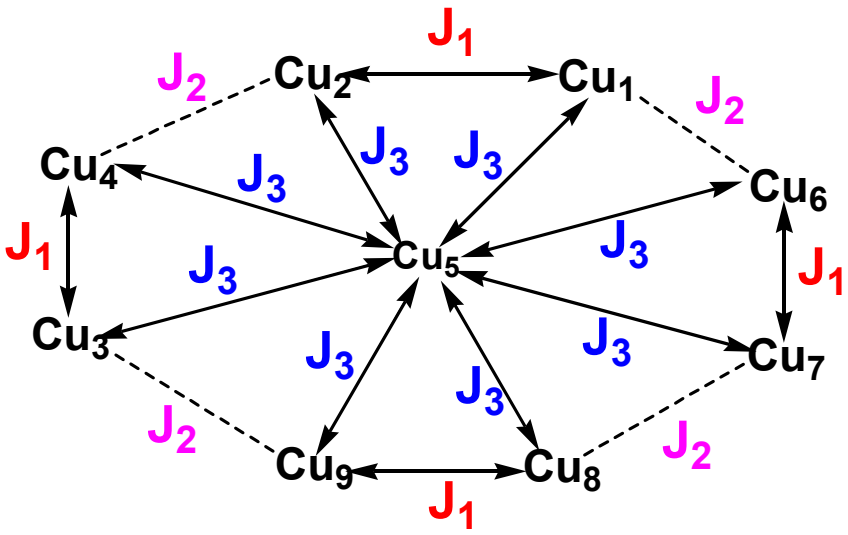

Figure 7.10: Coupling Scheme.

As an approach to the *J* coupling constants, a fit based on the interaction was performed by means of the CLUMAG program, which uses the irreducible tensor operator formalism (ITO) on the Hamiltonian. Best fit parameters are in good accordance with the expected values for the three kinds of bridges, $J_1 = -189.1$ cm^{-1}, $J_2 = -22.7$ cm^{-1}, $J_3 = -45.7$ cm^{-1}, $g = 2.29$ with a R agreement factor ($R = (\chi_M^{calc} - \chi_M^{exp})^2/(\chi_M^{exp})^2$) of 1.37×10^{-4}. In this case, attempts to fit the system with a "*three-J*" scheme give good mathematical fits and realistic coupling constants values.

Magnetostructural correlations have been found to be very successful in the description of the Cu...Cu coupling in binuclear complexes with double bridging ligands. It has been shown that if the Cu-O-Cu angle exceeds 97.5°, an antiferromagnetic interaction is observed, if less a ferromagnetic interaction.[23] Significant decrease of the values of exchange coupling constants was observed due to the displacement of the Cu_2O fragment from planarity due to displacement of metal ions from the ligand plane.[24] To avoid over parameterization in the calculation for the compound **17**, only the interactions deemed most likely to dominate the coupling were considered. It is clear from the vast amount of research that the nature and the strength of the exchange are chiefly affected by the Cu-O-Cu angle. In general, the coupling is antiferromagnetic and J decreases as Cu-O-Cu angle becomes more acute. For each type of bridge there is predicted critical value of Cu-O-Cu angle where J changes sign to become ferromagnetic. The antiferromagnetic interaction is favoured by the nature of the bridge in the order OPh > OR > OH. Other electronic and geometric factors have also been found to exert a particular influence on the value of J, such as the coordination geometry around Cu(II),[20] the Cu-O bond distances,[21] or the electronegativity of the additional ligands bound to the metals.[22] Because of the approximations included in this analysis, however, the numbers obtained must be regarded for scepticism. The structural differences of this cluster **17** prevent a systematic comparison between their J values. However, the strongest interaction, which controls the coupling, can be compared.

As expected, the magnetic response of compounds **17** is dominated by the strong antiferromagnetic coupling through the alkoxo bridge in the $\{Cu_2L\}^+$ which shows large Cu–O–Cu bond angles. A strong antiferromagnetic exchange is expected when the Cu-O-Cu bridging angle is close to 180°, whereas for angles close to 90°, the interaction is expected to be either ferromagnetic or weakly antiferromagnetic. Therefore, in spite of the relatively similar coupling constants, the exchange coupling through different Cu-O-Cu bond angle based on alkoxo, hydroxo and alkoxo-hydroxo bridge has non-trivial

features that should be analyzed separately. In spite of a different coordination polyhedron, the interaction through alkoxo bridge coupling reaches a J value comparable to that obtained for the interaction between the two copper planes with $d_{x^2-y^2}$ interaction. Owing to the square pyramidal geometry of Cu(1) and Cu(2), the metallic components of their magnetic orbitals is $d_{x^2-y^2}$ which points towards the equatorial ligands. As a consequence strong overlap is expected with the alkoxo-bridge. From the structural data, the coupling constant associated with the alkoxo bridge (J_1) should be high in view of the large Cu–O–Cu bond angle and weaker value should be expected for the interaction through the enolized μ_2-O-hydroxo bridge (J_2) due to countercomplementary interactions promoted by the exogenous hydroxo bridge and expected to be weaker compared to the interaction mediated through alkoxo bridge only and are in good agreement with entities reported elsewhere. So it can be anticipated that the observed weaker antiferromagnetic coupling(J_2) compared to that of alkoxo bridge exchange interaction (J_1) results from a competition between the two different magnetic orbital overlap pathways, viz. Cu-O_{enol}-Cu and Cu-O(H)-Cu, which may have opposite face relative to each other. On the other hand the hydroxo subunit should correspond to a moderate antiferromagnetic superexchange interaction (J_3) is due to $d_{x^2-y^2}||d_{z^2}$ pathway.

For the compound **17**, in which the environment of the eight copper ions is practically square pyramidal (4+1) with unpaired electron in the $d_{x^2-y^2}$ orbital, except the central copper ions Cu(5) is in an octahedral environment with the unpaired electron in d_{z^2} orbital, due to the Jahn-Teller distortion, which is evidenced in the X-ray structure. The strong interaction mediated through alkoxo bridges in the $\{Cu_2L\}^+$ unit is thus well justified and comparable to the reported[25] values in the range J = -111 to -380 cm^{-1}. The moderately large Cu-O-Cu angles result in good overlap between the copper $d_{x^2-y^2}$ and alkoxo p_x and p_y orbitals. That the J_2 coupling is much smaller in comparison to J_1 coupling could be explained very nicely due to the countercomplementary interaction promoted by the exogenous hydroxo group and can be compared with literature survey, documented well.[8,9b,10,25f,26-27] It is to be also mentioned that though the Cu-O-Cu angle is very large (131°) but the interaction is reduced by the countercomplementary exchange interaction promoted by the carboxylate group and in one case the interaction between the copper ions mediated through alkoxo-hydroxo is ferromagnetic in nature (J = + 17 cm^{-1})[10] due to the countercomplementary interaction mediated through the hydroxo bridge.

7.6 References:

(1) (a) H. Saarinen and M. Orama, *Acta Chem. Scand*., 1998, **52**, 1209; (b) M. Orama, H. Saarinen and J. Korvenranta, *Acta Chem. Scand*., 1989, **43**, 407

(2) B. F. Becket and J. Hoskins, *J. Chem. Soc. Dalton Trans*., 1972, 291

(3) (a) A. Graham, S. Meier, S. Parsons and R. E. P. Winpenny, *J. Chem. Soc. Chem. Commun*., 2000, 811; (b) X. Lin, D. M. J. Doble, A. J. Blake, A. Harrison, C. Wilson and M. Schröder, *J. Am. Chem. Soc*., 2003, **125**, 9476; (c) D. M. J. Doble, C. H. Benison, A. J. Blake, D. Femske, M. S. Jackson, R. D. Kay, W-S. Li and M.Schröder, *Angew. Chem. Int. Ed. Engl.,* 1999, **38**, 1915

(4) G. S. Papaefstathiou, A. Escuer, R. Vicente, M. Font-Bardia, X. Solans and S. P. Perlepes, *J. Chem. Soc. Chem. Commun*., 2001, 2414

(5) (a) U. H. Crawford, H. W. Richardson, J. R. Wasson, D. J. Hodgson and W. E. Hatfield, *Inorg. Chem*. 1976, **15**,2107; (b) D. J. Hodgson, *Prog.Inorg. Chem*. 1975, **19**,173

(6) (a) P. J. Hay, J. C. Thibeault and R. Hoffmann, *J. Am. Chem. Soc*., 1975, **97**, 4887; (b) O.Kahn, *Inorg. Chim. Acta*. 1978, **31**,11

(7)(a) V. Mckee and J. Smith, *J. Chem. Soc. Chem. Commun*., 1983, 1465; (b) M. G. B. Drew, J. Nelson, F. S. Esho, V. Mckee and S. M. Nelson, *J. Chem. Soc. Dalton Trans*., 1982, 1837

(8) (a) Y. Nishida and S. Kida, *J. Chem. Soc. Dalton Trans*., 1986, 2633; (b) Y. Nishida and S. Kida, *Inorg. Chem*. 1988, **27**, 447

(9) (a) T. Mallah, M-L. Bailot, O. Kahn, J. Gouteron, S. Jeannin and Y. Jeannin, *Inorg. Chem*., 1986, **25**, 3058; (b) V. Mckee, M. Zvagulis and C. A. Reed, *Inorg. Chem*., 1985, **24**, 2914; (c) V. Mckee, J. V. Dagdigian, R. Bau and C. A. Reed *J. Am. Chem. Soc*., 1981, **103**, 7000

(10) W. Mazurek, K. J. Berry, K. S. Murray, M. J. O'Connor, M. R. Snow, and A. G. Wedd, *Inorg. Chem*. 1982, **21**, 3071

(11) (a) V. A. Milway, V. Niel, T. S. M. Abedin, Z. Xu, L. K. Thompson, H. Grove, D. O Miller, and S. R. Parsons, *Inorg. Chem*., 2004, **43**, 1874; (b) X. Ottenwaelder, J. Cano, Y. Journaux, E. Riviere, C. Brennan, M. Nierlich and R. Ruiz-Garcia, *Angew. Chem. Int. Ed. Engl.,* 2004, **43**, 850; (c) L. Zhao, Z. Xu, L. K. Thompson, S. L. Heath, D. O. Miller and M. Ohba, *Angew. Chem. Int. Ed. Engl.,* 2000, **39**, 3114

(12) (a) A. Mukherjee, I. Rudra, M. Nethaji, S. Ramashesa and A. R. Chakravorty, *Inorg. Chem*., 2003, **42**, 463; (b) K. Geetha, M. Nethaji and A. R. Chakravorty, *Inorg. Chem*.,1997, **36**, 6134; (c) A. Mukherjee, M. Nethaji and A. R. Chakravorty, *Angew. Chem. Int. Ed. Engl.,* 2004, **43**, 87

(13) (a) S. K. Tandon, L. K. Thompson, J. N. Bridson and C. Beneli, *Inorg. Chem*., 1995, **34**, 5507; (b) A. Escuer, M. Salah, E. Fallah, R. Vicente, N. Sanz, M. Font-Bardia, X. Solans and F. A. Mautner, *J. Chem. Soc. Dalton Trans*., 2004, 1867, (c) V. Mckee, M. Zvagulis, J. V. Dagdigian, M. G. Patch and C. A. Reed, *J. Am. Chem. Soc*., 1984, **106**, 4765

(14) P. Chaudhuri, *Coord. Chem. Rev* 2003, **243**, 143

(15) (a) V. Pavlischuk, F. Birkelbach, T. Weyhermüller, K.Wieghardt and P. Chaudhuri. *Inorg. Chem*., 2002, **41**, 4405; (b) J. Faus, F. Lloret, M. Julve, M. J. Clemente-Juan, M. Munoz, X. Solans, M. Font-Bardia, *Angew. Chem. Int. Ed. Engl.,* 1996, **35**, 1485; (c) V. V. Pavlischuk, S. V. Kolotilov, A. W. Addison, M. J. Prushan, R. J. Butcher and L. K. Thompson, *Inorg. Chem*., 1999, **38**, 1759; (d) T. Weyhermüller, R. Wagner, S. Khanra and P. Chaudhuri, *J. Chem. Soc. Dalton Trans*., 2005, 2539; (e) P. Chaudhuri and T. Weyhermüller, unpublished results.

(16) (a) S. Ross, T. Weyhermüller, E. Bill, E. Bothe, U. Flörke, K. Wieghardt and P. Chaudhuri, *Eur.J.Inorg.Chem.*, 2004, 984; (b) S. Ross, T. Weyhermüller, E. Bill, K. Wieghardt and P. Chaudhuri, *Inorg. Chem.*, 2001, **40**, 6656

(17) D. Gatteschi and L. Pardi, *Gazz. Chim. Ita*., 1993, **123**, 231

(18) A. W. Addison, T. N. Rao, J. Reedijk and G. C. Vershcoor, *J. Chem. Soc., Dalton Trans.*, 1984, 1349

(19) K. Kambe, *J.Phys.Soc.,Jpn*. 1950, **5**, 48

(20) (a) P. J. Hay, J. C. Thibault and R. Hoffman, *J. Am. Chem. Soc*., 1975, **97**, 4884; (b) R. J. Butcher and E. Sinn, *Inorg. Chem*, 1976, **15**, 1604

(21) (a) E. Ruiz, P. Alemany, S. Alvarez and J. Cano, *Inorg. Chem*, 1997, **36**, 3683; (b) E. Ruiz, P. Alemany, S. Alvarez and J. Cano, *J. Am. Chem. Soc*., 1997, **119**, 1297

(22) H. Astheimer and W. Haase, *J. Chem. Phys*. 1986, **85**, 1427

(23) V. H. Crawford, H. W. Richardson, J. R. Wasson, D. J. Hodgson and W. E. Hatfield, *Inorg. Chem*, 1976, **15**, 2107

(24) H. Okawa, J. Nishio, M. Obha, M. Tadokoro, N. Matsumoto, M. Koikawa, S. Kida and D. E. Fenton, *Inorg. Chem*, 1993, **32**, 2949

(25) (a) A. Mukherjee, M. K. Saha, I. Rudra, S. ramasesha, M. Nethaji and A. R. Chakravarty, *Inorg. Chim. Acta*. 2004, **357**, 684; (b) H. Arif, Y. Funahashi, K. Jitsukawa, and H. Masuda, J. Chem. Soc., Dalton. Trans. 2003, 2115; (c) H. Grove, T. L. Kelly, L. K. Thompson, L. Zhao, Z. Xu, T. S. M. Sbedin, D. O. Miller, A. E. Goeta, C. Wilson and J. A. K. Howard, *Inorg. Chem* 2004, **43**, 4278; (e) B. Graham, M. T. W. Hearn, P. C. Junk, M. Kepert, F. E. Mabbs, B. Moubaraki, K. S. Murray and L. Spiccia, *Inorg. Chem* 2001, **40**, 1536; (f) H. Nie, S. M. J. Aubin, M. S. Mashuta, R. A. Porter, J. F. Richardson, D. N. Hendrickson and R. M. Buchanon, *Inorg. Chem* 1996, **35**, 3325; (g) D. Ghosh, N. Kundu, G. Maity, K-Y. Choi, A. Caneschi, A. Endo and M. Chaudhuri, *Inorg. Chem* 2004, **43**, 6015; (h) A. Escuer, M. S. E. Fallah, R. Vicente, N. Sanz, M. Font-Bardia, X. Solans and F. A. Mautner, J. Chem. Soc., Dalton. Trans. 2004, 1867; (i) P. E. Kruger, B. Moubaraki, G. D. fallon and K. S. Murray, J. Chem. Soc., Dalton. Trans. 2000, 713; (j) S. Wang, S. J. Terpanier, J-C. Zheng and M. J. Wagner, *Inorg. Chem* 1992, **31**, 2118, (k) M. Mikuriya, K. Minowa and R. Nukuda, *Bull. Chem. Soc. Jpn*., 2002, **75**, 2595, (l) Y. Song, C. Massera, O. Roubeau, P. Gomez, A. M. M. Lanfredi and J. Reedijk, *Inorg. Chem* 2004, **43**, 6842

(26) W. Mazurek, B. J. Kennedy, K. S. Murray, M. J. O'Connor, J. R. Rodgers, M. R. Snaw, A. G. Wedd and P.R. Zwack, *Inorg. Chem* 1985, **24**, 3258

(27) Y-C. Chou, S-F. Huang, R. Koner, G-H. Lee, Y. wang, S. Mohanta and H-H. Wei, *Inorg. Chem* 2004, **43**, 2759

CHAPTER-8

CONCLUSION AND PERSPECTIVES

The attempt to design oximate based polynuclear complexes in the field of molecular magnetism is the main goal of this work. Careful design of these polynuclear complexes has allowed us to isolate complexes with the desirable geometry and the results have led to valuable structural and magnetochemical insights. The main information and conclusions concerning this work are summarized and some perspectives are suggested. To conclude, the following points of this study deserve particular attention:

CHAPTER–2

The ligation property of a metal complex, tris(pyridine-2-aldoximato) nickel(II), has been explored to generate heterometal complexes like $\mathbf{Ni^{II}Mn^{III}Ni^{II}}$ and $\mathbf{Ni^{II}Cr^{III}Ni^{II}}$. The thermodynamic stability of the *in-situ* generated monoanion, $[Ni(PyA)_3]^-$ with facially disposed three pendent oxime oxygen atoms, makes it possible to isolate linear trinuclear complexes.

The exchange interaction between the central Mn(III) and neighboring Ni(II) is of antiferromagnetic in nature, albeit weak, and the exchange pathway $d_z^2 || \sigma_{sp}^2 || d'^2_z$ determines the strength and sign of J for the Mn(III)•••Ni(II) pair in complex **1**. On the contrary, the overall exchange interaction for complex **2**, $\mathbf{Ni^{II}Cr^{III}Ni^{II}}$, is ferromagnetic. The Cr(III)•••Ni(II) interaction in the $\mathbf{Ni^{II}Cr^{III}Ni^{II}}$ complex (**2**) is a classic example for intramolecular ferromagnetic coupling, which is predominantly due to the orthogonality of the magnetic orbitals. This is in accord with the Goodenough-Kanamori orthogonality rule as expressed by Ginsberg's symbols: e_g (Ni^{II}) $||$ $\sigma_{NO} \perp t_{2g}$ (Cr^{III}). It is to be emphasized here that two different exchange interactions are operative in the linear trinuclear $\mathbf{Ni^{II}Cr^{III}Ni^{II}}$ complex. The nearest neighbor exchange interaction between Cr(III)•••Ni(II) is found to be + 0.60 cm^{-1}, while the interaction between the terminal Ni(II) ions is evaluated to be - 0.90 cm^{-1}. The assumption occasionally made that no coupling prevails between the terminal ions may yield a miss assigned ground state.

Isolation of complex **3**, a triangular trinickel(II) complex, containing the neutral unit $[Ni(PyA)_2(PyAH)]^0$, is in accord with the reported[23] thermodynamic data that the neutral unit is more stable than the mono anionic species $[Ni(PyA)_3]^-$. It must be noted in this connection that isolation of triangular Ni(II) is very much dependent on the precipitation conditions. Our attempt to prepare a trinickel(II) compound with the linear structure like that of **1** and **2**,

$[Ni^{II}(PyA)_3Ni^{II}(PyA)_3Ni^{II}]^0$ starting from Nickel(II) acetate resulted in a compound consisting of two monomeric $[Ni(PyA)_2(PyAH)]$units held together by two O...H...O bridges.

The nickel(II) centers in the triangular unit of complex **3** are disposed as a scalene triangle with three different Ni...Ni distances. In spite of that, an excellent fit of the experimental magnetic moment data with an isosceles triangular model of three spins with S = 1.0 is possible, presumably due to only two types of bridging ligands. The triplet ground state $|1,2\rangle$ is only 8.4 cm^{-1} below the first excited singlet state $|0,1\rangle$ for **3**.

It has been established that the ground state is determined not by the absolute values of J and J' but by their ratio, $\rho = J'/J$. For $\rho \leq 1/2$, the ground state is E(1,2), and for $\rho \geq 2$, is E(1,0). On the other hand for $1/2 \leq \rho \leq 2$, the ground state is E(0,1). As a whole, the situation may be described as follows : the antiferromagnetic interaction between Ni(1) Ni(2) and Ni(1) Ni(3) polarizes the spins around Ni(2) and Ni(3) in a ferromagnetic fashion. Any antiferromagnetic interaction along Ni(2) Ni(3) opposes this effect. When $|J'|$ is small enough ($\rho \leq 1/2$), the ferromagnetic polarization takes over. When $|J'|$ is large enough ($\rho \geq 2$), the antiferromagnetic interaction takes over. When the ferromagnetic polarization and the antiferromagnetic interaction are of the same order of magnitude, the system looks for a compromise. The spin vectors around Ni(2) and Ni(3) are neither parallel nor antiparallel. Particularly interesting are the two situations $\rho = 1/2$ and $\rho = 2$. For both the cases the ground state is accidentally degenerate and the spins are unable to decide which state to be and the system is frustrated. At this point it is really worth-mentioning that, *the ratio, $\rho = J'/J$ determines the ground state in the isosceles triangular model where all the local spins are of integer values*, this important consideration was overlooked previously, in some cases,[18] led to a miss assigned spin ground state.

CHAPTER -3

The dinucleating oxime ligand acts as a backbone for the synthesis of linear tetranuclear complexes where Me_3Tacn acts as the terminal ligand. The results described in chapter-3 show that it is possible to stabilize the tris(2,6-diformyl-4-methyl phenoldioximato) bis manganese(II) pentaanion by complexation with the $[Me_3TacnM^{III}]^{3+}$, where M = Mn(III), Fe(III) or Cr(III) unit. Tris(2,6-diformyl-4-methyl phenoldioximato) bis manganese(II) pentaanion is capable of functioning as bridging ligands to give rise to linear homo- and heterotetranuclear complexes and can mediate a varying range of exchange interactions, including weak to moderate antiferromagnetic and even ferromagnetic exchange. Because of the quasi-isostructural nature these materials are unique and ideally suited for the study of intramolecular exchange interactions between the paramagnetic transition metal ions as a function of their respective d^n

electronic configurations. Five complexes were isolated and they are abbreviated as **$B^{III}Mn^{II}Mn^{II}B^{III}$ (4), $Mn^{III}Mn^{II}Mn^{II}Mn^{III}$ (5), $Mn^{IV}Mn^{II}Mn^{II}Mn^{IV}$ (6), $Fe^{III}Mn^{II}Mn^{II}Fe^{III}$ (7) and $Cr^{III}Mn^{II}Mn^{II}Cr^{III}$ (8)**.

All the complexes exhibit overall antiferromagnetic interactions. The magnetic susceptibility data for **4** demonstrates antiferromagnetic exchange coupling between the two paramagnetic high-spin Mn(II) [$S_{Mn(II)}$ = 5/2] centers. The exchange coupling constant was evaluated to be J = - 8.4 cm^{-1}. The evaluated value of the isotropic exchange interactions between the central Mn(II) centers, in complex **4** was employed to extract the exchange interactions parameter in the tetranuclear complexes **5**, **6**, **7** and **8**. The obtained values resemble quite satisfactorily in case of complexes **5, 7** and **8,** where $J_{Mn(II)...Mn(II)}$ were evaluated to be - 8.2 cm^{-1}, - 8.0 cm^{-1} and - 8.75 cm^{-1} respectively. The nearest neighbor Mn(III)...Mn(II) and Mn(IV)...Mn(II) interactions were assigned as weak ferromagnetic in nature, while the interaction between the Fe(III)...Mn(II) and Cr(III)...Mn(II) are of weak antiferromagnetic in nature.

Complex ***6*** *is the first structurally characterized tris-(oximato) bridged* ***$Mn^{IV}Mn^{II}Mn^{II}Mn^{IV}$*** *tetranuclear complex* and the parallel spin coupling, albeit weak (J = + 0.8 cm^{-1}) between the neighboring Mn(IV) and Mn(II) ions, falls at the lower end of the observed range for all similar compounds known in the literature.[2] Thus the contribution of the path e' $||$ sp^2 $||$ e' to the overall interaction becomes very important, since the e' orbitals centred on Mn(IV) and Mn(II) are empty and half-filled, respectively, leading to ferromagnetic interaction. It is interesting to note that the related isostructural $Cr^{III}Mn^{II}Mn^{II}Cr^{III}$ complex exhibits weak antiferromagnetic interaction (J = - 2.4 cm^{-1}) between the nearest neighbor Cr(III) and Mn(II) ions. Thus the contribution of the path $t_{2g}(Cr^{III})$ $||$ sp^2 $||$ $t_{2g}(Mn^{II})$ to the overall interaction becomes important, as, this path provides antiferromagnetic contribution.

CHAPTER-4

The results described in chapter-4 reveal that heterotetranuclear butterfly complexes can be synthesized by using "*metal-complexes"* as ligands. (2,6-diacetylpyridinedialdoximato) copper (II) anion is capable of functioning as bridging ligands and by complexation with $[Me_3TacnM]^{3+}$, where M = Fe(III) or Cr(III), to give rise to heterotetranuclear butterfly complexes **$Fe^{III}_2Cu^{II}_2$ (9)**, **$Cr^{III}_2Cu^{II}_2$ (10)**, where Cu(II) occupy the "*body*" and Fe(III) or Cr(III) occupy the "*wing-tip*" positions of the *butterfly*.

This study confirms that there are indeed three different coupling constants, $J_A = J_{wb}$, $J_B = J_{wb}$, $J_C = J_{bb}$ operative in the tetranuclear butterfly **$Fe^{III}_2Cu^{II}_2$** complex. Full matrix diagonalization method produced best fit parameters, $J_A = J_{wb}$ = - 125.0 cm^{-1} and $J_B = J_{wb}$ = - 6.0

cm^{-1}, $J_C = J_{bb} = -50.0\ cm^{-1}$. *VTVH measurement suggests that, it is indeed a high-spin molecule with* $\boldsymbol{S_T = 4}$ *ground state*. Simulation of the VTVH magnetic data, provides the information about exchange coupling constants with $J_A = J_{wb} = -125.0\ cm^{-1}$ and $J_B = J_{wb} = -6.0\ cm^{-1}$, $J_C = J_{bb} = -50.0\ cm^{-1}$, $D_{Fe} = +2.7\ cm^{-1}$.

Due to the presence of competing exchange interactions the ratio of the exchange coupling constants determines the ground state, not their absolute magnitudes. The strong magnetic interaction between the Fe(III) and Cu(II) ions can be interpreted by the combinations of the symmetry allowed $Fe(d_{x^2-y^2}) \,||\, (O) \,||\, Cu(d_{x^2-y^2})$ and $Fe(d_{x^2-y^2}) \,||\, \sigma_{NO} \,||\, Cu(d_{x^2-y^2})$, π- and σ-super exchange pathways respectively. Presence of strong J_{wb} over J_{bb} induces spin frustration in the butterfly $\mathbf{Fe^{III}_2Cu^{II}_2}$ core congeners**.**

In order to provide a theoretical basis for the observed magnetic properties of $\mathbf{Cr^{III}_2Cu^{II}_2}$, a "two-J" model was employed to fit and interpret the experimental data. Full matrix diagonalization method produced best fit of the parameters, $J_A = J_{wb} = -81.0\ cm^{-1}$ and $J_B = J_{wb} = -16.0\ cm^{-1}$. *VTVH measurement suggests that the molecule possesses an* $\boldsymbol{S_T = 2}$ *ground state and is indeed a "high-spin" molecule*. Simulation of the VTVH magnetic data provides the information about exchange coupling constants with $J_A = J_{wb} = -81.0\ cm^{-1}$ and $J_B = J_{wb} = -16.0\ cm^{-1}$. *Interestingly, the coupling between the* Cr^{III} *and* Cu^{II} *ions in* ***10*** *is antiferromagnetic in nature in contrast to that reported*[9-11] *for oxime bridged heteronuclear Cr(III)Cu(II) complexes*

Due to the presence of competing exchange interactions the ratio of the exchange coupling constants determines the ground state, not their absolute magnitudes. Presence of strong J_{wb} over J_{bb} induces spin frustration in the butterfly $\mathbf{Cr^{III}_2Cu^{II}_2}$ core congeners**.** $\mathbf{Cr^{III}_2Cu^{II}_2}$ species exhibits irregular spin state structure. The level ordering is a result of the mutual influence of the two different interactions which may lead to ground state variability.

These results show that it is possible to stabilize "high-spin" ground states, due to the molecular topology of the paramagnetic centers, despite antiferromagnetic interactions prevailing between the spin carriers. In the light of the present state of knowledge, the strategy of "*irregular spin-state*" structure resulting from particular spin topology is more effective in obtaining "high-spin" molecules than the common strategy of obtaining ferromagnetically coupled systems through involvement of symmetry related strict orthogonality of the magnetic orbitals of the interacting metal centers.

CHAPTER-5

The results described in this chapter show that tetramanganese clusters with different molecular topologies can be synthesized and led to interesting magnetic properties. The ligands Hppi and

salicylaldoxime act as the backbone for the synthesis of **Mn^{II}_4 (11)** and **Mn^{III}_4 (12)** complexes respectively with different topologies like "*star-shaped*", "*tetrahedral*" etc. There are very few examples of tetranuclear clusters with centred planar topology. The presented tetramanganese(II) cluster with "*star-shaped"* geometry is one of the rare example in this area.

*Complex **11** is a rare example of ferromagnetically coupled tetramanganese(II) cluster*. Detailed analysis of the temperature and field dependent magnetic behavior demonstrates a very weak ferromagnetic interaction is operative between the central and peripheral Mn(II) ions, which leads to *high-spin ground states* (**S_T = 10**). In order to provide a theoretical basis for the observed magnetic properties of **Mn^{II}_4**, a "two-J" model was employed to fit and interpret the experimental data. Full matrix diagonalization method produced best fit parameters: $J_{12} = J_{13} = +$ 0.32 cm^{-1} and $J_{14} = -$ 0.2 cm^{-1}.

*The high-spin Mn(II) centers with S = 5/2 exhibit weak ferromagnetic coupling in the Mn^{II}_4 molecule as is evidenced from both the magnetic susceptibility and variable temperature variable field (VTVH) measurements, yielding high-spin molecule with **S_T = 10** ground state.* Simulation of the VTVH magnetic data, provides the information about exchange coupling constants with $J_{12} = J_{13} = +$ 0.47 cm^{-1} and $J_{14} = -$ 0.2 cm^{-1}.

$[Mn^{III}_4(salox)_4(salox\ H)_4]$ (**12**) complex is a ferromagnetically coupled "*high-spin*" tetramanganese(III) cluster of tetrahedral geometry. The study also confirms that there are indeed two different coupling constants, $J_{12} = J_{23} = J_{34} = J_{14}$ and $J_{14} = J_{23}$ are operative in the *tetrahedral tetramaganese(III)* cluster **12**. Full matrix diagonalization method produced best fits of the parameters, $J_{12} = J_{23} = J_{34} = J_{14} = +$ 1.9 cm^{-1}; $J_{14} = J_{23} = -$ 1.6 cm^{-1} and $D_1 = D_2 = D_3 = D_4 =$ $|3|$ cm^{-1}

*The high-spin Mn(III) centers with S = 2 exhibit weak ferromagnetic coupling in the Mn^{III}_4 molecule as is evidenced from both the magnetic susceptibility and variable temperature variable field (VTVH) measurements, yielding high-spin molecules with **S_T = 8** ground state*. Simulation of the VTVH magnetic data, provides the information about exchange coupling constants with $J_{12} = J_{23} = J_{34} = J_{14} = +$ 1.9 cm^{-1}; $J_{14} = J_{23} = -$ 1.6 cm^{-1} and $D_1 = D_2 = D_3 = D_4 =$ $|3|$ cm^{-1}.

CHAPTER-6

Magnetostructural study of two hexanuclear manganese and one hexanuclear copper clusters is presented in this chapter. Two new hexanuclear mixed-valence, isostructural manganese complexes **13** and **14** have been prepared from the pentadentate dapdo ligand. The hexanuclear mixed-valence **$Mn^{III}_4Mn^{II}_2$** complexes containing the structural core **$[Mn^{III}_4Mn^{II}_2(\mu_4\text{-}O)_2]$** are

rather uncommon compared to compounds with [$\mathbf{Mn^{II}_4Mn^{III}_2(\mu_4\text{-}O)_2}$] core. *Complexes **13** and **14** are the first structurally characterized discrete hexanuclear complexes with [$\mathbf{Mn^{III}_4Mn^{II}_2(\mu_4\text{-}O)_2}$] core congener.* These two hexanuclear $\mathbf{Mn^{III}_4Mn^{II}_2}$ complexes represent the examples of "*edge- sharing tetrahedra*".

The magnetic susceptibility data for [$\mathbf{Mn^{III}_4Mn^{II}_2(\mu_4\text{-}O)_2}$] core congeners **13** and **14** exhibit both intramolecular antiferromagnetic and ferromagnetic exchange coupling. A "four-J" model was employed to fit and interpret the experimental data. *The system may be envisaged of two ferromagnetically coupled antiferromagnetic triangles and the fact that $J_A >> J_C$ clearly stabilize a local S = 5/2 ground state in each triangular unit, the ferromagnetic pathway J_D leads to an S_T = 5 ground state. So it is a "high-spin" molecule and $\mathbf{S_T = 5}$ is also evidenced from the variable-temperature-variable field (VTVH) magnetic measurements.*

By using the **ITO** mathematical approach the exchange interaction was found to be J_A = - 12.6 cm^{-1}, J_B = - 4.6 cm^{-1}, J_C = + 2.4 cm^{-1}, J_D = + 1.9 cm^{-1}, g_{Mn} = 1.98, $D_1 = D_3 = D_5 = D_6 = D_{Mn(III)}$ = 4.0 cm^{-1}. The exchange interaction between Mn(III)...Mn(III) is antiferromagnetic in nature, while the interactions between Mn(III)...Mn(II) [d^4(HS)/d^5(HS)] were found to be both antiferromagnetic and ferromagnetic, albeit weak, as the average Mn^{III}-O-Mn^{II} bond angle of 100° prevents the better overlap between the magnetic orbitals. This gives rise to ferromagnetic exchange interaction (J_B).

The main lesson from this study is that high nuclearity Mn_x complexes can be prepared which have either pairwise ferromagnetic Mn^{II}...Mn^{III} or Mn^{III}...Mn^{III} interactions or a combination of pairwise antiferromagnetic interactions or in the third possibility combination of pairwise ferromagnetic-antiferromagnetic interactions that lead to molecules with $S_T \neq 0$ ground state. Based on combination of pairwise exchange interactions, competing exchange interaction, and topology the polynuclear manganese complexes are stabilized in *high-spin* ground states.

The hexadentate oxime ligand generates a new hexanuclear copper(II) cluster(**15)**, consisting two linked Cu_3O core. Several trinuclear copper(II) structures with central O^{2-} or OH^- groups have been structurally characterized, however this *structure with two such triangles linked by a proton appears to be novel*.

The oximate ligands generally mediate strong antiferromagnetic exchange coupling between the d^9 copper(II) ions with a $d_{x^2-y^2}$ ground state as each copper(II) ions are in a square pyramidal coordination environment. The simulation of the magnetic data affords an antiferromagnetic exchange interaction in complex **15**, in accordance with the large Cu-O-Cu angles of 113.65 and 114.32° respectively in each triangular unit. A "two-J" model was used to

analyze the magnetic data. From the best fit, the intra-and interdimer antiferromagnetic exchange coupling constants are obtained to be J_A = - 614.1 cm^{-1} and J_B = - 114.5 cm^{-1} respectively. The overall coplanar Cu_3O core structure permits larger magnetic exchange interaction. As both the oximate and oxo groups transmit strong exchange coupling between the copper(II) ions, the overall effect of both of these transmissions is reflected in strong antiferromagnetic exchange interaction in this hexanuclear copper(II) cluster. Values of J ~ - 1000 cm^{-1} have been reported for other imino-oximate complexes.

CHAPTER-7

This chapter describes the structure and magnetic properties of two rare examples of nonanuclear copper(II) and nickel(II) clusters. Two new nonanuclear nickel(II) (**16**) and copper(II) (**17**) complexes have been isolated with the ligand syn-2-pyridinealdoxime and N,N'-(2-hydroxypropane-1,3-diyl)bis(benzoylacetoneimine) respectively.

Chemically significant hydrogen bonding may stabilize the nonanuclear Ni^{II} cluster. The magnetic susceptibility data for **16** exhibits an antiferromagnetic coupling between the paramagnetic Ni(II) (S_{Ni} = 1) centers and gives rise to $\mathbf{S_T}$ **=1** ground state. Antiferromagnetic exchange coupling is mediated through an average Ni(II)....Ni(II) separation of 3.38 Å . A close examination of the structure indicates that there are five different types of bridging groups for transmission of exchange coupling between the Ni(II) centers with S_{Ni} = 1.0 : i) diatomic -NO-, ii) μ_3-oximate -N-O, iii) μ_2-OH, iv) μ_3-OH , and v) μ_2-OH_2. Two avoid overparametarization a "two-J" model was employed to simulate the experimental magnetic data and resulted in moderate antiferromagnetic exchange interaction of the value J_1 = - 26.5 cm^{-1} and J_2 = - 7.0 cm^{-1}. The stronger J_1 interaction through the diatomic NO-bridging as oppose to J_2 interaction mediated through the μ_3-oximate oxygen is in accord with the literature. *This is the second example of the magnetostructurally characterized nonanuclear nickel(II) cluster. The ZFS (D) parameter of the S_T = 1 ground state is found to be $D_{S=1}$ = + 2.7 cm^{-1}*.

The polynuclear copper(II) cluster (**17**) is a rare example of magnetostructurally characterized $[Cu^{II}_9(OH)_4]^{14+}$ core congener. This cluster has a novel metallamacrocyclic core which is generated from the self-assembly process. The magnetic susceptibility data for Cu^{II}_9 complex exhibits overall antiferromagnetic coupling between the copper(II) centers and result in a non-diamagnetic ground state.

This complex also belongs to the class of *irregular spin state structure,* as is evidenced from the minima observed in the magnetic susceptibility plot. *This is due to the presence of competing exchange interactions between the spin carriers.*

To avoid the over-parameterization, three different exchange coupling constants were taken into consideration and from the best fit, the values: J_1 = - 189.1 cm^{-1}, J_2 = - 22.7 cm^{-1}, J_3 = - 45.7 cm^{-1} are obtained. J_1, J_2 and J_3 define the exchange interactions between the copper(II) ions mediated through alkoxo, alkoxo-hydroxo and hydroxo bridges respectively. As expected, the magnetic response of compound **17** is dominated by the strong antiferromagnetic exchange interaction through the alkoxo bridge in the $\{Cu_2L\}^+$ unit which shows large Cu-O-Cu bond angles. J_2 coupling constant is much smaller in comparison to J_1 coupling and could be explained very nicely due to the *countercomplementary* interaction promoted by the exogenous hydroxo group.

Magnetostructural Correlation:

In the last few years, the idea of synthesizing polynuclear complexes involving "metal-oximates" as building blocks has become quite popular. In the near future new chemistry is expected to be developed that enables chemists to synthesize a wide variety of the ligands possessing the versatility of the functioning both as bridging and polynucleating group. Thus, larger polynuclear assemblies are expected to be synthesized through modular approaches by choosing suitable ligands. The ultimate goal, obviously, is the development of the area of molecular magnetism. Oximate groups can mediate exchange interactions of varying range, weak and moderate ferromagnetic to strong antiferromagnetic. A problem concerning such exchange coupled systems is the lack of availability of isostructural polynuclear complexes with varying d^n electron configurations. Investigation of a series of isostructural polynuclear complexes will be much more informative compared to those comprising singly isolated exchange coupled clusters only. Although most of the compounds discussed in this work, along with the structurally characterized oximate based polynuclear complexes reported earlier, little can be said about the magnetostructural trends. This thesis is focused on such exchange coupled polynuclear complexes containing the bridging core M-N-O-M' originating from metal oximates. Qualitative rules allowing the prediction of the nature of interaction between two spin carriers according to the symmetry of the magnetic orbitals were proposed in the 1950's by Goodenough and Kanamori. The concepts of natural orbital and overlap integral allow the generalization and extension of Goodenough-Kanamori rules. *However, no such relation have been established between the exchange coupling constant and the metrical parameters of the diatomic bridge like oximate(N-O), azine (N-N) or oxalate*. Discussion, in detail, needs to be concentrated on such system where considerable structural and magnetochemical work have been reported. This thesis concentrates one of such parameter, e.g. the role of the dihedral angle

comprising the planes between M-N-O and O-N-M' in exchange interaction and such work is worth doing. In other words, it appears tedious, if not impossible, *to extract a qualitative understanding* of the relation between dihedral angle and exchange interaction. Table 8.1 summarizes dihedral angle comprising the planes between the planes M(O-N) and (O-N)M' and the exchange coupling constant of some magnetostructurally characterized oximato based polynuclear complexes irrespective of nuclearity.

Table 8.1: Magnetostructural parameters of some oximato complexes

Compounds	Average dihedral angle between the planes comprising M-O-N and O-N-M' atoms	Exchange coupling constants	References :
1. $[(Me_3Tacn)Mn^{III}Mn^{II}(PyA)_3]^{2+}$	32.8	+ 1.6	i
2. $[(Me_3Tacn)Mn^{III}(dmg)_3Mn^{II}Mn^{III}(Me_3Tacn)]^{2+}$	13.3	+ 4.7	ii
3. $[(Mcoe)_3Mn^{II}Mn^{III}Mn^{II}(Mcoe)_3]^{+}$	9.3	-1.3	iii
4. $[(TapTacn)Mn^{II}(\mu\text{-}O_2COMe)Mn^{III}Mn^{II}(TapTacn)]^{+}$	2.1	+ 2.0	iv
5. $[(Me_3Tacn)Mn^{III}Mn^{II}(dfmp)_3Mn^{II}Mn^{III}(Me_3Tacn)]^{+}$	30.3	+ 2.8	Complex 5
6. $[Mn^{II}Mn^{IV}Mn^{II}(pko)_4(OMe)_2(OCN)_2]$	3.75	+ 4.1	v
7. $[Mn^{II}Mn^{IV}Mn^{II}(pko)_4(OMe)_2(Cl)_2]$	14.8	+ 3.9	v
8. $[(Me_3Tacn)Mn^{IV}Mn^{II}(dfmp)_3Mn^{II}Mn^{IV}(Me_3Tacn)]^{3+}$	17.0	+ 0.8	Complex 6
9. $[Mn^{II}Mn^{IV}Mn^{II}(pko)_4(OMe)_2(SCN)_2]$	34.3	+ 3.1	vi
10. $[(Me_3Tacn)Fe^{III}(dmg)_3Mn^{II}Fe^{III}(Me_3Tacn)]^{2+}$	4.8	- 6.7	vii
11. $[(Me_3Tacn)Fe^{III}Mn^{II}(PyA)_3]^{2+}$	32.1	- 6.1	viii
12. $[(Me_3Tacn)Fe^{III}Mn^{II}(dfmp)_3Mn^{II}Fe^{III}(Me_3Tacn)]^{+}$	29.8	- 1.8	Complex 7
13. $[(Me_3Tacn)Cr^{III}Mn^{II}(PyA)_3]^{2+}$	31.4	+ 1.5	ix
14. $[(Me_3Tacn)Fe^{III}(\mu\text{-}O..H..O\text{-}\mu)Cu^{II}{}_2(dapdo)_2(\mu\text{-}Cl)\,FFe^{III}(Me_3Tacn)]^{2+}$	5.7	- 125.0	Complex 9
15. $[(Me_3Tacn)Cr^{III}(dmg)_3Cu^{II}Cr^{III}(Me_3Tacn)]^{2+}$	9.1	+ 18.5	x
16. $[(Me_3Tacn)Cr^{III}(OMe)Cu^{II}(dopn)(H_2O)]^{2+}$	21.8	+ 18.5	xi
17. $[(Me_3Tacn)Cr^{III}Cu^{II}(PyA)_3]^{2+}$	34.0	+ 1.8	xii
18. $[(Me_3Tacn)Cr^{III}(\mu\text{-}OH)_2Cu^{II}{}_2(dapdo)_2(Br_2)\,Cr^{III}(Me_3Tacn)]^{2+}$	76.7	- 16.0	Complex 10
19. $[(Me_3Tacn)Fe^{III}Cu^{II}(PyA)_3]^{2+}$	32.1	- 42.5	viii

20. $[(Me_3Tacn)Fe^{III}(dmg)_3Cu^{II}Fe^{III}(Me_3Tacn)]^{2+}$	10.6	- 53.0	xx
21. $[(Me_3Tacn)Mn^{III}(OOCMe)Cu^{II}(dopn)]^{2+}$	24.5	+ 54.0	xi
22. $[(Me_3Tacn)Mn^{III}(dmg)_3Cu^{II}Mn^{III}(Me_3Tacn)]^{2+}$	26.5	- 63.0	ii
23. $[(Me_3Tacn)Fe^{III}(Cl)Cu^{II}(MeOH)Ni^{II}(MeOH)_2(L_{OX})]^{2+}$	47.1	- 19.8	xii
24. $[(Me_3Tacn)Fe^{III}Ni^{II}(dfmp)_2Ni^{II}(MeCOO)_2$ $(MeOH)_2Fe^{III}(Me_3Tacn)]^{2+}$	31.1	- 6.8	xxi
25. $[(Me_3Tacn)Fe^{III}(dmg)_3Ni^{II}Fe^{III}(Me_3Tacn)]^{2+}$	24.1	- 32.0	xxii
26. $[(Me_3Tacn)Fe^{III}(NCS)Ni^{II}(H_2O)(NCS)$ $Ni^{II}(NCS)_2(H_2O)(L_{OX})]$	28.2	- 9.3	xiii
27. $[(Me_3Tacn)Fe^{III}Ni^{II}(PyA)_3]^{2+}$	39.5	- 34.0	viii
28. $[(PyA)_3Ni^{II}Fe^{III}Ni^{II}(PyA)_3]^{+}$	38.4	- 31.0	xiv
29. $[(Me_3Tacn)Cr^{III}Ni^{II}(PyA)_3]^{2+}$	38.8	- 9.2	ix
30. $[(Me_3Tacn)Cr^{III}Ni^{II}(PPyA)_3]^{2+}$	20.8	0.0	ix
31. $[(Me_3Tacn)Cr^{III}(dmg)_3Ni^{II}Cr^{III}(Me_3Tacn)]^{2+}$	25.9	- 0.7	x
32. $[(PyA)_3Ni^{II}Cr^{III}Ni^{II}(PyA)_3]^{+}$	35.2	+ 0.6	Complex 2
33. $[\{Ni(Dien)\}_2(\mu_3\text{-}OH)_2\{Ni_2(Moda)_4\}]^{2+}$	7.2	- 20.3	xv
34. $[Ni_4(MeOH)_2(pko)_6]^{2+}$	36.5	-24.0	xvi
35. $[(Me_3Tacn)Ni_2(PyA)_3]^{2+}$	43.1	- 33.0	xvii
36. $[Ni_3(PyA)_5(PYAH)]^{+}$	24.1	-8.3	Complex 3
	75.8	-2.0	
37. $[Ni_4(TapHTacn)_3]^{2+}$	36.4	-13.4	iv
38. $[Ni_6(amox)_6(\mu_6\text{-}O)(\mu_3\text{-}OH)_2]^{2+}$	44.0	-25.0	xix
39. $[Ni_3(Dtox)(Dtox\ H)_2]^{2+}$	37.5	-14.0	xviii
	58.0	-7.3	

The obvious question is: can we find some relation between these parameters? The results obtained are summarized below:

(a) When we consider dihedral angle and exchange coupling constants in a general manner, we *can not find any correlation*. Figures 8.1a and b show such plots where little can be said about the influence of the dihedral angles on exchange interaction.

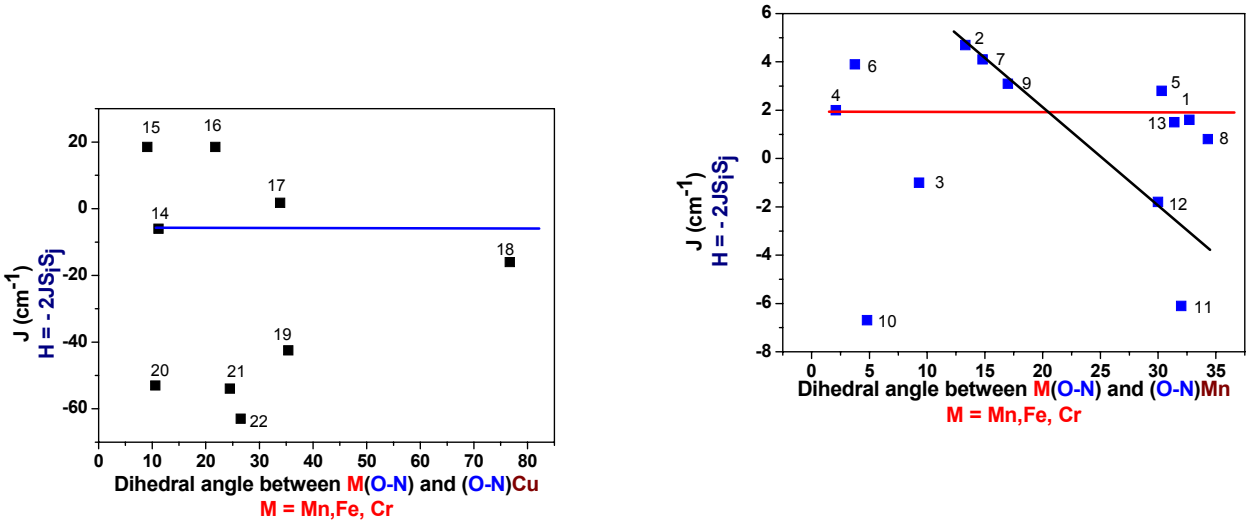

(a) **(b)**

Figure 8.1: Plot of dihedral angles comprising the planes between M(O-N) and (O-N)M' and exchange coupling constant (J)

(b) W*hen we consider each individual pair, it seems that there is certain influence of the dihedral angles on exchange interactions.*

According to Kahn, Goodenough and Kanamori $Cr^{III}Ni^{II}$ [d^3d^8(octahedral)], $Cr^{III}Cu^{II}$ [d^3d^9(octahedral)], and $Mn^{IV}Mn^{II}$ [d^3d^5(HS)(octahedral)] interactions are expected to be ferromagnetic due to the $t_{2g}\perp e_g$ magnetic orbitals as several strictly ferromagnetic paths are available..

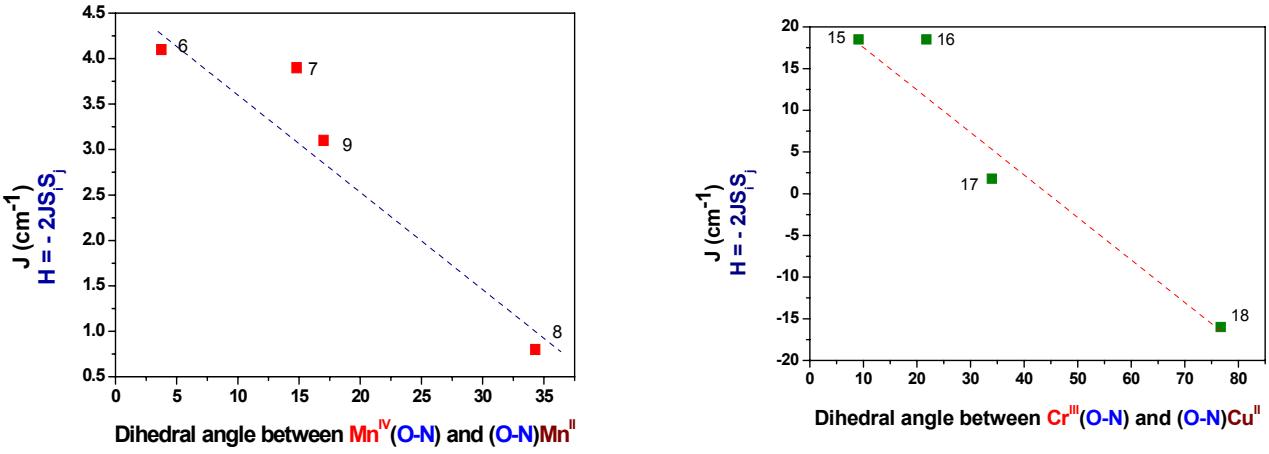

(a) **(b)**

Figure 8.2 : Plot of dihedral angles comprising the planes between Mn^{IV}(O-N) and (O-N)Mn^{II} and exchange coupling constant (J) (a) and dihedral angles comprising the planes between Cr(O-N) and (O-N)Cu and exchange coupling constant (J) (b)

Figures 8.2 and 8.3 suggest that there is a decreasing tendency of ferromagnetic exchange coupling constants with increasing dihedral angles. This observation leads us to the conclusion that with increasing dihedral angle there may be some deviation from orthogonality, which in turn, causes better overlap between the magnetic orbitals results and is reflected in increasing antiferromagnetic coupling with increasing dihedral angle. Deviation from such behavior of the complexes **16** and **32** may be due to the influence of subtle coordination differences around metal centers.

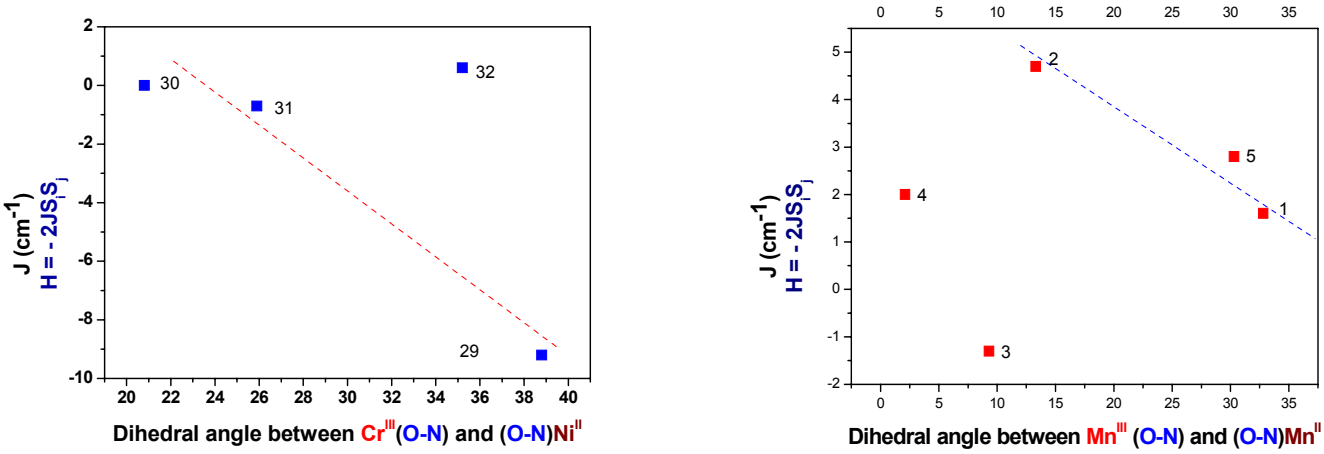

Figure 8.3: Plot of dihedral angles comprising the planes between Cr(O-N) and (O-N)Ni and exchange coupling constant (J)

The similar trend is also observed in case of Mn^{II}…Mn^{III} cases. However Mn^{II}...Mn^{III} exchange interaction value of J = - 1.3 cm^{-1} in **3**, which results from Mn(III)-O-N-Mn(II) superexchange pathways can be compared with the related dimethylgyoximato (**2**), diformyl-4 methylphenoldioximato (**5**) and pyridinealdoximato(**1**)- bridging in the work of Birkelbach, compound **5** and Chaudhuri and co-workers in which Mn(II)...Mn(III) interactions were found to be ferromagnetic. The difference of sign of these Mn(II)-N-O-Mn(III) interaction results from the net effect of the ferromagnetic and antiferromagnetic contributions to $J_{Mn(II)...Mn(III)}$ Which, in turn, will be influenced by subtle coordination differences on the Mn(III) and Mn(II) centers, and to a lesser degree by the terminal bridging groups. Linear trinuclear $Mn^{II}Mn^{III}Mn^{II}$ congener (**4**) does not fit in the trends. Careful examination reveals that the exchange coupling in this complex mediated mainly by two-types of bridges, a single atom -O-bridge and a two

atom N-O linkage, of which the later contribution is expected to be small. The angle at the bridging oxygen would be expected to be important, this affects the nature of σ and π overlap between the metal magnetic orbitals and the oxygen p_x, p_y and p_z orbitals mediate the exchange. $Mn(1)^{II}$-O-$Mn(2)^{III}$ and $Mn(2)^{III}$-O-$Mn(3)^{II}$ angles are 97.5 and 108° respectively. However, the magnetic response in this complex was analyzed by using a "one-J" mode, which is not strictly true. So a "two-J" model seems to be more appropriate and $Mn(1)^{II}$...$Mn(2)^{III}$ interactions is expected to be more ferromagnetic compared to the exchange interaction between $Mn(3)^{II}$...$Mn(2)^{III}$.

From the above observation it can be concluded that with increasing dihedral angle antiferromagnetic exchange interaction increases.

(c) For $Fe^{III}Cu^{II}$ complex, antiferromagnetic exchange interaction decreases, with the increase of dihedral angle and the observed result is opposite compared to that of previous one. Fe(III)...Cu(II) is expected to be antiferromagnetic due to presence of several antiferromagnetic paths in the exchange coupling constant. Reduction of antiferromagnetic exchange coupling constant suggests that lesser overlap is prevailing between the magnetic orbitals with increasing angle.

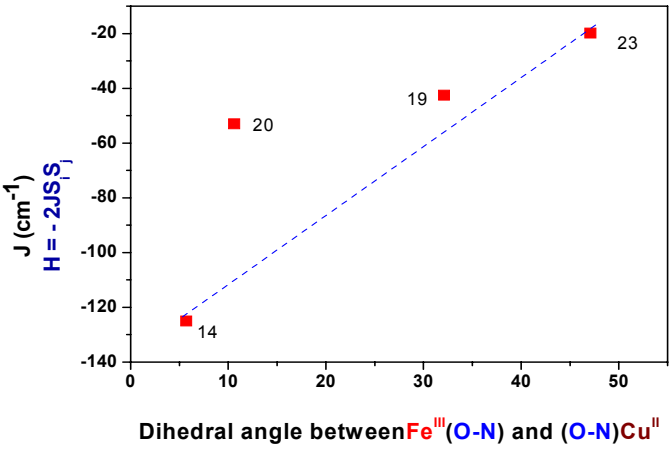

Figure 8.4: Plot of dihedral angles comprising the planes between Fe(O-N) and (O-N)Cu and exchange coupling constant (J)

(d) In the Ni-N-O-Ni case little can be said about the trends, but it can be concluded that the interaction through diatomic NO bridge is stronger than the interaction mediated through μ_3-oximate oxygen. Comparison of exchange coupling constants in complexes

34, **35**, **36**, **37** and **38** reveals that each oximate (NO) may transmit J = - 10.5 ± 1.5 cm^{-1} antiferromagnetic exchange coupling. While comparison of the exchange coupling constants in the Fe^{III}-O-N-Ni^{II} complexes reveal that each oximate may transmit J = ~ - 11cm^{-1} antiferromagnetic exchange interaction irrespective of the dihedral angles.

Summarizing some of the results of the exchange-coupled oximate -bridged polynuclear complexes reported in the literature, along with some of the complexes in this work, it appears that no strong correlation between structural and magnetic properties for such complexes has been obtained. Hence obtaining any such correlation requires isostructural purely octahedral dinuclear complexes. The importance of designed synthesis lies there in.

Perspectives:

A few ideas and perspectives, in the continuation of this work are outlined below:

(1) Synthesis and magnetostructural characterization of linear trinuclear $Mn^{II}Mn^{III}Mn^{II}$ complex of syn-2-pyridinealdoxime ligand, isostructural with the complexes **1** and **2** need to be explored.

(2) Experimental determination of the exchange coupling constant for complex **4** by using X- and Q-band EPR techniques and comparison of the values obtainable from spectroscopic technique with the evaluated value from SQUID measurement.

(3) HFEPR measurement of the complex **9 ($Fe^{III}_2Cu^{II}_2$)** to verify the ground state of the cluster.

(4) Alternating current (AC) susceptibility measurement of the Mn^{II}_4 complex (**11**), to check whether this complex can be a single molecule magnet (SMM).

(5) AC-susceptibility and HFEPR measurement of the complex **12 (Mn^{III}_4)** to verify the ground state of the complex and for the precise determination of the sign and magnitudes of zero-field splitting parameter (D).

(6) AC-susceptibility measurement of the complex **14 ($Mn^{III}_4Mn^{II}_2$)**, for the precise determination of the sign and magnitude of the zero-field splitting parameter and to check SMM properties.

(7) Synthesis and magnetostructural characterization of the Cr^{III}_4 and V^{III}_4 core congeners isostructural with Mn^{III}_4 (**12**)

(8) In traversing the first-row d-block elements we have noticed that paramagnetic Ti and V-oximates remain relatively unexplored, probably because of difficulties in

synthesis and stability. Clearly, these aspects need to be further experimentally explored.

References:

(i) P. Chaudhuri and U. Flörke, Unpublished result.

(ii) F. Birkelbach, U. Flörke, H-J. Haupt, C. Butzlaff, A. X. Trautwein, K. Wieghardt and P. Chaudhur, *Inorg. Chem.,* 1998, **37**, 2000

(iii) D. J. Price, S. R. Batten, K. J. Berry, B. Moubaraki and K. S. Murray, *Polyhedron*, 2003, **22**, 165

(iv) V. Pavlischuk, F. Birkelbach, T. Weyhermüller, K. Wieghardt and P. Chaudhuri, *Inorg. Chem.,* 2002, **41**, 4405

(v) M. Alexiou, C. M. Zeleski, C. Dendrinou-Samara, J. Kampf, D.P. Kessissoglou, V. L. Pecoraro, *Z. Anorg. Allg.Chem.,* 2003**, 629**, 2348

(vi) M. Alexiou, C. Dendrinou-Samara, A. Kasagianni, S. Biswas, C. M. Zeleski, J. Kampf, D. Yoder, J. E. Penner-Hahn, V. L. Pecoraro, D.P. Kessissoglou, *Inorg. Chem.,* 2003**, 42**, 2185

(vii) P. Chaudhuri and U. Flörke, Unpublished result.

(viii) S. Ross, T. Weyhermüller, E. Bill, E. Bothe, U. Flörke, K. Wieghardt and P. Chaudhuri, *Eur. J. Inorg. Chem.,* 2004, 984

(ix) S. Ross, T. Weyhermüller, E. Bill, K. Wieghardt and P. Chaudhuri, *Inorg. Chem.,* 2001, **40**, 6656

(x) D. Burdinski, F. Birkelbach, T. Weyhermüller, U. Flörke, H-J. Haupt, M. Lengen, A. X. Trautwein, E. Bill, K. Wieghardt and P. Chaudhuri, *Inorg. Chem.,* 1998**, 37**, 1009

(xi) F. Birkelbach, M.Winter, U. Flörke, H-J. Haupt, C. Butzlaff, M. Lengen, E. Bill, A. X. Trautwein, K. Wieghardt and P. Chaudhuri, *Inorg. Chem.,* 1994, **33**, 3990

(xii) C. N. Verani, T. Weyhermüller, E. Rentschler, E. Bill and P.Chaudhuri, *J. Chem. Soc., Chem. Commun.,* 1998, 2475

(xiii) C. N. Verani, E. Rentschler, T. Weyhermüller, E. Bill and P. Chaudhuri, *J. Chem. Soc.,Dalton Trans.,* 2000, 4263

(xiv) P. Chaudhuri and T. Weyhermüller, Unpublished result

(xv) V. V. Pavlischuk, S. V. Kolotilov, A. W. Addison, M. J. Prushan, D. Schollmeyer, L. K. Thompson and E. A. Goreshnik, *Angew. Chem. Int. Ed*., 2001, **40**, 4734

(xvi) M. Alexiou, C. Dendrinou-Samara, C. P. Raptopoulou, A. Terzis, V. Tangoulis and D. P. Kessisoglou, *Eur. J. Inorg. Chem*., 2004, 3822

(xvii) P. Chaudhuri, T. Weyhermüller, R. Wagner and S. Khanra, Unpublished result

(xviii) V. V. Pavlischuk, S. V. Kolotilov, A. W. Addison, M. J. Prushan, R. J. Butcher and L. K. Thompson, *Inorg. Chem*., 1999, **38**, 1759

(xix) Y-B. Jiang, H-Z. Kou, R-J. Wang and J. Ribas, *Inorg. Chem*., 2005, **44**, 709

(xx) P. Chaudhuri, M. Winter, P. Fleischhauer, W. hasse, U. Flörke and H-J. Haupt, *J. Chem. Soc., Chem. Commun.,* 1990, 1728

(xxi) C. Krebs, M.Winter, T. Weyhermüller, E. Bill, K.Wieghardt and P.Chaudhuri, *J. Chem. Soc., Chem. Commun.,* 1995, 1913

(xxii) P. Chaudhuri, M. Winter, B. P. C. Della Vedova, P. Fleischhauer, W. hasse, U. Flörke and H-J. Haupt, *Inorg. Chem*., 1991, **30**, 4777

(xxiii) (a) H. Saarinen and M. Orama, *Acta Chem. Scand*., 1998, **52**, 1209; (b) M. Orama, H. Saarinen and J. Korvenranta, *Acta Chem. Scand*., 1989, **43**, 407

CHAPTER- 9

EQUIPPMENT AND EXPERIMENTAL WORK

9.1 METHODS AND EQUIPMENTS

All the analyses were performed at the Max-Planck-Institut für Bioanorganische Chemie, Mülheim an der Ruhr, unless otherwise mentioned. Commercial grade chemicals were used for the synthetic purposes and solvents were distilled and dried before use.

Infrared Spectroscopy

Infrared spectra were measured from 4000 to 400 cm^{-1} as KBr pellets at room temperature on a '*Perkin-Elmer* FT-IR-Spectrophotometer 2000'.

NMR Spectroscopy

^{1}H- and ^{13}C- NMR spectra were measured using a '*Bruker* ARX 250, DRX 400 or DRX 500'. The spectra were referenced to TMS, using the ^{13}C or residual proton signals of the deuterated solvents as internal standards.

Mass Spectroscopy

Mass spectra in the Electron Impact mode (EI; 70 eV) were recorded on a Finnigan MAT 8200 mass spectrometer. Only characteristic fragments are given with intensities. The spectra were normalized against the most intense peak having intensity 100. Electron Spray Ionization (ESI) mass spectra were recorded either on a Finnigan Mat 95 instrument or a Hewlett-Packard HP 5989 mass spectrometer. ESI- and EI- spectra were measured by the group of Dr. W. Schrader at the Max-Planck-Institute for Coal Research, Mülheim an der Ruhr.

Elemental Analysis

The determination of the C, H, N and metal content of the compounds was performed by the 'Mikroanalytischen Labor H. Kolbe', Mülheim an der Ruhr, Germany.

UV-VIS Spectroscopy

UV-VIS spectra were recorded on a '*Perkin-Elmer* UV-VIS Spectrophotometer Lambda 19'or on a Hewlett-Packard HP 8452A diode array spectrophotometer in the range 200-1200 nm. For UV-VIS spectro-electrochemical investigations the HP 8452A diode array spectrophotometer was used, by employing a coulometry cuvette and Bu_4NPF_6 as supporting electrolyte.

Electrochemistry

Cyclic voltammetry, square wave voltammetry and linear sweep voltammetry experiments were performed using an 'EG&G Potentiostat / Galvanostat 273A'. A standard three-electrode-cell was employed with a glass-carbon working electrode, a platinum-wire auxiliary electrode and Ag/AgCl (saturated LiCl in EtOH) reference electrode. Measurements were made under an inert atmosphere at room temperature. The potential of the reference electrode was determined using Fc^{+}/Fc as the internal standard.

Magnetic Susceptibility Measurements

The measurements of the temperature or field dependent magnetization of the sample were performed in the range 2 to 290 K at 1, 4 or 7 T on a '*Quantum Design* SQUID-Magnetometer MPMS'. The samples were encapsulated in gelatin capsules and the response functions were measured four times for each given temperature, yielding a total of 32 measured points. The resulting volume magnetization from the samples had its diamagnetic contribution compensated and was recalculated as volume susceptibility. Diamagnetic contributions were estimated for each compound by using Pascal's constants. The experimental results were fitted with the program JULIUS calculating through full-matrix diagonalization of the Spin-Hamiltonian. The following Hamiltonian-operators were used:

$H_{ZE} = \mu_B \sum g_i \hat{S}_i \,.\mathbf{B}$

$H_{HDVV} = -2 \sum J_{ij} \hat{S}_i \,.\, \hat{S}_j$

$H_{ZFS} = \sum D_i[\hat{S}_{iz}^2 - \{S_i(S_i+1)/3\} + E_i/D_i(\hat{S}_{ix}^2 - \hat{S}_{iy}^2)]$

Indexes i,j indicate individual spins. For the magnetic measurement the calculated g values obtained during simulation is the isotropic.

EPR Spectroscopy

First derivative X-Band EPR spectra of powdered or frozen solution samples were measured with a '*Bruker* ESP 300 Spectrometer' coupled to an '*Oxford Instruments* ESR 910-Cryostat'.

^{57}Fe-Mössbauer Spectroscopy

^{57}Fe-Mössbauer spectra were measured with an *Oxford Instruments* Mössbauer spectrometer in the constant acceleration mode. ^{57} Co/Rh was used as the radiation source. The minimum experimental linewidths were 0.24 mm/s. The temperature of the sample was controlled by an '*Oxford Instruments* Variox Cryostat'. Isomer shifts were determined relative to α-iron at 300K. The measurements were carried out at 80K and 100K with solid samples containing the isotope ^{57}Fe.

Crystallography

X-ray diffraction data were collected on an '*Enraf-Nonius* CAD4 Diffractometer' or on a '*Siemens* Smart System'. Graphite-monochromatized Mo-Kα with λ = 0.71073 Å was employed. Data were collected by the 2θ-ω scan method (3≤2θ≤50°). The data were corrected for absorption and Lorenz polarization effects. The structures were solved by direct methods and subsequent Fourier-difference techniques, and refined anisotropically by full-matrix least-squares on F^2 with the program SHELXTL PLUS. Hydrogen atoms were included at calculated positions with U < 0.08 $Å^2$ in the last cycle of refinement.

GC / GC-MS Analysis

GC of the organic products were performed either on HP 6890 instruments using RTX-5 Amine 13.5 m S-63 columns respectively. GC-MS was performed using the above column coupled with a HP 5973 mass spectrometer with mass selective detector.

9.2 SYNTHESIS

$Me_3TacnFeCl_3$,[1] ***$Me_3TacnCrBr_3$***[2], ***[$Cu(dapdoH_2)](ClO_4)_2$***[3] and the ligand, **2-hydroxy-1,3-propanediylbis(benzoylacetoneimine)**[4] (L^2H_3) were prepared according to the literature procedure.

9.2.1 LIGANDS

2,6-Diacetylpyridine dioxime [$dapdoH_2$]

This synthesis is a modification of Hartkamp's method. 2,6-Diacetylpyridine (2.9 g, 18 mmol) was dissolved in MeOH (35 cm^3), a solution of hydroxylamine hydrochloride (2.8 g, 40 mmol) and NaOH (1.6 g, 40 mmol) in MeOH:H_2O (20 cm^3, 1:1 by vol) was prepared and added to the diacetylpyridine solution. The resulting solution was refluxed with stirring for 2 h. A white precipitate began to form after 5 min heating. After 2 h, the mixture was cooled in ice and the white precipitate was collected by suction filtration and recrystallized from MeOH. ^1H NMR (CD_3COCD_3, 80 MHz): δ 2.32 (6H, s, CH_3), 7.71 (1H, t, Py-4H), 7.85 (1H, d, Py-3H), 10.64 (2H, s, NO-H). MS: m/z 193 (M^+, 100 %).

Yield: 3.16 gm (92 %), *MP*: 236°C

Molecular Weight: 193 g/mol $C_9H_{11}N_3O_2$

Elemental Analysis:

	%C	%H	%N
Calculated	55.96	5.7	21.76
Found	55.9	5.6	21.73

Infrared Spectrum:

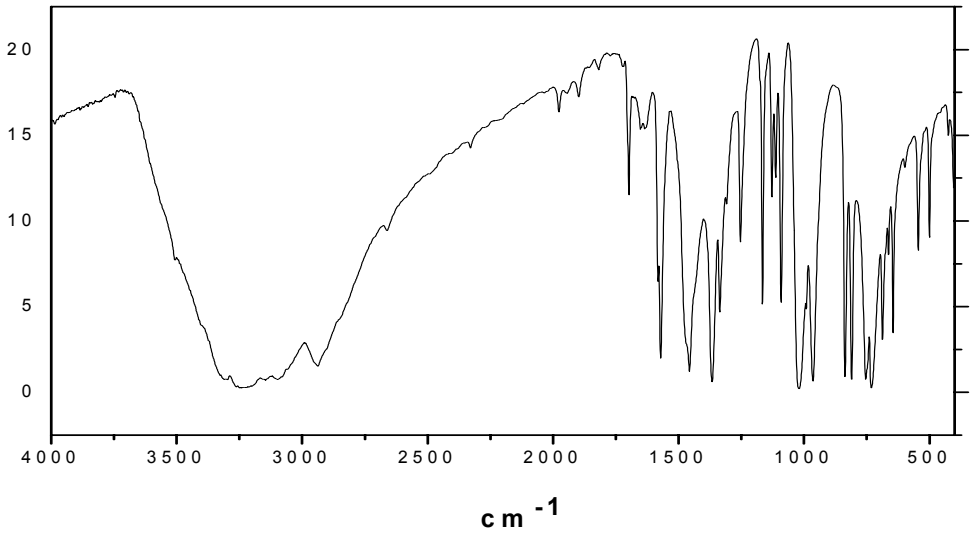

Synthesis of 2,6-Bis-iminomethyl-(4,6-di-tertbutyl-2-iminophenol)-4-methyl-phenol (H_3dfmp)

2,6-Diformyl-4-methylphenol was synthesized as described in ref. The corresponding dioxime, H_3dfmp, was prepared in the following way: To a suspension of 2,6-diformyl-4-methylphenol (3.36 g; 20 mmol) and $NH_2OH{\bullet}HCl$ (3.13 g; 50 mmol) in water (45 ml), warmed at 80^{o}C, was added methanol with stirring until a clear orange solution was obtained. The solution was stirred at 80^{o}C for 1 h. The solution was cooled to room temperature, followed by addition of enough water, so that the solution just started to become turbid. After keeping it at ambient temperature for ca. 24 h, the crystalline solid was removed by suction filtration, washed thoroughly with water and dried in air. The dioxime can be recrystallized from a methanol-water mixture. IR (KBr, medium and strong selective bands only): 3380, 3329, 1623, 1604, 1465, 1307, 1265, 1061, 1027, 934, 793, 757, 696 cm^{-1}. ^{1}H NMR (CD_3OD, 80 MHz): δ 2.34 (3H, s, CH_3), 7.37 (2H, s, Ar), 8.37 (2H, s, oxime). ^{13}C NMR ($CDCl_3$): δ 20.31 ($ArCH_3$), 119.78, 129.84, 130.85 (C-Ring), 149.17 (CN), 154.48 (C-OH). MS: m/z 194 (M^+, 100 %).

Yield: 4.5 gm (70 %), *MP*: 186-188 °C

Molecular Weight: 194 $C_9H_{10}N_2O_3$

Elemental Analysis:

	%C	%H	%N
Calculated	55.67	5.15	14.43
Found	55.7	5.2	14.3

Infrared Spectrum:

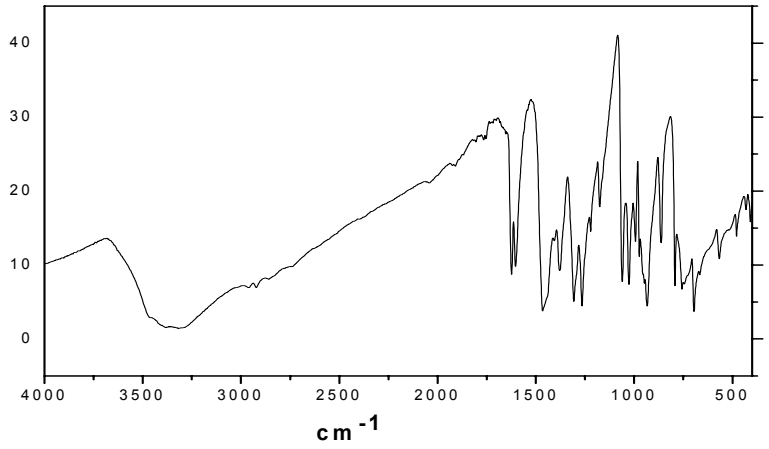

9.2.2 COMPLEXES:

Synthesis of $[Ni^{II}(PyA)_3Mn^{III}(PyA)_3Ni^{II}](ClO_4)$ (1)

To a light green solution of $NiCl_2 .6H_2O$ (0.47 g; 2 mmol) and $Mn(ClO_4)_2 .6H_2O$ (0.46 g; 1 mmol) in distilled methanol (25 ml), solid pyridine-2-aldoxime(0.72g; 6 mmol) was added with stirring, followed by addition of 7 ml of $[Bu_4N][OCH_3]$ (20% in CH_3OH). The resulting red brown solution was stirred for 0.5 h and filter to procure red-brown microcrystalline solid. X-ray quality crystals were obtained from a dimethylformamide solution, in which methanol was allowed to diffuse.

Yield: 830 mg (81 %)

Molecular Weight: 998.49 $C_{36}H_{30}ClMnN_{12}Ni_2O_{10}$

Elemental Analysis:

	%C	%H	%N	%Ni	%Mn
Calculated	43.43	3.04	16.88	11.8	5.22
Found	43.3	3.0	16.9	11.9	5.1

Infrared Spectrum:

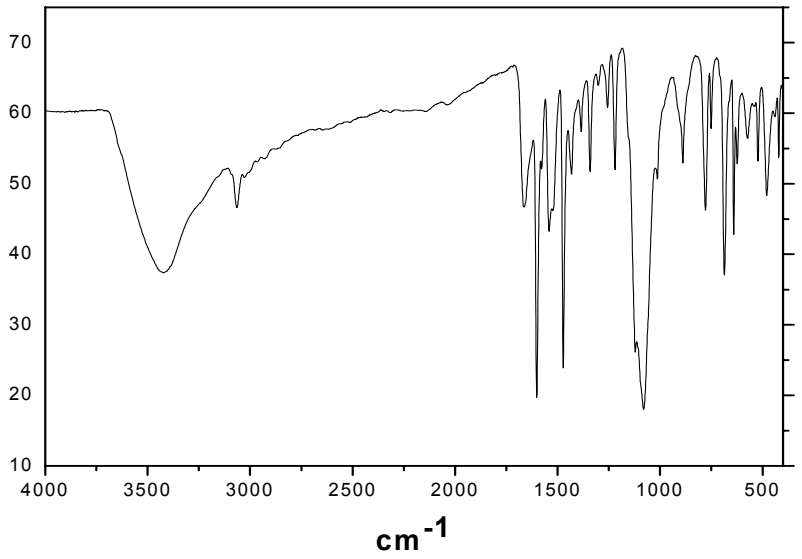

Synthesis of $[Ni^{II}(PyA)_3Cr^{III}(PyA)_3Ni^{II}](ClO_4)$ (2)

To a light green solution of $NiCl_2 .6H_2O$ (0.47 g; 2 mmol) and $Cr(ClO_4)_3 .6H_2O$ (0.46 g; 1 mmol) in distilled methanol (25 ml), solid pyridine-2-aldoxime(0.72g; 6 mmol) was added with stirring, followed by addition of 7 ml of $[Bu_4N][OCH_3]$ (20% in CH_3OH). The resulting red brown solution was stirred for 0.5 h and filter to procure red-brown microcrystalline solid. X-ray quality crystals were obtained from a dimethylformamide solution, in which methanol was allowed to diffuse.

Yield: 720 mg (73 %)

Molecular Weight: 995.59 $C_{36}H_{30}ClCrN_{12}Ni_2O_{10}$

Elemental Analysis:

	%C	%H	%N	%Ni	%Cr
Calculated	43.43	3.04	16.88	11.8	5.22
Found	43.3	3.0	16.9	11.9	5.1

Infrared Spectrum:

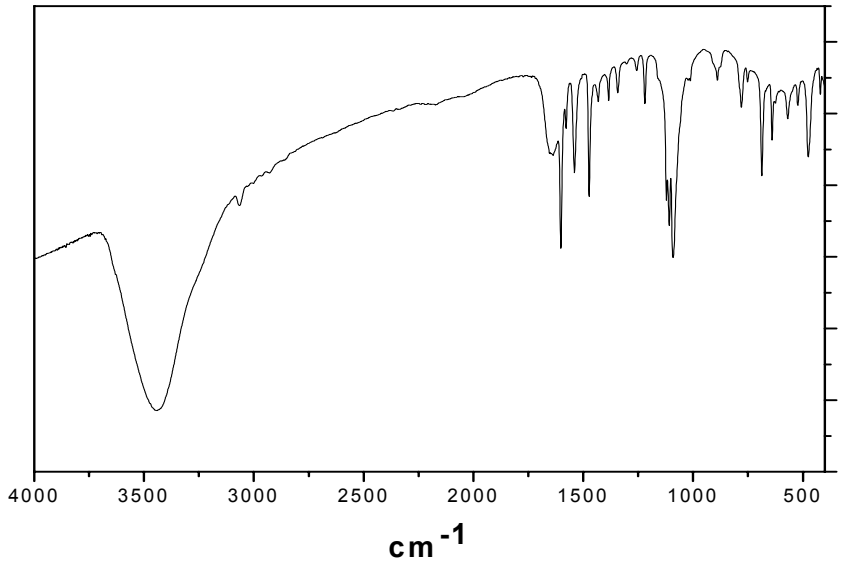

Synthesis of $[Ni^{II}_3(PyA)_5((PyAH)](ClO_4).\ CH_3CN$ (3)

Solid pyridine-2 aldoxime (0.36 g; 3 mmol) was added to a solution of $Ni(ClO_4)_2.\ 6H_2O$(0.55 g; 1.5 mmol) in methanol(25mL) to yield a deep brown solution. 4.5 ml of $[Bu_4N][OCH_3]$ (20% in CH_3OH) were added, which upon stirring yielded a red brown solution. After 0.5 h stirring the precipitated red brown microcrystalline substance was filtered and air dried. X-ray quality deep red-brown crystals were obtained from a solution of 8 in CH_3CN.

Yield: 550 mg (53 %)

Molecular Weight: 1044.36 $C_{38}H_{34}ClN_{13}Ni_3O_{10}$

Elemental Analysis:

	%C	%H	%N	%Ni
Calculated	43.7	3.28	17.44	16.86
Found	43.8	3.4	17.6	17.0

Infrared Spectrum:

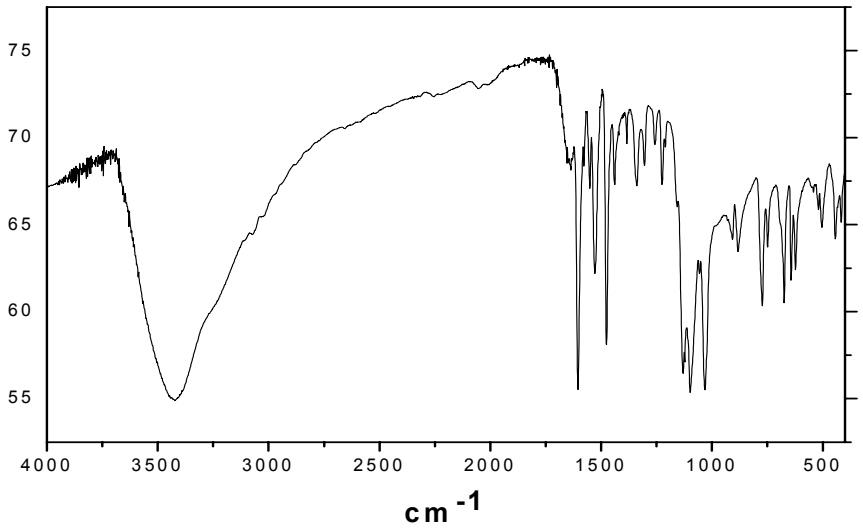

Synthesis of $[(CH_3)B\{(dfmp)_3Mn^{II}Mn^{II}\{B(CH_3)]$ (Et_3NH) (4)

To a solution of H_3dfmp (300 mg, 1.5 mmol) and $Mn(ClO_4)_2$. $6H_2O$ (370 mg, 1 mmol) in methanol (40 ml) was added triethylamine (0.6 ml, 4.5 mmol) and the suspension was stirred 10 min. To this dark solution methylboronic acid $[CH_3B(OH)_2]$, (60 mg, 1 mmol) was added. The solution was stirred at ambient temperature for 0.5 h in the air, after which the precipitated deep yellowish solid was collected by filtration and air-dried. The yellowish solid was recrystallized from a solvent mixture of dichloromethane-ethanol (2:1). IR (KBr, cm^{-1}): 1610, 1593, 1580, 1450, 1305, 1208, 1047, 1008, 946, 935, 833, 761, 738, 705. ESI-MS (m/z): 735 (100 %).

Yield: 290mg (40%)

Molecular Weight: 883.33 $C_{37}H_{49}N_7O_{10}B_2Mn_2$

Elemental Analysis:

	%C	%H	%N	%Mn
Calculated	50.18	5.14	11.7	13.15
Found	49.8	4.85	11.56	13.19

Infrared spectrum:

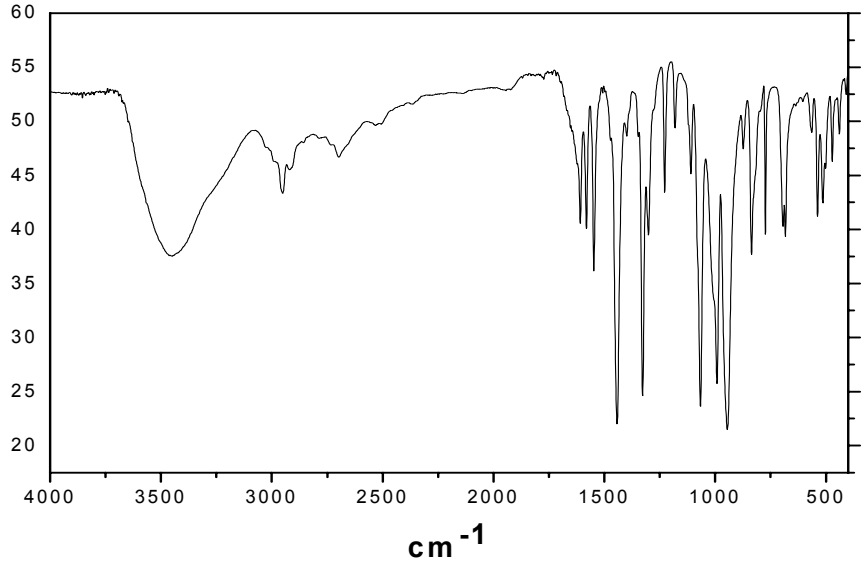

Synthesis of $[(Me_3Tacn)Mn^{III}\{(dfmp)_3Mn^{II}Mn^{II}\}Mn^{III}(Me_3Tacn)](ClO_4)$ (5)

To an argon blanketed atmosphere 300 mg (1.5 mmol) H_3dfmp was dissolved in 30 mL methanol and 0.4 mL (3 mmol) Triethylamine was added in it and it was stirred for 10 min. Then 0.24 g (1 mmol) $Mn^{II}(CH_3COO)_2 .4H_2O$ was added and stirred. In another round bottom flask 0.17 g (1 mmol) 1,4,7-trimethyl 1,4,7-triazacyclononane and $[Mn^{III}_3(\mu_3\text{-}O)(\mu\text{-}CH_3COO)_6(H_2O)_3](CH_3COO)$ (0.26 g) was dissolved in 20 mL methanol and was stirred for20 minutes. This solution was added to the previous solution and then it was refluxed for 20 minutes and the resulting solution turned brown black. After cooling it was filtered off and 0.24 g (2 mmol) $NaClO_4$ was added and after few minutes brown solid precipitated out, was collected by filtration and air-dried. Suitable single crystal for X-ray quality was grown from Acetonitrile-methanol (3:1) mixture. IR (KBr, cm^{-1}): 1607, 1567, 1542, 1460, 1438, 1322, 1229, 1144,1120,1107,1089 1006, 988, 705,624. ESI-MS (m/z): 567 (100 %) $[\mathbf{M} - 2(ClO_4)]^{2+}$, 1135 (9 %) $[\mathbf{M} - ClO_4]^{+}$.

Yield: 400 mg (37 %).

Formula Weight: 1308.38 $C_{48}H_{70}N_{13}O_{14}ClMn_4$

Elemental Analysis:

	%C	%H	%N	%Mn
Calculated	44.06	5.39	13.91	16.8
Found	43.93	5.2	13.8	16.64

Infrared spectrum:

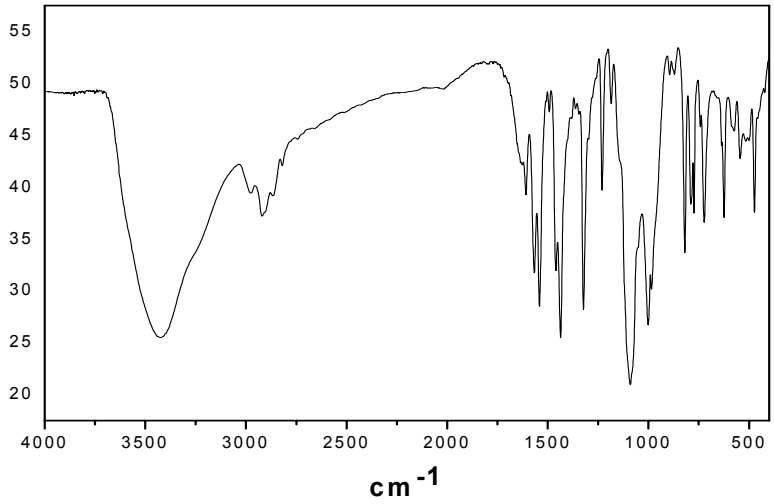

Synthesis of $[(Me_3Tacn)Mn^{IV}\{(dfmp)_3Mn^{II}Mn^{II}\}Mn^{IV}(Me_3Tacn)](ClO_4)_3$ (6)

300 mg (1.5 mmol) H_3dfmp was dissolved in 30 mL methanol and 0.4 mL (3 mmol) triethylamine was added in it and it was stirred for 10 min. Then 0.24 g (1 mmol) $Mn^{II}(CH_3COO)_2$.$4H_2O$ was added and stirred. In another round bottom flask 0.17 g (1 mmol) 1,4,7-trimethyl 1,4,7-triazacyclononane and $[Mn^{III}_3(\mu_3\text{-}O)(\mu\text{-}CH_3COO)_6(H_2O)_3](CH_3COO)$ (0.26 g) was dissolved in 20 mL methanol and was stirred for 20 minutes. This solution was added to the previous solution and then it was refluxed for 20 minutes and the resulting solution turned brown black. After cooling it was filtered off and 0.24 g (2 mmol) $NaClO_4$ was added and after few minutes brown solid precipitated out, was collected by filtration and air-dried. Suitable single crystal for X-ray quality was grown from Acetonitrile-ethanol (3:1) IR (KBr, cm^{-1}): 1607, 1567, 1542, 1460, 1438, 1322, 1229, 1144,1120,1107,1089 1006, 988, 705,624. ESI-MS (m/z): 567 (100 %) [**M** - $2(ClO_4)]^{2+}$, 1135 (9 %) [**M** - $ClO_4]^+$.

Yield: 300 mg (29 %).

Molecular Weight: 1481.73 $C_{46}H_{67.5}N_{12.5}O_{22.5}Cl_3Mn_4$

Elemental Analysis:

	%C	%H	%N	%Mn
Calculated	37.29	4.6	11.8	14.83
Found	37.4	4.73	11.7	14.62

Infrared spectrum:

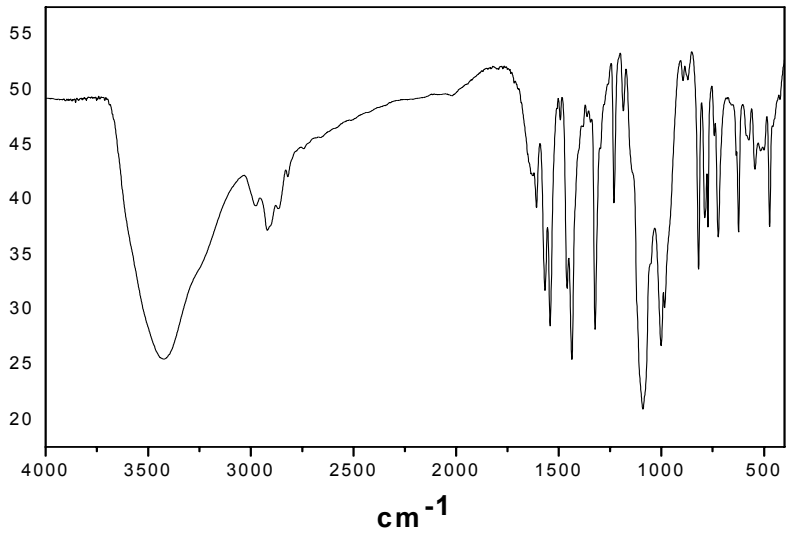

Synthesis of [(Me$_3$Tacn)Fe^{III}{(dfmp)$_3$Mn^{II}Mn^{II}}Fe^{III}(Me$_3$Tacn)](ClO$_4$) (7)

300 mg (1.5 mmol) H_3dfmp was dissolved in 30 mL methanol and 0.5 mL (4 mmol) triethylamine was added in it and it was stirred for 10 min. Then 0.24 g (1 mmol) $Mn^{II}(CH_3COO)_2$ .4H_2O was added and stirred, followed by L'$FeCl_3$ (0.33 g, 1 mmol) and then it was refluxed for 20 minutes under argon and the resulting solution turned brown black. After cooling it was filtered off and 0.24 g (2 mmol) $NaClO_4$ was added and after few minutes red brown solid precipitated out and it was filtered through suction filtration was washed with diethyl ether and then dried in air. Suitable single crystal for X-ray quality was grown from Acetonitrile-dichloromethane (1:3). IR (KBr, cm^{-1}): 1607, 1579, 1560, 1460, 1444, 1305, 1226, 1031, 1006, 988, 705. ESI-MS (m/z): 1137 (100 %) [**M** - $ClO_4]^+$.

Yield: 390 mg (36 %).

Molecular Weight: 1236 $C_{47.5}H_{67}N_{13}O_{13}Cl_2Mn_2Fe_2$

Elemental Analysis:

	%C	%H	%N	%Mn	%Fe
Calculated	43.18	5.1	13.78	8.33	8.46
Found	43.22	4.95	13.57	8.21	8.39

Infrared Spectrum:

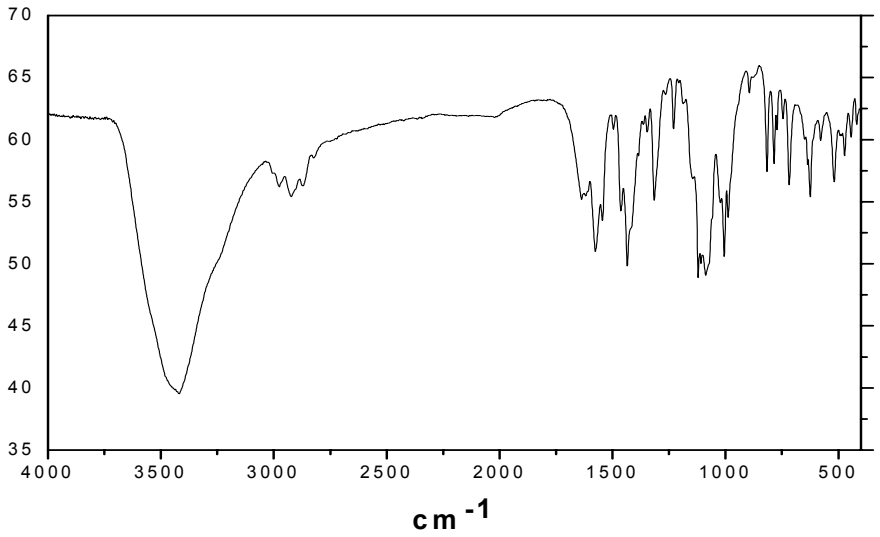

Synthesis of $[(Me_3Tacn)Cr^{III}\{(dfmp)_3Mn^{II}Mn^{II}\}Cr^{III}[(Me_3Tacn)](ClO_4)$ (8)

300 mg (1.5 mmol) H_3dfmp was dissolved in 30 mL Methanol and 0.5 mL(4 mmol) triethylamine was added in it and it was stirred for 10 min. Then 0.24 g (1 mmol) $Mn^{II}(CH_3COO)_2$.$4H_2O$ was added and stirred. To a suspension of 0.46 g (1 mmol) of L'$CrBr_3$ in 30 mL methanol was slowly added 0.63 g of $AgClO_4$ (3 mmol) with stirring. The suspension was refluxed under argon for 0.5 h; during this time a blue-violet solution with a concomitant formation of AgBr resulted. Precipitated AgBr was filtered off, and the clear blue-violet solution was charged to the previous methanolic solution and then it was refluxed for 20 minutes under argon and the resulting solution turned brown black. After cooling it was filtered off and green brown solid precipitated out and it was filtered through suction filtration was washed with diethyl ether and then dried in air. Yield: 390 mg (36 %). IR (KBr, cm^{-1}): 1607, 1579, 1560, 1460, 1444, 1305, 1226, 1031, 1006, 988, 705. ESI-MS (m/z): 1129 (100 %) $[\mathbf{M} - ClO_4]^+$.

Yield: 390 mg (36 %).

Molecular Weight: 1236 $C_{45}H_{63}N_{12}O_{13}ClMn_2Cr_2$

Elemental Analysis:

	%C	%H	%N	%Mn	%Cr
Calculated	43.18	5.1	13.78	8.33	8.46
Found	40.13	4.95	13.60	8.71	8.59

Infrared Spectrum:

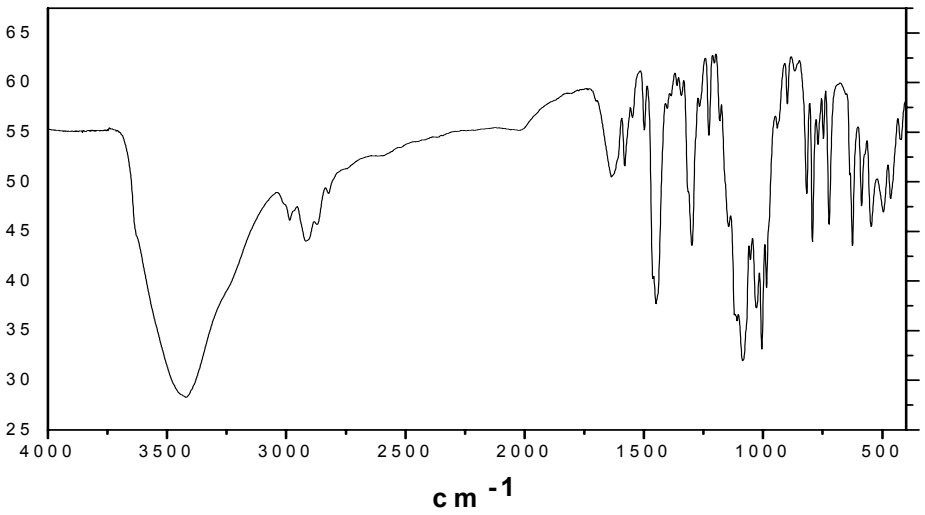

Synthesis of $[(Me_3Tacn)_2Fe^{III}_2L_2Cu^{II}_2(O..H..O)Cl](ClO_4)_2$ (9)

$[Cu(dapdoH_2)_2]$ $(ClO_4)_2$ (0.32 g, 0.5 mmol) was dissolved in 30 mL methanol. Then L'$FeCl_3$ (0.33 g, 1 mmol) was also added into the methanolic solution of $[Cu(dapdoH_2)_2]$ $(ClO_4)_2$, followed by Et_3N (0.26 mL, 2 mmol). The resulting solution was refluxed for 30 minutes and then $NaClO_4$ (0.36 g, 3 mmol) was added and then it was stirred for another 15 minutes. On cooling black microcrystalline solid precipitated out. It was then filtered through suction filtration and washed with diethyl ether. Suitable quality X-ray crystal was grown from CH_3CN-C_2H_5OH mixture. IR (KBr, cm^{-1}): 2906, 1593, 1502, 1545, 1459, 1444, 1297, 1163, 1077, 1006, 990, 781,623. ESI-MS (m/z): , 516(100 %) [**M** - $2ClO_4]^{2+}$; 1131(5%) [**M** - $ClO_4]^+$

Yield: 290 mg (45%).

Formula Weight: 1295.18 $C_{38}H_{69}N_{12}O_{16}Cl_3Cu_2Fe_2$

Elemental Analysis:

	%C	%H	%N	%Cu	%Fe
Calculated	35.24	5.37	12.98	9.8	8.6
Found	34.9	5.3	12.98	9.7	8.46

Infrared spectrum:

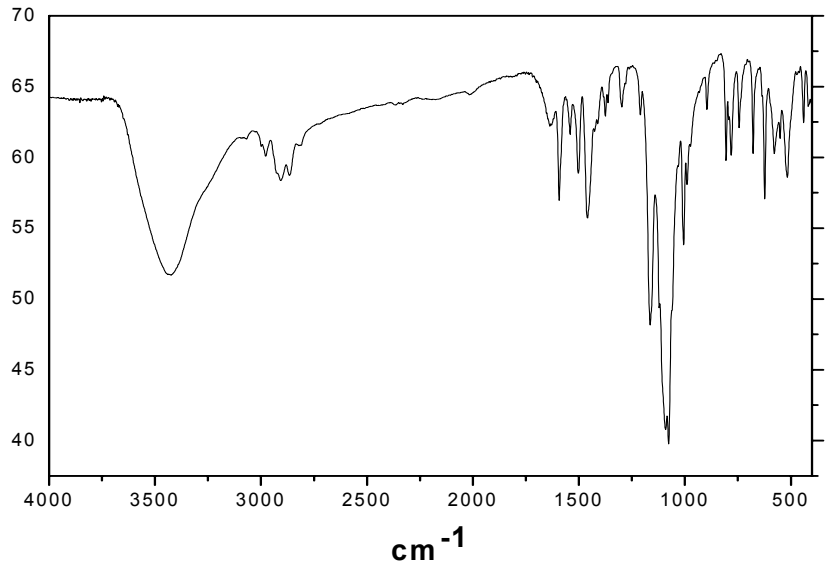

Synthesis of $[(Me_3Tacn)_2Cr^{III}_2L_2Cu^{II}_2(OH)_2Br_2](ClO_4)_2$ (10)

To a suspension of 0.46 g (1 mmol) of L'$CrBr_3$ in 30 mL methanol was slowly added 0.46 g of $AgClO_4$ (2 mmol) with stirring. The suspension was refluxed under argon for 0.5 h; during this time a blue-violet solution with a concomitant formation of AgBr resulted. Precipitated AgBr was filtered off, and the clear blue-violet solution was charged with a solid sample (0.32 g, 0.5 mmol) of $[Cu(dapdoH_2)_2]$ $(ClO_4)_2$ and 0.26 mL (2 mmol) Et_3N. The resulting green-brown solution was refluxed for 0.5 h, upon stirring at ambient temperature, the mixture deposited green amorphous solid. These were filtered off and air dried. Suitable quality X-ray crystal was grown from CH_3CN-C_2H_5OH mixture. IR (KBr, cm^{-1}): 2916, 1595, 1560, 1461, 1295, 1164, 1090, 1004, 984, 794,624. ESI-MS (m/z): , 579(100%)$[(\mathbf{2} - 2ClO_4+0.5H_2O)/2]^{2+}$.

Yield: 230 mg (29%).

Molecular Weight: 1480.95 $C_{42}H_{72}N_{15}O_{14.5}Br_2Cl_2Cu_2Cr_2$

Elemental Analysis:

	%C	%H	%N	%Cu	%Cr
Calculated	34.06	4.9	14.2	8.58	7.02
Found	33.8	4.87	14.1	8.41	7.09

Infrared Spectrum:

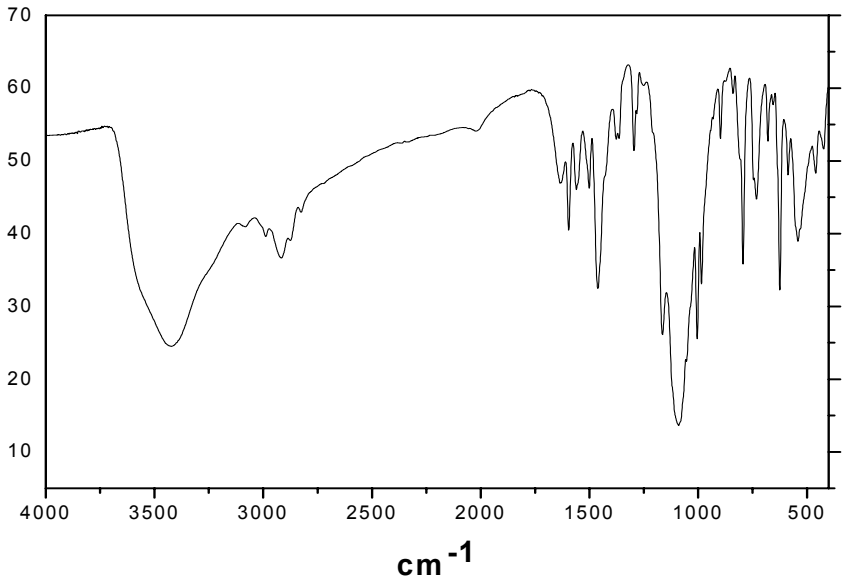

Synthesis of $[Mn^{II}_4(ppi)_6](BF_4)_2 .2CH_3CN . H_2O$ (11)

The mononuclear precursor complex $[Mn^{II}L_2]$ was prepared by reacting a solution of Hppi (0.396 g, 2 mmol) in acetone (20 mL) with $Mn(acac)_2$ (0.25 g, 1 mmol) in acetone (30 mL). Upon addition of the ligand solution to the yellow slurry an immediate color change to deep red observed. After stirring for 1 hr the red solid was isolated by filtration and washed with acetone to yield 0.45 g $[Mn^{II}L_2]$ complex.

$[Mn^{II}_4(ppi)_6](BF_4)_2$ was prepared by reacting $[Mn^{II}(ppi)_2]$ (0.45 g, 1 mmol) with $Mn(CH_3COO)_2 .4H_2O$ (0.09 g, 0.33 mmol) in 3:1 ration in acetonitrile-methanol mixture (30 mL, 1:1). It was stirred in air for 30 minutes and then NBu_4BF_4 (0.96 g, 3 mmol) was added into the black solution. Red solid precipitated out and washed with diethyl ether and dried in air. X-ray quality single crystal was grown by diffusing diethyl ether in concentrated acetonitrile solution of the complex. IR(KBr, cm^{-1}): 3053, 1585, 1479, 1457, 1298, 1280, 1146, 1083, 1061, 865, 750. ESI-MS (m/z): 701(100 %) $[M - 2(BF_4)]^{2+}$, 1489 (10 %) $[M - BF_4]^+$.

Yield: 220 mg (40 %).

Molecular Weight: 1676.78 $C_{76}H_{62}B_2F_8Mn_4N_{14}O_7$

Elemental Analysis:

	%C	%H	%N	%Mn
Calculated	54.44	3.73	11.7	13.11
Found	54.37	3.62	11.6	13.15

Infrared Spectrum:

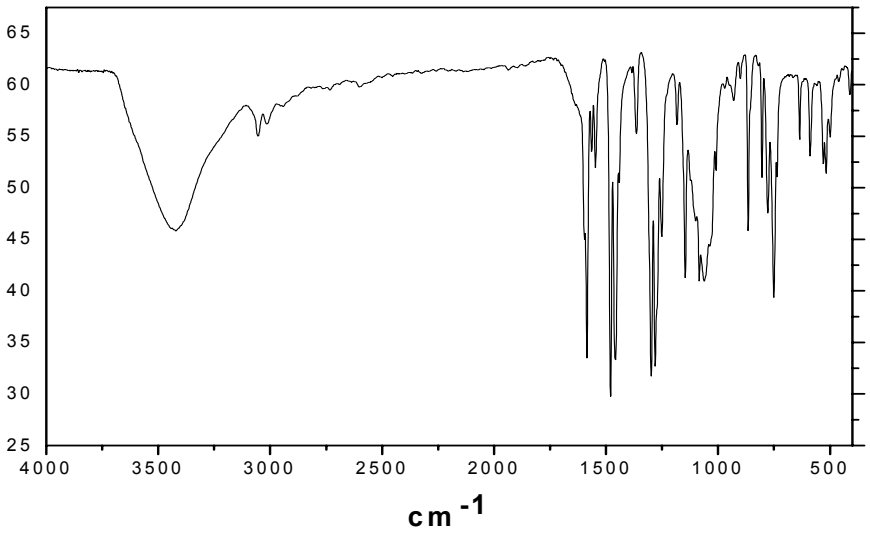

Synthesis of $[Mn^{III}_4(salox)_4(salox\ H)_4]$ 2.5 CH_3OH (12)

Complex 12 was prepared by the addition of 1 mmol (0.198 g) of $MnCl_2$ .4 H_2O into a 40 mL methanol solution of 2 mmol (0.27 g) of salicylaldoxime in presence of triethylamine (4 mmol, 0.52 mL) in argon blanketed atmosphere. Then the solution was refluxed for 30 minutes and then exposed in air and the solution turned to black. Brown black solid precipitated out while cooling the solution. The X-ray quality single crystal was grown by slow evaporation from 2:1 CH_2Cl_2-CH_3OH solution of the complex. IR (KBr, cm^{-1}): 3422, 2899, 1598, 1536, 1473, 1434, 1268, 1205, 1151, 1122, 1014, 909, 755, 666. ESI-MS (m/z): 1032(100 %) $[M - 2(salox\ H)]^+$, 1304 (10 %) [M]

Yield: 180 mg (40 %).

Molecular Weight: 1384.86 $C_{58.5}H_{54}Mn_4N_8O_{18.5}$

Elemental Analysis:

	%C	%H	%N	%Mn
Calculated	50.74	3.93	8.09	15.87
Found	50.57	3.84	8.04	15.93

Infrared Spectrum:

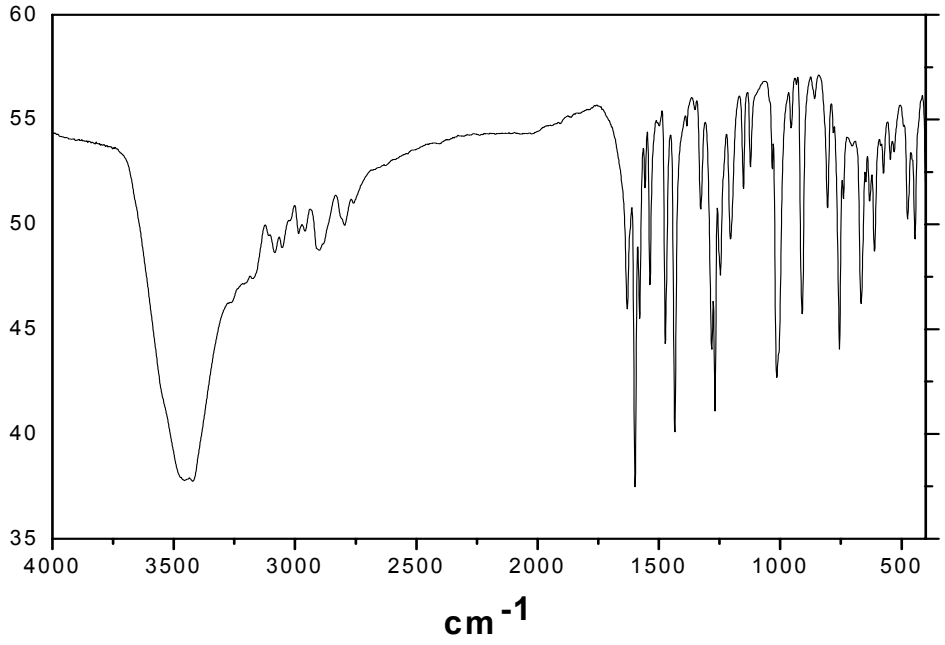

Synthesis of $[(dapdo)_2(dapdoH)_4(\mu\text{-}O)_2(\mu\text{-}OMe)_2Mn^{III}_4Mn^{II}_2](ClO_4)_2$ (13)

To a solution of $dapdoH_2$ (0.19 g, 1 mmol) in 30 mL methanol was added 0.26 g $[Mn^{III}_3(\mu_3\text{-}O)(\mu\text{-}CH_3COO)_6(H_2O)_3](CH_3COO)$, then 0.26 mL (2 mmol) Et_3N. The solution then turned brown, and it was then refluxed for 0.5 h whereupon a brown microcrystalline solid was precipitated out. It was filtered and washed with diethyl ether and air dried. Suitable quality of X-ray crystal was grown by diffusion of diethyl ether into the DMF-CH_3CN solution. IR (KBr, cm^{-1}): 3425, 2805, 1597, 1542, 1375, 1141, 1121, 1052, 952, 811, 661, 624, 559. ESI-MS (m/z): 787(100 %) $[M - 2(ClO_4)]^{2+}$

Yield: 150 mg (33 %)

Molecular Weight: 1922.03 $C_{66}H_{84}Cl_2N_{18}Mn_6O_{26}$

Elemental Analysis:

	%C	%H	%N	%Mn
Calculated	40.73	4.35	12.96	16.94
Found	40.6	4.4	12.83	17.01

Infrared Spectrum:

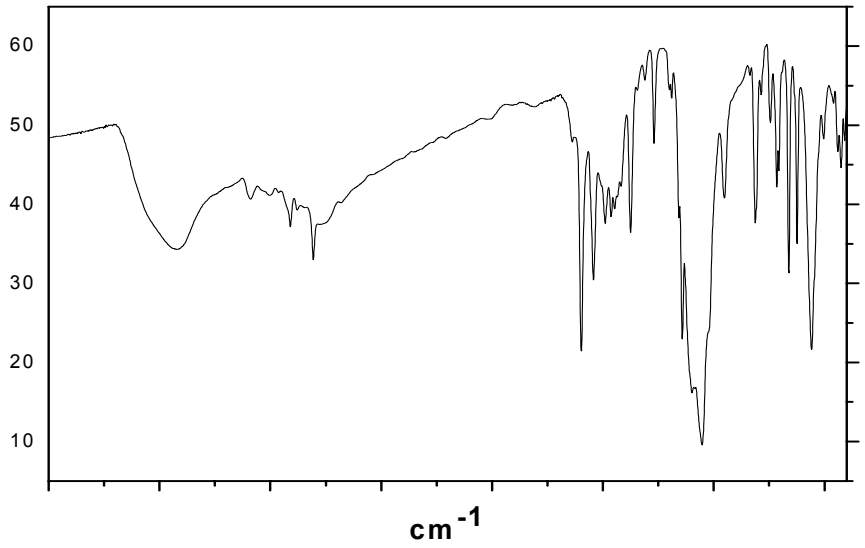

Synthesis of $[(dapdo)_2(dapdoH)_4(\mu\text{-}O)_2(\mu\text{-}OH)_2Mn^{III}_4Mn^{II}_2](ClO_4)_2$ (14)

To a solution of $dapdoH_2$ (0.19 g, 1 mmol) in 30 mL methanol was added 0.36 g $Mn(ClO_4)_2.6H_2O$, then 0.26 mL (2 mmol) Et_3N. The solution then turned brown, and it was then refluxed for 0.5 h whereupon a brown microcrystalline solid was precipitated out. It was filtered and washed with diethyl ether and air dried. Suitable quality of X-ray crystal was grown from concentrated CH_3CN solution. IR (KBr, cm^{-1}): 3425, 2805, 1598, 1542, 1375, 1141, 1121, 1080, 1052, 952, 812, 661, 624, 559. ESI-MS (m/z): 755(100 %) $[M - 2(ClO_4)]^{2+}$

Yield: 100 mg (20 %).

Molecular Weight: 1992 $C_{66}H_{78}Cl_2N_{24}Mn_6O_{24}$

Elemental Analysis:

	%C	%H	%N	%Mn
Calculated	39.8	3.95	16.88	16.55
Found	39.94	3.84	16.85	16.42

Infrared Spectrum:

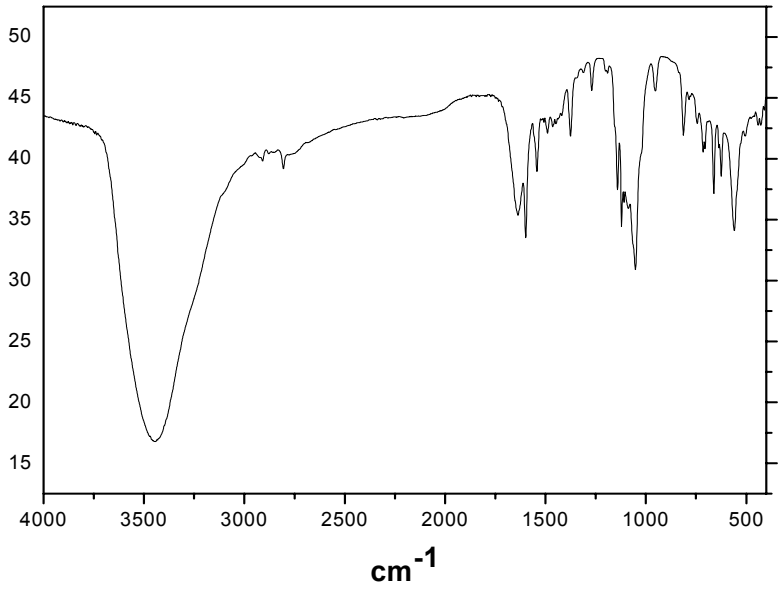

Synthesis of $[L_3(\mu\text{-}O)(\mu\text{-}OH)\ Cu^{II}_6(H_2O)_6](BF_4)_3$ (15)

To a light yellow solution of dioxime ligand (0.30 g; 1 mmol), $Cu(CH_3COO)_2\ .H_2O$ (0.40 g; 2 mmol) in distilled methanol (30 ml) was added with stirring, followed by addition of 0.3 ml of Et_3N. The resulting green solution was refluxed for 0.5 h and then NBu_4BF_4 (0.64 g, 2 mmol) was added to procure dark green microcrystalline solid. X-ray quality crystals were obtained from a mixture of CH_3OH-CH_3CN solution. IR (KBr, cm^{-1}): 3421, 1628, 1534, 1446, 1379, 1220, 1121, 1089, 687, 624 ESI-MS (m/z): 755(100 %) $[M - 3(BF_4)]^{2+}$

Yield: 170 mg (25 %).

*MolecularWeight:*1683.85 $C_{48}H_{73}B_3N_{12}Cu_6O_{14}F_{12}$

Elemental Analysis:

	%C	%H	%N	%Cu
Calculated	34.24	4.37	9.98	22.64
Found	34.38	4.4	9.91	22.55

Infrared Spectrum:

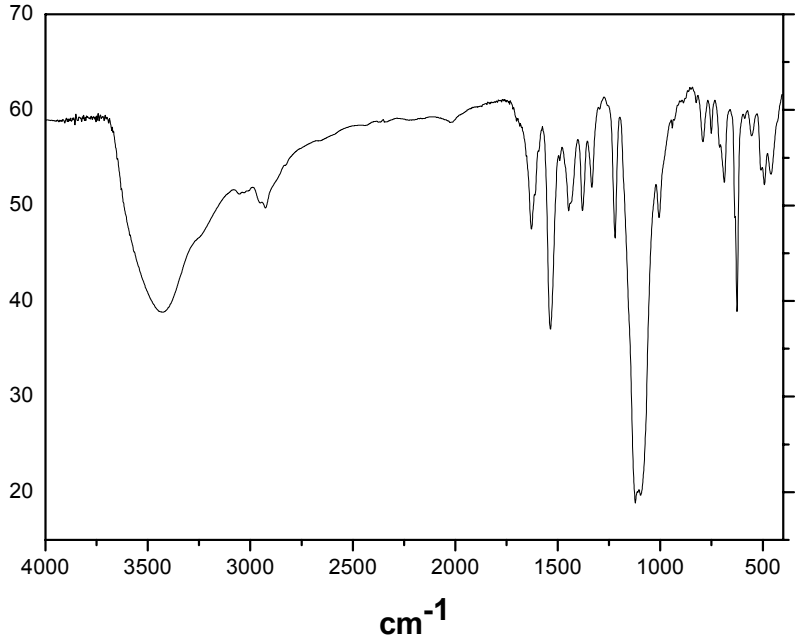

Synthesis of $[Ni^{II}_9(PyA)_{10}(\mu_3\text{-}OH)_2(\mu_2\text{-}OH)_2((\mu_2\text{-}OH_2)_2(H_2O)_6](ClO_4)_4 \cdot 12H_2O$ (16)

To a light green solution of $NiCl_2 .6H_2O$ (0.47 g; 2 mmol) in water (25 ml), solid pyridine-2-aldoxime(0.24g; 2 mmol) was added with stirring, followed by addition of NaOH(0.10 g) to adjust the pH of the solution to 8. $NaClO_4$ (0.36 g, 3 mmol) was added as counter anion to isolate the light orange microcrystalline solid. X-ray quality crystals were obtained by slow evaporation of the H_2O-CH_3OH (4:1) solution of the light orange microcrystalline solid. IR (KBr, cm^{-1}): 3441, 1604, 1540, 1476, 1223, 1141, 1120, 1088, 775, 683 626. ESI-MS (m/z): 781(100 %) $[(PyA)_5Ni_3]^+$, 478(10 %) $[(PyA)_3Ni_2]^+$,555(10 %) $[(PyA)_3Ni_3(O)]^+$, 1058(10 %) $[(PyA)_6Ni_4(ClO_4)]^+$

Yield: 200 mg (25 %).

MolecularWeight: 2565.74 $C_{60}H_{94}Cl_4N_{20}Ni_9O_{50}$

Elemental Analysis:

	%C	%H	%N	%Ni
Calculated	28.9	3.7	10.92	20.59
Found	28.7	3.59	10.94	20.52

Infrared Spectrum:

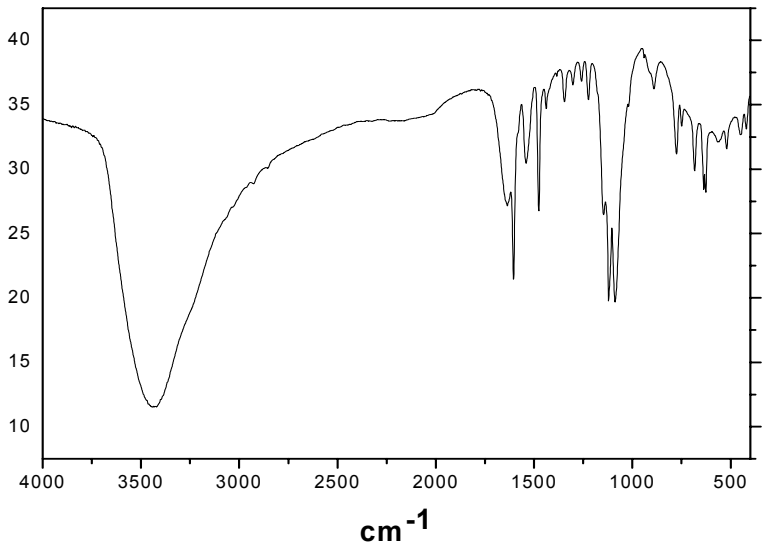

Synthesis of $[Cu^{II}_9L^1_4(\mu_3\text{-}OH)_4(MeOH)_2](ClO_4)_2$. 6MeOH (17)

To a light solution of the ligand (0.19 g; 0.5 mmol), $Cu(ClO_4)_2$.$6H_2O$ (0.37 g; 1 mmol) in distilled methanol (30 ml) was added with stirring, followed by addition of 0.5 ml of Et_3N. The resulting green solution was refluxed for 0.5 h and filter to procure dark green microcrystalline solid. X-ray quality crystals were obtained from a mixture of CH_2Cl_2-CH_3OH solution. IR (KBr, cm^{-1}): 3463, 1607, 1512, 1485, 1409, 1121, 1089, 704, 623. ESI-MS (m/z): 1021(100%) $[L_2Cu_4(OH)]^+$, 1523(50 %) $[L_3Cu_6(OH)]^+$, 501(33 %) $[LCu_2]^+$, 2075(15 %) $[L_4Cu_8(OH)_4]$

Yield: 300 mg (50 %).

Molecular Weight: 2596.86 $C_{100}H_{128}Cl_2N_8Cu_9O_{32}$

Elemental Analysis:

	%C	%H	%N	%Cu
Calculated	46.25	4,97	4.31	22.02
Found	46.10	4.83	4.4	22.1

Infrared Spectrum:

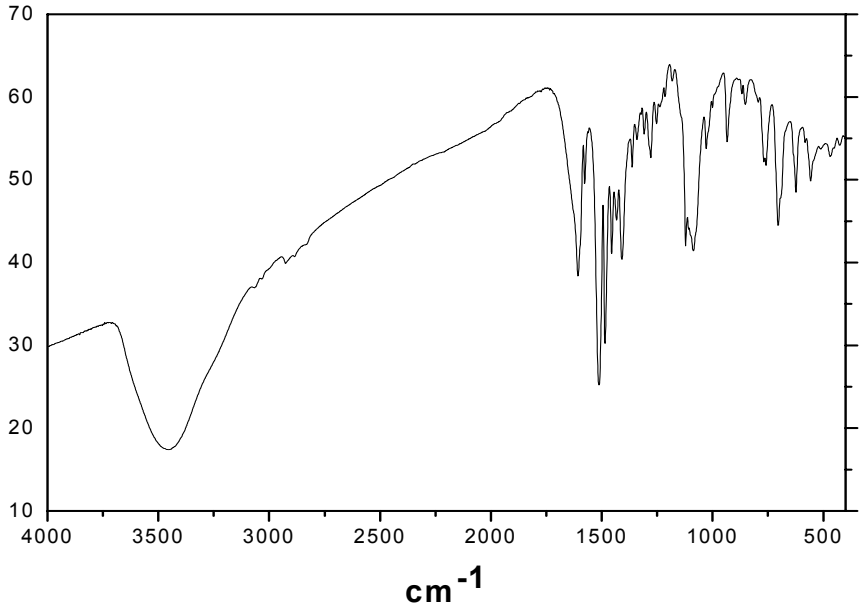

References:

(1) P. Chaudhuri, M. Winter, K. Wieghardt, S. Gehring, W. Haase, B. Nuber and J. Weiss, *Inorg. Chem*., 1988, **27**, 1564

(2) P. Chaudhuri, M. Winter, H. J. Kueppers, K. Wieghardt, B. Nuber and J. Weiss, *Inorg. Chem*., 1987, **26**, 3302

(3) C. W. Glynn and M. M. Turnbull, *Transition. Met. Chem*., 2002, **27**, 822

(4) Y. Nishida and S. Kida, *J. Chem. Soc., Dalton Trans*., 1986, 2633

APPENDICES:

(1) Crystallographic Data
(2) Magnetochemical Data
(3) Curriculum Vitae

(1) Crystallographic Data

Crystal data and structure refinement for 1, 2 and 3

	1	**2**	**3**
Empirical formula	$C_{36}H_{32}N_{12}O_{11}ClMnNi_2$	$C_{36}H_{30}N_{12}O_{10}ClCrNi_2$	$C_{38}H_{34}N_{13}O_{10}ClNi_3$
Formula weight	1016.55	999.59	1044.36
Temperature (K)	100(2)	100(2)	100(2)
Wavelength (Å)	0.71073	0.71073	0.71073
Crystal system	Rhombohedral	Trigonal	Monoclinic
Space group	R-3	R-3	P2(1)/n
Unit cell dimensions	a = 13.7375(4) Å	a = 13.6398(3) Å	a = 11.1498(3) Å
	b = 13.7375(4) Å	b = 13.6398(3) Å	b = 15.8194 (3) Å
	c = 21.5674(6) Å	c = 21.5949(5) Å	c = 23.9548(6) Å
	α = 90 deg.	α = 90 deg.	α = 90deg
	β = 90deg.	β = 90deg.	β = 102.13(1) deg.
	γ = 120 deg.	γ = 120 deg.	γ = 90deg.
Volume ($Å^3$);Z	3524.87(18); 3	3479.35(13); 3	4130.9(2); 4
Density (cal.) (Mg/m^3)	1.437	1.425	1.679
Absorp. coeff. (mm^{-1})	1.180	1.155	1.494
F(000)	1554	1521	1510
Crystal size	0.12 x 0.09 x 0.09 mm	0.10 x 0.10 x 0.10 mm	0.15 x 0.12 x 0.08 mm
θ range for data collection	3.55 to 28.31 deg.	4.12 to 31.04 deg.	3.09 to 31.03 deg.
Index ranges	-18<=h<=18,	-19<=h<=19,	-16<=h<=16,
	-18<=k<=18,	-19<=k<=19,	-22<=k<=22,
	-28<=l<=28	-31<=l<=31	-34<=l<=34
Reflections collected	20351	2998	106567
Independent reflections	1941[R(int) = 0.0355)]	2467[R(int) = 0.0306)]	13148[R(int) = 0.0525)]
Absorption correction	not corrected	not corrected	not corrected
Data / restraints / parameters	1941 / 21 / 127	2467 / 19 / 132	13132 / 1 / 593
Goodness-of-fit on F^2	1.091	1.110	1.052
Final R indices	R1 = 0.0325,	R1 = 0.0349,	R1 = 0.0355,
[I>2σ(I)]	wR2 = 0.0944	wR2 = 0.1088	wR2 = 0.0726
R indices (all data)	R1 = 0.0359,	R1 = 0.0383,	R1 = 0.0461,
	wR2 = 0.0970	wR2 = 0.1118	wR2 = 0.0821

Crystal data and structure refinement for 4, 5, 6 and 7

	4	**5**	**6**	**7**
Empirical formula	$C_{37}H_{49}B_2N_7O_{10}Mn_2$	$C_{48}H_{70}ClN_{13}O_{14}Mn_4$	$C_{46}H6_{7.5}Cl_3N_{12.5}O_{22.}Mn_4$	$C_{47.5}H_{67}Cl_2N_{13}O_{13}Mn_2Fe_2$
Formula weight	883.33	1308.38	1481.73	1320.62
Temperature	100(2) K	100(2) K	100(2) K	100(2) K
Wavelength (MoKα)	0.71073 Å	0.71073 Å	0.71073	0.71073 Å
Crystal System	Trigonal	Monoclinic	Triclinic	Monoclinic
Space group	$P3_121$	P2(1)/c	P-1	P2(1)/c
Unit cell dimensions	a = 11.269(3) Å	a = 16.485(2) Å	a = 17.026(4) Å	a = 14.411(4) Å
	b = 11.269(3) Å	b = 14.494(2) Å	b = 18.267(4) Å	b = 16.699(6) Å
	c = 27.733(7) Å	c = 24.365(3) Å	c = 23.598(6) Å	c = 25.02(8) Å
	α = 90°	α = 90°	α = 101.44 (1)°	α = 90°
	β = 90°	β = 90.26(2)°	β = 108.57(1)°	β = 104.82(4)°
	γ = 120°	γ = 90°	γ = 105.65(1)°	γ = 90°
Volume ($Å^3$); Z	3050.4(14); 3	5821.6(13); 4	6366.2; 4	5820.8(3); 4
Density (calc.) Mg/m^3	1.443	1.493	1.546	1.507
Absorp. coeff. (mm^{-1})	0.686	1.043	0.984	1.075
F(000)	1380	2712	3048	2732
Crystal size (mm)	0.18 x 0.17 x 0.12	0.11 x 0.06 x 0.02	0.12 x 0.10 x 0.05	0.06 x 0.05 x 0.05
θ range for data collect.	3.04 to 30.48°	3.18 to 22.50°	2.92 to 27.5°	2.08 to 30.55°
Reflections collected	63879	49350	114428	65527
Independent reflect.	6165	7587	29183	17765
	[R(int.) = 0.424]	[R(int.) = 0.1044]	[R(int.) = 0.0721]	[R(int.) = 0.0631]
Absorpt. correction	not measured	not measured	Gaussian, face indexed	not measured
Data/restraints/param.	6157 / 9 / 281	7587 / 8 / 711	29183 / 906 / 1655	17632 / 7 / 760
Goodness-of-fit on F^2	1.107	1.216	1.029	1.012
Final R indices	R_1 = 0.0379	R_1 =0.1044	R_1 = 0.0756	R_1 = 0.0527
[I>2σ(I)	wR_2 = 0.0980	wR_2 = 0.1595	wR_2 = 0.1929	wR_2 = 0.1263
R indices (all data)	R_1 = 0.0420	R_1 = 0.1430	R_1 = 0.1075	R_1 = 0.0856
	wR_2 = 0.1130	wR_2 = 0.1737	wR_2 = 0.2143	wR_2 = 0.1494

	9	**10**
Empirical formula	$C_{38}H_{69}N_{12}O_{16}Cl_3Cu_2Fe_2$	$C_{42}H_{72}N_{15}O_{14.5}Br_2Cl_2Cr_2Cu_2$
Formula weight	1295.18	1480.95
Temperature (K)	100(2)	100(2)
Wavelength (Å)	0.71073	0.71073
Crystal system	Monoclinic	Triclinic
Space group	C2/c	P-1
Unit cell dimensions	a = 27.449(6) Å	a = 14.607(4) Å
	b = 8.976(2) Å	b = 15.153 (4) Å
	c = 24.038(6) Å	c = 15.186(5) Å
	α = 90 deg.	α = 88.13(4) deg.
	β = 119.883(6) deg.	β = 86.56(4) deg.
	γ = 90 deg.	γ = 62.57(4) deg.
Volume ($Å^3$);Z	5135.2(2); 4	2798.00(15); 2
Density (cal.) (Mg/m^3)	1.675	1.652
Absorp. coeff. (mm^{-1})	1.605	2.563
F(000)	2324	1510
Crystal size		
θ range for data collection	3.91 to 31.02 deg.	2.97 to 31.06 deg.
Index ranges	-39<=h<=39,	-21<=h<=21,
	-13<=k<=13,	-21<=k<=21,
	-34<=l<=34	-21<=l<=21
Reflections collected	48703	85582
Independent reflections	8163[R(int) = 0.0589)]	18949[R(int) = 0.0396)]
Absorption correction	not corrected	Gaussian, face indexed
Data / restraints / parameters	8163 / 0 / 339	18883 / 101 / 772
Goodness-of-fit on F^2	1.025	1.019
Final R indices	R1 = 0.0348, wR2 = 0.0709	R1 = 0.0345, wR2 = 0.0806
[I>2σ(I)]		
R indices (all data)	R1 = 0.0477, wR2 = 0.0755	R1 = 0.0452, wR2 = 0.1026

Crystal data and structure refinement for 9, and 10

Crystal data and structure refinement for 11 and 12

	11	**12**
Empirical formula	$C_{76}\ H_{62}\ B_2\ Mn_4\ N_{14}\ O_7F_8$	$C_{58.5}\ H_{54}\ Mn_4\ N_8\ O_{18.5}$
Formula weight	1676.78	1384.86
Temperature (K)	100(2)	100(2)
Wavelength (Å)	0.71073	0.71073
Crystal system	Tetragonal	Triclinic
Space group	$I4_1/a$ No. 88	P-1
Unit cell dimensions	a = 17.0154(9) Å	a = 12.3968(9) Å
	b = 17.0154(9) Å	b = 14.715(2)Å
	c = 53.619(4) Å	c = 16.716(2)Å
	α =90 deg.	α = 84.15(1) deg.
	β = 90deg.	β = 84.11(1)deg.
	γ = 90deg.	γ = 89.48(1) deg.
Volume ($Å^3$);Z	15524.0(16); 8	3017.4(6); 2
Density (calculated) (Mg/m^3)	1.435	1.524
Absorption coefficient (mm^{-1})	0.717	0.898
F(000)	6832	1418
Crystal size (mm)	0.23 x 0.17 x 0.13	0.04 x 0.01 x 0.01
θ range for data collection	2.24 to 26.35 deg.	2.93 to 22.50
Index ranges	-21<=h<=20,	-13<=h<=12,
	-21<=k<=20,	-15<=k<=15,
	-66<=l<=66	-17<=l<=17
Reflections collected	53622	21974
Independent reflections	7932 [R(int) = 0.0338]	7884 [R(int) = 0.0931]
Absorption correction	Gaussian, face-indexed	Not measured
Data / restraints / parameters	7843 / 0 / 570	7884 / 12 / 837
Goodness-of-fit on F^2	1.028	1.032
Final R indices	R1 = 0.0353,	R1 = 0.0600,
[I>2σ(I)]	wR2 = 0.930	wR2 = 0.1137
R indices (all data)	R1 = 0.0571,	R1 = 0.1215,
	wR2 = 0.1742	wR2 = 0.1365

Crystal data and structure refinement for 13, 14 and 15

	13	**14**	**15**
Empirical formula	C_{66} H_{84} Cl_2 Mn_6 N_{18} O_{26}	C_{66} $H_{78}Cl_2$ Mn_6 N_{24} O_{24}	C_{48} $H_{73}B_3Cu_6$ F_{12} N_{12} O_{14}
Formula weight	1922.03	1992.06	1683.85
Temperature (K)	100(2)	100(2)	100(2)
Wavelength (Å)	0.71073	0.71073	0.71073
Crystal system	Triclinic	Triclinic	Cubic
Space group	P-1	P-1	Pa-3, No. 205
Unit cell dimensions	a = 10.636(2) Å	a = 10.9213(9) Å	a = 23.8313(9) Å
	b = 13.270(3) Å	b = 13.5592(12)Å	b = 23.8313(9) Å
	c = 15.515(3) Å	c = 15.444(2)Å	c = 23.8313(9) Å
	α =65.48(2) deg.	α = 101.75(1) deg.	α = 90 deg.
	β = 82.81(2) deg.	β = 107.72(1)deg.	β = 90deg.
	γ = 84.62(2) deg.	γ = 98.08(1) deg.	γ= 90 deg.
Volume ($Å^3$);Z	1974.5(7); 1	2081.9(4); 1	13534.5(9); 8
Density (calculated) (Mg/m^3)	1.616	1.589	1.653
Absorption coefficient (mm^{-1})	1.087	1.034	1.951
F(000)	986	1018	6832
Crystal size (mm)	0.04 x 0.03 x 0.03	0.06 x 0.04 x 0.04	0.36 x 0.32 x 0.22
θ range for data collection	2.3 to 25.00 deg.	3.43 to 27.50	3.01 to 27.50 deg.
Index ranges	-13<=h<=13,	-14<=h<=15,	-31<=h<=30,
	-16<=k<=16,	-19<=k<=19,	-31<=k<=31,
	-19<=l<=19	-20<=l<=20	-31<=l<=31
Reflections collected	25689	23688	118922
Independent reflections	6943 [R(int) = 0.0824]	9500 [R(int) = 0.0857]	5319 [R(int) = 0.0570]
Absorption correction	Not measured	Not measured	Gaussian, face-indexed
Data / restraints / parameters	6879 / 95 / 570	9385 / 3 / 568	5319 / 95 / 314
Goodness-of-fit on F^2	1.050	1.010	1.057
Final R indices	R1 = 0.0598,	R1 = 0.0543,	R1 = 0.0427,
[I>2σ(I)]	wR2 = 0.1180	wR2 = 0.0916	wR2 = 0.1139
R indices (all data)	R1 = 0.1108,	R1 = 0.1180,	R1 = 0.0531,
	wR2 = 0.1397	wR2 = 0.1139	wR2 = 0.1246

Crystal data and structure refinement for 16 and 17

	16	**17**
Empirical formula	$C_{60}H_{94}Cl_4N_{20}Ni_9O_{50}$	$C_{100}H_{128}N_8O_{32}Cl_2Cu_9$
Formula weight	2565.74	2596.86
Temperature (K)	100(2)	100(2)
Wavelength (Å)	0.71073	0.71073
Crystal system	Monoclinic	Triclinic
Space group	C2/c , No. 15	P-1
Unit cell dimensions	a = 24.704(2) Å	a = 13.0636(4) Å
	b = 31.015(3) Å	b = 15.2420 (6) Å
	c = 26.032(2) Å	c = 16.0330(6) Å
	α = 90 deg.	α = 107.71(1) deg.
	β = 100.13(2) deg.	β = 112.03(1) deg.
	γ = 90 deg.	γ = 101.11(1) deg.
Volume ($Å^3$);Z	19635.3(2); 8	2643.47(15); 1
Density (cal.) (Mg/m^3)	1.736	1.631
Absorp. coeff. (mm^{-1})	1.899	1.907
F(000)	10512	1335
Crystal size	0.28x0.06x0.06 mm	0.16x0.15x0.10 mm
θ range for data collection	2.97 to 22.50 deg.	2.99 to 31.10 deg.
Index ranges	-26<=h<=26,	-18<=h<=18,
	-33<=k<=33,	-22<=k<=22,
	-28<=l<=28	-23<=l<=21
Reflections collected	103240	66247
Independent reflections	12807[R(int) = 0.0984)]	16905[R(int) = 0.0513)]
Absorption correction	Gaussian, face indexed	Gaussian, face indexed
Data / restraints / parameters	12807 /93 0 / 1467	16905 / 1 / 702
Goodness-of-fit on F^2	1.111	1.040
Final R indices	R1 = 0.0717, wR2 = 0.1593	R1 = 0.0446, wR2 = 0.0989
[I>2σ(I)]		
R indices (all data)	R1 = 0.0926, wR2 = 0.1703	R1 = 0.0616, wR2 = 0.1026

(2) Magnetochemical Data

Complex $Ni^{II}Mn^{III}Ni^{II}$ (1)

MW = 837.0 g/mol, χ_{dia} = -425.0 x 10^{-6} cm^3 mol^{-1}
m = 32.57 mg , H = 1.000 T

No	T(K)	$\chi.T_{exp.}$	$\chi.T_{calc.}$	μ_{exp}	$\mu_{calc.}$
1	1.951	0.33602	0.01984	1.6393	0.39835
2	5.116	0.83956	0.33326	2.59122	1.63257
3	10.144	1.37563	0.89542	3.31688	2.67604
4	15.046	1.79121	1.44128	3.78488	3.39511
5	20.003	2.14802	1.92967	4.14475	3.92845
6	30.002	2.70188	2.66048	4.6485	4.61274
7	39.999	3.09273	3.13414	4.97337	5.00655
8	50.006	3.38002	3.45382	5.19923	5.25568
9	60.043	3.59354	3.68111	5.36094	5.42586
10	70.058	3.7587	3.84908	5.48275	5.54827
11	80.067	3.8952	3.978	5.58141	5.64042
12	90.09	4.00346	4.08005	5.65845	5.71231
13	100.1	4.09563	4.16253	5.72321	5.76976
14	110.15	4.1709	4.23085	5.77556	5.81692
15	120.12	4.2364	4.28772	5.82074	5.85589
16	130.17	4.28919	4.33647	5.85689	5.88908
17	140.18	4.34007	4.37826	5.89153	5.91739
18	150.19	4.38152	4.41461	5.91959	5.9419
19	160.19	4.42087	4.44647	5.94611	5.96331
20	170.22	4.45514	4.47473	5.96912	5.98223
21	180.22	4.48471	4.49983	5.98889	5.99898
22	190.22	4.51229	4.52233	6.00728	6.01396
23	200.24	4.53428	4.54265	6.0219	6.02746
24	210.16	4.55519	4.56089	6.03577	6.03954
25	220.26	4.57663	4.57778	6.04996	6.05072
26	230.26	4.59272	4.59306	6.06058	6.06081
27	240.26	4.6115	4.60709	6.07296	6.07006
28	250.26	4.62828	4.62	6.084	6.07856
29	260.27	4.64631	4.63194	6.09584	6.08641
30	270.26	4.66375	4.64299	6.10727	6.09366
31	280.27	4.67325	4.65327	6.11349	6.1004
32	290.27	4.69206	4.66284	6.12578	6.10667

Complex $Ni^{II}Cr^{III}Ni^{II}$ (2)

MW = 995 g/mol, χ_{dia} = -420 x 10^{-6} cm^3 mol^{-1}
m = 63.45 mg , H = 1.000 T

No	T(K)	$\chi.T_{exp.}$	$\chi.T_{calc.}$	μ_{exp}	$\mu_{calc.}$
1	1.912	2.93923	3.39597	4.84837	5.21148
2	5.089	3.99861	4.11896	5.65502	5.73949
3	9.999	4.11023	4.09724	5.7334	5.72434
4	14.959	4.05373	4.02934	5.69386	5.67671
5	20.004	3.99144	3.98056	5.64994	5.64224
6	29.999	3.9079	3.92252	5.59051	5.60095
7	39.996	3.86411	3.88978	5.5591	5.57753
8	50.009	3.83246	3.86892	5.53628	5.56255
9	60.047	3.82229	3.8545	5.52893	5.55218
10	70.052	3.81195	3.844	5.52145	5.54461
11	80.068	3.81108	3.83599	5.52082	5.53883
12	90.105	3.80872	3.82967	5.51911	5.53427
13	100.12	3.81586	3.82458	5.52428	5.53059
14	110.11	3.81745	3.82039	5.52543	5.52756
15	120.12	3.82319	3.81687	5.52958	5.52501
16	130.11	3.82085	3.81389	5.52789	5.52285
17	140.18	3.82048	3.81129	5.52762	5.52097
18	150.19	3.80833	3.80905	5.51883	5.51935
19	160.21	3.79812	3.80708	5.51142	5.51792
20	170.21	3.79525	3.80535	5.50934	5.51667
21	180.22	3.79464	3.80379	5.5089	5.51554
22	190.23	3.7969	3.8024	5.51054	5.51453
23	200.24	3.79574	3.80115	5.5097	5.51362
24	210.24	3.79607	3.80001	5.50994	5.51279
25	220.27	3.79687	3.79898	5.51052	5.51205
26	230.26	3.79938	3.79803	5.51234	5.51136
27	240.25	3.80528	3.79716	5.51662	5.51073
28	250.26	3.81294	3.79636	5.52217	5.51015
29	260.16	3.81381	3.79563	5.5228	5.50962
30	270.25	3.82078	3.79494	5.52784	5.50912
31	280.25	3.8247	3.7943	5.53067	5.50865
32	290.25	3.83429	3.79371	5.5376	5.50822

Complex Ni^{II}_3 (3)

MW = 1044 g/mol, χ_{dia} = -430 x 10^{-6} cm^3 mol^{-1}
m = 54.25 mg , H = 1.000 T

No	T(K)	$\chi.T_{exp.}$	$\chi.T_{calc.}$	μ_{exp}	$\mu_{calc.}$
1	1.96	0.80356	0.98983	2.53507	2.81358
2	5.11	0.97353	1.02925	2.79032	2.86906
3	9.99	1.0331	1.00545	2.87442	2.8357
4	15.02	1.12205	1.07778	2.99561	2.93592
5	20.01	1.2452	1.21	3.15572	3.1108
6	30.00	1.51542	1.50578	3.48134	3.47025
7	40.01	1.75747	1.76298	3.74907	3.75494
8	50.01	1.9538	1.96718	3.95293	3.96645
9	60.02	2.10845	2.12762	4.1064	4.12502
10	70.06	2.23365	2.25491	4.22656	4.24663
11	80.07	2.33672	2.35677	4.32298	4.34148
12	90.09	2.42075	2.4402	4.40002	4.41766
13	100.12	2.49276	2.50933	4.46498	4.4798
14	110.13	2.55149	2.56741	4.51727	4.53134
15	120.14	2.60448	2.61687	4.56394	4.57478
16	130.16	2.64714	2.6595	4.60117	4.61189
17	140.18	2.68774	2.69656	4.63632	4.64392
18	150.14	2.72092	2.72887	4.66485	4.67166
19	160.2	2.75367	2.75771	4.69284	4.69628
20	170.21	2.78267	2.78323	4.71748	4.71796
21	180.22	2.80758	2.80609	4.73855	4.73729
22	190.23	2.83175	2.82667	4.7589	4.75463
23	200.24	2.85184	2.84529	4.77575	4.77027
24	210.24	2.87148	2.86221	4.79217	4.78443
25	220.25	2.88915	2.87767	4.80689	4.79733
26	230.26	2.90473	2.89184	4.81984	4.80913
27	240.25	2.92129	2.90484	4.83356	4.81993
28	250.25	2.93752	2.91686	4.84696	4.82989
29	260.27	2.95348	2.92801	4.86011	4.83911
30	270.25	2.96902	2.93832	4.87288	4.84762
31	280.26	2.98144	2.94794	4.88306	4.85555
32	290.24	2.99747	2.95689	4.89617	4.86292

Complex $Mn^{II}Mn^{II}$ (4)

MW = 837.0 g/mol, χ_{dia} = -425.0 x 10^{-6} cm^3 mol^{-1}
m = 32.57 mg , H = 1.000 T

No	T(K)	$\chi.T_{exp.}$	$\chi.T_{calc.}$	μ_{exp}	$\mu_{calc.}$
1	1.948	0.0677	0.01015	0.73581	0.01018
2	5.119	0.16488	0.02578	1.14832	0.45402
3	9.996	0.35264	0.21482	1.67936	1.31074
4	15.039	0.55982	0.43311	2.11595	1.86114
5	20.005	0.75228	0.63946	2.45284	2.26144
6	30.001	1.1297	1.04851	3.00581	2.89578
7	39.998	1.50433	1.4553	3.46857	3.41158
8	50.008	1.87591	1.86014	3.87334	3.85702
9	60.045	2.24432	2.2595	4.23664	4.25095
10	70.05	2.60378	2.64487	4.56333	4.59919
11	80.075	2.94663	3.0123	4.85447	4.90827
12	90.093	3.27157	3.35655	5.11514	5.18115
13	100.14	3.57341	3.6766	5.3459	5.42254
14	110.13	3.85239	3.96939	5.55066	5.63432
15	120.13	4.1087	4.2378	5.73234	5.8217
16	130.17	4.34608	4.4839	5.8956	5.98835
17	140.18	4.56144	4.70773	6.03991	6.136
18	150.19	4.76215	4.91199	6.17136	6.2677
19	160.21	4.94278	5.09873	6.28731	6.38573
20	170.22	5.11166	5.26937	6.39382	6.4917
21	180.22	5.26377	5.42559	6.48825	6.58723
22	190.24	5.40441	5.56934	6.57436	6.67392
23	200.24	5.53466	5.70136	6.65311	6.75256
24	210.25	5.65088	5.82325	6.7226	6.82436
25	220.25	5.76244	5.93581	6.78864	6.89
26	230.25	5.86172	6.0401	6.84687	6.95027
27	240.26	5.95191	6.13702	6.89934	7.00581
28	250.17	6.03728	6.22633	6.94864	7.0566
29	260.26	6.12128	6.31111	6.99682	7.10448
30	270.26	6.20203	6.38957	7.04282	7.1485
31	280.26	6.28144	6.46301	7.08776	7.18947
32	290.23	6.35298	6.53167	7.12801	7.22756

Complex $Mn^{III}Mn^{II}Mn^{II}Mn^{III}$ (5)

MW = 1234 g/mol, χ_{dia} = -630.0 x 10^{-6} cm^3 mol^{-1}
m = 34.79 mg , H = 1.000 T

No	T(K)	$\chi.T_{exp.}$	$\chi.T_{calc.}$	μ_{exp}	$\mu_{calc.}$
1	1.951	0.79064	0.53854	2.5146	2.07533
2	5.072	1.89519	1.48217	3.89319	3.44293
3	9.997	2.94776	2.69293	4.85541	4.64079
4	15.028	3.82114	3.69206	5.5281	5.43393
5	20.004	4.55633	4.50875	6.03652	6.00492
6	30	5.73805	5.74341	6.77426	6.77742
7	39.999	6.65335	6.61325	7.29457	7.27255
8	50.009	7.38764	7.27651	7.68656	7.62853
9	60.022	7.9832	7.81704	7.99039	7.9068
10	70.058	8.47748	8.27621	8.23404	8.1357
11	80.08	8.88361	8.67223	8.42896	8.32808
12	90.088	9.2187	9.01671	8.58646	8.49187
13	100.11	9.4894	9.3184	8.71162	8.63277
14	110.13	9.72049	9.58288	8.81705	8.75442
15	120.17	9.91151	9.81584	8.90327	8.86019
16	130.16	10.0726	10.0203	8.97533	8.95199
17	140.18	10.2081	10.2017	9.03549	9.03266
18	150.18	10.3344	10.3625	9.09122	9.10357
19	160.13	10.4319	10.5052	9.134	9.16604
20	170.2	10.5331	10.6344	9.1782	9.22223
21	180.23	10.6111	10.75	9.2121	9.27222
22	190.23	10.6783	10.853	9.24124	9.31688
23	200.24	10.7431	10.9479	9.26924	9.35718
24	210.24	10.7904	11.0332	9.28962	9.39356
25	220.26	10.8469	11.1111	9.31391	9.42666
26	230.25	10.893	11.1821	9.33369	9.45673
27	240.28	10.9354	11.2475	9.35183	9.48435
28	250.27	10.98	11.3073	9.37088	9.50953
29	260.27	11.007	11.3625	9.3824	9.53271
30	270.26	11.0346	11.4136	9.39415	9.55412
31	280.25	11.0707	11.4608	9.40951	9.57386
32	290.26	11.0718	11.5049	9.40998	9.59226

Complex $Mn^{IV}Mn^{II}Mn^{II}Mn^{IV}$ (6)

MW = 1433 g/mol, χ_{dia} = -700.0 x 10^{-6} cm^3 mol^{-1}
m = 33.63 mg , H = 1.000 T

No	T(K)	$\chi.T_{exp.}$	$\chi.T_{calc.}$	μ_{exp}	$\mu_{calc.}$
1	1.916	1.21603	1.75514	3.11854	3.74658
2	5.11	2.91624	3.31404	4.82938	5.14823
3	9.994	3.99506	4.62802	5.65251	6.08383
4	15.014	5.00867	5.45928	6.32908	6.60765
5	20.005	5.85464	6.11183	6.84273	6.99141
6	30.001	7.18731	7.23633	7.58163	7.60744
7	40	8.21043	8.21261	8.10331	8.10438
8	50.013	9.02793	9.04005	8.49715	8.50286
9	60.031	9.69277	9.72286	8.80447	8.81813
10	70.038	10.2385	10.2805	9.04894	9.06748
11	80.069	10.694	10.7386	9.24804	9.2673
12	90.089	11.0777	11.1163	9.41248	9.42887
13	100.13	11.39	11.432	9.54424	9.56182
14	110.13	11.6566	11.6969	9.65529	9.67197
15	120.14	11.8802	11.9228	9.74746	9.76492
16	130.16	12.0724	12.1171	9.82599	9.84416
17	140.17	12.234	12.2856	9.89153	9.91237
18	150.19	12.3887	12.433	9.95388	9.97166
19	160.14	12.4916	12.5621	9.99513	10.0233
20	170.21	12.6331	12.6779	10.05158	10.06939
21	180.23	12.7325	12.7808	10.09105	10.11017
22	190.23	12.8205	12.8729	10.12586	10.14653
23	200.23	12.9041	12.956	10.15882	10.17923
24	210.24	12.9741	13.0314	10.18634	10.20881
25	220.24	13.0507	13.1	10.21636	10.23564
26	230.25	13.1102	13.1628	10.23963	10.26015
27	240.24	13.159	13.2203	10.25867	10.28253
28	250.26	13.2152	13.2734	10.28055	10.30316
29	260.27	13.2625	13.3223	10.29893	10.32212
30	270.26	13.3201	13.3676	10.32127	10.33966
31	280.26	13.3867	13.4096	10.34704	10.35589
32	290.25	13.436	13.4488	10.36608	10.37101

Complex $Fe^{III}Mn^{II}Mn^{II}Fe^{III}$ (7)

MW = 1236 g/mol, χ_{dia} = -592.0 x 10^{-6} cm^3 mol^{-1}
m = 22.75 mg , H = 1.000 T

No	T(K)	$\chi.T_{exp.}$	$\chi.T_{calc.}$	μ_{exp}	$\mu_{calc.}$
1	1.959	1.32852	0.79258	3.25959	2.5177
2	5.01	2.77139	2.03779	4.70791	4.037
3	9.996	4.22679	3.66287	5.81413	5.4124
4	14.994	5.31265	4.95719	6.51831	6.29647
5	20.005	6.17474	5.97047	7.0273	6.91009
6	30	7.45581	7.35645	7.72195	7.67032
7	40.002	8.39672	8.26324	8.19472	8.12933
8	50	9.14143	8.94522	8.5504	8.45814
9	60.038	9.76769	9.51563	8.83843	8.72365
10	70.056	10.2858	10.0168	9.06982	8.95043
11	80.089	10.7361	10.4698	9.26622	9.15058
12	90.1	11.1224	10.8813	9.43145	9.32867
13	100.12	11.4475	11.2574	9.5683	9.48852
14	110.13	11.7448	11.6005	9.69175	9.63203
15	120.14	11.9972	11.9139	9.79534	9.76127
16	130.17	12.2252	12.2007	9.88798	9.87806
17	140.19	12.4247	12.4626	9.96833	9.98352
18	150.19	12.6103	12.7019	10.04251	10.07891
19	160.2	12.7793	12.9215	10.10958	10.16567
20	170.22	12.9289	13.1233	10.16858	10.24474
21	180.23	13.0787	13.3089	10.22732	10.31693
22	190.24	13.2042	13.4801	10.27627	10.38307
23	200.24	13.3299	13.6381	10.32507	10.44375
24	210.24	13.4435	13.7844	10.36897	10.49961
25	220.26	13.5514	13.9206	10.4105	10.55136
26	230.25	13.6678	14.0468	10.45511	10.59908
27	240.25	13.7637	14.1645	10.49173	10.64339
28	250.26	13.8558	14.2746	10.52677	10.68468
29	260.27	13.9436	14.3776	10.56007	10.72316
30	270.25	14.0124	14.4738	10.58609	10.75897
31	280.17	14.1152	14.5637	10.62485	10.79233
32	290.26	14.2252	14.6496	10.66617	10.82411

Complex $Cr^{III}Mn^{II}Mn^{II}Cr^{III}$ (8)

MW = 1228 g/mol, χ_{dia} = -625.0 x 10^{-6} cm^3 mol^{-1}
m = 39.54 mg , H = 1.000 T

No	T(K)	$\chi.T_{exp.}$	$\chi.T_{calc.}$	μ_{exp}	$\mu_{calc.}$
1	1.952	0.59263	0.25479	2.17707	1.42748
2	5.138	1.36712	0.8418	3.30661	2.59469
3	9.969	1.81119	1.55265	3.80594	3.52384
4	15.007	2.18216	2.14702	4.17756	4.14379
5	20.005	2.53284	2.61344	4.50073	4.57178
6	30	3.19519	3.297	5.05508	5.13498
7	39.998	3.80295	3.8081	5.51493	5.51866
8	50.01	4.33953	4.24381	5.89116	5.82582
9	60.034	4.82463	4.64128	6.21171	6.09254
10	70.055	5.25082	5.01295	6.48027	6.33178
11	80.069	5.62698	5.36218	6.70837	6.54862
12	90.093	5.96075	5.68979	6.90446	6.74571
13	100.13	6.24829	5.99551	7.06903	6.92456
14	110.13	6.5057	6.27796	7.21317	7.0858
15	120.11	6.72787	6.53843	7.33531	7.2313
16	130.16	6.93391	6.78015	7.44678	7.36375
17	140.18	7.11205	7.00194	7.54183	7.48322
18	150.19	7.27804	7.2058	7.62933	7.59138
19	160.21	7.42578	7.39365	7.70638	7.68969
20	170.21	7.5584	7.56638	7.77489	7.77899
21	180.22	7.6811	7.72591	7.83774	7.86057
22	190.23	7.78637	7.87331	7.89127	7.9352
23	200.23	7.89224	8.0096	7.94474	8.00359
24	210.23	7.98217	8.13599	7.98987	8.06649
25	220.26	8.06887	8.25374	8.03315	8.12465
26	230.26	8.15133	8.36299	8.07409	8.17825
27	240.25	8.22445	8.46477	8.11022	8.22786
28	250.24	8.296	8.55985	8.14543	8.27394
29	260.27	8.36422	8.64917	8.17885	8.317
30	270.26	8.41954	8.73256	8.20585	8.357
31	280.26	8.48277	8.81094	8.23661	8.39442
32	290.15	8.5273	8.88388	8.2582	8.42909

Complex $Fe^{III}_2Cu^{II}_2$ (9)

MW = 1295.0 g/mol, χ_{dia} = -620.0 x 10^{-6} cm^3 mol^{-1}
m = 18.61 mg , H = 1.000 T

No	T(K)	$\chi.T_{exp.}$	$\chi.T_{calc.}$	μ_{exp}	$\mu_{calc.}$
1	1.947	6.15347	6.18609	7.01519	7.03376
2	5.025	8.40454	8.49109	8.19854	8.24064
3	10.058	8.39965	8.34069	8.19615	8.16734
4	15.031	7.95016	7.90105	7.97384	7.94917
5	20.003	7.62678	7.58346	7.80998	7.78777
6	30	7.21982	7.19946	7.59876	7.58804
7	39.997	6.99787	6.98533	7.48105	7.47434
8	50.009	6.86339	6.85034	7.40881	7.40177
9	60.01	6.76545	6.75804	7.35576	7.35173
10	70.055	6.6945	6.69076	7.31709	7.31505
11	80.075	6.64977	6.63989	7.29261	7.28719
12	90.094	6.61113	6.60007	7.27139	7.2653
13	100.11	6.57834	6.56814	7.25333	7.24771
14	110.1	6.55335	6.5422	7.23954	7.23338
15	120.15	6.53128	6.52081	7.22734	7.22155
16	130.16	6.51287	6.5034	7.21715	7.2119
17	140.18	6.49725	6.48937	7.20849	7.20412
18	150.19	6.48503	6.47844	7.20171	7.19805
19	160.2	6.48535	6.47042	7.20188	7.19359
20	170.22	6.46962	6.46519	7.19314	7.19068
21	180.21	6.49148	6.46268	7.20529	7.18929
22	190.23	6.46212	6.46283	7.18897	7.18937
23	200.24	6.46348	6.46557	7.18973	7.19089
24	210.24	6.46667	6.47083	7.1915	7.19382
25	220.26	6.4667	6.47854	7.19152	7.1981
26	230.25	6.47453	6.48859	7.19587	7.20368
27	240.15	6.4784	6.50074	7.19802	7.21042
28	250.26	6.48892	6.51531	7.20387	7.2185
29	260.27	6.50329	6.53173	7.21184	7.22759
30	270.25	6.51218	6.54996	7.21677	7.23767
31	280.26	6.52818	6.56996	7.22563	7.24871
32	290.26	6.55049	6.59152	7.23796	7.26059

Complex $Cr^{III}_2Cu^{II}_2$ (10)

MW = 1348 g/mol, χ_{dia} = -610.0 x 10^{-6} cm^3 mol^{-1}
m = 37.89 mg , H = 1.000 T

No	T(K)	$\chi.T_{exp.}$	$\chi.T_{calc.}$	μ_{exp}	$\mu_{calc.}$
1	1.949	1.25667	2.4444	3.17022	4.42146
2	5.091	2.56664	2.81681	4.53066	4.74633
3	10.153	2.85421	2.87389	4.77774	4.79418
4	15.046	2.85834	2.86638	4.78119	4.78791
5	20.005	2.82607	2.83215	4.75413	4.75924
6	30	2.72395	2.72977	4.66744	4.67243
7	40.001	2.63192	2.626	4.58792	4.58276
8	50.01	2.55155	2.53778	4.51733	4.50512
9	60.041	2.48523	2.46667	4.45823	4.44155
10	70.055	2.43778	2.41147	4.41547	4.39158
11	80.049	2.40619	2.37065	4.38676	4.35425
12	90.107	2.38338	2.34285	4.36592	4.32864
13	100.11	2.36909	2.32739	4.35281	4.31434
14	110.13	2.36202	2.323	4.34631	4.31027
15	120.15	2.36645	2.32848	4.35039	4.31535
16	130.16	2.37514	2.34248	4.35837	4.3283
17	140.18	2.39356	2.36369	4.37524	4.34785
18	150.19	2.41592	2.39075	4.39563	4.37267
19	160.21	2.44451	2.42249	4.42156	4.4016
20	170.21	2.48274	2.45773	4.456	4.4335
21	180.22	2.5103	2.49561	4.48066	4.46753
22	190.16	2.54717	2.53501	4.51345	4.50266
23	200.25	2.58604	2.57615	4.54775	4.53905
24	210.23	2.62565	2.61743	4.58245	4.57527
25	220.25	2.6658	2.65901	4.61735	4.61147
26	230.25	2.70577	2.7003	4.65184	4.64714
27	240.26	2.74667	2.74115	4.68687	4.68216
28	250.26	2.78569	2.78127	4.72004	4.7163
29	260.27	2.82566	2.8206	4.75378	4.74952
30	270.26	2.86462	2.85889	4.78644	4.78165
31	280.27	2.89995	2.89622	4.81587	4.81277
32	290.24	2.93601	2.93234	4.84572	4.84269

Complex Mn^{II}_4 (11)

MW = 1576 g/mol, χ_{dia} = -770.0 x 10^{-6} cm^3 mol^{-1}
m = 35.14 mg , H = 1.000 T

No	T(K)	$\chi.T_{exp.}$	$\chi.T_{calc.}$	μ_{exp}	$\mu_{calc.}$
1	1.95	7.98	12.903	7.9906	10.15839
2	5.08	19.09	19.4542	12.35687	12.47344
3	10.14	19.31	19.4838	12.42805	12.48292
4	15.05	18.81	18.9431	12.26628	12.30849
5	19.99	18.45	18.5727	12.14849	12.18756
6	29.99	18.107	18.1414	12.0338	12.04522
7	40.00	17.9295	17.9079	11.97467	11.96745
8	50.00	17.8172	17.7628	11.93711	11.91887
9	60.04	17.7392	17.6639	11.91095	11.88564
10	70.05	17.6572	17.5926	11.88339	11.86163
11	80.08	17.6318	17.5386	11.87484	11.84341
12	90.089	17.5972	17.4964	11.86318	11.82916
13	100.1	17.554	17.4625	11.84861	11.81769
14	110.08	17.52	17.4347	11.83713	11.80828
15	120.13	17.4909	17.4113	11.8273	11.80035
16	130.16	17.4592	17.3915	11.81657	11.79364
17	140.18	17.4322	17.3746	11.80743	11.78791
18	150.19	17.41	17.3598	11.79991	11.78289
19	160.19	17.396	17.3469	11.79517	11.77851
20	170.21	17.3765	17.3355	11.78855	11.77464
21	180.23	17.3689	17.3254	11.78598	11.77121
22	190.23	17.3438	17.3163	11.77746	11.76812
23	200.24	17.3315	17.3081	11.77328	11.76533
24	210.15	17.3147	17.3008	11.76757	11.76285
25	220.24	17.3035	17.294	11.76377	11.76054
26	230.25	17.3072	17.2878	11.76502	11.75843
27	240.25	17.295	17.2821	11.76088	11.75649
28	250.25	17.282	17.2769	11.75646	11.75472
29	260.26	17.2788	17.2721	11.75537	11.75309
30	270.26	17.2627	17.2677	11.74989	11.75159
31	280.23	17.2561	17.2636	11.74764	11.7502
32	290.24	17.2568	17.2597	11.74788	11.74887

Complex Mn^{III}_4 (12)

MW = 1384 g/mol, χ_{dia} = -650.0 x 10^{-6} cm^3 mol^{-1}
m = 29.59 mg , H = 1.000 T

No	T(K)	$\chi.T_{exp.}$	$\chi.T_{calc.}$	μ_{exp}	$\mu_{calc.}$
1	1.966	5.7165	6.90638	6.76152	7.43198
2	5.094	14.5492	15.6427	10.78696	11.18498
3	9.999	16.7753	16.9447	11.58283	11.64116
4	14.994	16.1334	15.9428	11.35906	11.29176
5	20.004	15.3838	15.2949	11.09203	11.05994
6	29.999	14.3461	14.5037	10.7114	10.77008
7	40	13.7333	14.0042	10.48013	10.58299
8	50.008	13.3568	13.6506	10.33548	10.44853
9	60.035	13.0962	13.385	10.23416	10.34638
10	70.059	12.9027	13.1782	10.15827	10.26615
11	80.056	12.7774	13.0129	10.10882	10.20156
12	90.101	12.6807	12.8769	10.0705	10.14811
13	100.12	12.5933	12.7639	10.03573	10.10348
14	110.13	12.5281	12.6682	10.00972	10.06553
15	120.14	12.47	12.5862	9.98648	10.03291
16	130.16	12.4259	12.5151	9.96881	10.00453
17	140.18	12.3819	12.4529	9.95114	9.97963
18	150.13	12.3487	12.3984	9.93779	9.95777
19	160.19	12.3258	12.3495	9.92858	9.93812
20	170.22	12.3047	12.3058	9.92007	9.92052
21	180.23	12.2882	12.2666	9.91342	9.9047
22	190.23	12.2529	12.2312	9.89917	9.8904
23	200.24	12.2308	12.199	9.89024	9.87737
24	210.24	12.2064	12.1697	9.88037	9.86551
25	220.26	12.1763	12.1427	9.86818	9.85456
26	230.26	12.1583	12.118	9.86088	9.84453
27	240.26	12.129	12.0951	9.84899	9.83522
28	250.25	12.1031	12.074	9.83847	9.82664
29	260.27	12.0814	12.0544	9.82965	9.81866
30	270.26	12.0595	12.0361	9.82074	9.8112
31	280.14	12.05	12.0193	9.81687	9.80435
32	290.26	12.0524	12.0032	9.81785	9.79779

Complex $Mn^{III}_4Mn^{II}_2$ (13)

MW = 1774 g/mol, χ_{dia} = -740 x 10^{-6} cm^3 mol^{-1}
m = 22.95 mg , H = 1.000 T

No	T(K)	$\chi.T_{exp.}$	$\chi.T_{calc.}$	μ_{exp}	$\mu_{calc.}$
1	1.954	5.71186	5.53098	6.75878	6.6509
2	5.076	8.99394	7.83852	8.48114	7.91765
3	9.994	9.72196	8.43898	8.81772	8.21532
4	15.014	9.67494	8.61716	8.79637	8.30159
5	20.005	9.53456	8.75954	8.73232	8.3699
6	30.001	9.40964	9.09982	8.67493	8.53092
7	39.999	9.55658	9.49414	8.7424	8.71379
8	50.011	9.90966	9.91632	8.90243	8.90543
9	60.046	10.34882	10.35492	9.09756	9.10024
10	70.052	10.80894	10.79858	9.2976	9.29315
11	80.059	11.27654	11.23944	9.49658	9.48095
12	90.105	11.73602	11.67076	9.68813	9.66115
13	100.12	12.1494	12.08298	9.85727	9.83029
14	110.13	12.54018	12.473	10.01455	9.98769
15	120.13	12.88962	12.8384	10.15312	10.13293
16	130.12	13.21522	13.17852	10.28056	10.26627
17	140.19	13.50796	13.49652	10.3938	10.3894
18	150.2	13.78836	13.78898	10.50112	10.50136
19	160.21	14.03658	14.05928	10.59522	10.60379
20	170.21	14.27676	14.30878	10.68548	10.69746
21	180.22	14.49874	14.53964	10.76824	10.78341
22	190.23	14.68712	14.7532	10.83796	10.86232
23	200.24	14.87638	14.95098	10.90757	10.93489
24	210.24	15.03404	15.13426	10.96522	11.00171
25	220.25	15.19804	15.30468	11.02486	11.06347
26	230.25	15.34708	15.4631	11.07879	11.12059
27	240.26	15.47818	15.6109	11.12601	11.17361
28	250.26	15.61206	15.74874	11.17402	11.22283
29	260.27	15.73	15.8778	11.21615	11.26872
30	270.26	15.80874	15.99844	11.24419	11.31145
31	280.24	15.9287	16.11154	11.28677	11.35136
32	290.26	16.06634	16.21826	11.33543	11.38889

Complex $Mn^{III}_4Mn^{II}_2$ (14)

MW = 1744 g/mol, χ_{dia} = -720 x 10^{-6} cm^3 mol^{-1}
m = 15.34 mg , H = 1.000 T

No	T(K)	$\chi.T_{exp.}$	$\chi.T_{calc.}$	μ_{exp}	$\mu_{calc.}$
1	1.954	5.71186	5.53098	6.75878	6.6509
2	5.076	8.99394	7.83852	8.48114	7.91765
3	9.994	9.72196	8.43898	8.81772	8.21532
4	15.014	9.67494	8.61716	8.79637	8.30159
5	20.005	9.53456	8.75954	8.73232	8.3699
6	30.001	9.40964	9.09982	8.67493	8.53092
7	39.999	9.55658	9.49414	8.7424	8.71379
8	50.011	9.90966	9.91632	8.90243	8.90543
9	60.046	10.34882	10.35492	9.09756	9.10024
10	70.052	10.80894	10.79858	9.2976	9.29315
11	80.059	11.27654	11.23944	9.49658	9.48095
12	90.105	11.73602	11.67076	9.68813	9.66115
13	100.12	12.1494	12.08298	9.85727	9.83029
14	110.13	12.54018	12.473	10.01455	9.98769
15	120.13	12.88962	12.8384	10.15312	10.13293
16	130.12	13.21522	13.17852	10.28056	10.26627
17	140.19	13.50796	13.49652	10.3938	10.3894
18	150.2	13.78836	13.78898	10.50112	10.50136
19	160.21	14.03658	14.05928	10.59522	10.60379
20	170.21	14.27676	14.30878	10.68548	10.69746
21	180.22	14.49874	14.53964	10.76824	10.78341
22	190.23	14.68712	14.7532	10.83796	10.86232
23	200.24	14.87638	14.95098	10.90757	10.93489
24	210.24	15.03404	15.13426	10.96522	11.00171
25	220.25	15.19804	15.30468	11.02486	11.06347
26	230.25	15.34708	15.4631	11.07879	11.12059
27	240.26	15.47818	15.6109	11.12601	11.17361
28	250.26	15.61206	15.74874	11.17402	11.22283
29	260.27	15.73	15.8778	11.21615	11.26872
30	270.26	15.80874	15.99844	11.24419	11.31145
31	280.24	15.9287	16.11154	11.28677	11.35136
32	290.26	16.06634	16.21826	11.33543	11.38889

Complex Cu^{II}_6 (15)

MW = 1657 g/mol, χ_{dia} = -660 x 10^{-6} cm^3 mol^{-1}
m = 35.32 mg , H = 1.000 T

No	T(K)	$\chi.T_{exp.}$	$\chi.T_{calc.}$	μ_{exp}	$\mu_{calc.}$
1	1.922	0.33836	0.0033	1.64501	0.16246
2	5.19	0.59442	0.1963	2.18035	1.25297
3	9.991	0.61462	0.4496	2.21709	1.89624
4	15.013	0.59928	0.5582	2.18924	2.11288
5	20.005	0.61975	0.6107	2.22633	2.21001
6	30	0.65456	0.6608	2.28799	2.29887
7	40.003	0.68417	0.6847	2.33916	2.33916
8	50.006	0.70997	0.7	2.38286	2.38286
9	60.03	0.7283	0.71	2.41344	2.41344
10	70.051	0.74367	0.72	2.43876	2.43876
11	80.045	0.7599	0.73	2.46523	2.46523
12	90.082	0.76789	0.74	2.47816	2.47816
13	100.12	0.77633	0.74	2.49173	2.49173
14	110.12	0.78415	0.75	2.50426	2.50426
15	120.14	0.79109	0.76	2.51532	2.51532
16	130.16	0.7976	0.76	2.52565	2.52565
17	140.17	0.80391	0.78	2.53561	2.53561
18	150.13	0.81065	0.79	2.54621	2.54621
19	160.2	0.81785	0.8	2.55751	2.55751
20	170.21	0.82507	0.82	2.56877	2.56877
21	180.22	0.83312	0.83	2.58127	2.58127
22	190.22	0.8412	0.84	2.59376	2.59376
23	200.22	0.85044	0.85	2.60796	2.60796
24	210.23	0.85998	0.86	2.62255	2.62255
25	220.25	0.87022	0.88	2.63811	2.63811
26	230.24	0.88141	0.89	2.65503	2.65503
27	240.25	0.8924	0.9	2.67153	2.67153
28	250.25	0.90446	0.92	2.68951	2.68951
29	260.27	0.91742	0.93	2.70871	2.70871
30	270.25	0.93045	0.944	2.72789	2.72789
31	280.25	0.94357	0.956	2.74705	2.74705
32	290.24	0.95801	0.968	2.76799	2.76799

Complex Ni^{II}_9 (16)

MW = 2347 g/mol, χ_{dia} = -990 x 10^{-6} cm^3 mol^{-1}
m = 24.91 mg , H = 1.000 T

No	T(K)	$\chi.T_{exp.}$	$\chi.T_{calc.}$	μ_{exp}	$\mu_{calc.}$
1	1.958	0.43884	0.2031	1.87341	1.27448
2	5.116	0.55179	0.62	2.10071	2.22677
3	10.168	0.69449	0.83	2.35674	2.57643
4	15.043	0.88835	0.99	2.66546	2.81382
5	20.005	1.09873	1.17	2.96432	3.05895
6	30.002	1.49451	1.51	3.45723	3.4751
7	40.003	1.83462	1.83	3.83048	3.82565
8	50.005	2.1308	2.11	4.12811	4.10791
9	60.038	2.38751	2.37	4.3697	4.35365
10	70.053	2.61174	2.6	4.5703	4.56001
11	80.065	2.81625	2.808	4.74586	4.7389
12	90.087	2.99803	2.9972	4.89663	4.89595
13	100.13	3.16516	3.168	5.03127	5.03352
14	110.1	3.31166	3.32	5.14639	5.15286
15	120.14	3.45017	3.46	5.2529	5.26038
16	130.17	3.57094	3.58	5.34405	5.35083
17	140.18	3.68455	3.699	5.4284	5.43903
18	150.18	3.78576	3.8	5.50244	5.51279
19	160.2	3.88302	3.89	5.57268	5.57769
20	170.21	3.96987	3.98	5.63466	5.64184
21	180.22	4.04943	4.06	5.69084	5.69826
22	190.24	4.12616	4.13	5.7445	5.74718
23	200.24	4.19321	4.2	5.79099	5.79568
24	210.16	4.25886	4.26	5.83615	5.83693
25	220.24	4.32103	4.32	5.87859	5.87789
26	230.26	4.37688	4.37	5.91646	5.91181
27	240.26	4.43332	4.42	5.95448	5.94553
28	250.25	4.48225	4.47	5.98725	5.97906
29	260.27	4.52742	4.514	6.01734	6.00842
30	270.26	4.57264	4.56	6.04732	6.03896
31	280.26	4.61571	4.59	6.07573	6.05879
32	290.26	4.66497	4.63	6.10807	6.08513

Complex Cu^{II}_9 (17)

MW = 2595 g/mol, χ_{dia} = -1260 x 10^{-6} cm^3 mol^{-1}
m = 22.53 mg , H = 1.000 T

No	T(K)	$\chi.T_{exp.}$	$\chi.T_{calc.}$	μ_{exp}	$\mu_{calc.}$
1	2	0.90783	0.84	2.69452	2.5919
2	5	1.13652	1.222	3.01487	3.12619
3	10	1.32429	1.3644	3.2544	3.30332
4	15	1.40389	1.408	3.35078	3.35568
5	20	1.43277	1.423	3.38507	3.37351
6	30	1.43319	1.4189	3.38557	3.36865
7	40	1.41523	1.4016	3.36429	3.34805
8	50	1.40297	1.3875	3.34968	3.33116
9	60.04	1.4014	1.3835	3.34781	3.32636
10	70.05	1.40066	1.3921	3.34692	3.33668
11	80.06	1.41961	1.414	3.36949	3.36282
12	90.09	1.45108	1.4482	3.40663	3.40325
13	100.09	1.49328	1.4928	3.45581	3.45526
14	110.16	1.54608	1.5462	3.51638	3.51651
15	120.14	1.60616	1.6057	3.58405	3.58353
16	130.16	1.66997	1.6701	3.65455	3.65469
17	140.13	1.739	1.7372	3.72932	3.72739
18	150.19	1.8095	1.8068	3.80416	3.80132
19	160.19	1.88111	1.8767	3.8787	3.87415
20	170.2	1.95163	1.9467	3.95074	3.94574
21	180.21	2.02169	2.016	4.02102	4.01536
22	190.23	2.09067	2.084	4.08905	4.08252
23	200.24	2.15602	2.1567	4.15246	4.15312
24	210.24	2.22219	2.2153	4.2157	4.20916
25	220.25	2.28414	2.2781	4.27406	4.26841
26	230.24	2.33785	2.3387	4.32402	4.32481
27	240.24	2.39403	2.3971	4.37567	4.37847
28	250.25	2.44631	2.4535	4.42319	4.42968
29	260.26	2.4959	2.5	4.46779	4.47146
30	270.27	2.54654	2.55	4.51289	4.51595
31	280.26	2.59664	2.609	4.55707	4.5679
32	290.26	2.65603	2.6575	4.60889	4.61016